

Mining Science and Technology

Горные науки
и технологии

Vol. 8 №4
2023





Activities of the *Mining Science and Technology (Russia) (Gornye nauki i tekhnologii)* international journal are aimed at developing international scientific and professional cooperation in the field of mining.

The journal target audience comprises researchers, specialists in the field of mining, representatives of academic and professional communities.

The journal publishes original papers describing research findings, experience in the implementation of projects in mining industry, review publications.

The journal seeks to develop interdisciplinary areas that contribute to progress in mining, for example, technological and environmental safety, project organization and management in mining industry, development of territories, legal aspects of natural resource use, and other areas studied by researchers and practitioners. The journal always welcomes new developments. Papers are accepted in English or Russian.

EDITOR-IN-CHIEF

Vadim L. Petrov, Prof., Dr.Sci.(Eng.), National University of Science and Technology MISIS, Moscow, Russian Federation

DEPUTIES EDITOR-IN-CHIEF

Oleg I. Kazanin, Prof., Dr.Sci.(Eng.), National Mineral Resources University "University of Mines", St. Petersburg, Russian Federation

Svetlana A. Epshtein, Dr.Sci.(Eng.), National University of Science and Technology MISIS, Moscow, Russian Federation

EDITORIAL BOARD

Zach Agioutantis, Prof., Ph.D., University of Kentucky, Lexington, Kentucky, USA

Maksim A. Bogdasarou, Prof., Dr.Sci.(Geol. and Min.), Brest State A. S. Pushkin University, Brest, Belarus

Grigory Yu. Boyarko, Prof. Dr. Sci. (Econ.), Cand. Sci. (Geol. and Miner.), National Research Tomsk Polytechnic University, Tomsk, Russian Federation

Xuan Nam Bui, Prof., Dr.Sci., Hanoi University of Mining and Geology, Duc Thang – Bac Tu Liem, Hanoi, Vietnam

Carsten Drenstedt, Prof., Ph.D., Freiberg University of Mining and Technology, Freiberg, Germany

Faramarz Doulati Ardejani, Prof., Ph.D., Colledge of Engineering, University of Tehran, Tehran, Iran

Mikhail S. Ershov, Prof., Dr.Sci.(Eng.), National University of Oil and Gas "Gubkin University", Moscow, Russian Federation

Akper A. Feyzullaev, Prof., Dr.Sci.(Geol. and Min.), Institute of Geology and Geophysics of the National Academy of Sciences of Azerbaijan, Baku, Azerbaijan

Ochir Gerel, Prof., Dr.Sci.(Geol. and Min.), Geoscience Center, the Mongolian University of Science and Technology, Ulaanbaatar, Mongolia

Zoran Gligorić, Prof., Dr.Sci. (Mining-Underground Mining), University of Belgrade, Belgrade, Republic of Serbia

Monika Hardygora, Prof., Ph.D., Wrocław University of Technology, Wrocław, Poland

Nikolae Ilias, Prof., Dr.Sci.(Eng.), University of Petrosani, Petrosani, Romania

Vladislav Kecojevic, Prof., Ph.D., Benjamin M. Statler College of Engineering and Mineral Resources, West Virginia University, Morgantown, West Virginia, USA

Aleksey A. Khoreshok, Prof., Dr.Sci.(Eng.), Gorbachev Kuzbass State Technical University, Kemerovo, Russian Federation

Vladimir I. Klishin, Prof., Dr.Sci.(Eng.), Institute of Coal, Siberian Branch, Russian Academy of Sciences, Kemerovo, Russian Federation

Vladimir N. Koshelev, Prof., Dr.Sci.(Chem.), National University of Oil and Gas "Gubkin University" (Gubkin University), Moscow, Russian Federation

Jyant Kumar, Prof., Ph.D-Geotech.Eng., Indian Institute of Science, Bengaluru, India

Vladimir A. Makarov, Prof., Dr.Sci.(Geol. and Min.), Siberian Federal University, Krasnoyarsk, Russian Federation

Sergey I. Malafeev, Prof., Dr.Sci.(Eng.), Vladimir State University named after Alexander and Nikolay Stoletovs, Vladimir, Russia

Oleg S. Misnikov, Prof., Dr.Sci.(Eng.), Tver State Technical University, Tver, Russian Federation

Valery V. Morozov, Prof., Dr.Sci.(Eng.), National University of Science and Technology MISIS, Moscow, Russian Federation

Igor M. Petrov, Dr.Sci.(Eng.), Infomine Research Group LLC, Moscow, Russian Federation

Bakhadirzhan R. Raimzhanov, Prof., Dr.Sci.(Eng.), Uzbekistan Research, Design and Survey Institute for Geotechnology and Nonferrous Metallurgy – O'zGEORANGMETLITI, Tashkent, Uzbekistan

Bayan R. Rakishev, Prof., Dr.Sci.(Eng.), Kazakh National Research Technical University named after K.I. Satpayev, Alma-Ata, Kazakhstan

Oscar Jaime Restrepo Baena, Prof., Ph.D., National University of Colombia, Medellín, Colombia

Alexander N. Shashenko, Prof., Dr.Sci.(Eng.), National Mining University, Dnipro, Ukraine

Vadim P. Tarasov, Prof., Dr.Sci.(Eng.), National University of Science and Technology MISIS, Moscow, Russian Federation

Denis P. Tibilov, Prof., Dr.Sci.(Econ.), Moscow State Institute of International Affairs (University) under the Ministry of Foreign Affairs of Russia, Moscow, Russian Federation

Niyaz G. Valiev, Prof., Dr.Sci.(Eng.), The Ural State Mining University, Ekaterinburg, Russian Federation

Natalia Zhuravleva, Prof., Dr.Sci.(Eng.), West Siberian Testing Center JSC (WSTCenter JSC), Novokuznetsk, Russian Federation

Vera V. Yurak, Assoc. Prof., Dr. Sci. (Econ.), Ural State Mining University, Yekaterinburg; Institute of Economics, Ural Branch of the Russian Academy of Sciences, Yekaterinburg, Russian Federation

EDITORIAL COUNCIL

Yuri G. Agafonov, Assoc. Prof., Cand.Sci.(Eng.), National University of Science and Technology MISIS, Moscow, Russian Federation

Michael R. Filonov, Prof., Dr.Sci.(Eng.), National University of Science and Technology MISIS, Moscow, Russian Federation

Leonid A. Plaschansky, Prof., Cand.Sci.(Eng.), National University of Science and Technology MISIS, Moscow, Russian Federation

Yuri I. Razorenov, Prof., Dr.Sci.(Eng.), Platov South-Russian State Polytechnic University, Novocherkassk, Russian Federation

EXECUTIVE SECRETARY

Daria P. Galushka, National University of Science and Technology MISIS, Moscow, Russian Federation

QUARTERLY

FOUNDED in 2016

REGISTRATION

The journal science and applied research journal is registered by the Federal Service for Communication, IT and Mass Communication Control on August 10, 2015. Registration Certificate E-No. ФС77-62652

INDEXATION

Scopus, CAS, EBSCO, DOAJ, РИНЦ, ВИНТИ РАН, Dimensions, BASE, J-Gate, Jisc Library Hub Discover.

FOUNDER AND PUBLISHER



MISIS
UNIVERSITY

The National University of Science and Technology MISIS (NUST MISIS)

CONTACT

4 Leninsky Prospect, Moscow 119049, Russian Federation

Phone: +7 (495) 955-00-77

e-mail: send@misis.ru



This work is licensed under a
Creative Commons Attribution 4.0 License.



Деятельность научно-практического журнала «Горные науки и технологии» (Mining Science and Technology (Russia)) направлена на развитие международного научного и профессионального сотрудничества в области горного дела.

Целевая аудитория журнала – исследователи, специалисты в области горного дела, представители академического и профессионального сообществ.

В журнале публикуются оригинальные статьи, описывающие результаты исследований, опыт реализации проектов в горнопромышленном комплексе, обзорные публикации.

Журнал стремится развивать такие междисциплинарные направления, как технологическая и экологическая безопасность, организация и управление проектами в горной промышленности, развитие территорий, правовые аспекты использования природных ресурсов и другие, которые способствуют прогрессу в горном деле и реализуются исследователями и практиками.

ГЛАВНЫЙ РЕДАКТОР

Петров Вадим Леонидович, проф., д.т.н., НИТУ «МИСиС», г. Москва, Российская Федерация

ЗАМЕСТИТЕЛИ ГЛАВНОГО РЕДАКТОРА

Казанин Олег Иванович, проф., д.т.н., Санкт-Петербургский горный университет, г. Санкт-Петербург, Российская Федерация

Эпштейн Светлана Абрамовна, д.т.н., НИТУ «МИСиС», г. Москва, Российская Федерация

РЕДАКЦИОННАЯ КОЛЛЕГИЯ

Агиутантис Зак, проф., д-р наук, Университет Кентукки, г. Лексингтон, Кентукки, США

Богдасаров Максим Альбертович, проф., д.г.-м.н., Брестский государственный университет им. А.С. Пушкина, г. Брест, Беларусь

Боярко Григорий Юрьевич – проф., д.э.н., к.г.-м.н., Национальный исследовательский Томский политехнический университет, г. Томск, Российская Федерация

Буи Суан Нам, проф., д-р наук, Ханойский университет горного дела и технологии, г. Ханой, Вьетнам

Валиев Нияз Гадым оглы, проф., д.т.н., Уральский государственный горный университет, г. Екатеринбург, Российская Федерация

Герел Очир, проф., д.г.-м.н., Центр геолого-геофизических исследований, Монгольский университет науки и технологии, г. Улан-Батор, Монголия

Глигорич Зоран, проф., д-р наук, Белградский университет, г. Белград, Республика Сербия

Дребенштедт Карстен, проф., д-р наук, Технический университет Фрайбургская горная академия, г. Фрайберг, Германия

Дулати Ардежани Фарамарз, проф., д-р наук, Инженерный колледж, Тегеранский университет, г. Тегеран, Иран

Ершов Михаил Сергеевич, проф., д.т.н., Российский государственный университет нефти и газа (национальный исследовательский университет) им. И.М. Губкина, г. Москва, Российская Федерация

Журавлева Наталья Викторовна, проф., д.т.н., АО «Западно-Сибирский испытательный центр» (АО «ЗСИЦентр»), г. Новокузнецк, Российская Федерация

Илиаш Николае, проф., д.т.н., Университет Петрошани, г. Петрошани, Румыния

Кецоджевич Владислав, проф., д-р наук, Институт инженерного дела и минеральных ресурсов им. Бенджамина М. Статлера Университета Западной Вирджинии, г. Моргантаун, Западная Вирджиния, США

Клишин Владимир Иванович, проф., д.т.н., Институт угля Сибирского отделения Российской академии наук, г. Кемерово, Российская Федерация

Кошелев Владимир Николаевич, проф., д.х.н., Российский государственный университет нефти и газа им. И.М. Губкина, г. Москва, Российская Федерация

Кумар Джьянт, проф., д-р наук (геотехнический инжиниринг), Индийский институт науки (Indian Institute of Science), г. Бангалор, Индия

Макаров Владимир Александрович, проф., д.г.-м.н., Сибирский федеральный университет, г. Красноярск, Российская Федерация

Малафеев Сергей Иванович, проф., д.т.н., Владимирский государственный университет имени А.Г. и Н.Г. Столетовых, г. Владимир, Российская Федерация

Мисников Олег Степанович, проф., д.т.н., Тверской государственный технический университет, г. Тверь, Российская Федерация

Морозов Валерий Валентинович, проф., д.т.н., НИТУ «МИСиС», г. Москва, Российская Федерация

Петров Игорь Михайлович, д.т.н., ООО «Исследовательская группа «Инфолайн»», г. Москва, Российская Федерация

Раимжанов Бахадиржан Раимжанович, проф., д.т.н., Узбекский научно-исследовательский и проектно-изыскательский институт геотехнологии и цветной металлургии «O'zGEORANGMETLIT», г. Ташкент, Узбекистан

Ракишев Баян Ракишевич, проф., д.т.н., Казахский национальный исследовательский технический университет им. К.И. Сатпаева, г. Алма-Ата, Казахстан

Рестрепо Баэна Оскар Хайме, проф., д-р наук, Национальный университет Колумбии, г. Медельин, Колумбия

Тарасов Вадим Петрович, проф., д.т.н., НИТУ «МИСиС», г. Москва, Российская Федерация

Тиболов Денис Петрович, проф., д.э.н., Московский государственный институт международных отношений (Университет) Министерства иностранных дел России, г. Москва, Российская Федерация

Фейзуллаев Акпер Акпер оглы, проф., д.г.-м.н., Институт геологии и геофизики (ИГГ) Национальной Академии Наук Азербайджана, г. Баку, Азербайджан

Хорешок Алексей Алексеевич, проф., д.т.н., Кузбасский государственный технический университет им. М.С. Горбачева, г. Кемерово, Российская Федерация

Шашенко Александр Николаевич, проф., д.т.н., Национальный горный университет, г. Днепр, Украина

Хардигора Моника, проф., д-р наук, Вроцлавский технологический университет, г. Вроцлав, Польша

Юрак Вера Васильевна, доц., д.э.н., Уральский государственный горный университет, г. Екатеринбург; старший научный сотрудник, Институт экономики Уральского отделения Российской академии наук (ИЭ УРО РАН), г. Екатеринбург, Российская Федерация

Юрак Вера Васильевна, доц., д.э.н., Уральский государственный горный университет, г. Екатеринбург; старший научный сотрудник, Институт экономики Уральского отделения Российской академии наук (ИЭ УРО РАН), г. Екатеринбург, Российская Федерация

Юрак Вера Васильевна, доц., д.э.н., Уральский государственный горный университет, г. Екатеринбург; старший научный сотрудник, Институт экономики Уральского отделения Российской академии наук (ИЭ УРО РАН), г. Екатеринбург, Российская Федерация

Юрак Вера Васильевна, доц., д.э.н., Уральский государственный горный университет, г. Екатеринбург; старший научный сотрудник, Институт экономики Уральского отделения Российской академии наук (ИЭ УРО РАН), г. Екатеринбург, Российская Федерация

Юрак Вера Васильевна, доц., д.э.н., Уральский государственный горный университет, г. Екатеринбург; старший научный сотрудник, Институт экономики Уральского отделения Российской академии наук (ИЭ УРО РАН), г. Екатеринбург, Российская Федерация

Юрак Вера Васильевна, доц., д.э.н., Уральский государственный горный университет, г. Екатеринбург; старший научный сотрудник, Институт экономики Уральского отделения Российской академии наук (ИЭ УРО РАН), г. Екатеринбург, Российская Федерация

Юрак Вера Васильевна, доц., д.э.н., Уральский государственный горный университет, г. Екатеринбург; старший научный сотрудник, Институт экономики Уральского отделения Российской академии наук (ИЭ УРО РАН), г. Екатеринбург, Российская Федерация

Юрак Вера Васильевна, доц., д.э.н., Уральский государственный горный университет, г. Екатеринбург; старший научный сотрудник, Институт экономики Уральского отделения Российской академии наук (ИЭ УРО РАН), г. Екатеринбург, Российская Федерация

Юрак Вера Васильевна, доц., д.э.н., Уральский государственный горный университет, г. Екатеринбург; старший научный сотрудник, Институт экономики Уральского отделения Российской академии наук (ИЭ УРО РАН), г. Екатеринбург, Российская Федерация

Юрак Вера Васильевна, доц., д.э.н., Уральский государственный горный университет, г. Екатеринбург; старший научный сотрудник, Институт экономики Уральского отделения Российской академии наук (ИЭ УРО РАН), г. Екатеринбург, Российская Федерация

Юрак Вера Васильевна, доц., д.э.н., Уральский государственный горный университет, г. Екатеринбург; старший научный сотрудник, Институт экономики Уральского отделения Российской академии наук (ИЭ УРО РАН), г. Екатеринбург, Российская Федерация

Юрак Вера Васильевна, доц., д.э.н., Уральский государственный горный университет, г. Екатеринбург; старший научный сотрудник, Институт экономики Уральского отделения Российской академии наук (ИЭ УРО РАН), г. Екатеринбург, Российская Федерация

Юрак Вера Васильевна, доц., д.э.н., Уральский государственный горный университет, г. Екатеринбург; старший научный сотрудник, Институт экономики Уральского отделения Российской академии наук (ИЭ УРО РАН), г. Екатеринбург, Российская Федерация

Юрак Вера Васильевна, доц., д.э.н., Уральский государственный горный университет, г. Екатеринбург; старший научный сотрудник, Институт экономики Уральского отделения Российской академии наук (ИЭ УРО РАН), г. Екатеринбург, Российская Федерация

Юрак Вера Васильевна, доц., д.э.н., Уральский государственный горный университет, г. Екатеринбург; старший научный сотрудник, Институт экономики Уральского отделения Российской академии наук (ИЭ УРО РАН), г. Екатеринбург, Российская Федерация

Юрак Вера Васильевна, доц., д.э.н., Уральский государственный горный университет, г. Екатеринбург; старший научный сотрудник, Институт экономики Уральского отделения Российской академии наук (ИЭ УРО РАН), г. Екатеринбург, Российская Федерация

Юрак Вера Васильевна, доц., д.э.н., Уральский государственный горный университет, г. Екатеринбург; старший научный сотрудник, Институт экономики Уральского отделения Российской академии наук (ИЭ УРО РАН), г. Екатеринбург, Российская Федерация

Юрак Вера Васильевна, доц., д.э.н., Уральский государственный горный университет, г. Екатеринбург; старший научный сотрудник, Институт экономики Уральского отделения Российской академии наук (ИЭ УРО РАН), г. Екатеринбург, Российская Федерация

Юрак Вера Васильевна, доц., д.э.н., Уральский государственный горный университет, г. Екатеринбург; старший научный сотрудник, Институт экономики Уральского отделения Российской академии наук (ИЭ УРО РАН), г. Екатеринбург, Российская Федерация

Юрак Вера Васильевна, доц., д.э.н., Уральский государственный горный университет, г. Екатеринбург; старший научный сотрудник, Институт экономики Уральского отделения Российской академии наук (ИЭ УРО РАН), г. Екатеринбург, Российская Федерация

Юрак Вера Васильевна, доц., д.э.н., Уральский государственный горный университет, г. Екатеринбург; старший научный сотрудник, Институт экономики Уральского отделения Российской академии наук (ИЭ УРО РАН), г. Екатеринбург, Российская Федерация

Юрак Вера Васильевна, доц., д.э.н., Уральский государственный горный университет, г. Екатеринбург; старший научный сотрудник, Институт экономики Уральского отделения Российской академии наук (ИЭ УРО РАН), г. Екатеринбург, Российская Федерация

ПЕРИОДИЧНОСТЬ 4 раза в год

ОСНОВАН в 2016 году

РЕГИСТРАЦИЯ

Зарегистрирован Федеральной службой по надзору в сфере связи, информационных технологий и массовых коммуникаций 10 августа 2015 года.

Свидетельство о регистрации Эл № ФС77-62652.

ИНДЕКСИРОВАНИЕ

Scopus, CAS, EBSCO, DOAJ, РИНЦ, ВИНТИ РАН, Dimensions, BASE, J-Gate, Jisc Library Hub Discover.



Журнал открытого доступа.

УЧРЕДИТЕЛЬ И ИЗДАТЕЛЬ



Национальный исследовательский технологический университет «МИСиС» (НИТУ «МИСиС»)

АДРЕС УЧРЕДИТЕЛЯ И ИЗДАТЕЛЯ

119049, г. Москва, Ленинский проспект, д. 4

КОНТАКТЫ РЕДАКЦИИ

Адрес: 119049, г. Москва, Ленинский проспект, д. 4

Телефон: +7 (495) 955-00-77

e-mail: send@misis.ru



Контент доступен под лицензией Creative Commons Attribution 4.0 License.



CONTENTS

GEOLOGY OF MINERAL DEPOSITS

World's barite resources as critical raw material 264

G. Yu. Boyarko, L. M. Bolsunovskaya

Analysis and evaluation of prospects for high-quality quartz resources
in the North Caucasus 278

I. I. Bosikov, R. V. Klyuev, V. Ch. Revazov, N. V. Martyushev

MINING ROCK PROPERTIES. ROCK MECHANICS AND GEOPHYSICS

Physical simulation aspects of structural changes in rock samples
under thermobaric conditions at great depths 290

M. D. Ilyinov, D. N. Petrov, D. A. Karmanskiy, A. A. Selikhov

Simulation of ash dump embankment stability 303

O. G. Bessimbayeva, E. N. Khmyrova, E. A. Oleinikova, A. E. Kasymzhanova

BENEFICIATION AND PROCESSING OF NATURAL AND TECHNOGENIC RAW MATERIALS

Optimizing composition and application conditions of agents for modifying
spectral characteristics of diamonds in X-ray luminescence separation 313

V. A. Chanturiya, V. V. Morozov, G. P. Dvoichenkova, Yu. A. Podkamennyi, A. S. Timofeev

SAFETY IN MINING AND PROCESSING INDUSTRY AND ENVIRONMENTAL PROTECTION

Assessment of performance and environmental friendliness of a sorbent-based remediation
method for heavy metal and metalloids contaminated soils 327

V. V. Yurak, R. A. Apakashev, M. S. Lebzin, A. N. Malyshev

Chemical additive based on sodium oleate and linseed oil
for preparation coal dust suppression composition 349

V. A. Golubkov, G. A. Gorenkova, E. P. Vorozhtsov, M. A. Bespalova, S. V. Bortnikov

Monitoring of aerological risks of accidents in coal mines 350

S. V. Balovtsev

MINING MACHINERY, TRANSPORT, AND MECHANICAL ENGINEERING

Justification of the air distribution system of a down-the-hole hammer
with an efficient operating cycle 360

P. N. Tambovtsev, E. P. Rusin



СОДЕРЖАНИЕ

ГЕОЛОГИЯ МЕСТОРОЖДЕНИЙ ПОЛЕЗНЫХ ИСКОПАЕМЫХ

Мировые ресурсы барита – критического минерального сырья 264
Г.Ю. Боярко, Л.М. Болсуновская

Анализ и оценка перспективных участков высококачественного кварцевого сырья
на территории Северного Кавказа 278
И.И. Босиков, Р.В. Ключев, В. Ч. Ревазов, Н.В. Мартюшев

СВОЙСТВА ГОРНЫХ ПОРОД. ГЕОМЕХАНИКА И ГЕОФИЗИКА

Аспекты физического моделирования процессов структурных изменений образцов
горных пород при термобарических условиях больших глубин..... 290
М.Д. Ильинов, Д.Н. Петров, Д.А. Карманский, А.А. Селихов

Моделирование устойчивости ограждающих сооружений золотоотвала..... 303
О.Г. Бесимбаева, Е.Н. Хмырова, Е.А. Олейникова, А.Е. Касымжанова

ОБОГАЩЕНИЕ, ПЕРЕРАБОТКА МИНЕРАЛЬНОГО И ТЕХНОГЕННОГО СЫРЬЯ

Оптимизация состава и режима применения реагентов-модификаторов
спектральных характеристик алмазов в процессе рентгенолюминесцентной сепарации ... 313
В.А. Чантурия, В.В. Морозов, Г.П. Двойченкова, Ю.А. Подкаменный, А.С. Тимофеев

ТЕХНОЛОГИЧЕСКАЯ БЕЗОПАСНОСТЬ В МИНЕРАЛЬНО-СЫРЬЕВОМ КОМПЛЕКСЕ И ОХРАНА ОКРУЖАЮЩЕЙ СРЕДЫ

Оценка эффективности и экологичности сорбент-ориентированного метода
восстановления загрязненных тяжелыми металлами и металлоидами почв 327
В.В. Юрак, Р.А. Апакашев, М.С. Лебзин, А.Н. Малышев

Добавка на основе олеата натрия и льняного масла
для углепылеподавляющих растворов..... 341
В.А. Голубков, Г.А. Горенкова, Е.П. Ворожцов, М.А. Беспалова, С.В. Бортников

Мониторинг аэрологических рисков аварий на угольных шахтах 350
С.В. Баловцев

ГОРНЫЕ МАШИНЫ, ТРАНСПОРТ И МАШИНОСТРОЕНИЕ

Обоснование системы воздухораспределения погружного пневмоударника
с экономичным рабочим циклом..... 360
П.Н. Тамбовцев, Е.П. Русин



GEOLOGY OF MINERAL DEPOSITS

Review paper

<https://doi.org/10.17073/2500-0632-2023-02-85>

UDC 553.04:553.689.2

**World's barite resources as critical raw material**G. Yu. Boyarko   , L. M. Bolsunovskaya  

National Research Tomsk Polytechnic University, Tomsk, Russian Federation

 gub@tpu.ru**Abstract**

The relevance of the work is connected with the status of barite as a critical mineral raw material, as accepted in most industrialized countries.

Purpose: to study the dynamics of commodity flows (production, import, export, consumption) of barite throughout the countries, its world prices, sources of barite raw materials and the prospects for its production and consumption.

Methods: statistical, graphic, logical.

Results. The production of barite raw materials from 0,3 Mt/year in 1920s grew intensively and reached 8.0–9.6 Mt/year in the 2010. Initially, both the mining and processing of barite raw materials industries were located directly in the USA, Germany, Britain, Italy, and France. These countries accounted for over 90% of world production and 80–95% of world consumption. In the 1950s, a sharp increase in the consumption of barite as a weighting agent for drilling fluids began. This led to an increase in its production in large oil and gas producing countries (the USA, the USSR, Mexico, Canada), export flows (from Morocco and other countries), and cessation of exports from Germany, Britain and France. The share of international trade in barite also increased from 0,3–0,5 Mt/year in the 1950s to 4.2–6.0 Mt/year (55–70% of his income) in the 2010s. The cumulative world production of barite between 1920–2020 is expected to be 550 Mt. World barite resources in deposits prepared for exploitation are estimated at 740 Mt. The group of critical countries importing barite raw materials (imports over 50%) represents 38.8% of the GDP of the world economy (USA, European Union, Germany, Italy, Saudi Arabia, Canada, Kuwait, Norway, Oman, Algeria, Malaysia, Indonesia, UAE, Azerbaijan, Argentina). The group of countries exporting barite raw materials includes 31.0% of the GDP of the world economy (India, Morocco, China, Kazakhstan, Turkey, Iran, Laos, Mexico, Pakistan, Bulgaria). A decrease in the criticality of barite raw material supply is possible as a result in reducing consumption (Japan, France, Italy and the Czech Republic), increasing world barite production with the commissioning of new deposits, given the significant prepared resources of this raw material in Iran, Kazakhstan and Pakistan, as well as the search for new barite deposits, including chemogenic marine bottom sediments.

Keywords

critical minerals, barite, resources, production, world trade, consumption

Acknowledgements

The article was written as part of the grant from the Russian Science Foundation for 2022–2023 on the topic “Critical Mineral Products in the Russian and World Economy” (project No. 22-28-01742).

For citation

Boyarko G. Yu., Bolsunovskaya L. M. World's barite resources as critical raw material. *Mining Science and Technology (Russia)*. 2023;8(4):264–277. <https://doi.org/10.17073/2500-0632-2023-02-85>

ГЕОЛОГИЯ МЕСТОРОЖДЕНИЙ ПОЛЕЗНЫХ ИСКОПАЕМЫХ

Обзорная статья

Мировые ресурсы барита – критического минерального сырьяГ. Ю. Боярко   , Л. М. Болсуновская  

Национальный исследовательский Томский политехнический университет, г. Томск, Российская Федерация

 gub@tpu.ru**Аннотация**

Актуальность работы обусловлена статусом барита как критического минерального сырья, принятым в большинстве промышленно развитых стран.

Цель: изучение динамики товарных потоков (производства, импорта, экспорта, потребления) барита по странам мира, его мировых цен, сырьевой базы барита и перспектив его добычи и потребления.

Методы: статистический, графический, логический.



Результаты. Производство баритового сырья с 0,3 млн т в 1920 г. непрерывно растет и достигло в 2010-х годах 8,0–9,6 млн т/год. Первоначально и добывающие, и перерабатывающие баритовое сырье производства располагались непосредственно в США, Германии, Британии, Италии и Франции, на которые приходилось свыше 90 % его мировой добычи и 80–95 % мирового потребления. В 1950-х годах началось резкое увеличение потребления барита в качестве утяжелителя буровых растворов, что привело к увеличению его добычи в крупных нефтегазодобывающих странах (США, СССР, Мексика, Канада), появлению экспортных потоков (из Марокко и других стран), прекращению экспорта из Германии, Британии и Франции. Доля международной торговли баритом также возросла с 0,3–0,5 млн т/год в 1950-е годы до 4,2–6,0 млн т/год (55–70 % от его мировой добычи) в 2010-е годы. Накопленная мировая добыча барита за 1920–2020 гг. составила 550 млн т, имеющиеся мировые ресурсы барита в подготовленных для эксплуатации месторождениях оцениваются в 740 млн т. Группа критичных стран-импортеров баритового сырья (импорт свыше 50 %) представляет 38,8 % ВВП мировой экономики (США, Европейский союз, Германия, Италия, Саудовская Аравия, Канада, Кувейт, Норвегия, Оман, Алжир, Малайзия, Индонезия, ОАЭ, Азербайджан, Аргентина). Группа стран-экспортеров баритового сырья включает 31,0 % ВВП мировой экономики (Индия, Марокко, Китай, Казахстан, Турция, Иран, Лаос, Мексика, Пакистан, Болгария). Снижение критичности обеспеченности баритовым сырьем возможно путем снижения его потребления (что и осуществляется в Японии, Франции, Италии и Чехии), увеличения мировой добычи барита с вводом в эксплуатацию других баритовых месторождений, учитывая значительные подготовленные ресурсы этого сырья в Иране, Казахстане и Пакистане, а также поиска новых месторождений барита, в том числе хемогенных морских донных осадков.

Ключевые слова

критический минеральный продукт, барит, ресурсы, добыча, мировая торговля, потребление

Благодарности

Статья написана в рамках выполнения гранта Российского научного фонда на 2022–2023 гг. по теме «Критические минеральные продукты в российском и мировом хозяйстве» (проект № 22-28-01742).

Для цитирования

Boyarko G. Yu., Bolsunovskaya L. M. World's barite resources as critical raw material. *Mining Science and Technology (Russia)*. 2023;8(4):264–277. <https://doi.org/10.17073/2500-0632-2023-02-85>

Introduction

Barite (natural barium sulfate/fixed white/barium white) is predominantly used as a weighting agent for drilling fluids (75–88% of consumption), an inert filler in paint and varnish, rubber, paper, glass, cement and construction industries, in the production of plastics, ceramics (6–16%) and as a chemical raw material for the production of barium compounds (up to 6%) [1–3].

The world leaders in barite production are China, India and Morocco, and the leaders in its consumption are the USA, China, India and Saudi Arabia. In the United States, despite significant domestic production of barite (400–700 kt/year), due to imports of up to 87% of its consumption, this commercial product is considered a critical material [3, 4]. The same is the case with barite raw materials in the European Union, which imports up to 82% of its consumption [5]¹. In China, despite its world leadership in mining, barite is also a critical (strategic) commercial product [3, 6, 7]. In Russia, the demand for barites is satisfied by its production from a single source (Tolcheinskoye deposit in the Republic of Kha-

kassia), which is a risk factor of significant import dependence occurrence [3].

The earliest mention of mineral raw materials as a critical material was at the 1953 hearing in the U.S. Senate when discussing “Stocks and Availability of Strategic and Critical Materials for the United States in Time of War”². In the late 1990s, the concept of “critical minerals” (Critical mineral raw materials) was firmly established in the economies of the leading industrialized and rapidly developing countries. This denotes a material that is practically indispensable for the latest industrial technologies, but extremely presents a supply logistics risk [7]. The main indicator of the criticality of mineral raw materials is the level of its import dependence for the national economy. In the list of US critical mineral products, a more fractional gradation of imports is proposed and is

² Stockpile and accessibility of strategic and critical materials to the United States in time of war. Hearings before the Special Subcommittee on Minerals, Materials, and Fuel Economics of the Committee on Interior and Insular Affairs, United States Senate, Eighty-third Congress, first-[second] session, pursuant to S. Res. 143. A resolution to investigate the accessibility and availability of supplies of critical raw materials. Part 6. Petroleum, gas, and coal. Industrial and labor representatives; state administrative and production experts on petroleum, gas, coal, and synthetic fuels. United States. Congress. Senate. Committee on Interior and Insular Affairs. Washington, U.S. Govt. Print. Off.; 1953.

¹ Study on the review of the list of critical raw materials: critical raw materials factsheets. European Commission, Directorate-General for Internal Market, Industry, Entrepreneurship and SMEs. Publications Office; 2017. <https://doi.org/10.2873/398823>



defined with thresholds of 15, 50, 70, 85, 90 and 95% of consumption³. A gradation of import dependence for Russia has been proposed consisting of three ranges: insignificant imports (up to 25%), significant imports (25–75%), and total imports (over 75%) [8]. The second indicator of the criticality of mineral raw materials determines the level of uncertainty of its supply from producers to consumers, and its assessment is subjective [9]. Therefore, the logistics of critical mineral raw materials for its separate types needs to be analyzed.

In China, despite its world leadership in mining, barite is also a critical (strategic) commercial product [3, 6, 7]. In Russia, the demand for barites is satisfied by its production from a single source (Tolcheinskoye deposit in the Republic of Khakassia), which is a risk factor of significant import dependence [3].

Research methods

Data on world production and world trade of barite raw materials for 1920–2020, as well as on its world prices was analyzed, in order to examine world barite resources and its commodity markets. Sources of information: Bulletins and reviews of the US Geological Survey⁴ and Britain Geological Surveys⁵, databases of the Federal Customs Service of Russia⁶, Federal State Statistics Service of Russia⁷ and the UN International Trade Department⁸, reviews of information centers⁹. Content analysis of scientific literature sources, national foreign and Russian reports and accounts, periodicals and ongoing publications devoted to existing problems in the world mineral resource base of barite was carried out. Resources, reserves, production, trade and consumption of barite raw materials are given in metric tons, while prices in US dollars per ton of barite. The indicators

of the share of imports and exports of barite for individual countries and the world are determined by the ratio of their volumes to the sum of the supply of this product (production plus import). Average world barite prices are calculated based on the total volumes and value of world exports.

Overview of world resources and commodity flows of barite raw materials

Barite is a fairly common mineral present in many geological formations (sedimentary, hydrothermal, exogenous, etc.), and forms independent monomineral deposits. It is also present as an associated component in complex (mainly polymetallic) deposits.

Commercially significant barite deposits are represented by four mineral types [3, 10]:

- bedded-sedimentary (stratiform);
- bedded-volcanic (stratiform);
- metasomatic (including carbonatites);
- residual (weathering crust/residuum).

Many more geological formations of barite deposits (carbonatite, nodular, barite-fluorite, barite-celestite, etc.) [10, 11] can also be identified. However, the bulk of barite mining is mainly carried out from the deposits of the above four types.

Barite deposits are geologically quite widespread. In terms of the location of extractive and consuming industries, they are world-wide and also developed on national territories (see Fig. 1).

Over the hundred-years from 1920 to 2020, the cumulative world production of barite amounted to 550 Mt. As at 1 January 2021. The world barite resources in deposits prepared for exploitation are estimated at 740 Mt¹⁰ (Fig. 2), which at current demand level is enough for 70–80 years of consumption.

If in 1920 world production and consumption of barite accounted for about 0.3 Mt, by 1940 it had increased to 1.0 Mt/year. Then from 1946, progressive growth developed to a local maximum in 1981 (8.4 Mt). After falling consumption of drilling barite in the 1980–90s at the level of 4.4–5.7 Mt/year, resumed growth up to 9.6 Mt in 2012 (see Figs. 3, 4).

In the first half of the 20th century, the industries producing and processing of barite raw materials were located directly in the USA, Germany, Britain, Italy and France. They accounted for over 90% of its world production and 80–95% of world consumption. The use of barite was mainly for the production of paint filler (over 50% of consumption) and barium

³ Final List of Critical Minerals 2018. Department of the Interior U.S. 83 Fed. Reg. 23295. 2018. URL: <https://www.federalregister.gov/documents/2018/05/18/2018-10667/final-list-of-critical-minerals-2018>

⁴ US Geological Survey. URL: <http://minerals.usgs.gov/minerals/pubs/commodity/tin/index.html#mcs>

⁵ Britain Geological Surveys. URL: <http://www.bgs.ac.uk/mineralsuk/statistics/worldStatistics.html>

⁶ Federal Customs Service of Russia. URL: <http://stat.customs.gov.ru/analysis>

⁷ Federal State Statistics Service of Russia. URL: <https://gks.ru/emiss>

⁸ UNdata. A world of information. URL: <https://data.un.org/Default.aspx>

⁹ Information And Analytical Center “Mineral”. URL: <http://www.mineral.ru/Center/index.html>

Market Research Group “Infomine”. URL: <https://infomine.ru/>

TrendEconomy. URL: <https://trendeconomy.ru/>

¹⁰ US Geological Survey. URL: <http://minerals.usgs.gov/minerals/pubs/commodity/tin/index.html#mcs>

Information and Analytical Center “Mineral”. URL: <http://www.mineral.ru/Center/index.html>

chemicals. However, over time, the national resources of barite were reduced and there was a transformation of commodity flows from producers to consumers [3].

At the end of the 1950s, there was a sharp increase in the consumption of barite as a weighting agent for drilling fluids. This led to an increase in its production in large oil and gas producing countries (USA, USSR, Mexico, Canada), new export flows (from Morocco, Mexico, Canada and others countries), import flows to other producing countries (Algeria, Venezuela, Trinidad/Tabago), as well as the formation of transit flows

of barite raw materials through the Netherlands, Belgium and Singapore [3].

In the 1980s, after the end of the energy crisis of the 1970s, there was a reduction in drilling and, accordingly, the consumption of barite raw materials, primarily in the United States.

In the 1990s and at the beginning of the 21st century, the world economy began to transform, due primarily to China's industrial potential. Own extraction of barite in China itself, as well as in India, Kazakhstan, Iran, Pakistan grew sharply.

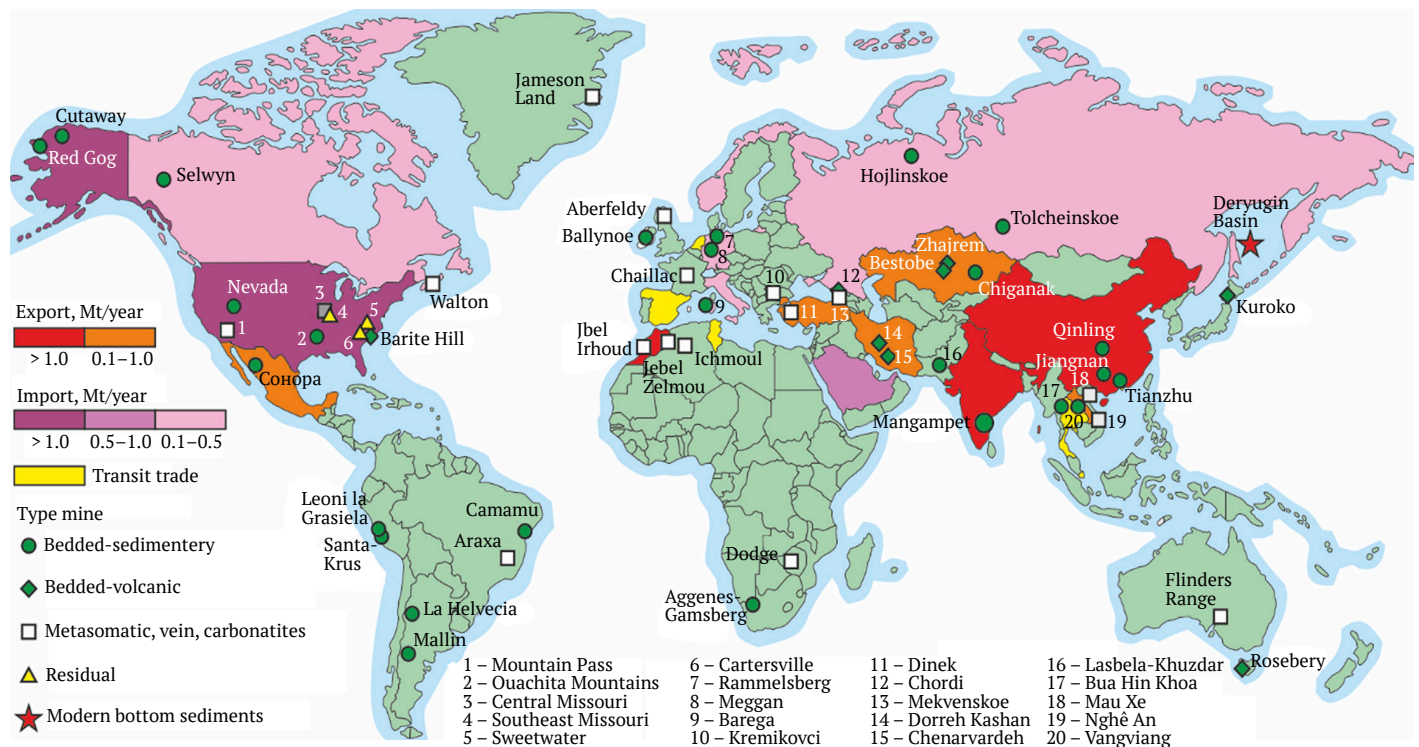


Fig. 1. Map of the world with the localization of barite deposits and lead countries in the international trade of barite raw materials (exporters, importers and transit countries)

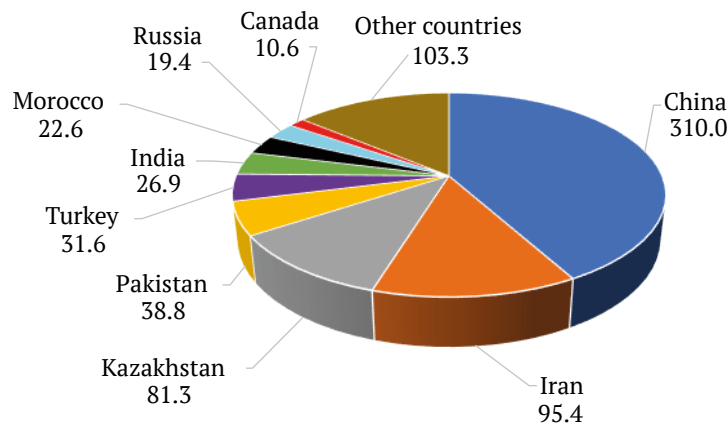


Fig. 2. Barite world resources in deposits prepared for exploitation (Mt)

Based on data provided in the US Geological Survey (<http://minerals.usgs.gov/minerals/pubs/commodity/tin/index.html#mcs>), the Information Center "Mineral" (<http://www.mineral.ru/Center/index.html>) and the Information Group "Infomine" (<https://infomine.ru/>)

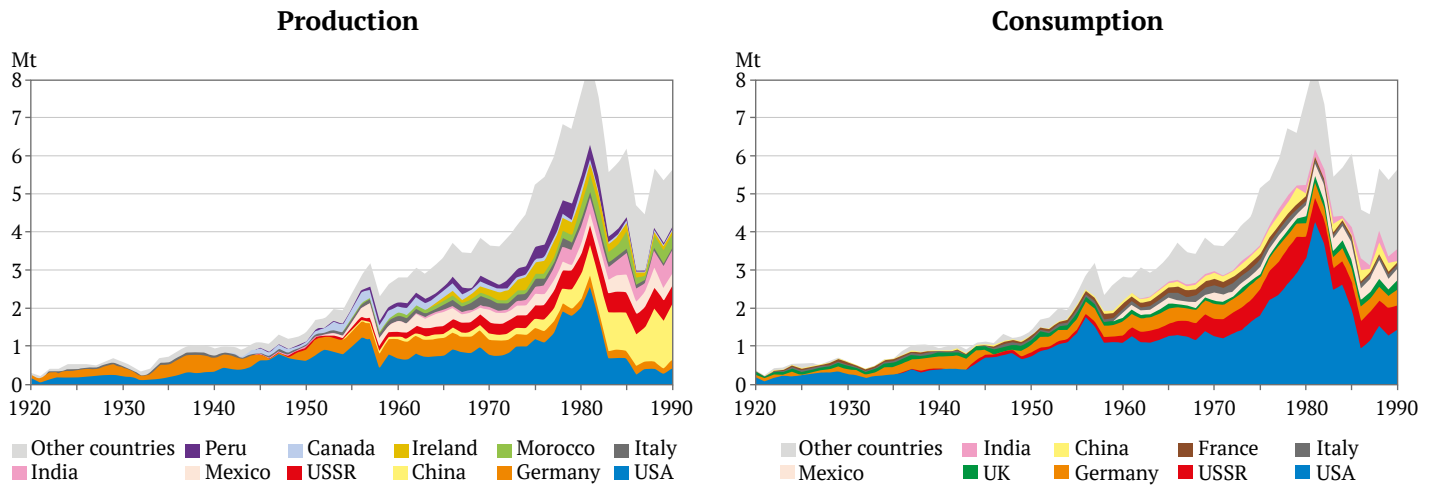


Fig. 3. Dynamics of world barite production and consumption for 1920–1990

Based on data provided in the US Geological Surveys (<http://minerals.usgs.gov/minerals/pubs/commodity/tin/index.html#mcs>) and Britain Geological Surveys (<http://www.bgs.ac.uk/mineralsuk/statistics/worldStatistics.html>), State Statistics Committee of the Russian Federation (<http://stat.customs.gov.ru/analysis>)

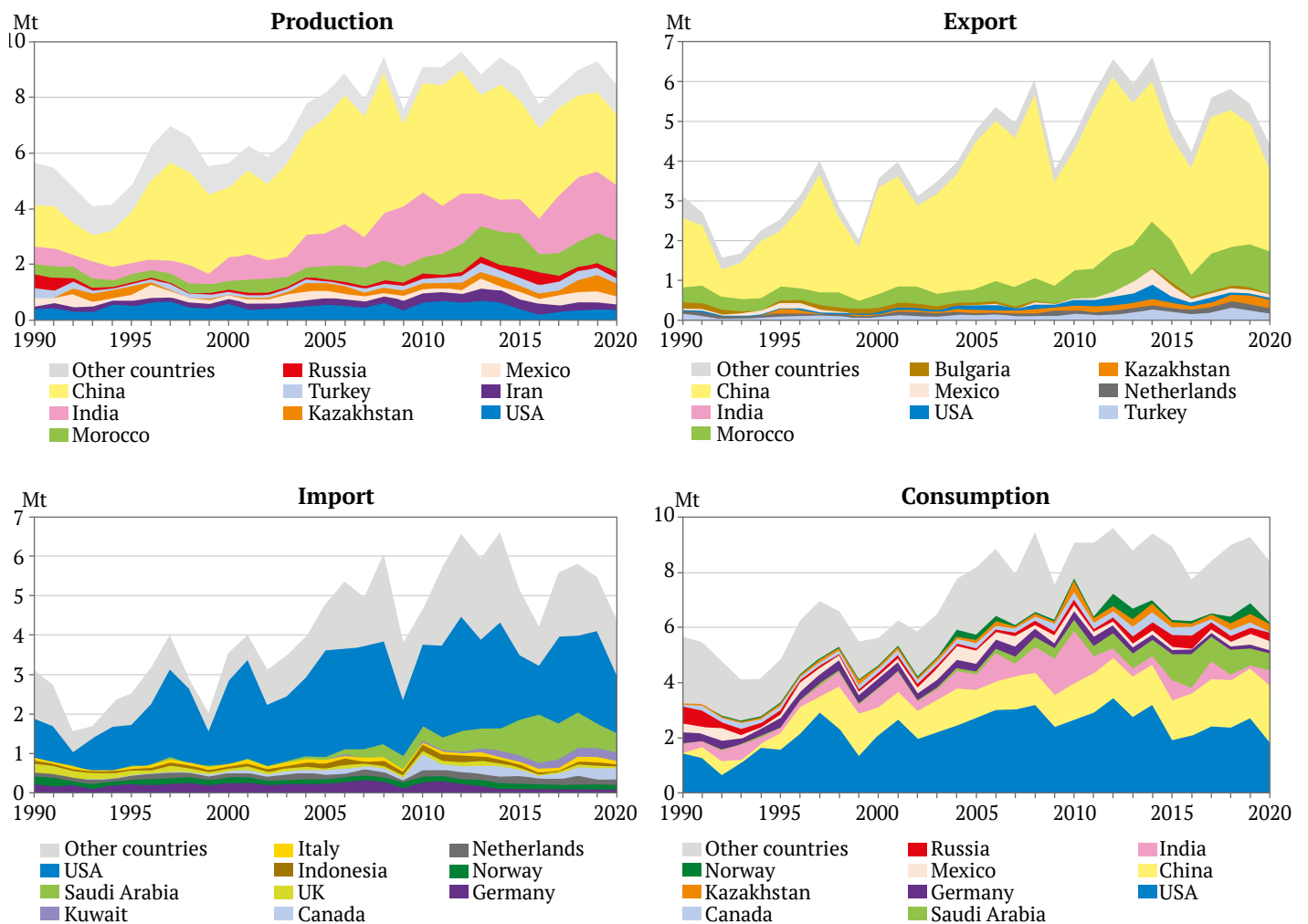


Fig. 4. Dynamics of world production, export, import and consumption of barite flows for 1990–2020

Based on data provided in the US Geological Surveys (<http://minerals.usgs.gov/minerals/pubs/commodity/tin/index.html#mcs>) and Britain Geological Surveys (<http://www.bgs.ac.uk/mineralsuk/statistics/worldStatistics.html>), the State Statistics Committee of the Russian Federation (<https://gks.ru/emiss>) and the Customs Service of the Russian Federation (<http://stat.customs.gov.ru/analysis>), the UN Department of International Trade (<https://data.un.org/Default.aspx>)



In recent years, due to the depletion of long-term developed oil fields, the volume of production drilling significantly increased. There was also an increase in the consumption of barite weighting agent (and, accordingly, imports) not only in the USA, Canada, Russia, but also in Saudi Arabia, Kazakhstan, Kuwait, Argentina, Indonesia, and the United Arab Emirates and Oman [3].

Major barite-producing countries. The *United States* has been the undisputed world leader in barite consumption throughout the entire study period. In 1941, it also became the leader in production, losing the last status only in 1983. The cumulative national production amounted to 63.3 Mt, the cumulative consumption – 146.6 Mt, and the remaining resources of the deposits – 7.6 Mt.

Numerous deposits of stratiform barite (Quachita/Washita Mountains, Red Dog, Cutaway basin and in Nevada), volcanogenic-sedimentary (Barite Hill), hydrothermal (Mountain Pass and in Missouri) and residual (Sweetwater, Cartersville and in Missouri) were developed in the United States type [1, 12, 13, 14]. Numerous deposits of stratiform barite (Quachita/Washita Mountains, Red Dog, Cutaway basin and in Nevada), volcanogenic-sedimentary (Barite Hill), hydrothermal (Mountain Pass and in Missouri) and residual (Sweetwater, Cartersville and in Missouri) were developed in the United States type [13]. The maximum level of production of barite raw materials in the United States was attained in 1981 (2.6 Mt), although it would fall by 1985 to a minimum of 269 kt.

In succeeding years, the level of national production of barite in the United States is 400–700 kt/year. Since 1986, the USA is a net importer of barite raw materials, importing 0.9–2.9 Mt/year (70–90% of consumption). National consumption of barite in the United States increased in the context of the rapid growth in the oil industry: from 0.7 Mt in 1946 to 1.7 Mt in 1956. In 1957–1974, it was at 1.1–1.7 Mt/year. After 1975, in connection with the development of secondary and tertiary technologies for oil production, consumption began to grow up to 4.3 Mt in 1981. This was followed by a recession of 0.9–1.5 Mt/year in 1986–1995. In the 21st century, the national consumption of barite raw materials in the USA is 1.7–3.4 Mt/year.

China, which mined only 25 kt of barite raw materials in 1955, intensified work on the development of the barite mining industry in the 1980s, and increased its production volumes, becoming the world leader in 1983. It then continued to increase production volumes up to a maximum of 5.0 Mt in 2008 [3]. The cumulative national production of barite in China is 108.3 Mt, the cumulative consumption is

39.1 Mt. Remaining resources amount to 310 Mt. The main volume of production of barite raw materials is related mainly to the deposits Qinling, Jiangnan and Tianzhu [12, 15–17].

Most of mined barite is exported, with China being the world leader in its international trade from 1980 to 2017. Exports of barite raw materials from China in 1980–1987 amounted to 20–36% of world trade. In 1988–2012, this increased to 45–66%. However since 2013, due to the increase in domestic consumption of barite, it has fallen to 12–39%. National consumption of barite raw materials in China increased from the level of 100–200 kt/year in 1964–1994. It then further increased to 1.5 Mt in 1998, and stabilized at the level of 1.0–1.3 Mt tons/year in 2000–2009, continuing to grow up to 2.0 Mt in 2020. The predominant use of barite in China is as a paint filler.

In the *USSR*, as in China, the mass production of barite began late, after the Second World War. It increased from 30 kt in 1946 up to a maximum of 540 kt in 1978. Later in Russia, there was a decline in industrial production of barite, accompanied by a decline in production to 50–85 kt/year in 1993–2007. However, since 2008, there has been an increase in the production up to 434 kt in 2016. The cumulative production of barite in the USSR/Russia amounted to 16.9 Mt, accumulated consumption – 24.3 Mt, residual resources – 19.4 Mt.

Barite raw materials are extracted at the Tolcheinskoye deposit in the Republic of Khakassia. Work at other previously developed deposits (Khoylinskoye, Kvartsitovaya Sopka) has ceased [3]. Barite was also imported: in the 1940–1950s – 20–70 kt/year (30–88% of consumption); in the 1960–1980s 100–400 kt/year (6–38%); in the 1990s and in the 21st century – 25–65 kt/year (10–30%). National consumption of barite in the USSR in the 1920–1940s was 5–20 kt/year. After 1944, it began to increase from 55–78 kt/year in 1944–1957 up to 950 kt in 1979. In the 1980s, it reached the level of 550–750 kt/year. National consumption of barite in Russia in the 1990s and in the 21st century is 100–450 kt/year.

India also began intensifying barite production in 1975, peaking at 2.3 Mt in 2010. Most of the mined barite is exported. Since 2018, India has become the world leader in the international trade of barite raw materials (up to 37% of the market), ahead of China [3]. Cumulative production of barite in India amounted to 43.0 Mt, cumulative consumption – 20.0 Mt, residual resources – 26.9 Mt. The main volume of production of barite raw materials are extracted at the unique Mangampet deposit [12, 18]. National consumption of barite in India in the 1920–1950s was 5–20 kt/year;



in the 1960–1970s it was 30–55 kt/year. After 1977, it grew 547 kt in 1993 and up to 1.9 Mt in 2010. In the future, the consumption of barite in India is estimated to be at the level of 500–600 kt/year.

Morocco began developing its own barite deposits in 1958: Jbel-Irhoud and Jebel-Zelmou. These were completely focused on the export of this raw material [19, 20]. For a long time (1980–2005), the level of production and export of barite was 0.4–0.5 Mt/year, later increasing to 0.7–1.2 Mt/year and Morocco traditionally ranks third in international trade barite raw materials (10–24% of the market) [3]. Cumulative production of barite in Morocco amounted to 24.6 Mt; cumulative consumption – 2.8 Mt; and residual resources – 22.6 Mt. There is the opportunity to significantly increase the resource base of barite [21, 22].

Mexico quickly brought the level of barite production to 200–400 kt/year for consumption in the national oil industry. This was achieved by developing the Sonora deposit in 1953 [23]. The cumulative production of barite raw materials in Mexico is 17.4 Mt; the cumulative consumption is 12.9 Mt; and the remaining resources are 3.8 Mt. In the 1950–1970s, 100–200 kt/year were exported (mainly to the USA). However, due to the increase in national consumption of the oil industry, export volumes fell in the 1980s to the 30–65 kt/year. In 1997, the export of barite raw materials practically ceased, resuming only after 2011.

Turkey is fortunately located near European consumers of barite raw materials. Since 1973, the Dinek deposit has remained active [24], exporting 100–300 kt/year. 50–100 kt/year are directed to own consumption. Turkey's cumulative production is 9.2 Mt; cumulative consumption is 3.4 Mt; and the remaining resources of barite raw materials are 31.6 Mt.

Barite-producing countries which have lost export status. Due to the depletion of their own deposits, many exporting countries of barite raw materials have practically left the international market: Yugoslavia in 1966; Germany in 1973; Greece in 1976; Peru in 1985; Ireland in 1995; and Bulgaria in 2009 [3].

Germany, originally in the 1920–1930s, was the world leader in the production and consumption of barite. Production was carried out at the Rammelsberg and Meggan fields [25, 26]. By 2020, the national cumulative production of barite raw materials amounted to 23.3 Mt; cumulative consumption – 26.8 Mt; and residual resources of own deposits – 1.2 Mt. Barite production volumes increased from 100 kt/year in the 1920s to 400 kt/year in the

1930–1960s (with a fall up to 2 kt/year during the Second World War). After 1972, they began to decline down to 34 kt in 2017. At the same time, an import flow of barite raw materials emerged (from 10% of imports from consumption in the 1960s to 70% in the late 1990s). By 1979, Germany had become its net importer of 100–300 kt/year of barite. The level of consumption of barite raw materials in Germany remained for a long time at 300–400 kt/year with a fall only during the economic crisis of 2008–2009. (174 kt in 2009) and with a decrease in demand from 2014 to the present (up to 130–160 kt/year).

Peru began development of the Leoni la Grasiela deposit in 1951 (100–435 kt/year, the vast majority was exported). Prior to 1985 it was a significant exporter of barite (up to 13% of the world market). The cumulative production of Peru amounted to 7.1 Mt; remaining resources – 3.4 Mt. At present, the Santa-Cruz de Kokachakra field is being developed in Peru with a production level of 15–105 kt/year.

Ireland began started development of the Ballynoe deposit in 1955 (100–370 kt/year). Almost all of the mined barite was exported (sometimes up to 22% of the world market). Production ceased in 1994. The cumulative production of Ireland amounted to 5.7 Mt; residual resources – 1.0 Mt.

Bulgaria began extracting barite as an associated useful component at the Kremikovtzi iron ore deposit (100–250 kt/year), most of which was exported. In 2009, as a result of the global economic crisis, production ceased and resumed only in 2014 at the level of 40–70 kt/year. The cumulative production of Bulgaria amounted to 4.5 Mt; the remaining resources – 9.5 Mt.

New countries extracting barite raw materials. New countries appeared with large-scale production of barite raw materials: Kazakhstan, Iran (up to 450 kt/year) and Laos (up to 400 kt/year) [3].

In *Kazakhstan* in the 1990s, in the context of an unfavorable economic environment, production from existing developed barite deposits (Karagai-ly, Zhairam, Bestobe and Chugunak [27]) was only 10–50 kt/year. Since 2003, the production of barite raw materials has increased to 170–270 kt/year. By 2019 it had grown to 600 kt/year. A significant part of the mined barite (100–220 kt/year) is exported to Azerbaijan, Turkmenistan, Uzbekistan and Russia. Intensive geologic exploration is under way, in order to increase Kazakhstan's barite raw materials. Since 1992, the cumulative production of barite in Kazakhstan in a short space of time rose to 6.0 Mt; the cumulative consumption of 3.6 Mt. Remaining resources are very large – 81.3 Mt.



Iran with its unique deposits of Dorreh Kashan and Chenarvarde [28, 29], (15–90 kt/year), since 1991 has increased production of barite raw materials up to 150–230 kt/year. Since 2009, volumes have increased up to 300–435 thousand t/year. Part of the mined barite is exported: 50–150 kt/year. The cumulative production of barite in Iran is 10.0 Mt; the cumulative consumption is 8.5 Mt; and remaining resources are very large – 95.4 Mt.

Laos, which was not previously of interest in terms of minerals, discovered the Vangviang deposit [30]. Thus rapid growth in barite production began from 27 kt in 2013 to 420 kt in 2019. 60–100 kt/year are exported.

Transit countries of barite raw materials.

Trade intermediaries have also emerged among producing countries and end-consumers of barite raw materials: the Netherlands, Spain, Tunisia, Thailand, Belgium, Hong Kong and Singapore.

The *Netherlands* is a convenient logistic point for receiving goods at the major ports of Amsterdam and Rotterdam with further transshipment to the countries of the central part of the European Union. In the absence of barite mining and the minimum volume of national consumption of 10–40 kt/year, the volume of imports and exports is 100–200 kt/year.

Until 2009, *Spain* independently mined up to 50–100 kt/year of barite with its own consumption of 50–70 kt/year. In 2010, the national production of barite raw material reduced. Consumption decreased to 20–40 kt/year, but imports increased to 50–100 kt/year and exports (30–50 kt/year).

Tunisia mines up to 10 kt/year of barite raw materials with a consumption of up to 5 kt/year. However, since 2008, it has been importing and exporting 30–80 kt/year of barite.

Thailand mines barite at the Bua Hin Khoa deposit (50–200 kt/year) with domestic consumption of 50–150 kt/year. Imports and exports of barite raw materials were previously at the level of 20–30 kt/year. However, since 2010, volumes have increased to 60–130 kt/year. This is partly the result of the transit trade of barite.

Transit flows of barite raw materials through Belgium, Singapore and Hong Kong are low – 20–40 kt/year.

Other barite producing countries in the G20.

Britain in the 1920–1930s produced 40–80 kt/year of barite raw materials. Maximum production of 100–120 kt/year was reached in the 1940s, after which there is a stable production of 30–60 kt/year up to the present day. The Aberfeldy field is under development [31]. National consumption is

also kept at a fairly stable level of 90–130 kt/year, requiring imports of 60–90 kt/year. Britain's cumulative production was 6.4 Mt, cumulative consumption was 12.3 Mt, and residual resources were 2.4 Mt.

Canada, has been developing the Selwyn and Walton deposits since 1944 (100–300 kt/year). Production has reduced to 30–50 kt/year since 1982. This level is maintained at this level to the present day. In the 1940s–1970s, mined barite raw materials were exported (100–200 kt/year), mainly to the USA. Nevertheless, the needs for the national oil and gas industry of Canada have reoriented commodity flows. Since 1979, exports have practically ceased, and since 1999 imports of barite began to grow (100–400 kt/year). Canada's cumulative production amounted to 6.8 Mt, cumulative consumption – 6.0 Mt, and residual barite resources – 10.6 Mt.

Italy in the 1920–1950s, barite raw materials were at a level of 20–100 kt/year. In the 1960–1980s: 100–200 kt/year. In the 1990s, production fell to 40–70 kt/year. The Barega and Mont-Aga deposits are under development. In terms of barite raw materials import, only 20–40 kt/year were purchased. Until the 1950s, the level of national consumption of barite in Italy was 20–50 kt/year. However, in the 1960–1980s, against the backdrop of the development of the chemical industry, it increased to 100–200 kt/year, and later stabilized at the level of 90–110 kt/year. Italy's cumulative production was 7.2 Mt; cumulative consumption was 8.8 Mt; and residual resources were 2.0 Mt.

France in the 1920–1960s produced barite raw materials at volumes of 30–100 kt/year; in the 1970–1980s – 100–200 kt/year; in the 1990s 40–70 kt/year. In 2007, mining operations ceased. The Chaillac deposit was under development. In terms of barite raw materials import, only 20–40 kt/year were purchased. France's cumulative production was 6.4 Mt; cumulative consumption was 7.3 Mt; and residual resources were 0.8 Mt.

The *European Union* is a complex conglomerate of its members. Some of them produce barite (Bulgaria, Britain, Germany, Slovakia), other countries only consume barite raw materials (Italy, Poland, Czech Republic, Austria), while other countries are involved in transit trade (Netherlands, Spain, Belgium). As a result, despite the criticality of barite raw materials for the EU in general (68–82% of imports from demand), there is also a significant counter-export flow (up to 25%). The cumulative production of the European Union is 63.0 Mt; the cumulative consumption is 77.5 Mt; and the remaining resources are 0.8 Mt.



Countries – net importers of barite raw materials. Saudi Arabia has been a consumer of barite raw materials for a long time at the level of 10–30 kt/year. Since 2004, due to the transition to secondary and tertiary oil production technologies, it has significantly increased the volume of drilling operations and, according the consumption of barite, (up to the maximum to 1.2 Mt in 2016). The accumulated national consumption of barite raw materials in Saudi Arabia is 9.8 Mt.

Norway began to develop North Sea oil and gas fields. It has been importing significant volumes of barite raw materials since 1979 (100–300 kt/year) [3]. The cumulative national consumption of barite in Norway is 5.6 Mt.

Barite consumption has also increased recently in Kuwait (up to 215 kt/year), Argentina (up to 180 kt/year), Indonesia (up to 150 kt/year) and the United Arab Emirates (up to 80 kt/year) [3].

The criticality of the world barite raw material trade. The share of international trade in barite raw materials has been continuously growing since the 1940s (5–14%) to 55–70%, and in the 2010s (see Fig. 5).

The following groups of countries can be defined according to the ratio of the import and export shares of barite raw materials (Fig. 6):

- critical level importing countries (imports over 50%) – Algeria, Germany, USA, European Union, Malaysia, Canada, Argentina, Italy, Azerbaijan, Oman, Kuwait, Saudi Arabia, Indonesia, UAE, Norway;

- importing countries with moderate imports – Britain, Russia, Brazil;

- exporting countries with a small share of exports (up to 50%) – Bulgaria, China, Mexico, Kazakhstan;
- exporting countries with a high share of exports – Morocco, Turkey, India, Pakistan, Laos, Iran;
- countries of transit trade of barite raw materials – the Netherlands, Tunisia, Spain, Thailand.

The total gross domestic product of importing countries of critical level barite raw materials is 38.8% of the world GNP, exporting countries (both with a small and with a high share of exports) – 31.0%, countries of transit trade – 3.2%. Thus, the criticality of the international trade market in barite is very high, primarily for members of the G20 (USA, European Union, Saudi Arabia, Indonesia and Argentina).

A decrease in the criticality in the barite raw material supply is possible by reducing its consumption, increasing barite production with the commissioning of prepared barite deposits, restoring previous extractive industries and searching for new deposits.

Reducing the consumption of barite raw materials by finding substitutes or eliminating its use. In the paint and varnish industry, barite filler has been replaced with titanium dioxide and bleached kaolin. However, this process is very slow, and linked to the traditional conservatism of consumers accustomed to familiar commercial products. Nevertheless, Japan, with a barite consumption of 100–150 kt/year in the 1980s and 1990s, reduced its demand to 25–40 kt/year by the 2010s. Consumption of barite raw materials also decreased in France, Italy, and the Czech Republic. In South Korea, small

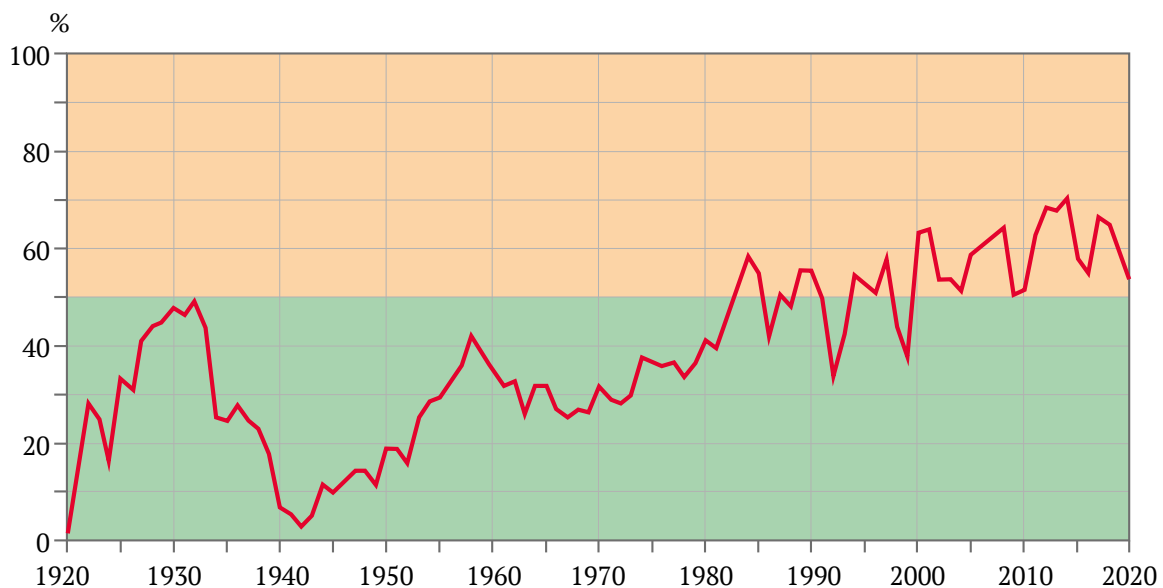


Fig. 5. Share of international trade volumes (export/import) on supply (production) of barite raw materials

volumes of barite was initially used (25–40 kt/year), indicating a planned limitation of its applicability. In principle, it is also possible to replace barite in the main segment of its consumption in drilling fluids with flaky hematite (in terms of physical and operational properties). However, in practice this replacement has not become widespread. Barite is used even in the new bromide-based super-heavy drilling fluids. It is used no longer as a weighting agent, but as a filler and fluid thickener.

The available world resources of barite raw materials (740 Mt) at the current level of its demand are enough for 70–80 years of consumption. Barite resources are most favorable in China, Iran and Kazakhstan. Difficulties arise from the fact that most are located outside the national territories of critical barite importing countries. Their development is

problematic due to the relative cheapness of barite raw materials. Therefore projects for their development are unattractive. Problematic projects for the development of barite deposits in the harsh conditions of the Subarctic are the Hojlin group in Russia, the Jameson Land Basin in Greenland and the Cutaway Basin in Alaska.

There are also logistical problems. For example, the centers for the extraction of barite raw materials in Kazakhstan are located far from seaports, significantly increasing the transport component in the cost of shipped products. Furthermore, political sanctions against certain countries (Iran, Russia, China, etc.) are viewed as a negative signal, already leading to a decrease in export deliveries of barite from China and Iran. Nevertheless, these complex issues can be resolved with new exploration projects in the territories

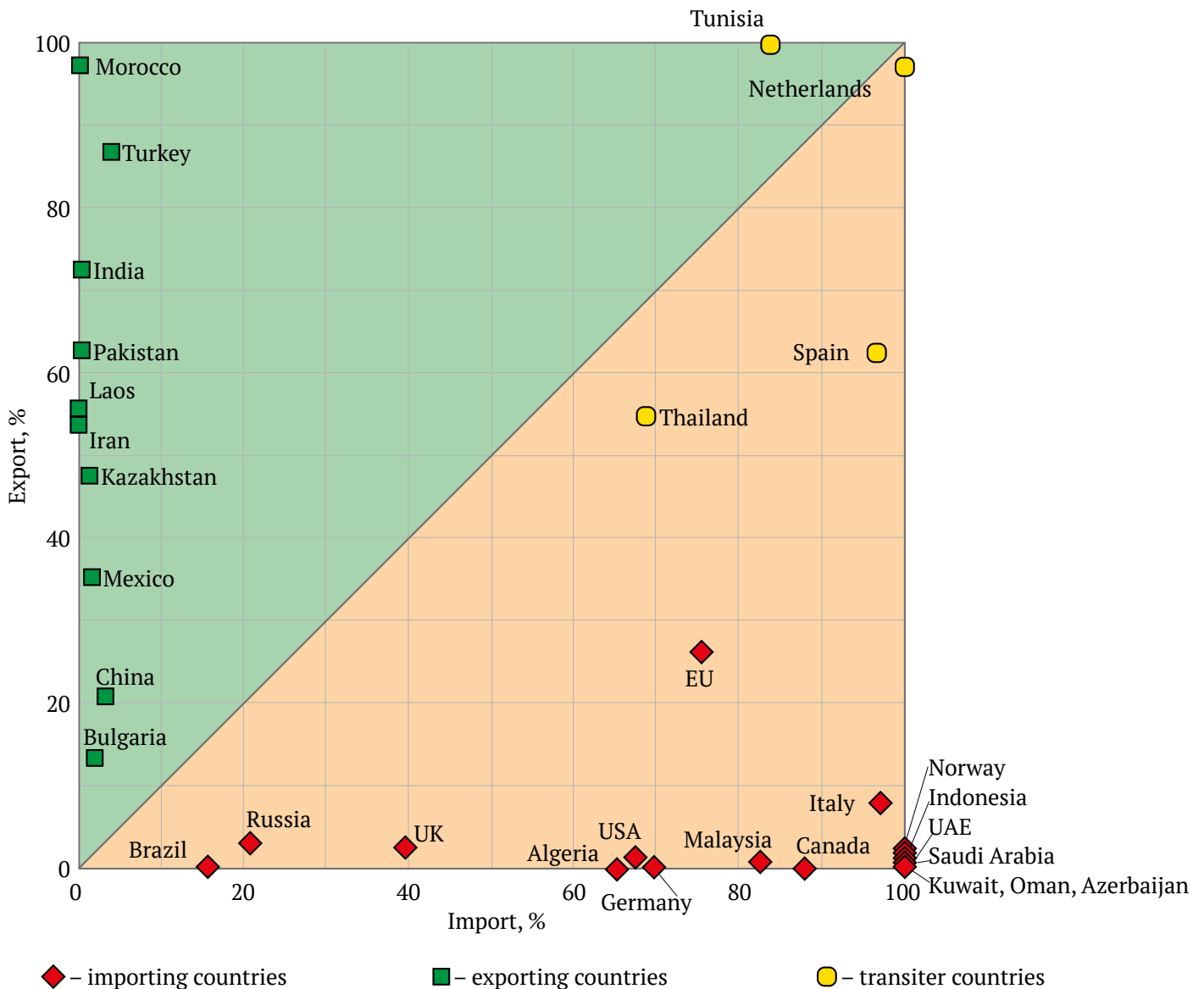


Fig. 6. Share diagram of import and export volumes on supply volumes (mining + import) of barite raw materials in 2020 for countries with commodity flows of barite over 50 kt



of new countries (for example, discoveries of barite deposits in Laos).

A fundamentally new source of barite raw materials can be modern chemogenic barite sediments found at the bottom of the Deryugin Basin in the Sea of Okhotsk (see Fig. 1) [32]. They are found in an area of up to 16 km² at relatively shallow depths of 1470–1480 m. They are in the form of travertine-like accumulations, concretions, and crusts. The resources of barite sediments in this field are up to 10 million tons of BaSO₄. This corresponds to an average concentration of barite formations up to 600 kg/m² [33, 34]. Similar recent marine barite sediments have also been found in other areas of the seabed of the World Ocean [35]. In addition to their chemogenic formation, a biogenic genesis of modern marine barite has also been proposed [36]. Previously, barites from bottom sediments of the seas were not even considered as a potentially useful resource. By analogy with projects for the development of deposits of deep-sea iron-manganese nodules, the development of underwater barite sediments is technically and economically feasible. In addition, the emergence of a new chemogenic type of barite deposits requires a rethinking of geological forecasts for searching of similar deposits in ancient bathyal and abyssal sedimentary formations.

Conclusions

The production of barite raw materials is continuously growing and reached 8.0–9.6 Mt/year in the 2010s. The share of barite international trade is also increased to 4.2–6.0 Mt/year or 55–70% of world production. Cumulative world production of barite for 1920–2020 amounted to 550 Mt; the available world resources of barite in deposits prepared for exploitation are estimated at 740 Mt.

Signs of the criticality in commodity flows of barite raw materials for the national economies of countries are a high share of imports from supply (over 50%) with significant import volumes (over 50 kt/year) and the excess of accumulated national consumption over national production.

The group of critical countries importing barite raw materials (imports over 50%) represents 38.8% of the GDP of the world economy. Imports in 2020 were as follows: USA (1.5 Mt, 68% of demand); the European Union (512 kt, 75%), including Germany (91 kt, 70%) and Italy (96 kt, 97%); Saudi Arabia (500 kt, 100%); Canada (290 kt, 88 %); Kuwait (208 kt, 100%); Norway (118 kt, 100%); Oman (95 kt, 100%); Algeria (75 kt, 65%); Malaysia (70 kt, 82%); Indonesia (62 kt, 100%); UAE (91 kt, 100%); Azerbaijan (59 kt, 100%); Argentina (51 kt, 88%).

The group of countries exporting barite raw materials includes 31.0% of the GDP of the world economy. Exports in 2020 were as follows: India (1.46 Mt, 73% of production); Morocco (1.07 Mt, 97%); China (541 kt, 21%); Kazakhstan (217 kt, 48%); Turkey (181 kt, 87%); Iran (162 kt, 54%); Laos (100 kt, 56%); Mexico (101 kt, 35%); and Pakistan (91 kt, 63%).

Barite raw materials are virtually impossible to replace in the production of drilling fluids, its main segment. There is a movement towards an increase in world consumption of weighted drilling fluids due to systemic changes in the development of oil and gas fields. This is due to a general increase in the depth of drilling to open oil and gas deposits from 1–2 km to 3–5 km and intensive involvement in the development of hard-to-recover reserves of shale oil and gas. This requires 5–8 times more production wells, in accordance with the technological drilling scheme.

The world demand for barite will only increase in the near future in view of growing consumption due to systemic changes in the development of oil and gas fields. This is associated with a general increase in drilling depth and intensive involvement in the development of hard-to-recover shale oil and gas reserves. Accordingly, there has been a growth in the consumption and import of critical barite raw materials to oil and gas producing countries: USA, Saudi Arabia, Kuwait, Indonesia, England, Canada and Norway.

The world barite raw material base has enabled an increase in production, both in traditional producing countries (Morocco, Mexico) and in new leading barite export countries (India, China). The state of barite mining in Russia although critical (the only mining enterprise), can be resolved by future commissioning of new deposits and the formation of controlled barite import flows from friendly countries (Kazakhstan, India, China, Iran).

A decrease in the criticality of barite raw material supply can be attained by reducing consumption in varnish and paint use (Japan, France, Italy and the Czech Republic), as well as by increasing world production of barite with the commissioning of new deposits, given the significant prepared resources of this raw material in Iran, Kazakhstan and Pakistan. There are potential new barite deposits in geologically poorly studied territories (Mongolia, Laos, Myanmar, Western Sahara, the shelf of the Moroccan coast, etc.), as well as searching for a new chemogenic type of barite deposits on the bottom of the seas and in ancient bathyal and abyssal sedimentary formations.



References

1. Bearden S.D. Barite: World sources and the US market. *Mining Engineering*. 1997;49(11):87–88.
2. Bonel K.A. *Mineral profile: Barites*. British Geological Survey; 2005. 28 p.
3. Boyarko G.Yu., Khatkov V.Yu. Current state of production and consumption of barite raw materials in Russia. *Bulletin of the Tomsk Polytechnic University. Geo Assets Engineering*. 2021;332(10):180–191. (In Russ.) <https://doi.org/10.18799/24131830/2021/10/3403>
4. Schulz K.J., DeYoung J.H., Seal R.R., Bradley D.C. (eds.) *Critical mineral resources of the United States – economic and environmental geology and prospects for future supply*. United States Geological Survey; 2017. 862 p. <https://doi.org/10.3133/pp1802>
5. Chen J.B., Huo W.M., Feng D.D. Analysis of strategic (critical) mineral resources situation in China and the U.S. and the EU. *Natural Resources. Economy of China*. 2020;33(8):9–17. (In Chinese)
6. Jiang Y., Wang T., Long T. Research on listing barite as a strategic mineral resource. *Acta Geoscientica Sinica*. 2021;42(2):297–302. (In Chinese) <https://doi.org/10.3975/cagsb.2020.110204>
7. Eremin N.I. Critical metals. *Geologiya Rudnyh Mestorozhdenij*. 2016;58(6):595–596. (In Russ.) <https://doi.org/10.7868/S0016777016060034>
8. Khatkov V.Y. Trade flows of import-dependent mineral products. *Mineral Recourses of Russia. Economics and Management*. 2017;(5):66–71. (In Russ.)
9. Singh R.K., Kumar A., Garza-Reyes J.A., de S´a M.M. Managing operations for circular economy in the mining sector: An analysis of barriers intensity. *Resources Policy*. 2020;69(4):101752. <https://doi.org/10.1016/j.resourpol.2020.101752>
10. Kasymov M.A. Formation types of barite deposits. *Proceedings of the Kyrgyz State Technical University named after I. Razzakov*. 2014;(33):108–112. (In Russ.)
11. Akhmanov G.G., Vasiliev N.G. *Mineral raw materials. Barite*. Handbook. Moscow: Geoinformmark; 1997. 39 p. (In Russ.)
12. Clark S.H.B., Poole F.G., Wang Z. Comparison of some sediment-hosted, stratiform barite deposits in China, the United States, and India. *Ore Geology Reviews*. 2004;24(1–2):85–101. <https://doi.org/10.1016/j.oregeorev.2003.08.009>
13. Howard K.W., Hanor J.S. Compositional zoning in the Fancy Hill stratiform barite deposit, Ouachita Mountains, Arkansas, and evidence for the lack of associated massive sulfides (USA). *Economic Geology*. 1987;82(5):1377–1385. <https://doi.org/10.2113/gsecongeo.82.5.1377>
14. Koski R.A., Hein J.R. Stratiform barite deposits in the Roberts Mountains allochthon, Nevada: a review of potential analogs in modern sea-floor environments. *Chapter H of Contributions to industrial-minerals research. United States Geological Survey Bulletin*. 2003;2209-H.
15. Wang F.-L., Huang Y., Fu Y. et al. A study of the enrichment mechanism of early Cambrian barite in Eastern Guizhou: Constraint from sulfur isotope. *Acta Geoscientica Sinica*. 2020;41(5):686–698. <https://doi.org/10.3975/cagsb.2020.081701> (In Chinese)
16. Zhou X., Li R., Tang D., Huang K.-J. et al. Cold seep activity in the early Cambrian: Evidence from the world-class shale-hosted Tianzhu barite deposit, South China. *Sedimentary Geology*. 2022;439:106220. <https://doi.org/10.1016/j.sedgeo.2022.106220>
17. Li Y., Zou H., Said N., Liu H. A new classification of barite deposits in China. *Ore and Energy Resource Geology*. 2023;14(3). <https://doi.org/10.1016/j.oreoa.2023.100019>
18. George B.G., Shalini N., Pandian M.S. et al. Strontium and Sulphur isotopic constraints on the formation of the Mangampeta barite deposit, Cuddapah basin. *Current Science*. 2013;105(4):499–504.
19. Rajlich P., Legierski J., Šmejkal V. Stable isotope study of base metal deposits from the Eastern High Atlas, Morocco. *Mineralium Deposita*. 1983;18(2):161–171. <https://doi.org/10.1007/BF00206206>
20. Jaillard L. The barite massive orebody at Tarhwacht, Western High Atlas, Morocco, hosted by an albitite of sedimentary origin. *Comptes Rendus – Academie des Sciences, Serie II*. 1987;304(14):847–853.



21. Jébrak M., el Wartiti M., Marcoux E., Zaharoui M. The Bouznika Cambrian barite deposit (Morocco), an early mineralization on the Iapetus margin. *Journal of African Earth Sciences*. 2011;60(3):53–62. <https://doi.org/10.1016/j.jafrearsci.2011.02.001>
22. Ibrahim D., Ahmed B., Habiba A. et al. Contribution of geophysics to the study of barite mineralization in the paleozoic formations of Asdaf Tinejdad (Eastern Anti Atlas Morocco). *Economic and Environmental Geology*. 2020;53(3):259–269. <https://doi.org/10.9719/EEG.2020.53.3.259>
23. González-Sánchez F., González-Partida E., Canet C. et al. Geological setting and genesis of stratabound barite deposits at Múzquiz, Coahuila in northeastern Mexico. *Ore Geology Reviews*. 2017;81(3):1184–1192. <https://doi.org/10.1016/j.oregeorev.2015.10.008>
24. Elmas N., Kumral M., Suner F., Tasdelen S. Stratiform barite deposits hosted in metamorphic assemblages of Dinek and surrounding regions, Isparta, Turkey. *Journal of Asian Earth Sciences*. 2012;48(4):150–159. <https://doi.org/10.1016/j.jseaes.2011.11.013>
25. Kekeliya S.A., Tvalchrelidze A.G., Yaroshevich V.Z. The geological and physicochemical conditions of formation of massive-sulfide-barite-base-metal deposits. *International Geology Review*. 1984;26(12):1437–1444. <https://doi.org/10.1080/00206818409466664>
26. Large D., Walcher E. The Rammelsberg massive sulphide Cu-Zn-Pb-Ba-Deposit, Germany: an example of sediment-hosted, massive sulphide mineralization. *Mineralium Deposita*. 1999;34(5/6):522–538. <https://doi.org/10.1007/s001260050218>
27. Tolmacheva T., Ryazantsev A., Degtyarev K., Nikitina O. Hydrothermal barite deposits in Upper Cambrian-Lower Ordovician siliceous successions of southern Kazakhstan. *Doklady Earth Sciences*. 2014;458(1):1077–1081. <https://doi.org/10.1134/S1028334X14090347>
28. Jamali H., Zohouri F.S., Tabatabaei Manesh S.M. Exhalative deposits in eocene volcano-sedimentary rocks in the middle part of the Urumieh-Dokhtar magmatic belt: Detailed evidence from Nabar deposit, west of Kashan, Urumieh – Dokhtar Magmatic Belt. *Journal of African Earth Sciences*. 2019;154(5):120–135. <https://doi.org/10.1016/j.jafrearsci.2019.03.011>
29. Derakhshi M.G., Mohammad R.H., Moayyed M., Maghfouri S. Metallogensis of Precambrian SEDEX-type Barite-(Pb-Cu-Zn) deposits in the Mishu mountain, NW Iran: Constrains on the geochemistry and tectonic evolution of mineralization. *Ore Geology Reviews*. 2019;107:310–335. <https://doi.org/10.1016/j.oregeorev.2019.02.024>
30. Ma Z., Ravelo A.C., Liu Z. et al. Export production fluctuations in the eastern equatorial Pacific during the Pliocene-Pleistocene: Reconstruction using barite accumulation rates. *Paleoceanography*. 2015;30(11):1455–1469. <https://doi.org/10.1002/2015PA002860>
31. Moles N.R. *Geology, geochemistry and petrology of the Foss stratiform barite-base metal deposit and adjacent Dalradian metasediments, near Aberfeldy, Scotland*. [Dissertation.] University of Edinburgh; 1985. URL: <http://hdl.handle.net/1842/11180>
32. Baranov B., Aloisi V., Degrachev A. Giant barite deposit mapped and the Derugin Basin (Okhotsk Sea). In: *Minerals of the Ocean – integrated strategies – 2*. 25–30 April, 2004. Saint Petersburg, Russia.
33. Astakhov A.S., Ivin V.V., Karnaukh V.N., et al. Barite mineralization in the Deryugin Basin of the Okhotsk Sea: Active processes and formation conditions. *Russian Geology and Geophysics*. 2017;58(2):200–214. <https://doi.org/10.1016/j.rgg.2017.01.002>
34. Andreev S.I., Kazakova V.E., Ivanova A.M., Smirnov A.N. Geology and minerals of the Far Eastern seas of Russia. In: *70 years in the Arctic, Antarctic and oceans. Collection of scientific papers*. St. Petersburg: All-Russian Research Institute of Geology and Mineral Resources of the World Ocean named after Academician I.S. Gramberg; 2018. Pp. 444–454.
35. Gwiazda P.X., Paull C.K., Caress D., Preston C.M., Johnson's S.B., Lundsten E.M., Anderson K. The Extent of Fault-Associated Modern Authigenic Barite Deposits Offshore Northern Baja California Revealed by High-Resolution Mapping. *Frontiers in Marine Science*. 2019;6:460. <https://doi.org/10.3389/fmars.2019.00460>
36. Gonzalez-Muñoz M.T., Martinez-Ruiz F., Morcillo F., et al. Precipitation of barite by marine bacteria: A possible mechanism for marine barite formation. *Geology*. 2012;40(8):675–678. <https://doi.org/10.1130/G33006.1>



Information about the authors

Grigory Yu. Boyarko – Dr. Sci. (Econ.), Cand. Sci. (Geol. and Min.), Professor, National Research Tomsk Polytechnic University, Tomsk, Russian Federation; ORCID [0000-0002-0715-7807](https://orcid.org/0000-0002-0715-7807), Scopus ID [56350674500](https://scopus.com/authorid/56350674500); e-mail gub@tpu.ru

Liudmila M. Bolsunovskaya – Cand. Sci. (Philolog.), Assistant Professor, National Research Tomsk Polytechnic University, Tomsk, Russian Federation; ORCID [0000-0002-1499-8970](https://orcid.org/0000-0002-1499-8970), Scopus ID [56350747600](https://scopus.com/authorid/56350747600); e-mail bolsunovskl@tpu.ru

Received 24.02.2023

Revised 20.03.2022

Accepted 21.03.2022



GEOLOGY OF MINERAL DEPOSITS

Research paper

<https://doi.org/10.17073/2500-0632-2023-10-165>

UDC 556.3



Analysis and evaluation of prospects for high-quality quartz resources in the North Caucasus

I. I. Bosikov¹  , R. V. Klyuev²   , V. Ch. Revazov¹  ,
N. V. Martyushev³  

¹North Caucasian Mining and Metallurgical Institute (State Technological University),
Vladikavkaz, Russian Federation

²Moscow Polytechnic University, Moscow, Russian Federation

³Kh. Ibragimov Complex Institute of the Russian Academy of Sciences, Grozny, Russian Federation

✉ kluev-roman@rambler.ru

Abstract

Quartz resources play a crucial role in the development of key economic sectors, particularly in the production of chemically pure silicon. The extraction and processing of these resources necessitate high-tech methods to obtain the desired silicon output. Presently, the demand for silicon stands at 5–6 Ktpa, while the supply remains at 2300 t. An analysis of the chemical properties of various rocks (quartzites, quartz sands, vein quartz) in the Republic of North Ossetia–Alania reveals that their parametric characteristics align with the requirements for silicon production. The researchers in North Ossetia have successfully grown single-crystal silicon and produced photovoltaic converters. Russian scientists have also achieved the first melting of metallurgical silicon into polycrystalline silicon using vacuum furnaces and electron-beam remelting, yielding promising results. The goal of this research is to analyze and assess the potential of high-quality quartz resources in the North Caucasus. The main objectives include identifying sites with optimal quartz deposits suitable for silicon production, conducting localization, estimating forecast resources, and designating areas for further investigation. The selected sites are expected to possess advantageous geographical and economic features, along with favorable mining conditions conducive to open-pit mining. The study focuses on the Fiagdon site in the Alagir District, RNO-Alania. Various methods, including laboratory work, sampling, examination of constructed sections, and a comprehensive review of mine workings and borehole documentation, were employed. Conclusions from mineralogical and petrographic analyses, alongside laboratory studies and process tests, contributed to the research methodology. The results of the research encompassed the analysis of statistical, economic, geological, and process-related information necessary for addressing primary geological objectives. Subsequent steps involved the selection of prospects for further exploration, specification of geological maps at a 1:10000 scale with accompanying legends and sections, determination of the conditions, morphology, and parameters of productive deposits, and preliminary studies on the quality and process characteristics of quartz resources. Furthermore, the P₂ forecast resources of high-quality quartz raw materials for silicon production were localized, estimated at 500 Kt, and rigorously tested. The study's discoveries have led to the formulation of recommendations for future exploration endeavors.

Keywords

quartz resources, silicon, prospects, mineralogical and petrographic analysis, process tests, productive deposits, quality and process characteristics of quartz resources

For citation

Bosikov I. I., Klyuev R. V., Revazov V. Ch., Martyushev N. V. Analysis and evaluation of prospects for high-quality quartz resources in the North Caucasus. *Mining Science and Technology (Russia)*. 2023;8(4):278–289. <https://doi.org/10.17073/2500-0632-2023-10-165>



ГЕОЛОГИЯ МЕСТОРОЖДЕНИЙ ПОЛЕЗНЫХ ИСКОПАЕМЫХ

Научная статья

Анализ и оценка перспективных участков высококачественного кварцевого сырья на территории Северного Кавказа**И. И. Босиков¹  , Р. В. Ключев²   , В. Ч. Ревазов¹  ,**
Н. В. Мартюшев³  ¹ Северо-Кавказский горно-металлургический институт (государственный технологический университет), г. Владикавказ, Российская Федерация² Московский политехнический университет, г. Москва, Российская Федерация³ Комплексный научно-исследовательский институт им. Х.И. Ибрагимова Российской академии наук, г. Грозный, Российская Федерация kluev-roman@rambler.ru**Аннотация**

Кварцевое сырье является стратегическим ресурсом, так как обеспечивает развитие важнейших отраслей экономики. При этом необходимо учитывать, что при его добыче и переработке следует применять высокотехнологичные методы, позволяющие получить в результате обогащения этого сырья химически чистый кремний. На сегодняшний день потребность в кремнии составляет 5–6 тыс. т в год при предложении 2300 т. Анализ особенностей химизма ряда горных пород (кварцитов, кварцевых песков, жильного кварца) Республики Северная Осетия – Алания показал, что они по своим параметрическим характеристикам могут отвечать требованиям, предъявляемым к кварцевому сырью для получения кремниевой продукции. К настоящему времени учёные Северной Осетии также имеют успешный опыт выращивания монокристаллического кремния и изготовления фотоэлектрических преобразователей. Российские учёные провели первые плавки металлургического кремния в поликристаллический в вакуумных печах способом электронно-лучевого переплава. Во всех случаях результаты обнадеживающие.

Цель, задачи: провести анализ и оценку перспективных участков высококачественного кварцевого сырья на территории Северного Кавказа. Основной задачей исследований является выявление объектов высококачественного кварцевого сырья для производства кремниевой продукции, локализация, оценка их прогнозных ресурсов и выделение участков для дальнейшего изучения. Выявленные объекты должны иметь благоприятные географо-экономические положение и горнотехнические условия, способствующие возможности их открытой (карьерной) отработки.

Объекты: Фиагдонский участок Алагирского района, РСО-Алания.

Методы: Проведение лабораторных работ, опробования, исследование построенных разрезов, изучение документации горных выработок и скважин, заключений минералого-петрографических, лабораторных исследований и технологических испытаний.

Результаты. После выполнения намеченного комплекса исследовательских работ проведен анализ статистической, экономической, геологической, технологической и другой информации, необходимой для решения основных геологических задач; выделены перспективные участки для дальнейших работ; уточнены геологические карты перспективных участков масштаба 1 : 10000 с легендами и разрезами к ним; определены условия залегания, морфология и параметры продуктивных залежей; предварительно изучены качество и технологические характеристики кварцевого сырья; локализованы, оценены и апробированы прогнозны ресурсы высококачественного кварцевого сырья для производства кремниевой продукции по категории P_2 – 500 тыс. т; разработаны рекомендации для проведения геологоразведочных работ.

Ключевые слова

кварцевое сырье, кремний, перспективные участки, минералого-петрографический анализ, технологические испытания, продуктивные залежи, качество и технологические характеристики кварцевого сырья

Для цитирования

Bosikov I. I., Klyuev R. V., Revazov V. Ch., Martynushev N. V. Analysis and evaluation of prospects for high-quality quartz resources in the North Caucasus. *Mining Science and Technology (Russia)*. 2023;8(4):278–289. <https://doi.org/10.17073/2500-0632-2023-10-165>



Introduction

Quartz resources play a pivotal role as strategic assets, crucial for the development of key economic sectors. The imperative development of effective technologies for processing these resources is vital to yield high-quality silicon [1, 2].

As of now, the demand for silicon stands at 5–6 Ktpa, with a supply of 2300 t. Encouragingly, Russian scientists have achieved a breakthrough by melting metallurgical silicon into polycrystalline silicon using vacuum furnaces and electron-beam remelting [3, 4].

In the pursuit of securing advantageous positions in the mining, production, and marketing of products derived from exceptionally pure quartz resources in Russia (e.g., Eastern Siberia’s “Solar Silicon” project, the Urals’ “Silicon–Ural,” and “Polar Quartz” projects), enterprises specializing in the deep processing of quartz resources are being established based on known deposits [5, 6]. Most quartz deposits are traditionally located in the Urals or Siberia [7, 8].

Chemical analysis of rocks (quartzites, quartz sands, vein quartz) from the North Caucasus [9, 10] has shown that their parametric characteristics can meet the requirements for quartz resources to produce silicon products.

Notably, in the Republic of North Ossetia–Alania, scientists have demonstrated successful experiences in cultivating single-crystal silicon and producing photovoltaic converters [11, 12].

The structure of quartz contains various impurity elements (IEs), such as Al, Fe, Ti, H, Li, Na, K, Cr, B, P, Ca, Mg, and Co, which directly impact resource quality.

A study of five vein quartz samples collected in 2019 from the Vodorazdelnoye occurrence by NIP SKGMI LLC (GTU) “Stroykomplekt-Innovations,” and conducted in the Rostec laboratory using atomic absorption methods (in flame and emission) in plasma, reveals that the impurities in the samples can be readily removed. Moreover, the quartz resources adhere to GOST 41-07-014–86 standards (Table 1).

In order to evaluate the suitability of quartz rocks within the territory of North Ossetia and identify research sites with significant resource potential, a preliminary analysis of available materials was conducted. The selection of these sites adhered to specific criteria:

- the examined rocks should exhibit homogeneity and be situated in favorable geographic and economic conditions, minimizing material costs for infrastructure preparation and road network development [13, 14];

- potential projects should possess necessary reserves and offer mining and technical conditions conducive to mechanized open-pit mining [15, 16].

Based on these criteria, four areas emerged as the most promising: Naro-Mamison, Fiagdon, Dzhimara, and Fiagdon-Kambileyevka. The research focus spans the central, predominantly eastern part of Mountainous Ossetia, specifically within the interfluvium of the Ardon–Kambileyevka Rivers situated in the Alagir District of North Ossetia.

The study area is delineated to the west by the Ardon River valley and to the east by the basin of the Kambileyevka River. The northern border aligns with parallel 43°00', and the southern border corresponds to the latitude of the Zakkadon River source. The selection of the work area in the Central Caucasus region is influenced by its highly dissected topography. Major watercourses include the Terek, Ardon, Fiagdon, Gizeldon, and Kambileyevka Rivers, along with numerous tributaries. The hydrological regime across all watercourses in the area exhibits a distinct seasonal nature.

Within this district, four areas have been designated for prospecting activities: Naro-Mamison, Fiagdon, Dzhimara, and Fiagdon-Kambileyevka. The geographical and economic positioning of these areas varies, reflecting the diverse characteristics of each.

The **Naro-Mamison area** situated in the upper reaches of the Ardon River and its tributaries (Zakkadon, Zrugdon, Vartsedon, and Mamisondon),

Table 1

Impurity element content in quartz from Vodorazdelnoye occurrence

Item No.	Sample No.	Element content, $n \cdot 10^{-4}$ %, ppm														
		B	P	Na	K	Li	Ca	Mg	Fe	Cu	Mn	Ni	Cr	Co	Al	Ti
1	KZh-1	–	–	23	40	10	5	2	5	0.3	10	1.5	0.5	1.5	15	1
2	KZh-2	–	–	23	20	10	7	3	10	0.7	10	2	0.5	2	20	2
3	KZh-3	–	–	35	40	15	10	10	30	1	10	3	1	3	30	6
4	No. 1	0.625	< 0.16	46.07	16.12	1.629	25.6	0.24	0.149	< 0.02	0.055	0.099	< 0.02	< 0.06	10.2	0.134
5	No. 2	0.295	0.2	22.62	5.656	0.68	169.1	2.547	0.521	< 0.02	0.214	0.049	< 0.02	< 0.06	13.24	0.124
Sum		0.92	0.28	149.69	121.78	37.31	216.7	17.79	45.67	2.02	30.27	6.65	2.02	6.56	88.44	9.26
Average		0.46	0.14	29.94	24.36	7.46	43.34	3.56	9.13	0.40	6.05	1.33	0.40	1.31	17.69	1.85



is categorized into three distinct zones: Vartse, Zrug, and Baikom, based on a comprehensive review of materials from geological archive. The Vartse site is positioned 0.4 km south of the Village of Vartse and 2.0 km southwest of the Village of Nar; the Zrug site is located 1.5 km south and southwest of the Village of Nar in the lower reaches of the Zrug gorge; while the Baikom site is confined to the left side of the valley of the Zakkadon River, situated 3 km northeast of the Village of Kesatikau.

Occupying a high-altitude expanse of the Main Caucasian Range, the Naro-Mamison area features a topography characterized by sharply dissected surfaces, slope angles reaching up to 30° in the northern part, and rocky serrated ridges with steep precipitous slopes exceeding 60° in the southern part. Elevations span from 1700 to 3200 m, with a relative difference in heights of 1500 m.

The river network well-branched, with major watercourses including the Mamisondon, Nardon, Zakkadon, and Zrugdon Rivers. Upon merging, the waters of the Mamisondon and Nardon rivers combine to form the Ardon River. The hydrological regime mirrors the area's climatic conditions, exhibiting a winter low-water period (1.5–3.0 m³/s in the Mamisondon and Nardon Rivers) and summer floods (6.0–8.0 m³/s), sourced primarily from glacial melt and rainwater in summer and ground and snow water in winter.

The climate is extremely continental, marked by significant daily temperature fluctuations. Winters are cold, while summers are cool and humid. The climate of broadly N–S and W–E oriented valleys differs from each other. The climate in W–E valleys (Mamisondon, Zakkadon, Nardon) is milder due to minimal impact from strong cold winds of N–S orientation. The average annual temperature is +4.6 °C, with January averaging –5.7 °C, July at +14.7 °C, and annual precipitation totaling 650 mm. In broadly N–S valleys (Zrugdon), frequent strong cold mountain-valley winds contribute to a further decrease in air temperature. The average annual temperature is +3.8 °C, with January averaging –6.4 °C, July at +13.8 °C. The absolute temperature ranges from a maximum of +28 °C to a minimum of –30 °C, and annual precipitation reaches 900 mm.

Exposure is uneven: on the northern slopes it is 40–45%, and on the southern slopes it is 50–65%.

The vegetation comprises flora from alpine and subalpine meadows, providing essential grazing pastures for cattle. Occasional low-growing forests and shrubs dot the northern slopes, while the absence of valuable wood species is notable.

The area boasts diverse wildlife, including auroch, chamois, lynx, wolf, bear, fox, and hare. No protected or conservation areas are present at the work sites.

Economically, the Naro-Mamison area is well-developed, intersected by major highways (Ossetian Military Road and Transcaucasian Highway). Residential villages are accessible by asphalted roads, with work sites linked by dirt roads, bridle paths, and foot trails. The region has been explored for mercury in the past.

The nearest settlement, the Village of Nar, is 1.5–2.0 km from the Vartse and Zrug sites, while the Baikom site is more distant at 17 km. Vladikavkaz and Alagir, with railway stations, are 92 and 52 km away. Power lines do not cross the work sites, but a 110 kW power line passes through the Village of Nar to the Republic of South Ossetia.

Water supply resources are abundant, with numerous outlets of fresh and mineral water. The area has an ample supply of skilled workers in mining professions. Seismicity is recorded at 9 points according to SNIIP-II–81.

The Fiagdon area encompasses the headwaters and upper reaches of the Fiagdon River (Fig. 1). Three distinct sites have been identified through preliminary material generalization: Arsikom, Bugulta, and Vodorazdelny. The first two are located on the right and left sides of the Bugultadon River valley, respectively, while the Vodorazdelny site is confined to the left side of the Dzamarashdon River valley. These river valleys are closely situated, with a spatial separation of no more than 3 km.

Situated in the high-altitude region of the Bokovoy Ridge, the Fiagdon area features a typical high-altitude topography, with elevations ranging from 2000 to 2750 m.

The primary river network consists of the Dzamarashdon and Bugultadon Rivers, which converge to form the Fiagdon River. The elevations of these rivers vary between 1900 and 2500 m, with the watershed elevations ranging from 2500 to 4000 m.

The flow patterns of the rivers and their numerous tributaries are influenced by both topographical features and climatic conditions, including winter low-water and summer floods.

The climate is continental and high-altitude, characterized by cold winters and cool, humid summers. In the valleys, the average annual temperature is +4 °C, with January averaging –7 °C and July reaching +14.5 °C. The absolute minimum temperature is –26 °C, the maximum is +28 °C, and the annual precipitation ranges from 600 to 900 mm.

Distinct vertical climatic zonality is evident, and the vegetation is primarily alpine-meadow. Up to

elevations of 2100–2200 m, shrubs and small woods are present on the western and northern slopes.

The area hosts a diverse range of wildlife. In the alpine highlands, auroch, chamois, and lynx can be found. Below an elevation of 2500 m, the region is inhabited by bear, wolf, hare, badger, and roe deer. The western boundary of the area coincides with the eastern border of the conservation area of the North Ossetian State Reserve.

In economic terms, the Fiagdon area exhibits a lesser degree of development compared to the Naro-Mamison area. The closest settlement is the village of Kharisdzhin, connected to the area by a 12 km long dirt road. The village of Verkhny Fiagdon is situated 4 km north of Kharisdzhin. The distance from the Village of Kharisdzhin to Vladikavkaz and Alagir, where railway stations are located, is 65 km each way, accessible via asphalted roads. A high-voltage power line (110 kW) traverses the area, but it is currently de-energized.

There are no limitations on technical and household water supply resources, and there is an ample number of skilled workers in mining professions in the area.

The seismicity of the area is 9 points.

The **Dzhimara area** encompasses the upper reaches of the Midagrabyndon River. A preliminary review of geological archive materials has led to the

identification of two distinct areas: Midagrabyndon and Shtyrdon (Fig. 2). Positioned on the left and right sides of the Midagrabyndon River valley, respectively, these sites are spatially close, with a mere 1.4 km distance between them.

Similar to the Fiagdon area, the Dzhimara area occupies a high-altitude expanse of the Bokovoy Ridge, featuring sharply dissected topography characteristic of its northern slope. Deep gorges, sharp ridges, steep cliffs (40–60°), significant elevations (2000–3000 m), and relative differences in height (1000–1300 m) pose challenges for geological studies from the surface. The highest elevations in this region include Shaukhokh (4636 m), Donchenta (4318 m), and Khaikalankhokh (4242 m). These peaks are the focal points for three glaciers: Lartsi-tsiti, Midagrabyndon, and Khrustalny.

The main river network in the Dzhimara area is defined by the Midagrabyndon River, a left tributary of the Gizeldon River. Characterized as a typical mountain river, the Midagrabyndon exhibits glacial feeding, an unstable water level, and flow rate, with frequent summer floods, rapids, and steep runoff. The water flow experiences abrupt fluctuations, ranging from winter low water (4–5 L/s) to summer floods and high water (20–25 L/s). During the summer, increased turbidity, carrying a significant amount of suspended matter, is observed due to snow and ice melting and heavy rains.



Fig. 1. Satellite image of the Eastern flank of the Fiagdon area:

1 – Lyadon quartz zone; 2 – Dargshuadon quartz occurrence; 3 – Dzagalym quartz occurrence

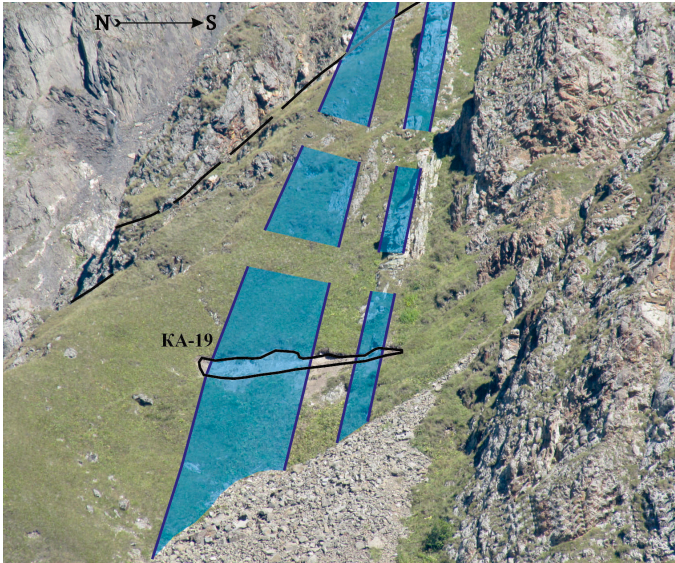


Fig. 2. Midagrabyyn site – silicification zones (KA-19 – ditch)

The climate in the region is distinctly high-altitude, featuring a relatively low average annual temperature (+3.5 °C), high precipitation levels (1000–1100 mm), a not excessively cold winter

(–6.5 °C), prolonged cold spring (+2.4 °C), cool summer (+13.5 °C), and sunny autumn (+4.0 °C). Frosts begin in late September and conclude in mid-May.

Vegetation predominantly consists of alpine-meadow formations within the alpine and subalpine belts, featuring forbs, *Alchemilla caucasica*, *Alchemilla sericea*, *Carum caasicum*, and *rhododendron*. Woody vegetation is limited to single low-growing birch shrubs.

The animal population is diverse, including auroch, chamois, and lynx in the alpine highlands, and bear, wolf, fox, badger, roe deer, and hare in the subalpine belt. There are no designated conservation zones in the Dzhimara area.

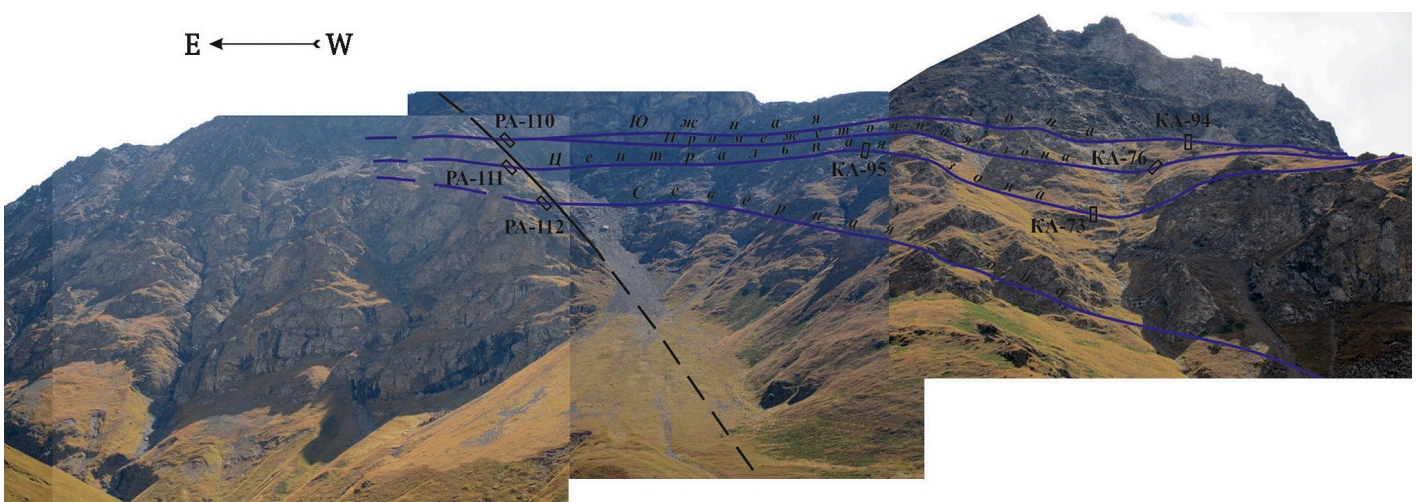


Fig. 3. Fiagdon site – Southern Zone, Intermediate Zone, Central Zone, Northern Zone

Economically, the Dzhimara area is less developed than other regions. The nearest settlement, the Village of Dzhimara, is located 6.5 km away and is connected by a dirt road, bridle paths, and foot trails. The distance from the Village of Dzhimara to the City of Vladikavkaz is 48 km, 45 km of which are asphalted roads. A 6 kW power line services the Village of Dzhimara.

There are no restrictions on technical and household water supply resources in the district, and there is an available workforce of mining professionals in Dzhimara, Fazikau, Dargavs, and other villages.

Seismic activity in the area is recorded at 9 points.

The **Fiagdon-Kambileyevka area** is situated between the valleys of the Fiagdon River to the west and the Kambileyevka River to the east, encompassing their middle course. A review of archive materials has led to the identification of six distinct sites: Fiagdon (Fig. 3), Mygvare-Barzond, and Kodakhdzhin in the western part of the area, within the Fiagdon River valley, and Tatarsky II, Medvezhegaysky, and Kambileyevka in the eastern part, within the Kambileyevka River valley. Spatially, the western three sites are located 25–30 km away from the eastern ones.

This area is situated in the low-altitude zone of Mountainous Ossetia, on the southern slope of the Lesisty Ridge.

The topography is characterized by typically low-altitude features, with gentle slopes (up to 30°), smooth peaks, and a landscape dissected by transverse river valleys. Elevations in this region range from 1000 to 1300 m, and the surface of all sites is covered with forests.

The river network is defined by the Fiagdon and Kambileyevka Rivers along with their tributaries. The river flow regime is influenced by climatic conditions, resulting in winter low-water levels and summer floods.



The snow cover in this area is unstable, lasting from December to February. Winds are periodic, originating from the north and northeast in winter and from the south and southwest in summer. The geographical conditions do not favor the formation of avalanches, mudflows, and landslides.

Vegetation is characterized by broad-leaved formations, including beech, hornbeam, maple, ash, linden, and oak. The soils are mountainous, brown forest, and relatively thin (up to 20 cm), with no agricultural value. Various plants such as wild pear, apple-tree, alycha, raspberry, dogwood, hazel, and blackberry are found throughout the area.

The animal population is diverse, featuring brown bear, forest cat, lynx, dormouse, marten, red deer, bison, among others. Birds such as siskin, bullfinch, woodpecker, etc., contribute to the rich biodiversity.

In economic terms, the area is reasonably well-developed. The distance from the western sites to the Villages of Mayramadag, Kodakhdzhin, Dzuarikau ranges from 3 to 5 km, while from the eastern sites to the Village of Tarskoye, it is between 1.0 and 3.2 km. The nearest railroad station (Vladikavkaz) is located 20 and 16 km away, respectively. Although there is no power line at the work sites, the nearby villages receive sufficient electricity.

The seismicity of the area is recorded at 8 points.

Statement of the problem

The primary objectives of the research are to identify sites with high-quality quartz resources suitable for silicon production, localize these sites, estimate forecast resources, and designate areas for further in-depth study. The chosen sites should possess favorable geographical and economic conditions, conducive to open-pit mining [17].

To achieve these goals, the research will involve addressing the following tasks:

- prospective areas for research to uncover high-quality quartz resources;
- conduct comprehensive research activities, including geological traverses, examination of previously drilled boreholes, and laboratory and laboratory-technological sampling;
- investigate morphostructural features and the internal structure of productive deposits;
- localize, evaluate, and test the forecast resources of high-quality quartz raw materials [18, 19];
- develop recommendations for exploration and licensing of identified prospects [20, 21].

In the initial stage of the research, materials from quartz rock development sites will be collected and synthesized, along with information on silicon

production methods and the regulatory requirements for raw materials.

Subsequently, the comprehensive study of the most promising sites will progress, incorporating studies that provide reliable, objective information on the mineralogical, chemical-spectral, and petrochemical composition of quartz rocks in these areas. Laboratory-analytical and mineralogical data will inform the calculation of process parameters for different types of quartz resources. Technological samples will be extracted from the quartz rock sites meeting theoretical regulatory requirements, forming the basis for classifying these rocks as suitable raw materials for silicon production. Simultaneously, the selection of sites with the most favorable mining and geographical-economic conditions will be made. Prospects will be used to calculate forecast resources and develop recommendations for further research and site preparation for licensing for subsoil use.

The complex set of methods employed to address these tasks includes prospecting traverses at a scale of 1:10,000, geological traverses for compiling reference lithological-structural sections at a scale of 1:500, sampling and sample processing, mineralogical and petrographic studies, laboratory-analytical assessments, process tests, and field data analysis.

Materials and methods

The laboratory and process studies of quartz sands involved several key parameters, including determining the particle-size distribution of the product fraction ($-0.25 + 0.1$ mm), assessing the light transmission coefficient (K_{lt}) of grains, analyzing the chemical composition (SiO_2 and impurity element content), and conducting mineralogical and petrographic analysis of the non-magnetic fraction.

The silicon dioxide content in the natural sand was found to be relatively low and did not fully comply with the requirements of GOST 2169–69 for quartz resources intended for the production of metallurgical (crystalline) silicon.

To gain insights into the material constitution and morphological features of impurity minerals, along with their quantitative interrelations influencing the process properties of the considered vein quartz, a semi-quantitative optical and mineralogical analysis was conducted. This analysis included the examination of electromagnetic, magnetic, heavy (2.67 g/cm^3), and light (2.63 g/cm^3) monofractions.

Data preparation and preliminary processing, such as regression plots in a two-dimensional configuration, were performed using MS Excel. Subsequent processing of experimental data involved the application of the simple b-spline method, similar

to previous studies [1*, 5*], implemented as scripts in the ViIMproved software (version 9.0) in the Python language. The construction of final three-dimensional plots was carried out using the gnuplot software.

Research results

Throughout the research, sites containing quartz rock suitable as raw materials for the production of solar-grade silicon products were identified. These selected sites fulfill essential criteria: they are situated in regions with favorable geographical and economic conditions, allowing for open-pit mining.

The investigation successfully identified high-tech raw materials conducive to a cost-effective approach for large-scale production of solar-grade (SG) silicon. The comprehensive set of studies resulted in the localization and estimation of forecast resources, accompanied by the formulation of recommendations for further exploration and development of these prospects.

Given the novelty of the problem and the absence of widely accepted requirements and methodological approaches, this type of work involves dealing with numerous specific factors.

The study areas were previously subjected to works primarily focused on identifying ore projects, with some attention given to construction materials, raw materials for basalt fiber production, alkaline bentonite clays for drilling fluids, among others.

However, these previous studies proved to be of limited information in addressing the objectives of the current research. Early reports on the aforementioned works, which had different primary goals, often lacked substantial information on quartz rocks and quartz raw materials. The Fiagdon-Kambileyevka area stands out as an exception, with in-depth studies conducted on sands intended for applications in silicate bricks, the glass industry, glass wool, and molding mixtures.

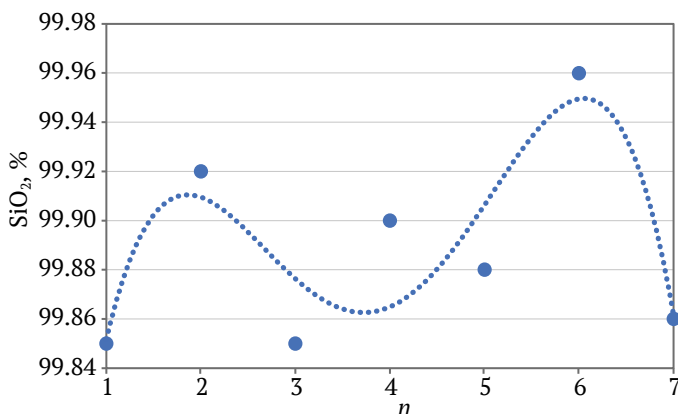


Fig. 4. Graphical representation of silica content variation based on occurrence type

During the conducted works, areas featuring quartz veining and silicification zones containing ore mineralization were documented. The primary focus was on studying the material constitution and interrelations of ore minerals and associated elements. This involved examining the internal structure, crystallization stages, the extent of alteration due to superimposed processes, volumetric characteristics related to the presence of rocks with different compositions, and the composition and parameters of quartz rocks (mineral resources)

Results and discussion

The relationship between the change in silica content (SiO₂) and the type of occurrence has been determined through the established polynomial equation (R² = 0.72, Fig. 4):

$$SiO_2 = -0.0034n^4 + 0.0529n^3 - 0.2775n^2 + 0.5712n + 99.509, \tag{1}$$

where SiO₂ is the silica content, %, and n is the occurrence number (1 – Arsikom; 2 – Lyadon I; 3 – Dzagalykom; 4 – Dargsuadon; 5 – Vartse; 6 – Baikom; 7 – Lyadon).

The evaluation of the qualitative characteristics of quartz rocks and their concentrates as raw materials for silicon product production has revealed the following findings:

1) quartz rocks of different genetic affiliations exhibit heterogeneity in chemical composition, particularly in SiO₂ content, dividing into two groups: – those with low SiO₂ content (≤ 98.2%) including quartz sands, quartzite-like sandstones, and quartz gravelstone);

– those with high SiO₂ content (> 98.2%) encompass vein milky-white coarse-grained quartz;

2) sedimentary (quartz sands) and sedimentary-metamorphic (quartzite-like sandstones and quartz gravelstone) rocks and concentrates derived from them are deemed non-processable and unsuitable as raw materials for producing high-purity quartz concentrates required for the production of “solar grade” silicon products;

3) vein milky-white coarse-grained quartz from the majority of occurrences in the Fiagdon and Naro-Mamison areas, in its natural form, meets the chemical composition requirements of GOST 2169–69 for quartz resources suitable for the production of metallurgical (crystalline) silicon.

Subsequently, the relationship between the change in light transmission and the type of occurrence was established with the following polynomial equation (R² = 0.73; Fig. 5):

$$K_t = 0.1993n^4 - 3.5249n^3 + 21.666n^2 - 53.562n + 49.121, \tag{2}$$

where K_{lt} is the light transmission value, %, and n is the occurrence number.

The identified extremely low value of light transmission ($K_{lt} = 31.1\%$) in vein quartz concentrates completely rules out their use as fusion raw material for manufacturing quartz crucibles.

In the final phase of the study, chemical composition parameters of impurities were obtained, summarized in Table 2.

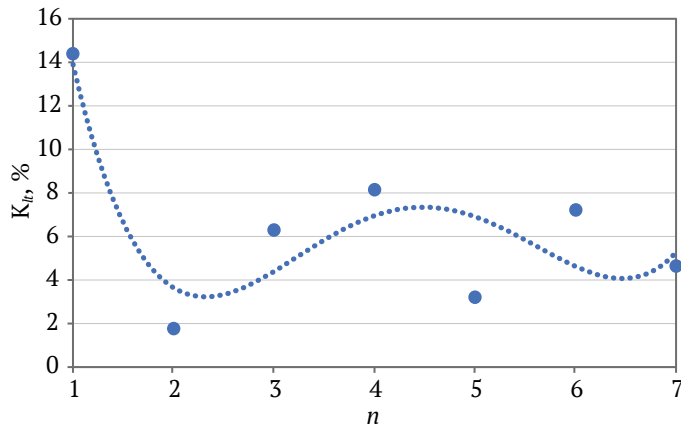


Fig. 5. Graphical representation of light transmission variation based on occurrence type

Elevated concentrations of Ti (45–65 ppm) and other elements such as Al, Ca, Mg, Na, K, Cu, Mn, and Fe in the concentrates indicate their unsuitability for the production of refined products intended for fusing on quartz glasses for various applications.

The mineralogical and petrographic analysis of the non-magnetic fraction revealed that quartz in sands consists of different generations, including water-transparent grains with a clean smooth surface and full transparency in reflected light. The bulk of the sand comprises 25.4–69.4% water-transparent grains.

“Quartzites” (quartzite-like sandstones) and quartz gravelstone from the Nazitkom, Lartsikom I and II, Skalny, Vodopadny, and Shtyrdon sites share the characteristic of containing significant amounts of feldspars (2.0–35.0%, occasionally up to 57%). They exhibit low quartz content (32.0–92.0%), a light transmission coefficient (K_{lt}) of 5.9–8.0%, and high values of impurity elements (IEs) such as Al, Ca, Mg, Na, K, Fe, and Ti.

The vein milky-white coarse-grained quartz within the Fiagdon and Naro-Mamison areas underwent the same sequential analysis as quartzite-like sandstones and gravelstone. After sample preparation, parameters such as chemical composition (SiO_2 and IE

Table 2

Summarized weighted average content of impurity elements in vein quartz concentrates from the Fiagdon and Naro-Mamison areas, ppm

Name of elements	n	Arsikom	Lyadon I	Dzagalykom	Dargshuadon	Vartse	Baikom	Lyadon
		1	2	3	4	5	6	7
High concentration								
IE	1	71.69	69.88	68.53	60.64	60.31	44.53	40.02
Al	2	47.7	46.3	33.93	25.47	38	34.29	21.36
Na	3	15.6	19.8	25.67	20.49	17	11.4	14.53
K	4	2.17	0.72	2.03	5.87	1	1.8	0.97
Ca	5	2.74	1.3	3.63	4.92	1.8	1.26	1.53
Low concentration								
Li	6	2.23	0.65	1	0.82	0.51	0.83	0.64
Fe	7	0.4	0.6	0.7	0.7	0.8	0.6	0.4
B	8	0.36	0.25	0.28	0.45	0.42	0.24	0.33
Ti	9	0.38	0.36	0.4	0.39	0.35	0.2	0.31
Mg	10	0.21	0.28	0.39	0.21	0.24	0.71	0.84
Mn	11	0.09	0.06	0.04	0.13	0.07	0.05	0.2
Cr	12	0.02	0.06	0.15	0.1	0.08	0.09	0.02
P	13	0.02	0.04	0.23	0.02	0.02	0.02	0.02
Cu	14	0.03	0.01	0.01	0.01	0.01	0.01	0.03
Ni	15	0.01	0.01	0.01	0.01	0.03	0.01	0.01
Co	16	0.01	0.01	0.01	0.01	0.01	0.01	0.01
Zr	17	0.01	0.01	0.01	0.01	0.01	0.005	0.01

oxide content), mineral composition, quantities of IEs in natural quartz, and processing middlings were determined, and mineralogical and petrographic analyses were conducted.

The analysis of Fig. 6 reveals the following: a) most vein quartz samples are most effectively processed for elements such as Ti, Ca, Mn, Cu, Mg, K, and Fe; less effectively for Al, Na, Li, B, and P; b) above-limit contents of Al, Na, K, and, less frequently, Ca and Fe relative to the KGO-3 grade in vein quartz concentrates exclude their application for producing quartz crucibles using the traditional “Siemens-process” for growing monocrystalline silicon; c) quartz concentrates from vein quartz of the Lyadon Zone, Arsikom, Dargshudon, Dzagalykom, Vartse, Lyadon I, and Baikom occurrences, with the total content of impurity elements (IE) ≤ 100 ppm and low Ti, B, and P contents, are potentially suitable for the production of “solar grade” silicon products. Minor deviations in their chemical compositions relative to regulated IEs (Ti, B, and P) may require slight process modifications.

Investigations of vein quartz from these areas have shown that most unprocessed samples meet the requirements of GOST 2169–69 ($\text{SiO}_2 \geq 98.2\%$, $\text{Fe}_2\text{O}_3 \leq 0.25\%$, $\text{CaO} \leq 0.25\%$, $\text{Al}_2\text{O}_3 \leq 0.6\%$) and are suitable for obtaining metallurgical (crystalline) silicon. Samples with increased calcite content (10.0–24.0%) taken at the Vodorazdelny Shtok and Bugultinsky sites are an exception.

The elevated calcite content in the veins of these sites is believed to be associated with the chemical composition of hosting rocks (diabase,

diabase porphyrites), influencing the composition of hydrothermal solutions that formed the vein bodies.

The data obtained indicate that vein quartz samples sometimes contain calcite, feldspars, sericite, and chlorite. Ore minerals such as pyrite and arsenopyrite are rarely present, and epidote, amphibole, and sillimanite group minerals are found in single samples.

Quartz in the samples is represented by transparent and milky-white grains, mostly isometric, occasionally elongated, with rare inclusions of hematite, magnetite, and muscovite.

Quartz grains may exhibit different structures, with some having smooth transparent flat faces, and others showing a wavy-ribbed structure and a greenish-gray color. Electron microscopy of the surface revealed the presence of Al (2.8%), K (1.48%), and Fe (0.42%) in addition to silicon and oxygen.

In summary, the studied vein quartz and concentrates are generally unsuitable for growing single-crystal silicon using the “Siemens-process” according to traditional technology. The above-limit content of alkali metals in the concentrates negatively impacts the thermal stability of crucibles, as alkalis act as flux, reducing the melting temperature of quartz glass products.

These quartz concentrates are considered promising for the production of silicon products, particularly for direct production of “solar grade” silicon products, without the process and environmental complications associated with the traditionally used “Siemens process”.

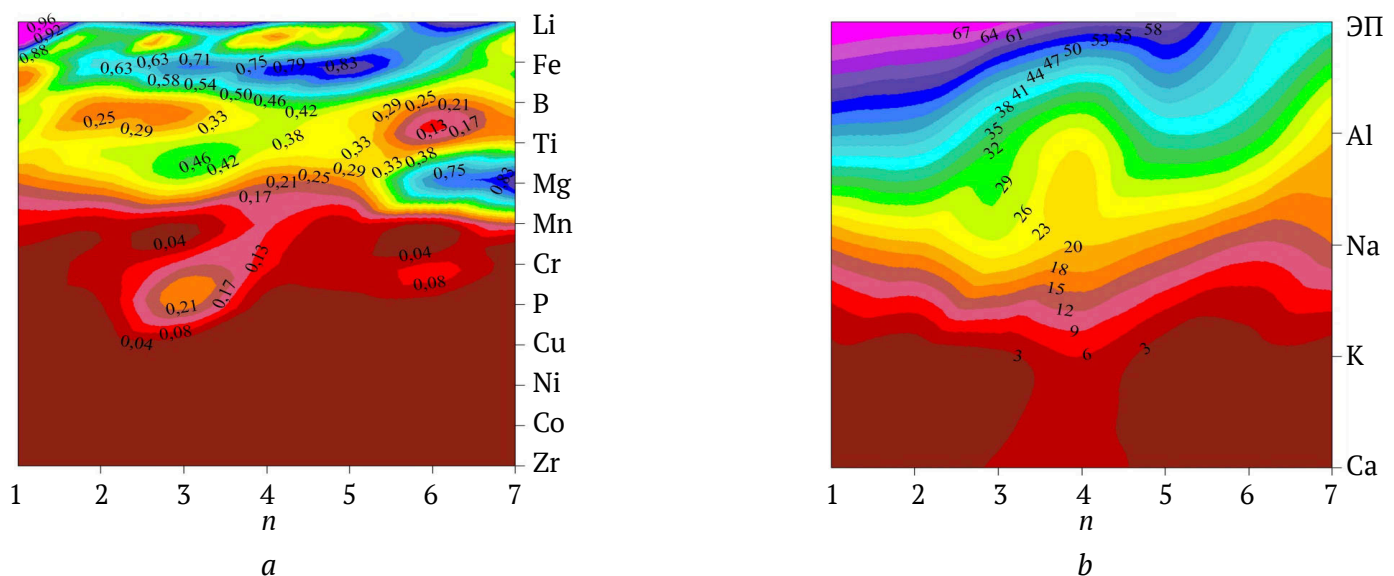


Fig. 6. Distribution of chemical elements concentration in impurities for occurrences of the Fiagdon and Naro-Mamison areas:

a – for elements of the “high concentration” group; *b* – for elements of the “low concentration” group



Conclusion

Following the completion of the planned research tasks and objectives, the following results have been achieved for the studied object:

- an analysis of materials, along with the generalization of statistical, economic, geological, and process information, necessary for addressing the primary research tasks, has been conducted;
- prospects for further research have been identified;
- geological maps of prospects, at a scale of 1:10,000, with legends and corresponding sections, have been specified;
- the conditions of occurrence, morphology, and parameters of productive deposits at the prospects have been determined;

– preliminary studies on the quality and process characteristics of quartz resources have been conducted;

- the forecast resources of high-quality quartz raw materials for the production of silicon products, falling under category P₂ (500 Kt), have been localized, estimated, and tested;
- recommendations for geological exploration and licensing have been developed;
- objects for licensing for subsoil use have been prepared.

These results have been obtained through a comprehensive approach involving laboratory work, sampling, the study of constructed sections, examination of mine workings and borehole documentation, as well as mineralogical and petrographic analyses, along with laboratory studies and process tests.

References

1. Fedorov A.M., Makrygina V.A., Nepomnyashchikh A.I., Eliseev I.A. Quartz resource potential of Eastern Siberia for high-purity quartz production. *Geografia i Prirodnye Resursy*. 2016;(6):55–59. (In Russ.) [https://doi.org/10.21782/GIPR0206-1619-2016-6\(55-59\)](https://doi.org/10.21782/GIPR0206-1619-2016-6(55-59))
2. Galiakhmetova L.Kh., Bydtaeva N.G., Nepryakhin A.E. Prospects of the Malo-Chipiketsky quartz-bearing zone for quartz raw materials of high quality. *Georesursy*. 2019;21(3):99–106. <https://doi.org/10.18599/grs.2019.3.99-106>
3. Nikolaev A.A., Kirpichyov D.E., Nikolaev A.V. Influence of material charging into plasma-arc furnace bath on energy parameters of reduction melting of quartz-leucoxene concentrate. *Fizika i Khimiya Obrabotki Materialov*. 2020;(1):36–41. (In Russ.) <https://doi.org/10.30791/0015-3214-2020-1-36-41>
4. Kaibichev A.V., Kaibichev I.A. Refining of technical silicon melts in the electrical field in helium. *Rasplavy*. 2019;(4):390–395. (In Russ.) <https://doi.org/10.1134/S0235010619040066>
5. Polenov Y.A., Ogorodnikov V.N., Kisin A.Y. History of prospecting and development of deposits of quartz raw materials in the Urals and the prospect of their further use. *News of the Ural State Mining University*. 2021;(2):48–59. (In Russ.) <https://doi.org/10.21440/2307-2091-2021-2-48-59>
6. Loginov V.G., Rudakov R.B., Koroteev N.D. Creating high-tech productions as a factor of raw material security (“Polar quartz” project). *News of the Ural State Mining University*. 2017;(1):84–87. (In Russ.) <https://doi.org/10.21440/2307-2091-2017-1-84-87>
7. Korekina M.A., Lyutoev V.P., Shanina S.N., Shtenberg M.V. Microelement composition of vein quartz of the Kuznechikhinskoe deposit (South Urals). *Obogashchenie Rud*. 2020;(5):23–29. (In Russ.) <https://doi.org/10.17580/or.2020.05.04>
8. Ogorodnikov V.N., Polenov Y.A., Savichev A.N. Extra pure quartz of the Ufaleysky quartziferous district (Southern Urals). *News of the Ural State Mining University*. 2018;(1):23–32. (In Russ.) <https://doi.org/10.21440/2307-2091-2018-1-23-32>
9. Klyuev R.V., Yegorova E.V., Bosikov I.I., Tsidaev B.S. Evaluation of use of effective technologies for increasing sustainable development of natural and technical system of oil and gas complex. *Sustainable Development of Mountain Territories*. 2018;10(3):392–403. <https://doi.org/10.21177/1998-4502-2018-10-3-392-403>
10. Bosikov I.I., Klyuev R.V. Assessment of Berezkinskoye ore field prospectivity using Micromine software. *Mining Science and Technology (Russia)*. 2022;7(3):192–202. <https://doi.org/10.17073/2500-0632-2022-3-192-202>
11. Golik V., Komashchenko V., Morkun V., Burdzieva O. Metal deposits combined development experience *Metallurgical and Mining Industry*. 2015;7(6):591–594.
12. Bosikov I.I., Klyuev R.V., Khetagurov V.N., Silaev I.V. Comprehensive assessment of hydrodynamic processes in the Klinskoye Quarry with the use of their control methods in rock masses. *Sustainable Development of Mountain Territories*. 2023;15(2):284–297. (In Russ.) <https://doi.org/10.21177/1998-4502-2023-15-2-284-297>



13. Tyulenev M.A., Markov S.O., Gasanov M.A., Zhironkin S.A. numerical modeling in the structural study of technogenic rock array. *Geotechnical and Geological Engineering*. 2018;36(5):2789–2797. <https://doi.org/10.1007/s10706-018-0501-3>
14. Rybak Y., Khayrutdinov M.M., Kongar-Syuryun Ch.B., Tyulyayeva Y.S. Resource-saving technologies for development of mineral deposits. *Sustainable Development of Mountain Territories*. 2021;13(3):405–415. (In Russ.) <https://doi.org/10.21177/1998-4502-2021-13-3-406-415>
15. Golik V.I., Gashimova Z.A., Liskova M.Yu., Kongar-Syuryun Ch.B. To the problem of minimizing the volume of mobile dust in the development of pits. *Occupational Safety in Industry*. 2021;(11):28–33. (In Russ.) <https://doi.org/10.24000/0409-2961-2021-11-28-33>
16. Kulikova E. Yu., Balovtsev S.V., Skopintseva O.V. Complex estimation of geotechnical risks in mine and underground construction. *Sustainable Development of Mountain Territories*. 2023;15(1):7–16. (In Russ.) <https://doi.org/10.21177/1998-4502-2023-15-1-7-16>
17. Khalkechev K.V., Khalkechev R.K., Levkin Yu.M. Mathematical model of the stress field in the pillars with due account taken of the main crack in coal fields. *Ugol'*. 2023;(7):56–58. (In Russ.) <https://doi.org/10.18796/0041-5790-2023-7-56-58>
18. Knutsson H., Knutsson K., Molin F., Zetterlund P. From flint to quartz: Organization of lithic technology in relation to raw material availability during the pioneer process of Scandinavia. *Quaternary International*. 2016;424:32–57. <https://doi.org/10.1016/j.quaint.2015.10.062>
19. Guan Q., Dong D., Zhang H., et al. Types of biogenic quartz and its coupling storage mechanism in organic-rich shales: A case study of the Upper Ordovician Wufeng Formation to Lower Silurian Longmaxi Formation in the Sichuan Basin, SW China. *Petroleum Exploration and Development*. 2021;48:813–823. [https://doi.org/10.1016/S1876-3804\(21\)60068-X](https://doi.org/10.1016/S1876-3804(21)60068-X)
20. Brand N.W., Bottrell S.H., Miller M.F. Concentrations of reduced Sulphur in inclusion fluids associated with black shale hosted quartz vein gold deposits: implications for mechanisms of transport and deposition of gold and a possible exploration tool. *Applied Geochemistry*. 1989;4:813–823. [https://doi.org/10.1016/0883-2927\(89\)90006-1](https://doi.org/10.1016/0883-2927(89)90006-1)
21. Sebutsoe T.C., Musingwini C. Characterizing a mining production system for decision-making purposes in a platinum mine. *The Journal of the Southern African Institute of Mining and Metallurgy*. 2017;117:199–206.

Information about the authors

Igor I. Bosikov – Cand. Sci. (Eng.), Assistant Professor, Head of the Department, North Caucasian Institute of Mining and Metallurgy (State Technological University), Vladikavkaz, Russian Federation; ORCID [0000-0001-8930-4112](https://orcid.org/0000-0001-8930-4112), Scopus ID [56919738300](https://scopus.org/56919738300); e-mail igor.boss.777@mail.ru

Roman V. Klyuev – Dr. Sci. (Eng.), Assistant Professor, Professor of the Department of Engineering and Technology of Mining and Oil and Gas Production, Moscow Polytechnic University, Moscow, Russian Federation; ORCID [0000-0003-3777-7203](https://orcid.org/0000-0003-3777-7203), Scopus ID [57194206632](https://scopus.org/57194206632); e-mail kluev-roman@rambler.ru

Vladimir Ch. Revazov – Cand. Sci. (Pedagogy), Assistant Professor the Department of Philosophy and Social and Humanitarian Technologies, North Caucasian Institute of Mining and Metallurgy (State Technological University), Vladikavkaz, Russian Federation; ORCID [0000-0003-1784-6531](https://orcid.org/0000-0003-1784-6531), Scopus ID [57201777428](https://scopus.org/57201777428); e-mail revazov.v@yandex.ru

Nikita V. Martjushev – Cand. Sci. (Eng.), Senior Researcher, Kh. Ibragimov Complex Institute of the Russian Academy of Sciences, Grozny, Russian Federation; ORCID [0000-0003-0620-9561](https://orcid.org/0000-0003-0620-9561), Scopus ID [36671592800](https://scopus.org/36671592800), ResearcherID [AAO-2653-2020](https://orcid.org/AAO-2653-2020); e-mail martjushev@tpu.ru

Received 22.10.2023

Revised 30.10.2023

Accepted 01.11.2023



MINING ROCK PROPERTIES. ROCK MECHANICS AND GEOPHYSICS

Research paper

<https://doi.org/10.17073/2500-0632-2023-09-150>

УДК 624.121



Physical simulation aspects of structural changes in rock samples under thermobaric conditions at great depths

M. D. Ilyinov , D. N. Petrov   , D. A. Karmanskiy  , A. A. Selikhov 

St. Petersburg Mining University, St. Petersburg, Russian Federation

 petrovgs@mail.ru

Abstract

When designing the parameters for the development of oil and gas field at significant depths, crucial to comprehend how certain factors affect the behavior of reservoir rocks and host rocks. These factors include the high level of rock stress, the ambient temperature field, and the hydro- and gas-dynamic processes within the mass. The impact of one or a combination of these factors can result in alterations to the construction, structure, composition, and properties of the rock mass and, ultimately leading to a mismatch between the design solutions and the actual conditions.

The purpose of the research is to establish a methodology for conducting laboratory studies that investigate the impact of the mode of occurrence of oil and gas field reservoirs at great depths on the properties of rock samples.

The research objectives encompass a theoretical analysis and the identification of the principal factors influencing rock behavior and changes in internal structure. Additionally, the objectives include developing laboratory research methods that comprehensively simulate these factors and conducting trial experiments to assess their effects.

As part of the project, tests were conducted on sandstone samples collected from depth ranging from 3.5 to 4 km within the hydrocarbon field. These studies were performed while simulating thermobaric reservoir conditions, which include temperature, rock pressure, and reservoir pressure.

The results of these experiments, aimed at examining the behavior of rock samples as closely as possible to their natural reservoir occurrence at depth of 3.5–4 km, are presented.

It has been observed that rock samples of the same lithology, collected from nearly identical depths, can exhibit significant differences in deformation characteristics, both in the pre- and off-limit regions of loading. The findings from these studies provide the initial data for the development and refinement of geomechanical model behavior for materials that take into account not only fracture strength criteria but also dilatancy processes at various stages of rock deformation.

Increasing lateral pressure within the range of 0 to 55 MPa causes relatively minor change in ultrasonic vibration velocities, typically ranging from 1 to 10%. This makes it challenging to determine the necessity of utilizing these results for indirectly assessing changes in rock properties within the mass. Nevertheless, within the context of geophysical studies, considering variations in velocity values enhances the quality of result interpretation, especially given the substantial geometric dimensions of the rock masses under investigation.

Research into the acoustic emissions of rocks in a complex stressed state enables the monitoring of spatial micro- and macrofracturing processes throughout the entire loading phase of samples. This provides a more comprehensive understanding of changes in their internal structure.

The article delves into the factors that impact structural changes in oil and gas field rocks, particularly as their development extends to greater depths. The study outlines methodological approaches that facilitate the investigation of physical and mechanical properties of rock samples, while accurately modeling complex thermobaric conditions. Additionally, it describes the technical specifications of the testing equipment, ensuring the closest possible replication of the actual conditions of reservoir rock occurrences. Lastly, the study reveals key features related to the deformation and fracture of rock samples during testing under lateral pressures of 55 MPa and pore pressures of 30 MPa, along with the creation of temperature fields up to 100 °C.

Keywords

rock, sample, stress, pore pressure, temperature, structure, acoustic emission, field, structural changes

For citation

Ilyinov M. D., Petrov D. N., Karmanskiy D. A., Selikhov A. A. Physical simulation aspects of structural changes in rock samples under thermobaric conditions at great depths. *Mining Science and Technology (Russia)*. 2023;8(4):290–302. <https://doi.org/10.17073/2500-0632-2023-09-150>



СВОЙСТВА ГОРНЫХ ПОРОД. ГЕОМЕХАНИКА И ГЕОФИЗИКА

Научная статья

Аспекты физического моделирования процессов структурных изменений образцов горных пород при термобарических условиях больших глубинМ. Д. Ильинов , Д. Н. Петров   , Д. А. Карманский  , А. А. Селихов *Санкт-Петербургский горный университет, г. Санкт-Петербург, Российская Федерация* petrovgs@mail.ru**Аннотация**

При проектировании параметров разработки нефтяных и газовых месторождений на больших глубинах необходимо иметь представление о влиянии на поведение пород-коллекторов и вмещающих их пород таких факторов, как высокий уровень напряженного состояния пород, температурное поле окружающей среды, гидро- и газодинамические процессы в массиве. Воздействие как одного, так и комбинации данных факторов могут привести к изменениям в строении, структуре, составе и свойствах породного массива и, как следствие, несоответствию реальным условиям принятых проектных решений.

Целью исследований является разработка методики лабораторных исследований влияния условий залегания коллекторов нефтяных и газовых месторождений на больших глубинах при изучении свойств образцов горных пород.

Задачи исследования: теоретический анализ и выявление основных факторов, влияющих на поведение и изменение внутренней структуры пород, разработка методики лабораторных исследований с комплексным моделированием данных факторов и проведение пробных экспериментов по оценке их влияния.

В рамках работы были выполнены испытания образцов песчаников, отобранных с глубин от 3,5 до 4 км месторождения углеводородов. Исследования проводились с моделированием термобарических пластовых условий залегания: температуры, горного и пластового давлений.

Представлены результаты экспериментов по исследованию поведения образцов горных пород с максимальным приближением к естественным условиям залегания пород коллекторов 3,5–4 км.

Установлено, что образцы пород одной литологической разности и отобранные практически с одинаковых глубин могут иметь существенные отличия в характере деформирования как в до-, так и запретельной области нагружения.

Результаты данных исследований служат исходными данными при разработке и уточнении геомеханических моделей поведения материалов, которые учитывают не только прочностные критерии разрушения, но и дилатансионные процессы на различных этапах деформирования пород.

Увеличение бокового давления в интервалах от 0 до 55 МПа приводит к относительно незначительному изменению скоростей ультразвуковых колебаний (от 1 до 10 %), что не позволяет судить о необходимости использования данных результатов при косвенной оценке изменения свойств горных пород в массиве. Однако в рамках геофизических исследований учет изменения численных значений скоростей позволит повысить качество интерпретации результатов, что связано с большими геометрическими размерами изучаемых массивов.

Исследования акустической эмиссии пород в сложнонапряженном состоянии позволяют отслеживать процессы пространственного образования и развития микро- и макротрещиноватости на всей стадии нагружения образцов и дают более полное представление об изменении их внутренней структуры.

В статье рассмотрены факторы, влияющие на процессы структурного изменения горных пород нефтяных и газовых месторождений, связанных с увеличением глубины их разработки. Разработаны методические подходы, позволяющие производить исследования физико-механических свойств образцов горных пород с моделированием сложных термобарических условий. Описаны технические характеристики испытательного оборудования, обеспечивающие максимальное воспроизведение реальных условий залегания пород-коллекторов. Выявлены особенности деформирования и разрушения образцов горных пород при их испытаниях в условиях бокового давления 55 МПа, порового 30 МПа с созданием температурного поля до 100 °С.

Ключевые слова

горная порода, образец, напряжение, поровое давление, температура, структура, акустическая эмиссия, месторождение, структурные изменения

Для цитирования

Ilyinov M. D., Petrov D. N., Karmanskiy D. A., Selikhov A. A. Physical simulation aspects of structural changes in rock samples under thermobaric conditions at great depths. *Mining Science and Technology (Russia)*. 2023;8(4):290–302. <https://doi.org/10.17073/2500-0632-2023-09-150>

Introduction

When designing the parameters for the development of oil and gas fields at significant depths, it's essential to understand the impact on the behavior of both reservoir and host rocks. These factors encompass a high level of rock stress, the ambient temperature field, and hydro- and gas-dynamic processes within the mass [1–3]. The influence of any single factor or a combination of these can lead to alterations in the construction, structure, composition and properties of the rock mass [4–6] and, ultimately resulting in a divergence from the design solutions intended for the actual conditions.

Currently, there are two prominent and contrasting theories regarding the origins of hydrocarbons: biogenic (organic) and abiogenic (inorganic) [7–9].

According to the biogenic (organic) theory, the formation of hydrocarbon fields involves several key stages. Initially, a layer of organic residues (oil source rocks) develops at the bottom of a water body. Subsequently, due to the Earth's crust movement

and sedimentation, there's a gradual subsidence of this layer to greater depths, leading to increased temperature and pressure. This, in turn, results in the creation of bitumoids (diffusion-dispersed oil) from organic matter. Over time, under the influence of gravity and tectonic forces, oil migrates from the source rocks through the reservoir rocks to the areas where fields form (Fig. 1) [10].

The most common types of reservoirs where oil accumulates are vaulted and tectonically shielded anticlinal traps [11, 12]. Vaulted traps form due to the combined horizontal and vertical deformation of strata without breaks (Fig. 2, *a*). Tectonically shielded traps develop when discontinuities such as downthrows, upcasts, or overthrusts occur, leading to impermeable formations overlapping the reservoir along the tectonic fault line due to formation displacement (Fig. 2, *b*).

The theory of abiogenic origin suggests that hydrocarbons form in mantle sources through inorganic synthesis at great depths, involving colossal pressures and high temperatures, using inorganic

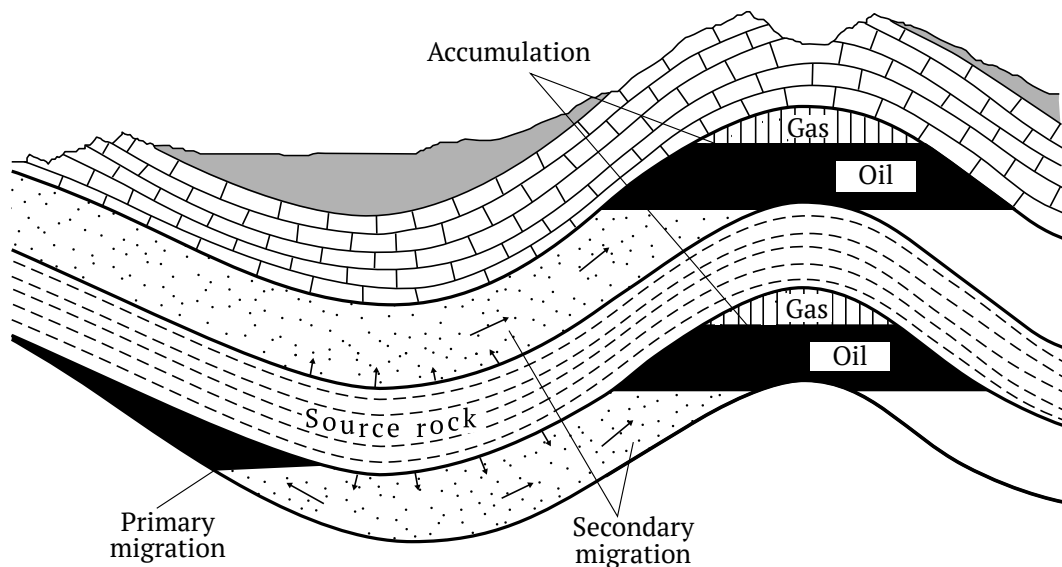


Fig. 1. Basic diagram of formation of oil deposits according to the biogenic theory [10]

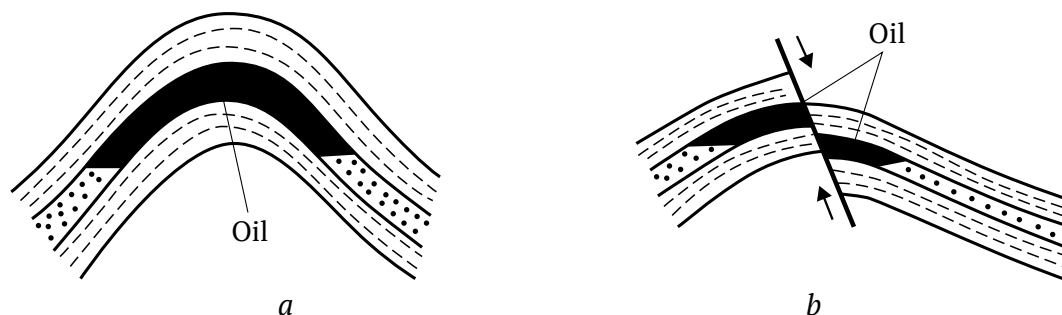


Fig. 2. Diagrams of formation of oil deposits: *a* – vaulted trap; *b* – tectonically shielded trap

carbon and hydrogen. According to this concept, these hydrocarbons are generated deep within the Earth's mantle and subsequently migrate along deep faults into the Earth's crust, accumulating in hydrocarbon fields [13–15].

If we set aside the fundamental differences in the genesis of hydrocarbon formation and focus solely on evaluating thermobaric and filtration processes, we can observe their qualitative similarity in both theories. In both cases, the formation of hydrocarbons and their migration through rocks occur under conditions of elevated rock pressure and temperature [16–18]. The divergence lies only in the numerical values of these indicators [19].

The influence of thermobaric conditions on the physical and mechanical properties of rocks is typically assessed through experimental methods involving the simulation of the real mode of occurrence, often utilizing testing equipment. In recent times, with advancements in software and computer technology, laboratory research results have been complemented with mathematical simulations based on various numerical methods [20–22]. These methods permit a more detailed examination of rock deformation and fracture processes, with the accuracy of their results hinging directly on the chosen geomechanical model and reasonable material behavior parameters. Consequently, identifying experimental patterns and dependencies that reflect the impact of specific factors on the behavior of rock samples serves as fundamental initial data for the subsequent evaluation of the behavior of both rocks and reservoir rocks within the mass [23, 24].

The purpose of this work is to develop a methodology for conducting laboratory studies to examine the impact of the mode of occurrence of oil and gas field reservoirs at great depths on the properties of rock samples. To accomplish this, the following objectives were established: conducting theoretical analyses to identify the primary factors affecting the behavior and structural changes in rocks, developing laboratory research methods that comprehensively simulate these factors, and conducting preliminary experiments to evaluate their influence.

Methods and techniques

The laboratory studies of rocks aim to fully mirror the structural influences that naturally occur within the mass during the formation of a hydrocarbon field [25–27]. As previously mentioned, porous and fractured reservoirs exhibit distinct types of voids. Pore voids develop due to rock compaction resulting from the pressure exerted on the rocks. Fracture voids, on the other hand, are associated tectonic plicative or disjunctive dislocations within the Earth's crust [28, 29].

In light of this, laboratory studies will be conducted on three types of samples:

- the first type comprises rock samples with pore-type voids (Fig. 3, *a*) without any additional external mechanical influences;

- the second type consists of rock samples with pore-type voids and the presence of natural or artificial micro- and macrofractures (Fig. 3, *b*), formed due to plastic deformations during the creation of the anticlinal folded structure of the reservoir;

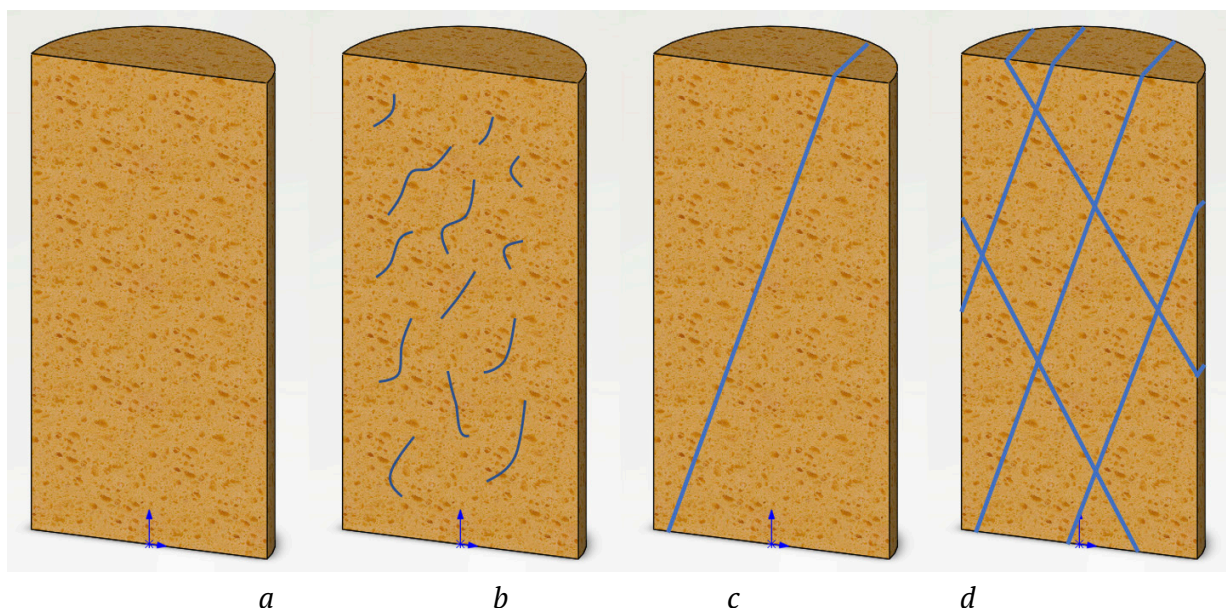


Fig. 3. Types of laboratory samples for research: *a* – first type; *b* – second type; *c* and *d* – third type

– the third type encompasses rock samples with the presence of both individual and systems of disjunctive faults, positioned at various angles to the sample (Fig. 3, *c d*), simulating the existence of tectonic faults in the rock formation.

The primary criterion for selecting samples for research within one lithotype of rocks is the high degree of homogeneity of the original core material.

When preparing the side and end surfaces of samples, it is imperative to adhere to the requirements outlined in regulatory documents for the preparation of rock samples intended for volumetric compression testing [30–32].

The boundary conditions set during the testing process should correspond to the depth at which reservoir rocks are typically found, which ranges from 6 to 10 km. These conditions should also account for a degree of variation, considering the heterogeneous nature of the Earth's crust structure. It has been determined that at these depths, the stress levels can range from 250 to 280 MPa, pore (reservoir) pressures can vary from 200 to 220 MPa, and rock temperatures can reach up to 300°C [33–35]. The process of fluid filtration through the sample body must be taken into account. In order to assess the factors influencing the changes in the internal structure and deformation under the conditions of volumetric stress in rock samples, a test chart is proposed (Fig. 4).

In order to achieve these specific boundary conditions, the use of advanced testing press systems is essential. Most press systems are typically designed

for standard testing methods outlined in GOST (State Standards). To address this, the servohydraulic testing system MTS 815, equipped with a 4600 kN force load frame and a triaxial compression chamber that allows the generation of lateral pressures up to 80 MPa, was retrofitted. This system also includes controllers and software designed for the automatic control of loading modes, as well as data collection from force and strain sensors in its basic configuration. In addition, thermal heaters with temperature control ranging from 20 to 200 °C were integrated into the triaxial compression chamber. Pumping units were added to facilitate the simulation of pore pressure at the inlet and outlet of the sample (P1 and P2, Fig. 5, *a*) within the range of 0 to 80 MPa. In this particular setup, the testing system is capable of investigating deformation and fracture characteristics of samples under the influence of mechanical loading. It also enables the determination of static deformation properties of rock samples, including elasticity and strain moduli, Poisson's and lateral strain ratios, as well as the assessment of volume changes (dilatancy) at various loading stages. Importantly, this configuration with the utilization of modern sensors provides higher signal accuracy from the measuring channels (accuracy class 0.2), consequently enhancing the overall reliability of the test results.

Another significant aspect of laboratory research involves the study of acoustic emission from rock samples during the testing process [36–38]. This

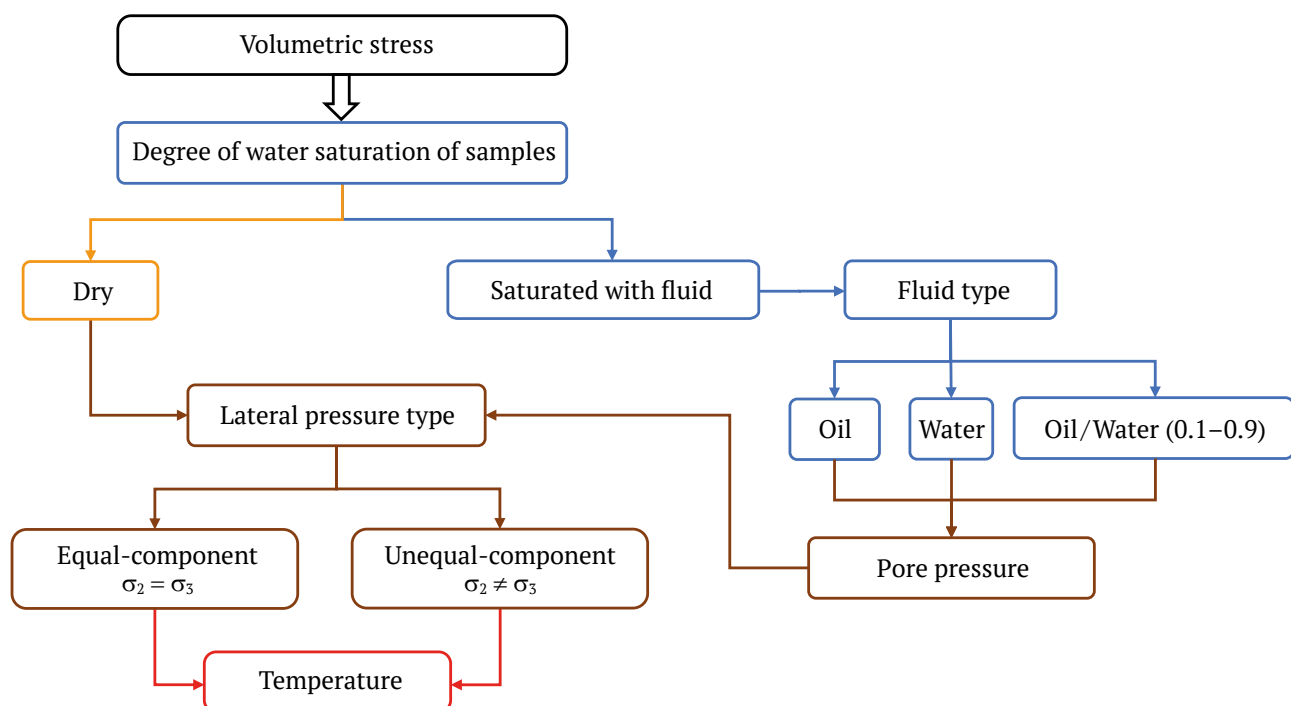


Fig. 4. Algorithm for creating boundary conditions when testing rock samples under volumetric stress

practice aims to enhance the level of detail in geophysical results obtained during field exploration by establishing correlations between the acoustic properties of rocks and their internal structure. From a theoretical standpoint, it allows for the acquisition of a comprehensive representation of the formation and development of micro- and macrofractures within the sample body during the loading process. To fulfill this purpose, the ErgoTech acoustic emission system was seamlessly integrated into the MTS 815 testing system, which facilitates the recording of acoustic emissions from rock samples within a triaxial compression chamber. The ErgoTech system comprises the following key components:

- a measuring unit that fully integrated into the triaxial compression chamber of the MTS 815 system, equipped with 6 ultrasonic sensors and 18 acoustic emission (AE) sensors (Fig. 5, *b*);

- a set of acoustic signal preamplifiers used for signal amplification and transmission to the information acquisition system;

- a unit dedicated to generating, collecting, and processing ultrasonic pulses, which is designed to determine wave velocities at various stages of the experiment.

The processing of test results is carried out using specialized software, namely PicoScope 6 and ASC InSite. PicoScope 6 was employed to ascertain the P- and S-wave velocities at different stages of sample loading. Meanwhile, the ASC InSite software was used to process signals from acoustic sensors and construct volumetric models depicting changes in signal locations and acoustic emission activity at different stages of sample testing.

In the laboratory studies, tests were conducted on sandstone samples collected from depths of 3.5 to 4 km within the hydrocarbon field. These studies were carried out while simulating thermobaric reservoir conditions, encompassing temperature, rock pressures, and reservoir pressures. The fundamental diagram illustrating the simulation of reservoir conditions during testing is depicted in Fig. 5, *a*.

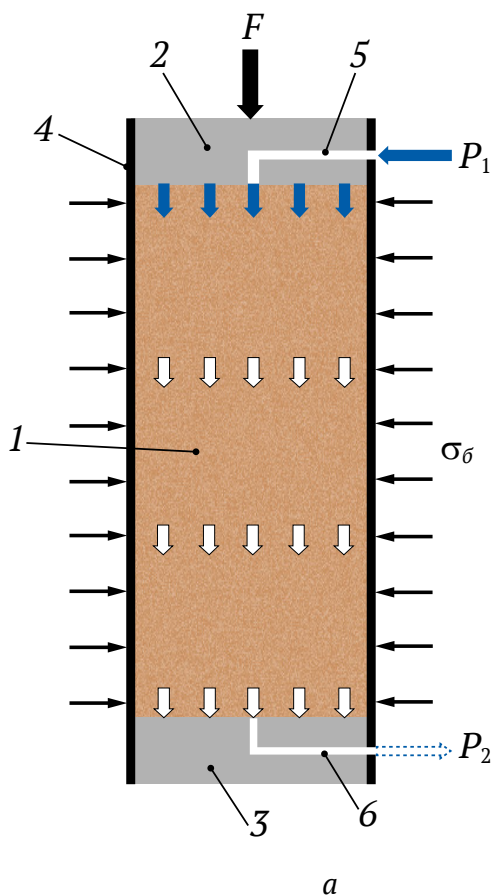


Fig. 5. Basic diagram of the experiment (*a*) and sample prepared for tests in the triaxial compression chamber (*b*) with installed acoustic emission sensors:

- 1 – sample; 2 – upper end lining; 3 – lower end lining; 4 – lateral waterproofing shell of the sample;
- 5 – channel in the upper end lining for water supply to the sample end; 6 – channel in the lower end lining for outflow of water filtered through the sample; F – differential axial load on the sample;
- σ_l – lateral pressure on the sample; P_1, P_2 – porous fluid pressure at the inlet and outlet of the sample

The testing process was as follows.

Samples with a diameter of 100 mm and a height of 200 mm, were crafted from “full-size” core material. These samples, prepared in accordance with GOST 21153.8 “Rocks. Method for determination of triaxial compressive strength”, were placed inside the triaxial compression chamber. Lateral pressure was incrementally increased at a rate of 1 MPa/min until reaching 55 MPa, and pore pressure was raised to 30 MPa. Then, the triaxial compression chamber was heated to 100 °C for two hours. Once the formation conditions for potential creep deformations were met, the sample was held until readings from longitudinal and transverse strain sensors had stabilized. The samples were then subjected to an axial load until they failed, with a strain rate of 1 mm/min. The specified boundary conditions remained constant throughout the entirety of the sample testing process. This approach ensured that laboratory tests, which included complex simulation of the rock mode of occurrence, closely approximated the real conditions of rock behavior within the mass, in stark contrast to conventional methods for determining strength and strain properties.

Results

The results of the tests showed that samples of the same lithotype, collected from approximately the same depth of occurrence, have different properties. They can be broadly categorized into three groups. A description of the behaviors observed in these sample groups is presented below.

During the phase of reaching the formation conditions, measurements were taken for P- and

S-wave velocities. Fig. 6 illustrates the dependences of changes in acoustic parameters of rocks on the lateral pressure value. The upper set of curves pertains to P-wave velocities, while the lower set relates to S-wave velocities. It's noteworthy that an increase in lateral pressure does not lead to a significant rise in the velocities of ultrasonic vibrations. Specifically, for P-waves within the range of lateral pressures from 0 to 55 MPa, there is an increase of 5–10% in velocity, and for S-waves, the increase is even smaller, around 1–5%. Since the velocity of ultrasonic oscillation is an indirect indicator of the material's (rock) density, we can infer that the formation conditions do not have a significant influence on the processes of compaction within the interior of the samples compared to normal atmospheric conditions.

Fig. 7, *a* illustrates the relationships between relative longitudinal and transverse strains and differential stress when testing these groups of sandstone samples under volumetric compression conditions. Samples in Group 3, which exhibit higher ultrasonic wave velocities, also demonstrate superior strength properties. The obtained variation in strength values, ranging from 80 to 220 MPa, under nearly identical testing conditions, indicates a significant discrepancy in the internal structure of the samples. This observation is further supported by the analysis of changes in volumetric deformations during sample loading (Fig. 7, *b*). For samples in Group 1, characterized by the lowest strength, both during the pre-limit deformation stage and the initial phase of off-limit deformation, a characteristic feature is the volume change in the negative region. This can be attributed to the processes of compaction and

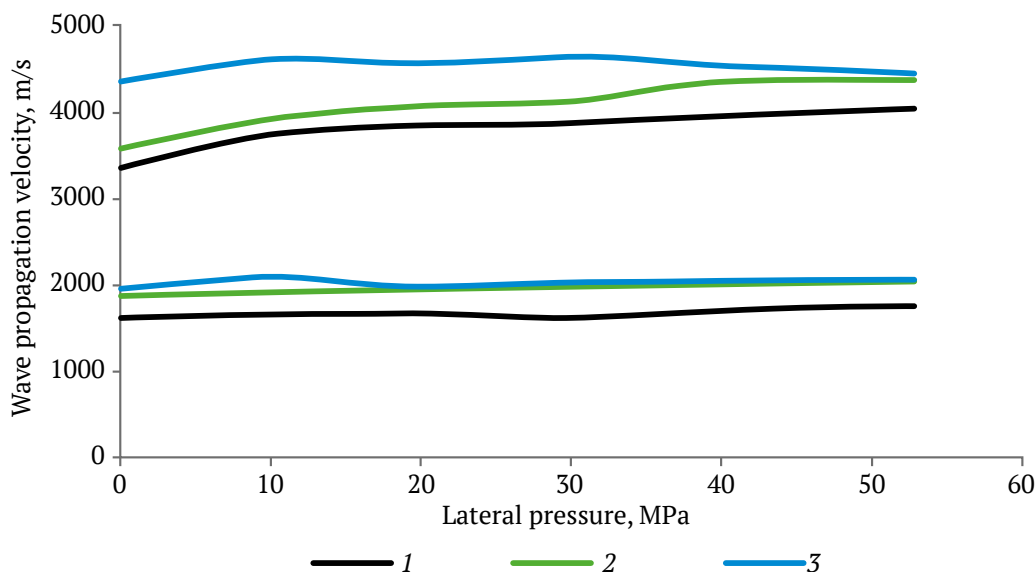


Fig. 6. Dependences of change in propagation velocities of P- and S-waves on the lateral pressure value: 1, 2, 3 – groups of sandstone samples

plastic yielding, which involve the closure of internal pore space without fracturing the rock skeleton. Samples in Groups 2 and 3 lack this negative volume change feature, with the transition from the negative to the positive region of volume change occurring prior to fracture. However, distinctions can still be observed, particularly concerning the intensity of volume increase in samples at stress levels close to the strength limit. Group 2 samples display a gradual increase in the rate of volumetric deformations throughout the entire loading range. On the other hand, Group 3 samples exhibit an intensified increase in intensity as they approach the strength limit, with fracture marked by a sudden spike in volumetric deformation values. These findings indicate the

presence of structural differences among the sample groups, stemming not from differences in constituent minerals but from variations in textural, structural features, and historical conditions during the rock stratum's formation. Based on this, it can be inferred that the samples in Group 3 likely possessed a more homogenous initial internal structure. The process of plastic yielding and eventual fracture in these samples primarily developed due to the accumulation of stresses within the sample's body exceeding the forces of internal bonds between particles. In contrast, the deformation and fracture of samples in Groups 1 and 2 were influenced to a greater extent by the presence of internal defects, layering, and other structural characteristics.

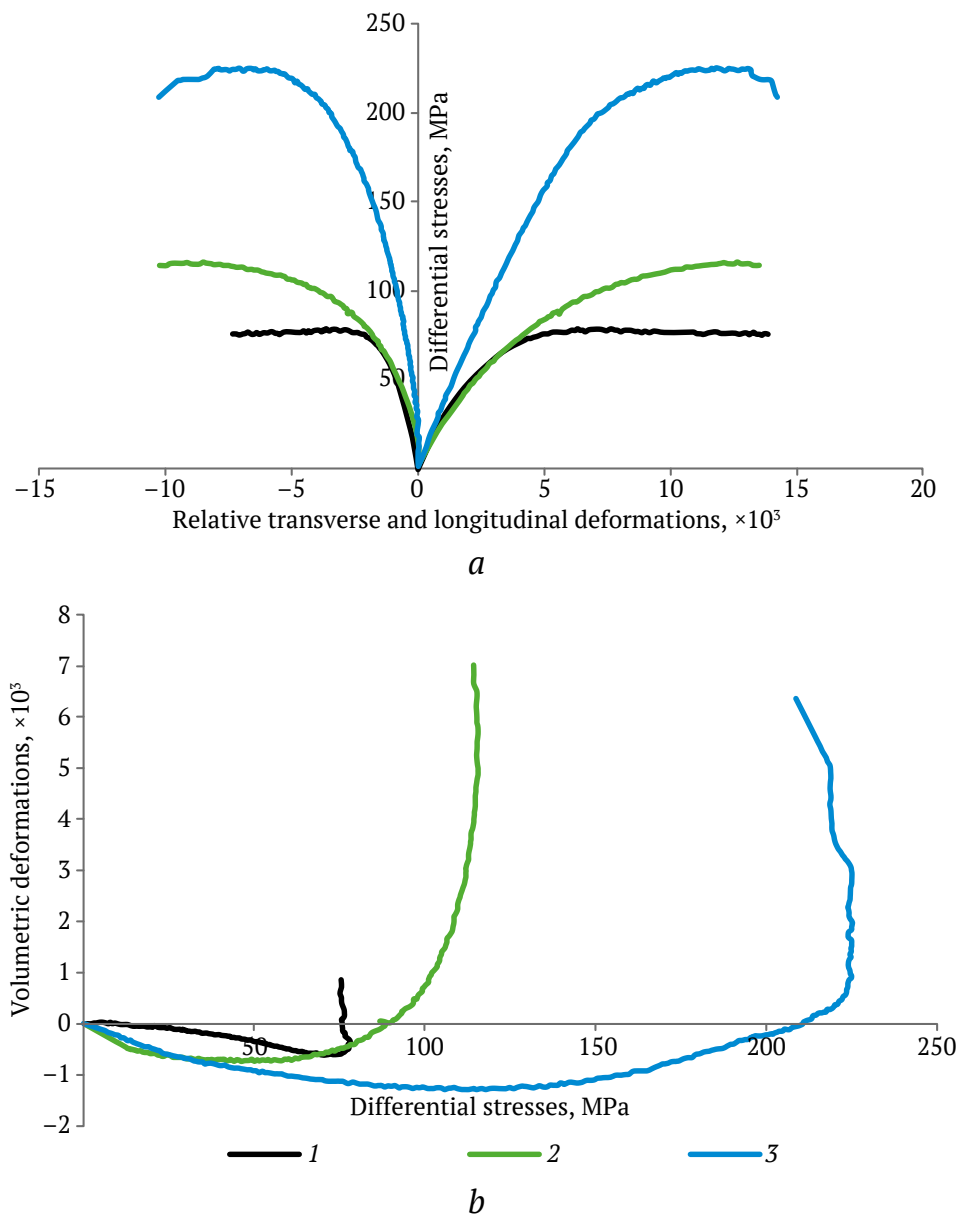


Fig. 7. Curves of dependences of changes in relative longitudinal and transverse deformations (a) and volumetric deformations (b) on the value of differential stress during volumetric compression testing of samples: 1, 2, 3 – groups of sandstone samples

The experiments conducted previously [39] demonstrated the fundamental viability of using the acoustic emission method to investigate the mechanisms of nucleation and subsequent development of micro- and macrofractures during the volumetric compression of rock samples. The results highlighted that the ErgoTech acoustic emission system for rocks allows us to ascertain the spatial and temporal distribution of hypocenters for acoustic emission events while recording amplitude and frequency parameters of signals. Fig. 8 presents the relationship between the intensity of acoustic emission signals and differential stress for rock samples of the same lithotype, tested at a lateral pressure of 40 MPa. In both cases, the maximum signal intensity is concentrated within the region of stress values closely approaching the breaking stress. This is attributed to the formation of

a diagonal shear surface, along which the subsequent fracture of the samples occurs. However, there are differences between the two samples. For the second sample, there is a systematic increase in signal intensity throughout the loading process. In contrast, the first sample, with a value of around 50% of its tensile strength, experiences a significant surge in signal intensity, nearly reaching the maximum value. An analysis of the signal locations at this loading stage revealed that in the first sample, there was the initiation and development of a weakening surface (fracture). However, after reaching certain stress values, the further growth of this surface halted, and failure occurred through a different shear surface. Additionally, there are some disparities in the location of acoustic signals at the time of sample fracture (as indicated in the right part of Fig. 8).

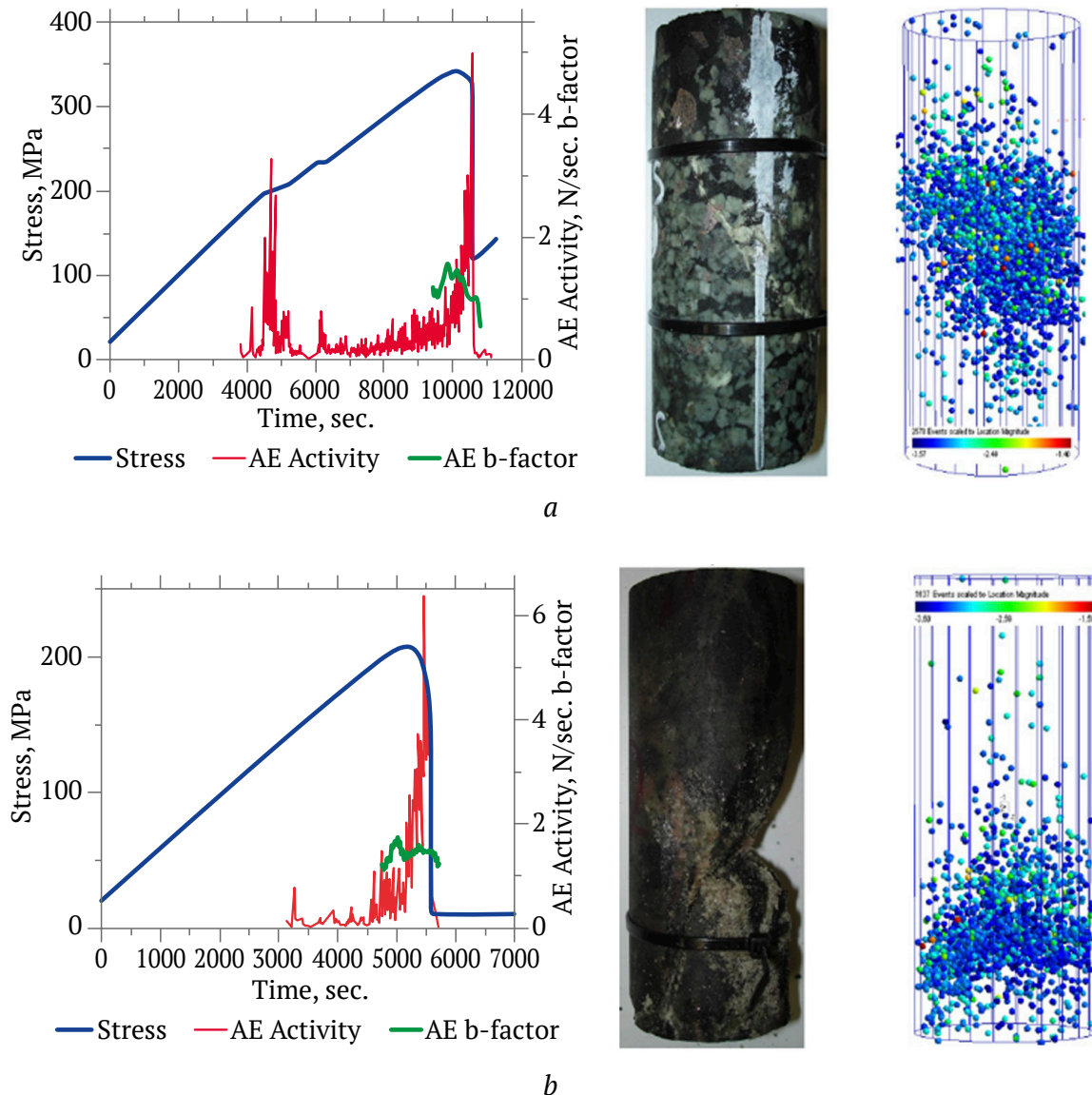


Fig. 8. Test results of two rock samples (*a*, *b*) under the conditions of volumetric stress with acoustic emission fixation [14]



Discussion of results

Methodological approaches to complex laboratory study of the factors influencing changes in the rock structure and including the type of the stress state, the values of principal stresses, and the values of pore pressure and temperature are presented. Existing regulatory documentation for testing rock samples under conditions of volumetric compression does not encompass the reproduction of the complex interplay of these factors during testing. This necessitates the introduction of additional requirements in the development of technical specifications for laboratory studies. Only under these conditions can the results accurately describe the behavior of reservoir rocks in their natural occurrences.

The research presents the results of experiments aimed at studying the behavior of rock samples with the highest possible approximation to the natural conditions of reservoir rock occurrence at depths of 3.5–4 km. It has been established that rock samples of the same lithology, collected from nearly identical depths, can exhibit significant differences in deformation characteristics, both in the pre- and off-limit regions of loading. These research findings serve as essential input data for the development and refinement of geomechanical models governing material behavior, including Coulomb–Mohr, Drucker–Prager, Hoek–Brown models, etc. These models consider not only strength criteria for fracture but also dilatancy processes at various stages of rock deformation, as described by the dilatancy angle formula [40]:

$$\psi = \arcsin \left(\frac{\dot{\varepsilon}_v^p}{-2\dot{\varepsilon}_l^p + \dot{\varepsilon}_v^p} \right),$$

where $\dot{\varepsilon}_v^p$ is the velocity of plastic volumetric deformations, and $\dot{\varepsilon}_l^p$ is the velocity of plastic principal maximum normal (longitudinal) deformations.

An increase in lateral pressure in the range from 0 to 55 MPa results in a relatively minor alteration in ultrasonic vibration velocities, typically ranging from 1 to 10%. This implies that the practical utility of these results for indirectly assessing changes in rock

properties within the mass may be limited. However, in the context of geophysical studies, where variations in numerical velocity values are considered, the interpretation of results is substantially enhanced. This is particularly relevant given the substantial geometric dimensions of the studied masses.

Investigations into acoustic emissions from rocks under complex stress conditions provide valuable insights into the spatial formation and development of micro- and macrofracturing processes throughout the entire sample loading stage. These findings contribute to a more comprehensive understanding of changes in the internal structure of the rock samples.

Conclusion

The study analyzes the factors that influence structural changes in rock samples under thermobaric conditions typical of great depths. This represents a pertinent area of scientific inquiry aimed at acquiring fresh insights into the existing structural condition of rocks and how it evolves in tandem with the geological history of the field.

The paper presents the results of comprehensive laboratory studies, highlighting the necessity for further, more extensive laboratory research to establish quantitative relationships that account for the impact of both individual factors and their cumulative influence on the nature of deformation and changes in the internal structure of rocks. Conducting such studies demands the involvement of highly qualified specialists, specialized press equipment, and a dedicated timeframe for experimentation.

Furthermore, the paper introduces approaches and a methodology for laboratory studies, which can be subsequently used in the revision and development of new regulatory documents within the realm of research on the physical and mechanical properties of reservoir rocks. The author team envisions continuing research endeavors aimed at broadening the scope of temperature and pressure effects on the behavior of reservoir rocks using different types of fluids.

References

1. Nguyen V.T., Rogachev M.K., Aleksandrov A.N. A new approach to improving efficiency of gas-lift wells in the conditions of the formation of organic wax deposits in the Dragon field. *Journal of Petroleum Exploration and Production Technology*. 2020;(10):3663–3672. <https://doi.org/10.1007/s13202-020-00976-4>
2. Petrakov D., Kupavykh K., Kupavykh A. The effect of fluid saturation on the elastic-plastic properties of oil reservoir rocks. *Curved and Layered Structures*. 2020;7(1):29–34. <https://doi.org/10.1515/cls-2020-0003>
3. Tananykhin D., Korolev M., Stecyuk I., Grigorev M. An investigation into current sand control methodologies taking into account geomechanical, field and laboratory data analysis. *Resources*. 2021;10(12):125. <https://doi.org/10.3390/resources10120125>



4. Litvinenko V. S., Vasiliev N. I., Lipenkov V. Y., Dmitriev A. N. Special aspects of ice drilling and results of 5G hole drilling at Vostok station, Antarctica. *Annals of Glaciology*. 2014;55(68):173–178. <https://doi.org/10.3189/2014AoG68A040>
5. Pavlovich A. A., Korshunov V. A., Bazhukov A. A., Melnikov N. Y. Estimation of rock mass strength in open-pit mining. *Journal of Mining Institute*. 2019;239:502–509. <https://doi.org/10.31897/PMI.2019.5.502>
6. Kochneva O. E., Nefedov U. V., Fedorov N. V. Establishing the correlation between reservoir properties and facies features of the Bashkir sediments of the Gagarinskoye field (Russian). *Oil Industry Journal*. 2019;(2):24–27. <https://doi.org/10.24887/0028-2448-2019-2-24-27>
7. Kazantseva T. T. The geodynamic concept of oil genesis. *Herald of the Russian Academy of Sciences of the Republic of Bashkortostan*. 2012;17(1):5–13. (In Russ.)
8. Kamaletdinov M. A., Ismagilov R. A. On some scientific results of petroleum geological investigations. *Herald of the Russian Academy of Sciences of the Republic of Bashkortostan*. 2011;(4):16–22. (In Russ.)
9. Kutcherov V. G. The genesis of hydrocarbons and the formation of deposits of oil and natural gas. *Vesti Gazovoi Nauki*. 2013;1(12): 86–91. (In Russ.)
10. Zakharova S. S. Basic concepts of the origin of oil and gas. *Nauka i Tekhnika v Yakutii*. 2003;(1):16–22. (In Russ.)
11. Egorov A. S., Prischepa O. M., Nefedov Y. V. et al. Deep structure, tectonics and petroleum potential of the western sector of the Russian arctic. *Journal of Marine Science and Engineering*. 2021;9(3):258. <https://doi.org/10.3390/jmse9030258>
12. Prishchepa O. M., Borovikov I. S., Grokhotov E. I. Oil and gas content of the understudied part in the northwest of the Timan-Pechora oil and gas province according to the results of basin modeling. *Journal of Mining Institute*. 2021;247:66–81. <https://doi.org/10.31897/PMI.2021.1.8>
13. Kutcherov V., Gerasimova I. Petroleum genesis: competition of paradigms. *Voprosy Filosofii*. 2019;(12):106–117. (In Russ.) <https://doi.org/10.31857/S004287440007530-8>
14. Gerasimova I. A. Petroleum genesis as a problem of transdisciplinary research. *Epistemology & Philosophy of Science*. 2020;57(3):125–141. (In Russ.) <https://doi.org/10.5840/eps202057346>
15. Dmitrievskii A. N. Polygenesis of oil and gas. *Doklady Earth Sciences*. 2008;419(2):373–377. <https://doi.org/10.1134/S1028334X08030033> (Orig. ver.: Dmitrievskii A. N. Polygenesis of oil and gas. *Doklady Akademii Nauk*. 2008;419(3):373–377. (In Russ.))
16. Ogadzhyanov V. A., Kerimov A. A., Mamedova V. A. Thermobaric criteria for predicting oil and gas prospects at the former Zhdanov field. *Izvestiâ vysših učebnyh zavedenij. Neft' i gaz*. 1988;(8):62–66. (In Russ.)
17. Ryzhov A. E., Zhukov V. S., Iselidze O. V., Grigoriev E. B. Influence of reservoir thermobaric conditions on the petrophysical characteristics of rock samples of the Achimov strata. *Vesti Gazovoy Nauki*. 2010;(1):145–156. (In Russ.)
18. Seredin V. V., Khrulev A. S. Variations of temperature in specimens of rocks and geomaterials under failure. *Journal of Mining Science*. 2016;54(4):683–688. <https://doi.org/10.1134/S1062739116041081> (Orig. ver.: Seredin V. V., Khrulev A. S. Variations of temperature in specimens of rocks and geomaterials under failure. *Fiziko-Tekhnicheskiye Problemy Razrabotki Poleznykh Iskopayemykh*. 2016;(4):63–69. (In Russ.))
19. Aleksandrova T., Nikolaeva N., Kuznetsov V. Thermodynamic and experimental substantiation of the possibility of formation and extraction of organometallic compounds as indicators of deep naphthogenesis. *Energies*. 2023;16(9):3862. <https://doi.org/10.3390/en16093862>
20. Karasev M. A., Nguyen T. T. Method for predicting the stress state of the lining of underground structures of quasi-rectangular and arched forms. *Journal of Mining Institute*. 2022;257:807–821. <https://doi.org/10.31897/PMI.2022.17>
21. Kochneva O. E., Nefedov U. V., Fedorov N. V. Establishing the correlation between reservoir properties and facies features of the Bashkir sediments of the Gagarinskoye field (Russian). *Oil Industry Journal*. 2019;(2):24–27. <https://doi.org/10.24887/0028-2448-2019-2-24-27>
22. Kotlov S. N., Shamshev A. A. Numerical geo-flow modeling of horizontal drainage holes. *Mining Information and Analytical Bulletin*. 2019;(6):45–55. (In Russ.) <https://doi.org/10.25018/0236-1493-2019-06-0-45-55>
23. Zhang P., Mishra B., Heasley K. A. Experimental investigation on the influence of high pressure and high temperature on the mechanical properties of deep reservoir rocks. *Rock Mechanics and Rock Engineering*. 2015;(48):2197–2211. <https://doi.org/10.1007/s00603-015-0718-x>



24. Gladkov E.A., Erofeyev L. Ya., Karpova E.G. et al. Geomechanical change of hydrocarbon deposits during their deformational metasomatic alterations. *Territorija Neftegaz*. 2016;(3):132–138. (In Russ.)
25. Abdelazim R. An integrated approach for relative permeability estimation of fractured porous media: laboratory and numerical simulation studies. *Journal of Petroleum Exploration and Production Technology*. 2020;10:1–18. <https://doi.org/10.1007/s13202-016-0250-x>
26. Adenutsi C.D., Li Z., Lai F., Hama A.E., Aggrey W.N. Pore pressure variation at constant confining stress on water–oil and silica nanofluid–oil relative permeability. *Journal of Petroleum Exploration and Production Technology*. 2019;9:2065–2079. <https://doi.org/10.1007/s13202-018-0605-6>
27. Brace W.F., Walsh J.B., Frangos W.T. Permeability of granite under high pressure. *Journal of Geophysical research*. 1968;73(6):2225–2236. <https://doi.org/10.1029/JB073I006P02225>
28. Pollard D.D. Theoretical displacements and stresses near fractures in rock: with applications to faults, joints, veins, dikes, and solution surfaces. *Fracture Mechanics of Rock*. 1987:277–349. <https://doi.org/10.1016/B978-0-12-066266-1.50013-2>
29. Zhang X.P., Wong L.N.Y. Cracking processes in rock-like material containing a single flaw under uniaxial compression: a numerical study based on parallel bonded-particle model approach. *Rock Mechanics and Rock Engineering*. 2012;(45):711–737. <https://doi.org/10.1007/s00603-011-0176-z>
30. Tiab Dj. *Petrophysics: theory and practice of measuring reservoir rock and fluid transport properties*. 2nd ed. Boston: Gulf Professional Pub.; 2004.
31. Khashper A.L., Aminev T.R., Fedorov A.I., Zhonin A.V. Research of dependence of rock permeability on its stress-strain state. *Geologicheskii Vestnik*. 2019;(1):133–140. (In Russ.) <https://doi.org/10.31084/2619-0087/2019-1-10>
32. Tsai B.N., Bondarenko T.T., Bakhtybaev N.B. On the dilatancy of rocks during their destruction. *Vestnik Satbayev University*. 2008;(5):21–36. (In Russ.)
33. Belokon A.V. Modeling of tectonic and temperature history of the drilling area of the Timan-Pechora deep reference well. *Vestnik Permskogo Natsional'nogo Issledovatel'skogo Politekhnicheskogo Universiteta. Geologiya. Neftegazovoye i Gornoye Delo*. 2000;(3):71–76. (In Russ.)
34. Tomkina A.V. Thermobaric conditions in ultra-deep depressions of the North Caucasus. In: Markevich V.P. (ed.) *Thermobaric Conditions and Geological Exploration in Ultra-Deep Depressions*. Moscow: Nauka Publ.; 1981. Pp. 13–26.
35. Timurzиеv A.I., Lastovetskii V.P. Quantitative assessment of parameters of stress- deformation state of rocks for allocation of areas of the relative extension (dilatation) and the hyperfracturing zones by results of mathematical modelling (on example of Ety-Purovsky oilfield polygon). Part 1. *Glubinnaya Neft'*. 2014;2(9):1499–1543. (In Russ.)
36. Eltsov I.N., Nazarov L.A., Nazarova L.A. et al. Interpretation of geophysical measurements in wells taking into account hydrodynamic and geomechanical processes in the penetration zone. *Reports of the Academy of Sciences*. 2012;445(6):677–677. (In Russ.)
37. Lockner D. The role of acoustic emission in the study of rock fracture. *International Journal of Rock Mechanics and Mining Sciences & Geomechanics Abstracts*. 1993;30(7):883–899. [https://doi.org/10.1016/0148-9062\(93\)90041-B](https://doi.org/10.1016/0148-9062(93)90041-B)
38. Armstrong B.H. Acoustic emission prior to rockbursts and earthquakes. *Bulletin of the Seismological Society of America*. 1969;59(3):1259–1279.
39. Rozanov A., Petrov D., Gladyr A., Korchak P. Acoustic emission analysis of brittle and ductile behavior of rocks at critical stresses. In: *82nd EAGE Annual Conference & Exhibition. European Association of Geoscientists & Engineers*. 2021;2021(1):1–5. <https://doi.org/10.3997/2214-4609.202011927>
40. Vermeer P.A., de Borst R. Non associated plasticity for soils, concrete and rock. *Heron*. 1984;29(3):51–64.

Information about the authors

Mikhail D. Ilyinov – Cand. Sci. (Eng.), Head of the Research Laboratory of Physical and Mechanical Properties and Rocks, Scientific Center of Geomechanics and Problems of Mining Production, Saint Petersburg Mining University, St. Petersburg, Russian Federation; ORCID [0009-0007-2185-8638](https://orcid.org/0009-0007-2185-8638); e-mail ilinov_md@spmi.ru

Dmitry N. Petrov – Cand. Sci. (Eng.), Associate Professor of the Department of Construction of Mining Enterprises and Underground Structures, Saint Petersburg Mining University, St. Petersburg, Russian Federation; ORCID [0000-0002-5513-1871](https://orcid.org/0000-0002-5513-1871), Scopus ID [56672478800](https://scopus.org/authorid/56672478800); e-mail kaf-sgp@spmi.ru



Daniil A. Karmanskiy – Leading Engineer of the Research Laboratory of Physical and Mechanical Properties and Destruction of Rocks, Scientific Center of Geomechanics and Problems of Mining Production, Saint Petersburg Mining University, St. Petersburg, Russian Federation; ORCID [0000-0002-3214-5322](https://orcid.org/0000-0002-3214-5322), Scopus ID [57209507897](https://scopus.com/authorid/57209507897); e-mail Karmanskij_DA@pers.spmi.ru

Alexander A. Selikhov – PhD-Student, Department of Construction of Mining Enterprises and Underground Structures, Saint Petersburg Mining University, St. Petersburg, Russian Federation; ORCID [0009-0005-8163-2249](https://orcid.org/0009-0005-8163-2249); e-mail s225059@stud.spmi.ru

Received 01.09.2023

Revised 22.09.2023

Accepted 25.09.2023



MINING ROCK PROPERTIES. ROCK MECHANICS AND GEOPHYSICS

Research paper

<https://doi.org/10.17073/2500-0632-2022-11-30>

UDC 627.431



Simulation of ash dump embankment stability

O. G. Bessimbayeva  , E. N. Khmyrova   , E. A. Oleinikova  , A. E. Kasymzhanova  

Karaganda State Technical University, Karaganda, Kazakhstan

 hmyrova@mail.ru

Abstract

Ash and slag materials are removed from boiler rooms of CHP “Combined Heat and Power Plant” (Теплоэлектростанция) by hydraulic transport and disposed in ash dumps. These are specially organized areas encircled by protective dams depending on the relief either along the entire perimeter or only in certain low-lying areas. The dams of hydraulic structures must provide stability to the whole structure against the following factors: shear; stability of slopes against sliding; filtration resistance of a dam body soils; reliable slope protection against possible failure due to atmospheric precipitation; as well as against wave action of water (within a settling pond); sufficient excess of dam crest over water level of a pond, etc. The study focuses on the design of ash and slag dump embankment (for storage of the ash and slag removed from the boiler rooms of Karaganda CHP by hydraulic transport). Ash dump design requires a broad range of problems to be solved. These include determination of location, design features and type of embankment, area of the basin and volume of the stored waste, strength of the embankment structures, etc. In order to assess the condition of the ash dump design, the stability of the facility embankment slopes for different combinations of loads, the conditions of possible watering of the dams, the presence of “geomembrane”, and pore pressure need to be analysed. A software program based on the finite element method allows simulation of ground (soil) conditions based on the strength and strain characteristics of the dam body filling soils and the base soils. Safety factors of the outer (downstream) slopes of hydraulic structures is determined taking into account the category and design of a structure, type of base (foundation), criticality of the design process stage, and other factors on the basis of conditions that ensure the prevention of the onset of limit states. The most critical and characteristic cross-sections across the perimeter of the ash dump embankment were selected for the computations, based on the analysis of the designed hydraulic structure base lithological composition. According to the computations performed, the outer slopes of the embankment at the paths of wells No. 373-19, No. 381-19, characteristic of almost the entire length of the embankment, are stable for different combinations of loads.

Keywords

Karaganda CHP, ash dump, embankment, structure, slopes, stability, simulation, soil, finite element method, load, factor of safety, drawdown curve, head gradient

For citation

Bessimbayeva O.G., Khmyrova E.N., Oleinikova E.A., Kasymzhanova A.E. Simulation of ash dump embankment stability. *Mining Science and Technology (Russia)*. 2023;8(4):303–312. <https://doi.org/10.17073/2500-0632-2022-11-30>

СВОЙСТВА ГОРНЫХ ПОРОД. ГЕОМЕХАНИКА И ГЕОФИЗИКА

Научная статья

Моделирование устойчивости ограждающих сооружений золоотвала

O. G. Бесимбаева  , E. N. Хмырова   , E. A. Олейникова  , A. E. Касымжанова  

Карагандинский государственный технический университет, г. Караганда, Казахстан

 hmyrova@mail.ru

Аннотация

Складирование золошлаковых материалов, удаляемых из котельных помещений ТЭЦ «Теплоэлектроцентраль» при помощи гидротранспорта, производится в золоотвалы: специально организованные участки местности, по границам которых, в зависимости от рельефа, возводятся ограждающие дамбы либо по всему периметру золоотвала, либо только на отдельных пониженных участках. Ограждающие дамбы гидротехнических сооружений должны обладать устойчивостью всего сооружения на сдвиг; устойчивостью откосов на оползание; фильтрационной прочностью грунта тела сооружения; надежностью защиты откосов от возможных разрушений в результате действия атмосферных осадков, а так-



же от волнового воздействия воды (в пределах отстойного пруда); достаточным превышением гребня дамбы над уровнем воды пруда и т.д. Основное внимание в исследовании сконцентрировано на вопросах проектирования ограждающих сооружений золошлаковых материалов, удаляемых из котельных помещений Карагандинской ТЭЦ при помощи гидротранспорта. При проектировании золоотвала решаются многие задачи, в том числе определяются местоположение, конструктивные особенности и тип ограждающих сооружений, площадь зеркала и объем складированных хвостов, прочность сооружений ограждающих дамб и т.д. С целью оценки состояния проектируемого золоотвала выполнен анализ устойчивости откосов ограждающей дамбы для различных сочетаний нагрузок, условий возможной обводненности дамбы, наличия «геомембраны» и порового давления. Расчетная программа, основанная на методе конечных элементов, позволяет моделировать состояние массива в соответствии с прочностными и деформационными характеристиками насыпных грунтов тела дамбы и грунтов пород основания. Коэффициент устойчивости внешних откосов гидротехнических сооружений определяется с учетом класса и конструкции сооружения, типа основания, ответственности расчетного технологического этапа и других факторов исходя из условий, обеспечивающих предупреждение наступления предельных состояний. На основании анализа геологического строения основания проектируемого гидротехнического сооружения выбраны наиболее ответственные и характерные поперечные расчетные сечения по периметру ограждающих дамб золоотвала. Согласно выполненным расчетам внешние откосы дамбы по линиям скважин № 373-19, № 381-19, которые являются характерными практически по всей длине ограждающей дамбы, являются устойчивыми для разных сочетаний нагрузок.

Ключевые слова

Карагандинская ТЭЦ, золоотвал, дамба, конструкция, откосы, устойчивость, моделирование, грунт, метод конечных элементов, нагрузка, коэффициент запаса, кривая депрессии, градиент напора

Для цитирования

Bessimbayeva O.G., Khmyrova E.N., Oleinikova E.A., Kasymzhanova A.E. Simulation of ash dump embankment stability. *Mining Science and Technology (Russia)*. 2023;8(4):303–312. <https://doi.org/10.17073/2500-0632-2022-11-30>

Introduction

Hydraulic structures have a number of features, so they differ significantly from other engineering structures. Their size, layout, types of individual elements significantly depend on local conditions: topography, hydrogeological conditions, geological structure (lithological composition) of a base, etc.

The dams of hydraulic structures must provide stability to the whole structure against the following factors: shear; stability of slopes against sliding; filtration resistance of a dam body soils; reliable slope protection against possible failure due to atmospheric precipitation; as well as against wave action of water (within a settling pond); sufficient excess of dam crest over water level of a pond, etc. [1].

Design solutions for embankment erection

Ash and slag materials are removed from boiler rooms of CHP “Combined Heat and Power Plant” (Теплоэлектростанция) by hydraulic transport and disposed in ash dumps. These are specially organized areas encircled by protective dams depending on the relief either along the entire perimeter or only in certain low-lying areas.

According to a detailed design for the construction of the 1st section of the Karaganda CHP ash dump, crest height was taken at 534.6 m, with a crest width of 8.0 m. According to design projections, the maximum filling level of the ash dump basin can reach 533.1 m. The design height of the dam on the inside

of the basin is 12 m with the dam slope ratio $m = 1 : 4$. The dam height on the outer side varies depending on the terrain with the dam slope ratio $m = 1 : 2.5$.

According to the findings of a geotechnical survey performed by “GeolProject and K” LLP in 2019 (in accordance with GOST 25100–2011 and GOST 20522–2012), the sequence of drilled rocks includes sediments of Upper Devonian Famennian stage (D3fm), eluvial sediments of Upper Devonian Famennian stage (el(D3fm)), Neogene (N) and Quaternary (Q) sediments, covered with topsoil and recent man-made sediments.

The Upper Devonian Famennian (D3fm) rocks are represented by rocky and semi-rocky sandstones. The Upper Devonian Famennian (el(D3fm)) rock eluvium is represented by a weathering crust: rubbly soil, rubbly and landwaste soil with sandy loam aggregate, rubbly and landwaste soil with loamy aggregate.

Based on the analysis of the spatial variability of particular indicators of soil properties and taking into account the features of the geological structure and lithological composition, three layers were identified in the sequence: 1st layer, topsoil; 2nd layer, clay alluvium (silt); 3rd layer, filled soil t(qiv). According to the degree of water permeability, 7 layers of geotechnical units (GTUs) can be determined: 1st GTU, loam; 2nd GTU, sandy loam; 3rd GTU, clay; 4th GTU, rubble-landwaste soil eld3fm; 5th GTU, landwaste soil eld3fm; 6th GTU, rubble soil eld3fm; 7th GTU, rock (sandstone) d3fm.



Hydrogeological conditions of the study area

According to drilling data, groundwater was intersected at a depth of 2.00–5.5 m. The elevations of standing-water levels are at 519.05–524.87 m. Under natural conditions, the level of groundwater is subject to seasonal fluctuations. The minimum standing-water level is observed in March, the maximum in early May.

The groundwater is fed by infiltration of precipitation, and, in the spring, by meltwater and floodwater. The recharge area is the area of the aquifer.

The amplitude of the level fluctuations in the study area is 1.0–1.5 m. In some years of high precipitation, the amplitude can reach 2.0–3.0 m.

The standard depths of freezing according to SP RK 5.01-102-2013 “Foundations of buildings and structures” are as follows: loam and clay, 1.41 m; sandy loam and dusty sand, 1.72 m; coarse and medium gravelly sands, 1.84 m; coarsely clastic soils, 2.09 m. The average depth of “0°C” penetration into the soils is 1.77 m.

The strength and strain characteristics of soils were established in studies conducted by Azimut Geology LLP, a chemical analysis laboratory in Karaganda.

In order to reduce filtration through the dam (embankment) body, the dam design provides for laying a geomembrane as a watertight barrier, covering the upstream slope of the dam and the bottom of the ash dump basin.

The dam detailed design provides for dewatering of the ash dump area, water diversion, and leveling the basin bottom to the elevation of 522.6 m. In this case, it is planned initially to remove the fertile soil layer, silts, and upper soil layers to the design elevation, in accordance with the requirements of SP RK 3.04-103–2014 “Bases of Hydraulic Structures”.

Depending on the terrain and the soil lithology, different soil layers will be removed: from loam to clay deposits [2, 3].

The project envisages filling the body of the dam with the soils removed during leveling. This is compliant with the requirements of SP RK 3.04-105–2014 “Dams made of soil materials”, which include loamy-sand and loamy soils. Analysis of the findings of the geotechnical survey performed by “GeolProject and K” LLP in 2019 shows that the most suitable are the Quaternary (Q) sediments represented by brown loam and sandy loam¹.

¹ Report “Geotechnical survey for design of ash dump of Karaganda CHP”, performed by “GeolProject and K” LLP in 2019.

Program of geotechnical survey performed by “GeolProject and K” LLP in 2019.

Based on the report “Geotechnical survey for design of ash dump of Karaganda CHP”, the characteristics of soils to be used in the construction of the embankment body, are given below.

The strength and strain characteristics for the 1st GTU layer, loam, were determined at natural moisture. The particular values of the strength properties of the loam at natural moisture, as well as those of density were subjected to statistical processing (according to the requirements of GOST 20522–2012). The resulting values² are shown in Table 1.

Table 1

Strength and strain characteristics of layers

Parameter	Angle of internal friction, degrees	Specific cohesion, MPa	Soil density, g/cm ³
1 st GTU, loam	22.39	0.060	2.02
2 nd GTU, sandy loam	17.24	0.013	1.97

The strain moduli according to laboratory tests at natural moisture vary from 6.17 to 13.96 MPa, with an average value of 8.23 MPa.

The layer of the 2nd GTU, sandy loam, is characterized by the physical parameters given in Table 1.

All types of soils are suitable for the formation of the main body of an earth-fill embankment [1] except for the following:

1) containing incompletely decomposed organic matter (plant residues) in an amount greater than 5% by mass or fully decomposed substances in an amorphous state in an amount greater than 8% by mass³;

2) containing water-soluble inclusions in the form of chloride and sulfate-chloride salts in an amount exceeding 5% by mass or sulfate salts in an amount exceeding 2% by mass. However, such soils may be placed in that part of the dam which is not exposed to seepage water.

The design provides for a single-layer barrier with one impervious element in the form of a polymer sheet (geomembrane) with a protective layer over it. It is planned to lay the geomembrane on the upstream slope of the dam and the bottom of the ash dump basin.

The single-layer barrier includes:

- an underlying layer of soil;
- an impervious element, which is a polymer sheet composed of flexible web products;
- a protective layer of soil.

² Ibid.

³ MSP (Interstate Building Rules) 3.04-101-2005 Determination of basic design hydrological characteristics.



In order to prevent mechanical impacts on the protective layer of soil (wave, ice, etc.), this layer on the dam slopes will be provided with additional protection, rock fill⁴ [2].

Also in order to assess the stability of the slopes of the designed ash dump, the computations were undertaken of embankment stability for the different combinations of the degree of loading, the conditions of the dam possible watering, the presence of “geomembrane”, and pore pressure.

Simulation of the designed structure stability

A detailed study of all factors affecting the process of displacement of rocks in an earthfill embankment is required, in order to justify the parameters of stable slopes of an embankment. It is of key importance to select a computation method which will meet the specific geotechnical and geological conditions and physical and mechanical properties of the rocks composing the body of dams and their bases. The computations should use methods which satisfy the equilibrium conditions of the wedge of failure and its elements in the limit state and take into account the stress state of a structure and its base.

A software program based on the finite element method allowing simulating ground conditions in accordance with the strength and strain characteristics of a dam body filling soils and a base soils was used to assess the stability of the ash dump dam (embankment) slopes. Phase2 applications automatically compare the stresses with the strength properties of soils and certain procedures were used to ensure that the stress pattern matches the equilibrium conditions and the specified properties of the soils.

The advantage of the finite element method [4] lies in its potential to investigate areas of any configuration and take into account different soil properties, each of which is unique in its boundary conditions and medium characteristics. It also provides for the possibility of arbitrary discretization of the investigated area, i.e. it is possible to thicken the finite element network in expected places of high gradients of investigated parameters.

The simulation of stability of the designed structure was carried out on the basis of the findings obtained on the basis of the analysis of topography,

⁴ SP RK 3.04-105-2014 “Dams made of soil materials”.
SP RK 3.04-101-2013 “Hydraulic structures”.
SNiP RK 3.04-40-2006 “Loads and impacts (wave, ice and from ships) on hydraulic structures”.
SP RK 3.04-103-2014 “Foundations of hydraulic structures”.
SP RK 2.03-30-2017 “Construction in seismic areas of the RK”.
SNiP RK 3.02-05-2010 “Automated system for monitoring of buildings and structures”.

hydrogeological conditions, lithological composition of the base, physical and mechanical characteristics of soils and wastes of the ash dump. The simulation also took into account the geotechnical survey data, the category of the structure, and operating conditions [3–5]. For each soil (ground) layer, its own physical and mechanical properties, density, bulk density, modulus of elasticity, and other parameters required to solve the problem, were prescribed.

Studies of the base soils, on which the designed dams are to be erected along the embankment perimeter were conducted in accordance with the report “Geotechnical survey for design of ash dump of Karaganda CHP”⁵. Four sections of different length with similar operating conditions in terms of hydrogeological conditions, lithological composition of the base, and a number of other factors were united into the computation zones.

The first section, 2.5 km long, according to the materials of the report is described by wells 374-19, 347-19, 346-19, 375-19, 345-19, 376-19, 377-19, 343-19, 378-19, 379-19, 341-19, 380-19, 340-19, 381-19, 339-19, 382-19, 338-19, 383-19, 385-19, which penetrated the following soil layers:

- clay alluvium and a 0.4–0.5 m thick topsoil;
- brown hard water-saturated loam 1.8 to 14.9 m thick;
- mottled or grayish-green hard water-saturated clay 8.0 to 10.9 m thick.

The second section, 0.75 km long, is similar to the previous one and described by well 328-19, intersecting hard sandy loam of brown and gray color with low degree of water saturation, up to 15.0 m thick; and wells 384-19, 330-19, 385-19, 327-19, 337-19, 326-19, intersecting the following soil lithologies:

- brown hard water-saturated loam 2.4 to 15 m thick;
- brown hard sandy loam of medium water saturation degree, 2.2 to 2.5 m thick;
- rock represented by gray massive sandstone of medium water saturation degree, 2.6 to 7.9 m thick.

The third section 300 m long, described by wells 324-19, 366-19 and 332-19, requires special attention. In terms of lithology, this section base is mainly presented by brown or red-colored hard water-saturated clay. The thickness varies from 5.5 to 8.5 m, and loam of low thickness (1.5–1.8 m). A gray hard loam 7.0 to 21 m thick occurs below this layer.

The fourth section, up to 3.7 km long, is the most solid base for the ash dump dams and is penetrated

⁵ Report “Geotechnical survey for design of ash dump of Karaganda CHP”, performed by “GeolProject and K” LLP in 2019.



by wells 323-19, 373-19 and up to well 350-19. The section is characterized by the following lithologies:

- brown hard water-saturated loam 1.7 to 15 m thick;
- rubbly hard water saturated soil with loamy and sandy loam aggregate from 1.5 to 10.4 m thick;
- rock and semi-rocky soil represented by gray massive sandstone of medium water saturation from 1.0 to 11.0 m thick.

The stability of a filling dam is strongly influenced by its base watering due to rising groundwater table⁶. This leads to a deterioration of the strength characteristics of base rocks and a decrease in their strength. Thus, the various combinations of the degree of watering of a dam and its base need to be considered when modeling [1, 2, 6, 7].

Based on the analysis of the designed hydraulic structure base lithology, the most critical and characteristic cross-sections across the perimeter of the ash dump embankment were selected.

The criterion for dam slope stability is the compliance (for the most dangerous wedges of failure) with inequality [3]:

$$\gamma_{fc} F(\gamma_f) \leq \frac{\gamma_c}{\gamma_n} R \left(\frac{1}{\gamma_g} \right),$$

where γ_{fc} is load combination factor; F is design value of generalized force impact, determined taking into account the load safety factor γ_f (f is resultant active forces or moments of these forces relative to the shear surface axis, which depends on the slope stability computation method); γ_c is condition load effect factor; γ_n is facility responsibility factor; R is design value of the generalized bearing capability of a “building – base” system, defined taking into account the safety factor for a soil γ_g , i.e. generalized design value of the ultimate shearing resistance forces along the surface in question.

When searching for a dangerous shear surface, a FoS dependence can be used

$$n_3 = \frac{R}{F} \geq \frac{\gamma_n \gamma_{fc}}{\gamma_c}.$$

For hydraulic structures of the II category of importance [2, 8, 9], to which the designed structure belongs, factor of safety (FoS) is equal to:

1) with a special combination of loads during operation:

$$n_3 = \frac{\gamma_n \gamma_{fc}}{\gamma_c} = \frac{1,2 \cdot 0,95}{1,0} = 1,14;$$

2) at the main combination of loads during operation:

$$n_3 = \frac{\gamma_n \gamma_{fc}}{\gamma_c} = \frac{1,2 \cdot 1,0}{1,0} = 1,2.$$

In order to study the stability of the designed dams and the correctness of the decisions made, simulation of altered characteristics of the designed embankment in various conditions of operation was performed. This was based on the provisions of regulatory documents (SNiP RK 3.04-40-2006 “Loadings and impacts (wave, ice and from ships) on hydraulic structures”)⁷.

The following computations were performed in the course of the simulation:

- 1) hydrostatic pressure at maximum filling without a dam watering;
- 2) hydrodynamic head at minimum filling with a watered dam;
- 3) pore pressure at maximum filling without a dam watering;
- 4) pore pressure at minimum filling with a watered dam;
- 5) hydraulic pressure gradient at full filling of the ash dump basin;
- 6) hydraulic pressure gradient in the initial period of operation;
- 7) volumetric moisture at full filling of the ash dump basin;
- 8) volumetric moisture in the initial period of operation;
- 9) computations of the embankment inner slope stability for different combinations of the embankment watering degree;
- 10) computation of the stability of the embankment outer slope.

This paper presents the findings of inner slope stability computations for the most characteristic cross-section at well 373-19 for various combinations of dam watering. It also takes into account the presence/absence of “geomembrane”, and pore pressure values, as well as the complicated part of the embankment next to well 324-19. The computations were performed using the “Phase2” computer program for different combinations of loads: filled soils with standard strength characteristics, compaction factor of 1.75, ash dump basin filling for the initial period of 0.4 m, and up to the level of 533.1 m. The slurry composition by content was 1/10-1/14. The characteristic cross-sections were compiled based on the lithological units found in the wells closest to the cross-section

⁶ SP RK 3.04-103-2014 “Foundations of hydraulic structures”

⁷ SNiP RK 3.04-40-2006 “Loads and impacts (wave, ice and from ships) on hydraulic structures”.

tions⁸. The physical and mechanical characteristics of soils were taken according to the research of soils in wells drilled along the perimeter of the territory, allocated for the ash dump. The computations showed that factor of safety (FoS) of the inner slope of the dam at the cross-section passing through well No. 373-19 without watering (the inner slope is reinforced with geomembrane and rock fill) is 1.718, and, with dam watering, 1.064.

Computations for the complicated embankment part near well 324-19 carried out, in order to assess the stability of the inner slopes of the embankment showed that FoS of the inner slope of the dam at well 324-19 without watering (with the inner slope strengthened by geomembrane and rock fill) is 1.672, and, with watering, 0.986. Fig. 1 shows the computa-

⁸ Report “Geotechnical survey for design of ash dump of Karaganda CHP”, performed by “GeolProject and K” LLP in 2019.

Program of geotechnical survey performed by “GeolProject and K” LLP in 2019.

tion using the “Phase2” program of the embankment inner slope stability at characteristic cross-section 324-19 (near well 324-19) when the dam is watered.

The area allocated for the ash dump has difficult hydrogeological conditions, so resolving the problem of prior dewatering of the area and water diversion is paramount, in order to ensure the stability of erected structures. The simulation shows that in order to ensure the stability of the inner and outer slopes when the dam is watered, pipe drainage needs to be installed.

The Phase2 program was used to calculate the stability of the outer slope of the selected sections. This takes into account the homogeneity of the soil mass, composed of filled soils (loam) with pipe drainage in place. Computation of the stability of the outer slope in cross-section no. 373-19 showed that FoS of the outer slope is 1.806, and for a special combination of loads at a seismic impact of 5 points (Fig. 2), 1.533.

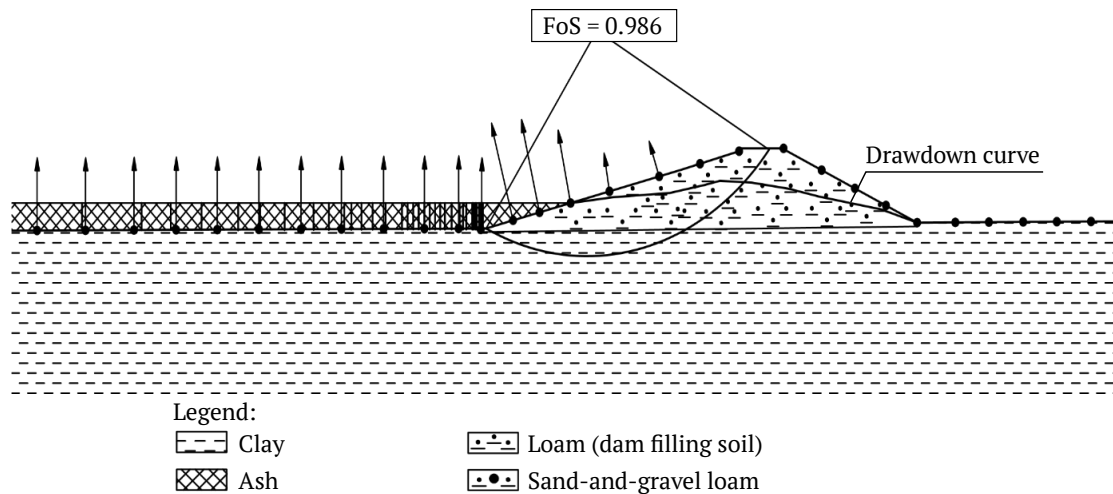


Fig. 1. Computations of embankment inner slope stability at characteristic cross-section 324-19 when the dam is watered

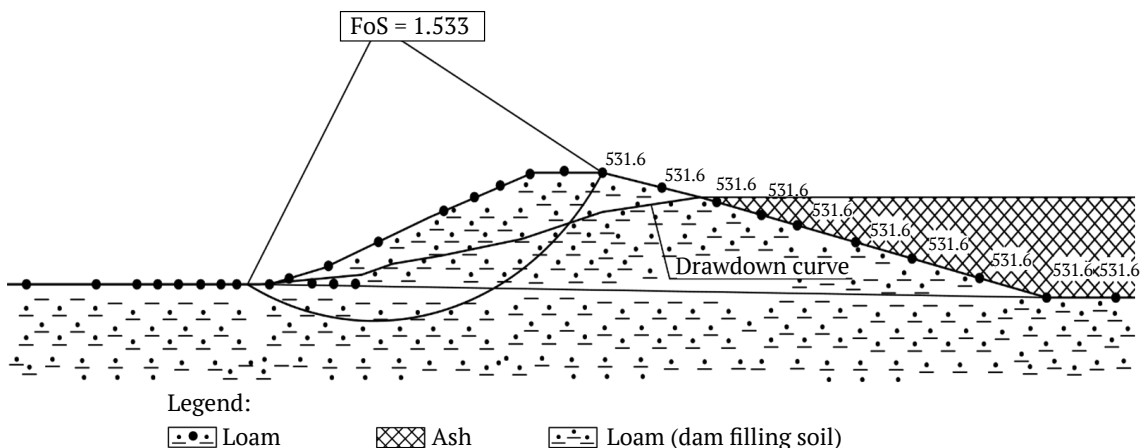


Fig. 2. Embankment outer slope stability computations for cross-section 373-19 at a special combination of loads

The calculated position of the depression curve was determined by filtration computation using the FEM (finite element method). Filtration strength of soils, as well as that of impervious barriers, was estimated on the basis of the appropriate computations and experimental studies of soils at the head gradients acting in a structure. This also took into account the stress-strain state of the structure and its base, design features, construction methods, and operating conditions [6–9].

Fig. 3 shows the depression curve and the calculated head gradient in the downstream (outer) slope of the embankment. According to filtration computation, the maximum design value of the effective head gradient in the downstream slope ranges from 0.523 to 0.360.

An outer slope strength analysis was performed in Phase2 for the weakest cross-section through well 324-19 with pipe drainage. The GLE/Morgenstern-Price method was used, taking into account the distribution of the main limit equilibrium with surcharged dam body. The method uses artificial loading as a basis, in order to identify weaknesses and possible failure points (Fig. 4). In this particular case, the weakest in terms of the stability factor is sector 3 on cross-section no. 324-19 (see Fig. 4).

During the analysis, a possible shear line for each sector is constructed separately. The computations show that the critical factor of safety at cross-section no. 324-19 is 1.026 (Fig. 5). This does not meet the requirements and criteria for the dam slope stability, which should be equal to 1.2.

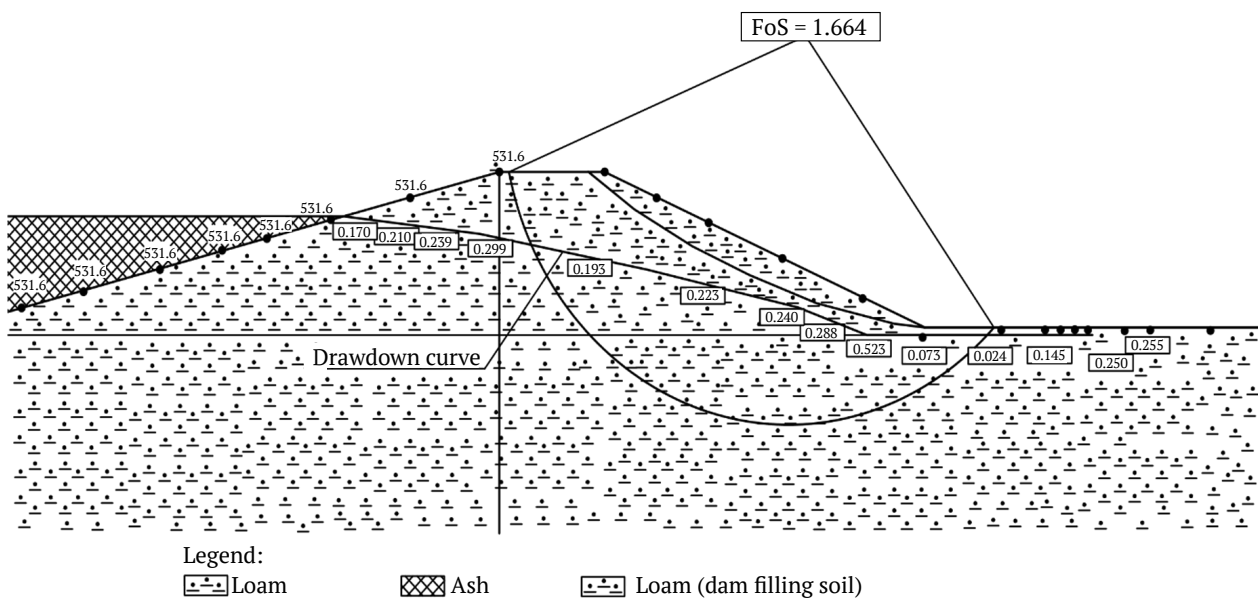


Fig. 3. Drawdown curve and head gradient readings

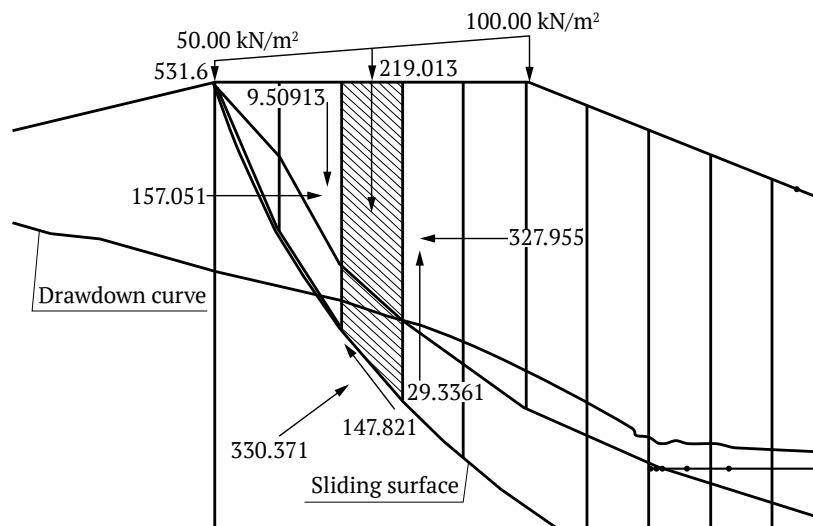


Fig. 4. Computation for cross-section no. 324-19 to identify weaknesses and possible failure points

According to the computations performed, the structural concept for the erection of an embankment made of a homogeneous soil mass (loam) with a clay base and without a cutoff wall will not ensure the stability of a dam next to the cross-section through well No. 324-19.

In order to ensure embankment stability, pipe drainage and a cutoff wall in the base of the dam for reliable connection with the base were applied. The designed dam body made of heterogeneous soil mass (loam with admixtures of sandstone and gravel) was used. The structural cross-section of the design dam body is shown in Fig. 6.

Computations of the stability according to the second option of the dam design for the cross-section defined by wells 324-19, 366-19 and 332-19 300 m long with a clay base showed $FoS = 1.664$ for the main combination of loads, and $FoS = 1.430$ for a special combination of loads under seismic action.

Conclusions

The stability of the embankment and separating dams of a TSF is determined by a complex of geotechnical, hydrogeological, and anthropogenic factors. The following have the greatest influence: physical and mechanical characteristics of soils and tailings (wastes); the process of construction and operation of a structure; nature of its base; hydrodynamic, hydrostatic, seismic, and dynamic forces⁹.

When designing embankment structures of dumps for ash and slag materials removed from boiler rooms of CHPs, many factors need to be established. These include: selection of the location of a dump and embankment; determination of the geological characteristics (lithology) of the embankment and dam bases; modeling the type and parameters of structures depending on the volume of waste

⁹ MSP (Interstate Building Rules) 3.04-101-2005 Determination of basic design hydrological characteristics.

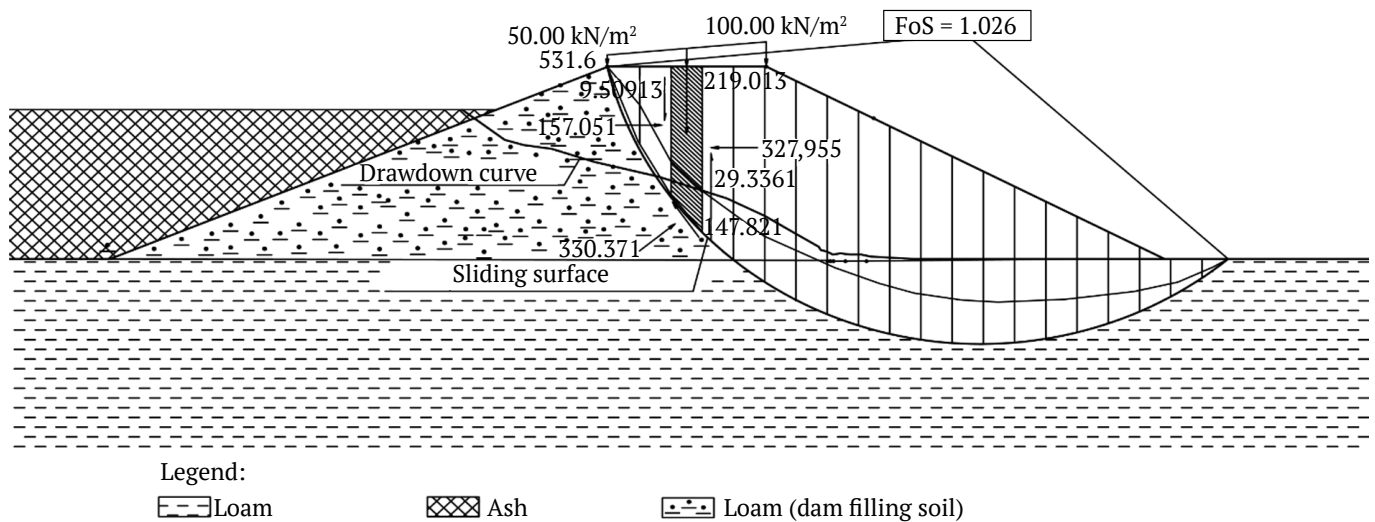


Fig. 5. Computation of outer slope stability for the weakest cross-section through well 324-19 with pipe drainage in place

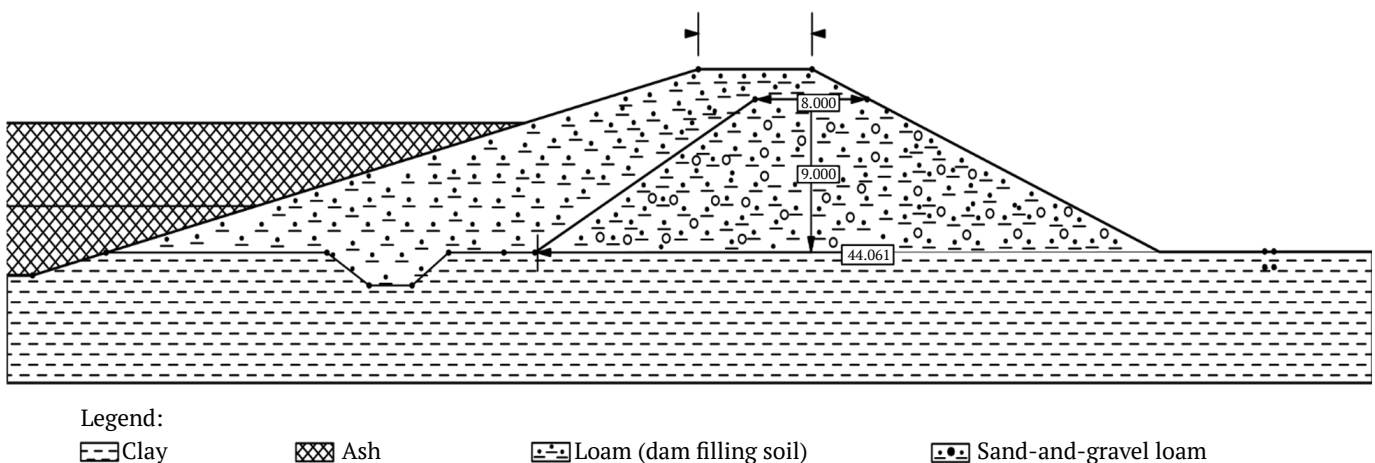


Fig. 6. Structural cross-section of the dam body with cutoff wall and pipe drainage



disposed; determination of materials for the construction of an embankment body based on possible close location of a quarry as a source of building materials; determination of the structural features of an embankment body, which should ensure required strength of an erected facility.

1. When designing the embankment of ash dump No. 3 of Karaganda CHP-3, a software program based on the finite element method allowing for ground conditions to be simulated in accordance with the strength and strain characteristics of a dam body filling soils and a base soils, was used.

2. The computations were performed using the “Phase2” computer program for different combinations of loads for filled soils with standard strength characteristics and a compaction factor of 1.75, ash dump basin filling for the initial period of 0.4 m and up to the level of 533.1 m. The slurry composition by content was 1/10-1/14. The computations were made taking into account the homogeneity of the dam slope soil mass composed of bulk soils (loam) and pipe drainage in place at the base. The inner slope is reinforced with a geomembrane and a rockfill.

3. The simulation showed that the calculated values of the characteristic cross-sections exceeded the regulatory values of the stability factor for structures of category II, which are equal to 1.2 and 1.14, respectively, except for the section with a clay base. The stability of filling dams is practically ensured along the entire perimeter of the embankment except for the section with a clay base.

4. When modeling the 300 m long (approx) dam body section, the base of which consists of red-colored and brown hard water-saturated clay with thickness from 5.5 to 8.5 m and loam of small thickness (1.5–1.8 m), it should be considered that the stability of a filling dam is strongly affected by the watering of its base due to rising groundwater table¹⁰. This leads to a deterioration of the strength characteristics of the base soils and a decrease in their strength. Thus, when

simulating, it becomes necessary to consider various combinations of the degree of watering of a dam and its base.

5. Computations of the stability of the dam built of homogeneous soil for the section with clay base in the worst conditions with maximum moisture of soils and minimum values of their strength characteristics showed that the condition of the dam slopes is close to the limit. The critical factor of safety at cross-section no. 324-19 is equal to 1,026, which does not meet the requirements and criteria for the dam slope stability.

Erection of an embankment made of homogeneous soil without additional structural elements to increase the structure strength can lead to violation of its integrity when the soil moisture and groundwater level increase.

6. In order to increase the strength of the embankment for the 300-m section with a clay base defined by wells 324-19, 366-19 and 332-19, the dam design, in addition to the built-in pipe drainage, provides for a cutoff wall in the base and a soil-fill toe (made of loam with sandstone and gravel admixtures), with the subsequent erection of the dam made of loam to the design parameters.

A structure option of the dam body at this specific section, developed on the basis of the simulation, provided a factor of safety values for the outer slope at well no. 324-19. This was FoS = 1.664 for the main combination of loads, and FoS = 1.430 for a special combination of loads under seismic action.

The ideal soil for the dam body construction is a soil, formed by large particles and clay-filled pores. Such a soil is characterized by a relatively high angle of internal friction, corresponding to a coarse-grained soil, and a low filtration coefficient, corresponding to a clay soil.

7. According to the filtration computations, the maximum calculated value of effective head gradient for well no. 324-19 will be 0.523; for well no. 373-19, 0.597; for well no. 381-19, 0.651; the regulatory value is not more than 1.3 [2, 6].

¹⁰ SP RK 3.04-103-2014 “Bases of hydraulic structures”.

References

1. Chugaev R.R. *Hydraulic structures*. Moscow: Agropromizdat; 1985. 318 p. (In Russ.)
2. Chugaev R.R. *Ground hydraulic structures*. Leningrad: Energy; 1967. 460 p. (In Russ.)
3. Kostyukov E.V., Prostov S.M., Bakhaeva S.P. Prediction of stability of hydraulic structure embankment on the basis of geoelectric control of their condition. *Bulletin of the Kuzbass State Technical University*. 2004;(2):14–18. (In Russ.) URL: <https://vestnik.kuzstu.ru/index.php?page=article&id=1637>
4. Zhang L., Peng M., Chang D., Xu Y., *Dam failure mechanisms and risk assessment*. John Wiley & Sons Singapore Pte. Ltd.; 2016. <https://doi.org/10.1002/9781118558522>
5. Panteleev V.G., Chugaeva G.A., Filippova E.A. et al. Composition of computation cases when analyzing slope stability of soil structures for various purposes. *Izvestiya VNIIG*. 1996;231. (In Russ.)



6. Ashraf M., Soliman A. H., El-Ghorab E., El Zawahry A. Assessment of embankment dams breaching using large scale physical modeling and statistical methods. *Water Science*. 2018;32(8):362–379.
7. Bakhayeva S.P., Prostov S.M., Kostyukov E.V., Seregin E.A. Comprehensive assessment of geomechanical processes in dams made of soil materials. *Mine Surveying Bulletin*. 2003;(2):62–66. (In Russ.)
8. Galperin A.M., Shafarenko E.M. *Rheological computations of mine-engineering structures*. Moscow: Nedra Publ.; 1977. 246 p. (In Russ.)
9. Kibirev V.I., Raylyan G.A., Sazonov G. T. et al. *Hydraulic disposition of beneficiation tailings*. Handbook. Moscow: Nedra Publ.; 1991. (In Russ.)
10. Wahl T.L. Uncertainty of predictions of embankment dam breach parameters. *Journal of Hydraulic Engineering*. 2004;130(5):389–397. [https://doi.org/10.1061/\(ASCE\)0733-9429\(2004\)130:5\(389\)](https://doi.org/10.1061/(ASCE)0733-9429(2004)130:5(389))
11. Wu W., Marsooli R., He Z. Depth-averaged two-dimensional model of unsteady flow and sediment transport due to noncohesive embankment break/breaching. *Journal of Hydraulic Engineering*. 2012;138(6):503–516. [https://doi.org/10.1061/\(ASCE\)HY.1943-7900.0000546](https://doi.org/10.1061/(ASCE)HY.1943-7900.0000546)
12. Wang L., Chen Z., Wang N. et al. Modeling lateral enlargement in dam breaches using slope stability analysis based on circular slip mode. *Engineering Geology*. 2016;209:70–81. <https://doi.org/10.1016/j.enggeo.2016.04.027>
13. Kostyukov E.V. *Research of physical condition and assessment of stability of ground dams of hydraulic structures at mining enterprises by geoelectric method*. [Ph.D. thesis in Eng. Sci.]. Kemerovo; 2005. 147 p. (In Russ.)

Information about the authors

Olga G. Bessimbayeva – Cand. Sci. (Eng.), Associate Professor of the Department of Mine Surveying and Geodesy, Karaganda State Technical University, Karaganda, Kazakhstan; ORCID [0000-0002-8132-1505](https://orcid.org/0000-0002-8132-1505), Scopus ID [57202620963](https://scopus.com/authorid/57202620963); e-mail bog250456@mail.ru

Elena N. Khmyrova – Cand. Sci. (Eng.), Head of the Department of Mine Surveying and Geodesy, Karaganda State Technical University, Karaganda, Kazakhstan; ORCID [0000-0001-5763-327X](https://orcid.org/0000-0001-5763-327X), Scopus ID [57202620896](https://scopus.com/authorid/57202620896); e-mail hmyrovae@mail.ru

Elena A. Oleinikova – Senior Lecturer, Department of Mine Surveying and Geodesy, Karaganda State Technical University, Karaganda, Kazakhstan; ORCID [0000-0002-6133-7630](https://orcid.org/0000-0002-6133-7630), Scopus ID [57202892706](https://scopus.com/authorid/57202892706)

Aizhan E. Kasymzhanova – Senior Lecturer, Department of Mine Surveying and Geodesy, Karaganda State Technical University, Karaganda, Kazakhstan; ORCID [0000-0002-6181-8637](https://orcid.org/0000-0002-6181-8637), Scopus ID [57191977084](https://scopus.com/authorid/57191977084)

Received 08.11.2022

Revised 21.02.2023

Accepted 10.03.2023



BENEFICIATION AND PROCESSING OF NATURAL AND TECHNOGENIC RAW MATERIALS

Research paper



<https://doi.org/10.17073/2500-0632-2023-09-154>

UDC 622.7

Optimizing composition and application conditions of agents for modifying spectral characteristics of diamonds in X-ray luminescence separation

V.A. Chanturiya  , V.V. Morozov  , G.P. Dvoichenkova   ,
Yu.A. Podkamennyi  , A.S. Timofeev  

*Research Institute of Comprehensive Exploitation of Mineral Resources of the Russian Academy of Sciences,
Moscow, Russian Federation*

 dvoigp@mail.ru

Abstract

One of the research areas focused on improving the efficiency of diamond-bearing kimberlite beneficiation processes involves the utilization of technology aimed at enhancing the recovery of weakly and anomalously luminescent diamonds during the X-ray luminescence separation process using luminophore-containing chemical agents. The objective of this research was to select the optimal composition of agents that modify the spectral characteristics of minerals and the conditions for their application. A crucial factor for process efficiency is the effective attachment of modifying agents to diamond crystals while avoiding similar attachment to kimberlite mineral surfaces. This is achieved through the use of organic collectors with an optimal composition, characterized by their ability to both adhere to the diamond surface and retain inorganic luminophore grains. The evaluation of luminophore attachment efficiency was performed using visometric analysis in the UV range. The capability of diamonds to retain luminophore collector droplets or films on their surfaces was evaluated using a technique to measure the three-phase limiting wetting angle. The spectral and kinetic characteristics of diamonds and their recovery during the X-ray luminescence separation process were determined using a separator “Polyus-M”. The feasibility of purposefully modifying the spectral characteristics of weakly and anomalously luminescent diamonds through luminophore-containing compositions based on zinc sulfides and zinc orthosilicate has been confirmed through the conducted studies. By considering the criterion of selectivity in the attachment of luminophore emulsion to diamonds and kimberlite minerals, calculated based on the measured surface concentrations of luminophores on the minerals, the optimal ratios between the masses of inorganic luminophore, organic collector, and the aqueous phase of the emulsion were determined. Dispersing agents that offer selective binding of luminophores to diamond crystals were identified, and rational parameters for the composition of the organic collector were established. The temperature range for treating diamond-containing material was defined. As a result of bench testing the modifying agents with the selected composition and conditions for their application in the diamond-containing material treatment cycle before XRF separation, it was confirmed that the recovery of anomalously and weakly luminescent diamonds could exceed 90%, while keeping the yield of kimberlite minerals in the concentrate below 1%.

Keywords

diamonds, kimberlite, spectral characteristics, luminophores, modifying agent, selectivity, luminescence, separation

Financing

The research was carried out at the expense of grant No. 21 of the Russian Science Foundation, <https://rscf.ru/project/17-00020>.

For citation

Chanturiya V.A., Morozov V.V., Dvoichenkova G.P., Podkamennyi Yu.A., Timofeev A.S. Optimizing composition and application conditions of agents for modifying spectral characteristics of diamonds in X-ray luminescence separation. *Mining Science and Technology (Russia)*. 2023;8(4):313–326. <https://doi.org/10.17073/2500-0632-2023-09-154>



ОБОГАЩЕНИЕ, ПЕРЕРАБОТКА МИНЕРАЛЬНОГО И ТЕХНОГЕННОГО СЫРЬЯ

Научная статья

Оптимизация состава и режима применения реагентов-модификаторов спектральных характеристик алмазов в процессе рентгенолюминесцентной сепарации

В.А. Чантурия  , В.В. Морозов  , Г.П. Двойченкова   ,
Ю.А. Подкаменный  , А.С. Тимофеев  

*Институт проблем комплексного освоения недр РАН,
г. Москва, Российская Федерация*

 dvoigp@mail.ru

Аннотация

Одним из направлений повышения эффективности процессов обогащения алмазосодержащих кимберлитов является применение технологии, способствующей извлечению слабо и аномально люминесцирующих алмазов в процессе рентгенолюминесцентной сепарации с применением люминофорсодержащих реагентов. Задача исследований заключалась в выборе рационального состава реагентов-модификаторов спектральных характеристик минералов и режима их применения. Основным условием эффективности процесса является интенсивное закрепление реагентов-модификаторов на кристаллах алмазов без аналогичного закрепления на поверхности кимберлита, что обеспечивается применением органических коллекторов оптимального состава, характеризующихся способностью как адгезионно закрепляться на поверхности алмазов, так и удерживать зерна неорганических люминофоров. Оценка эффективности закрепления люминофоров выполнена с использованием методики визиометрического анализа в УФ излучении. Оценка способности алмазов удерживать на поверхности капли или пленки коллектора с люминофорами выполнена с использованием методики измерения величины трехфазного краевого угла смачивания. Спектрально-кинетические характеристики алмазов и их извлечение в процессе рентгенолюминесцентной сепарации были определены на сепараторе «Полюс-М». В результате проведенных исследований установлена возможность целенаправленного модифицирования спектральных характеристик слабо и аномально светящихся алмазов люминофорсодержащими композициями на основе сульфидов цинка и ортосиликата цинка. С использованием критерия селективности закрепления люминофорсодержащей эмульсии на алмазах и минералах кимберлита, рассчитываемого по величинам измеренных поверхностных концентраций люминофоров на минералах, определены оптимальные соотношения между массами неорганического люминофора, органического коллектора и водной фазы применяемой эмульсии. Выбраны реагенты-диспергаторы, обеспечивающие селективное закрепление люминофоров на алмазных кристаллах. Установлены рациональные параметры состава органического коллектора. Определены границы температурного режима процесса обработки алмазосодержащего материала. В результате стендовой апробации реагентов модификаторов выбранного состава и режимов их применения в цикле обработки алмазосодержащего материала перед процессом РЛС установлена возможность достижения извлечения аномально и слабо люминесцирующих алмазов более чем на 90 % при значениях выхода кимберлита в концентрат, не превышающих 1 %.

Ключевые слова

алмазы, кимберлит, спектральные характеристики, люминофоры, реагент-модификатор, селективность, люминесценция, сепарация

Финансирование

Исследование выполнено за счет гранта Российского научного фонда № 21–17–00020, <https://rscf.ru/project/21-17-00020/>.

Для цитирования

Chanturiya V.A., Morozov V.V., Dvoichenkova G.P., Podkamennyi Yu.A., Timofeev A.S. Optimizing composition and application conditions of agents for modifying spectral characteristics of diamonds in X-ray luminescence separation. *Mining Science and Technology (Russia)*. 2023;8(4):313–326. <https://doi.org/10.17073/2500-0632-2023-09-154>



Introduction

A crucial resource for enhancing the efficiency of diamond mining enterprises lies in mitigating the so-called “methodical losses” of diamonds. These losses are linked to substantial and fundamental deviations in the raw material’s parameters from the settings of the utilized equipment. In the context of X-ray luminescence separation (XRF), methodological losses of diamonds arise from their unique composition and structure, leading to the absence or, conversely, excessive concentration of lattice defects or impurities, which induce distinct X-ray luminescence patterns [1, 2].

A promising trend for improving the efficiency of X-ray luminescence separation of diamonds involves the development of technologies to modify their spectral characteristics through the use of luminophore-containing modifying agents [3, 4]. This technology is design to target the recovery of weakly and anomalously luminescent crystals, characterized by X-ray luminescence of low intensity or significantly differing from the characteristics of the majority of diamonds.

The core components of these modifying agents are luminophore-containing compositions that incorporate both inorganic and organic luminophores, each possessing characteristics conducive to the desired alterations of the kinetic parameters of a diamond’s X-ray luminescence signal [5].

The primary criterion for selecting luminophores for the implementation of this technology is their ability to endow diamonds with X-ray luminescence signal parameters that closely resemble those of natural crystals and fall within the acceptable ranges of detector settings in X-ray luminescence separators.

An important condition for enhancing the effectiveness of this developed technology [3–5] is to establish selective conditions for the attachment of modifying agents to diamond crystals. This entails maintaining a satisfactory level of luminophore attachment to diamonds while minimizing their attachment to kimberlite mineral surfaces. The realization of this condition, adopted as the main approach to address the specified objectives, is achieved through the experimentally supported selection of organic collector components included in the modifying agents. These collectors are characterized by their capacity to be selectively adhered to the diamond surface while retaining inorganic luminophore grains within their structure. To determine the selectivity of luminophore attachment at the surfaces of diamonds and kimberlite, a method of visiometric analysis has been developed [4].

The necessary stability of diamond – collector – luminophore aggregates is achieved through hydrophobizing treatment of inorganic luminophores and by selecting the composition of organic fluids used as collectors [6]. The assessment of the adhesive ability of a collector to the diamond surface, which determines the ability of diamonds to retain the luminophore-containing composition on their surfaces, is conducted using the technique of measuring the three-phase limiting wetting angle in the system composed of mineral – collector drop – aqueous medium [7].

The ultimate objective of this research was to select the parameters of modifying agents and the conditions for their application that ensure the required selectivity in the X-ray luminescence separation process. This goal was attained by selecting rational agent compositions applicable for modifying the characteristics of the main types of non-extractable diamonds. This involves determining the composition and mass ratios of luminophores, collector and aqueous phase, identifying the composition of the organic collector, and choosing selective attachment regimes for luminophores on diamond crystals. This included the use of dispersing agents for the organic phase and agents to control collector attachment to kimberlite minerals.

Research methods

The treatment of diamond-containing kimberlite products with modifying agent was carried out using a specialized apparatus designed and manufactured with the support of the Russian Science Foundation under Grant No. 21-17-00020.

The intensity of luminophore attachment to diamonds was determined by assessing their surface concentration. This measurement was carried out using both luminescence and combined (ultraviolet-visible light) microscopy techniques, allowing for observation and registration of images of the elements within a luminophore-containing composition through the utilization of the photoluminescence effect [8, 9]. In this particular study, a “Micromed 3 LUM” luminescent microscope was employed.

The impact of control agents on the hydrophobic and oleophilic properties of the surfaces of both diamonds and hydrophobic minerals in kimberlite was evaluated through the measurement of limiting wetting angles [10]. Initially, the mineral surfaces were treated with the examined aqueous system, followed by the application of an organic substance droplet to the treated surface. The addition of the aqueous phase increased the level of the water-air

interface. Next, the limiting wetting angle and droplet size were measured within the mineral – collector drop – aqueous phase system.

These measurements were conducted using an “OCA 15EC Package 1” unit with an SD-DM direct dosing module. The measurement results were processed using the SCA 20 software package.

The efficiency of luminophores attachment to the surface of diamonds and kimberlite minerals was assessed based on images of luminescence produces by the examined objects under ultraviolet radiation. This assessment was carried out using a UVC-254/365 instrument equipped with UV light sources emitting at wavelengths of 254 and 365 nm. The obtained images were subjected to visimetric analysis, allowing for the estimation of luminophore concentration and distribution characteristics on the surface of the analyzed samples [2, 4].

To determine the spectral and kinetic characteristics of diamonds and kimberlite, as well as the recoverability of diamonds, a portable X-ray luminescence separator “Polyus-M” was employed. This equipment’s capabilities aligned closely with those of industrial X-ray luminescence separators [11, 12]. The built-in analog-to-digital registration system of the “Polyus-M” separator facilitated the separa-

tion process within the “selective” regime, which involved the use of kinetic characteristics of the X-ray luminescence signal, including the convolution S_V , attenuation time constant τ_{att} , amplitude of the slow component A_{SC} , amplitude of the fast component A_{FC} , and the ratio of amplitude components K_A [4, 12].

Findings and Discussion

1. Justification of process parameters for applied luminophores and compositions

One notable aspect of the research was the use of a specialized laboratory setup that performed the tasks of processing diamond-containing material with a modifying agent, separating the conditioned emulsion, and washing the treated material prior to the X-ray luminescent separation (XRF) operation (Fig. 1).

The use of this setup enables the processing and separation of diamond-containing material under conditions closely resembling industrial settings. The experimental methodology involved treating a mineral mixture in an emulsion of a modifying agent for 1 min, washing it with water for 30 s, subsequent drying, visimetric analysis, and capturing spectral and kinetic characteristics using the “Polyus-M” separator.

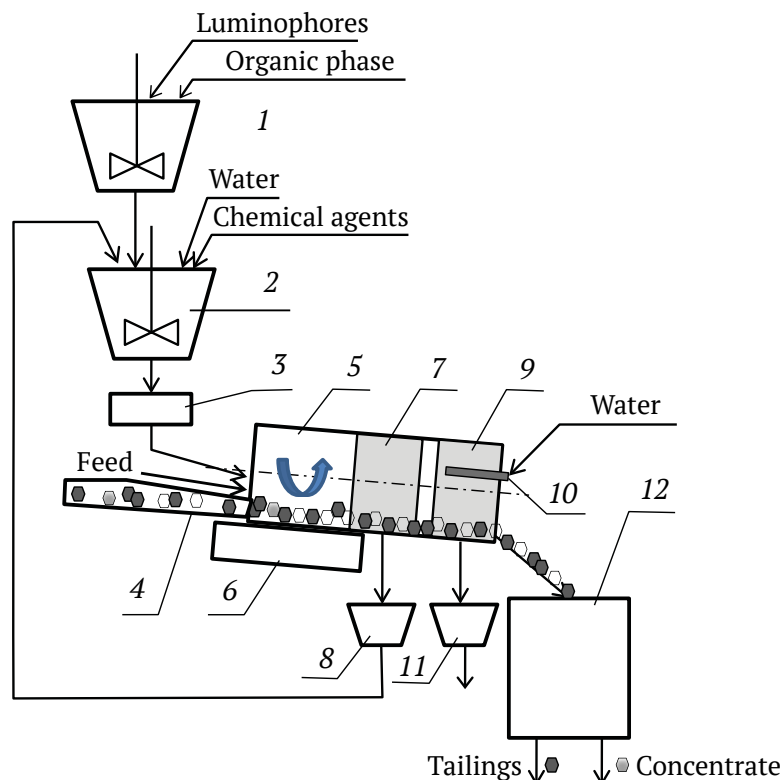


Fig. 1. Diagram of the setup for researching the technology of preparing diamond-containing products for the XRF process using modifying agents, where 1 – composition preparation unit; 2 – emulsion preparation unit; 3 – emulsion heating device; 4 – loading device; 5 – unit for diamond-containing material treatment with emulsion; 6 – roller drive; 7 – perforated section for removal of conditioned emulsion; 8 – emulsion receiver; 9 – perforated section for separation of washing water; 10 – distributor of washing water; 11 – receiver of washing water; 12 – X-ray luminescent separator

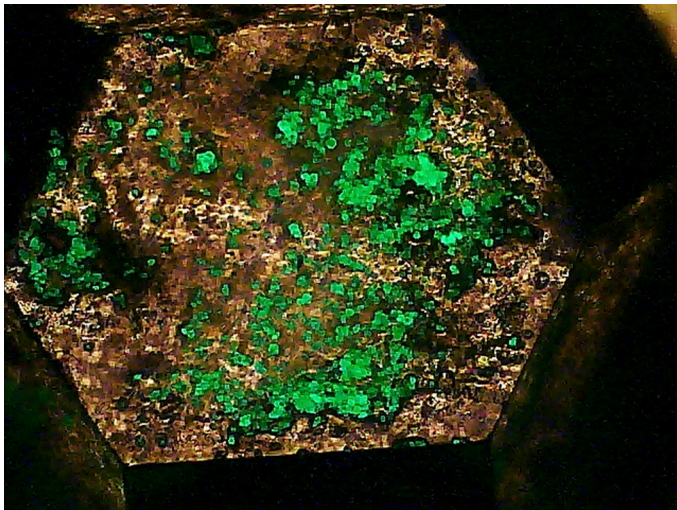
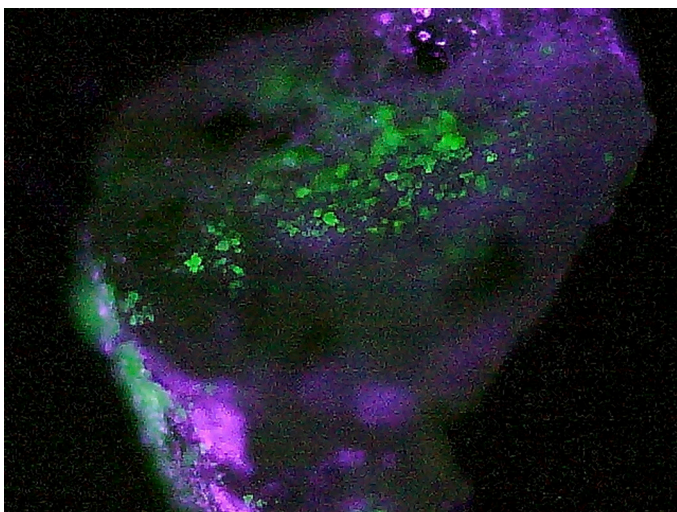
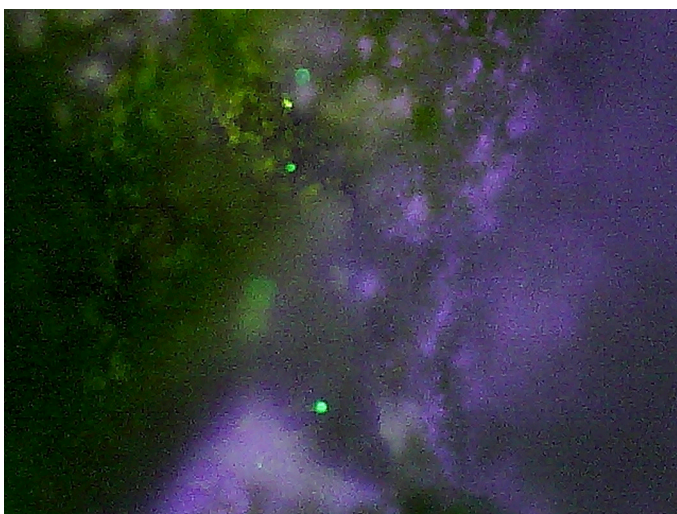
*a**b**c*

Fig. 2. Images in combined illumination of the surface of investigated minerals with attached luminophore (luminophore in green): *a* – synthetic diamond, *b* – natural diamond, *c* – kimberlite grains

The employed setup ensures effective contact between the emulsion and the diamond surface, allowing for the secure fixation of the luminophore composition on it. Our examination of the distribution and attachment of luminophores to the surface of diamond crystals, carried out using the Micromed-3-Lum microscope, revealed that the most pronounced fixation of luminophores was observed in the regions of crystal irregularities, both on synthetic and natural diamonds (Fig. 2, *a, b*). On the surface of kimberlite minerals, we observed the accumulation of luminophores at specific points, attributed to the fixation of an organic collector on naturally hydrophobic minerals (2, *c*).

The primary technological criterion for selecting of luminophore and collector compositions was their ability to confer the necessary spectral and kinetic characteristics upon diamonds for detection. The degree of resemblance between the waveform of the X-ray luminescence signal and that of a natural diamond served as the optimality criterion for a luminophore-containing composition. This criterion is illustrated in the graphs in Fig. 3, which demonstrate that the use of modifying agents with different composition (MLA-1, based on FL-530, and MLA-3, based on E-515-115) results in distinct shapes of the kinetic curves of the X-ray luminescence signal. Notably, within the conditions under consideration, the obtained characteristics closely resemble those of naturally recovered diamonds.

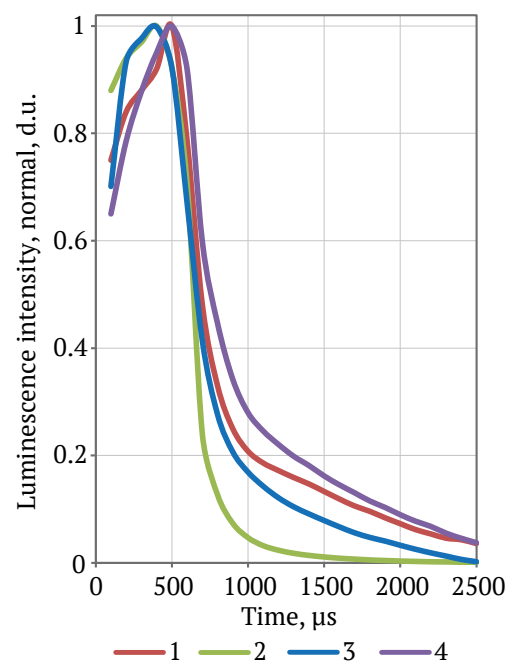


Fig. 3. Spectral and kinetic characteristics of diamonds before and after treatment: *1* and *2* – initial normal and anomalously luminescent diamonds, respectively; *3* and *4* – anomalously luminescent diamonds after treatment with modifying agents MLA-1 and MLA-3, respectively



The selection of luminophores for the studied compositions under study considered the need to alter the spectral characteristics of both types of non-extractable diamonds (weakly and anomalously luminescent). Previous research had indicated the promising potential of luminophores based on zinc orthosilicate, zinc sulfides, and cadmium sulfides for this purpose [6]. In this study, our objective was to validate and assess the effectiveness of the selected modifying agent compositions for the aforementioned categories of non-extractable diamonds.

The results of our investigations into the influence of the used luminophore compositions on the resulting spectral and kinetic characteristics of diamonds are presented in Table 1 and Fig. 4. These findings allowed us to assess the technological feasibility and efficiency of using the main types of modifying agents in the diamond-containing material treatment process preceding the X-ray luminescent separation procedure.

As evident from the provided data, in the case of weakly luminescent diamonds, the best outcomes were observed with the luminophore compositions of

modifying agents MLA-3 and MLA-4, both based on zinc sulfides. This is supported by the diagram in Fig. 3, which indicates that the resulting spectral and kinetic characteristics of weakly luminescent diamonds underwent a significant shift towards the detection range. This shift was attributed to the increased amplitudes of the fast and slow components.

The most favorable outcomes for anomalously luminescent diamonds were observed for MLA-1 and MLA-2 agents (based on zinc orthosilicate). However, the resulting signal form diamonds treated with the MLA-1 agent, particularly concerning the ratio of fast and slow components A_{SC} weakly luminescent diamonds, approaches the boundary of the detection zone (see Fig. 4, line 4).

In scenarios where both types of diamond crystals are simultaneous present in the initial diamond-containing product, the MLA-2 and MLA-3 agents prove to be the most effective for the purposeful modification of diamond luminescent properties. These agents endow the diamonds with spectral and kinetic characteristics that fall within the identification zone of the the detection system (see Fig. 4).

Table 1

Change in spectral and kinetic characteristics of diamonds resulting from treatment with modifying agents of different composition

No.	Mineral	Component	Before treatment	After treatment	Increase	K_A before treatment	K_A after treatment
MLA-1 (FL-530-G3 in CCHGO and BF)							
1	Weakly luminescent diamond	A_{SC}	109	574	465	3.88	1.27
		A_{FC}	423	730	307		
2	Anomalously luminescent diamond	A_{SC}	287	688	401	21.01	9.23
		A_{FC}	6030	6353	323		
MLA-2 (FL-530-G3 and anthracene in a ratio of 25-40 : 1 in CCHGO and BF)							
3	Weakly luminescent diamond	A_{SC}	102	545	443	4.20	2.01
		A_{FC}	428	1095	667		
4	Anomalously luminescent diamond	A_{SC}	287	810	523	21.25	8.66
		A_{FC}	6100	7011	911		
MLA-3 (E-515-115-G5 in CCHGO and BF)							
5	Weakly luminescent diamond	A_{SC}	100	488	388	4.00	4.80
		A_{FC}	400	2340	1940		
6	Anomalously luminescent diamond	A_{SC}	347	720	383	17.64	10.18
		A_{FC}	6120	7330	1210		
MLA-4 (FK-110-G5 in CCHGO and BF)							
7	Weakly luminescent diamond	A_{SC}	110	455	345	3.83	4.29
		A_{FC}	421	1954	1533		
8	Anomalously luminescent diamond	A_{SC}	326	647	321	18.53	10.83
		A_{FC}	6040	7008	968		
MLA-5 (FK-1 in CCHGO and BF)							
9	Weakly luminescent diamond	A_{SC}	109	425	316	3.65	5.09
		A_{FC}	398	2163	1765		
10	Anomalously luminescent diamond	A_{SC}	339	695	256	17.55	10.10
		A_{FC}	5950	7020	1070		

A separate series of studies was dedicated to experimentally substantiate the optimal fractional composition of an organic collector, which would ensure the maximum attachment of a luminophore-containing composition to diamonds. In order to unveil the underlying patterns of how an organic collector with a fractional composition based on CCHGO and BF influences the efficiency of luminophore attachment and aid in the reasonable selection of a chemical agent composition, a set of physicochemical investigation was carried out. This analysis included the measurement of the adhesive activity of the collector as the primary influencing factor. To assess and compare adhesion activity, the results of limiting wetting angle measurements in the diamond – collector drop – aqueous phase system were employed.

An analysis of the research findings revealed that an increase in the proportion of BF in the collector leads to an elevation in the value of the limiting wetting angle, signifying heightened adhesive activity. However, despite this increase in the limiting wetting angle, when the mass fraction of BF in the compound exceeds 15%, there is a decrease in the size of the

collector droplet retained on the diamond surface after the liquid level rises (Table 2).

This result can be mainly attributed to the following factors: a decrease in the viscosity of the collector, resulting in a reduction of the hysteresis effect, and a decrease in density, leading to an increase in detachment force as the liquid level rises.

The extreme pattern of luminophore fixation intensity dependence on the mass fraction of BF in the organic collector correlates with a similar dependence of the size of the retained collector droplet on the mineral surface on the compound composition (see Table 2). The likely explanation for this correlation is the pivotal role played by the amount of organic collector attached to a diamond surface. Pure CCHGO exhibits lower adhesion activity to a diamond surface compared to compounds containing BF, which results to a lower quantity of fixed compound and, consequently, a reduced amount of luminophore on the diamond. Increasing the proportion of BF in the collector beyond 15% leads to reduced detachment from the diamond surface. This reduction can be attributed to the increasing density difference relative to the aque-

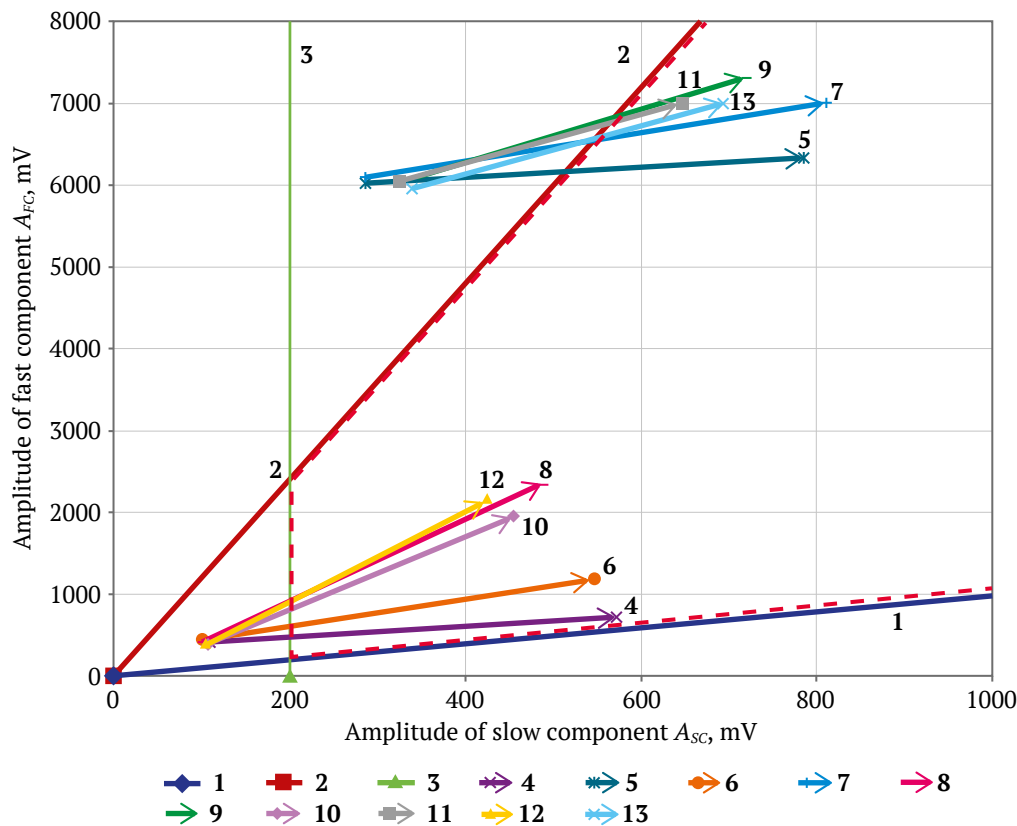


Fig. 4. Diagram showing changes in amplitude spectral and kinetic characteristics of non-extractable diamonds after treatment with luminophore-containing modifying agents: 1 – lower boundary of the positive diamond identification area based on K_A ; 2 – upper boundary of the positive diamond identification area based on K_A ; 3 – boundary of the positive diamond identification area based on A_{SC} ; 4, 6, 8, 10, 12 – shifting characteristics of weakly luminescent diamonds; 5, 7, 9, 11, 13 – shifting characteristics of anomalously luminescent diamonds after treatment: 4, 5 – MLA-1; 6, 7 – MLA-2; 8, 9 – MLA-3; 10, 11 – MLA-4; 12, 13 – MLA-5; [red dashed box] – area of positive identification (detection)

ous phase (with a density of BF at 0.867 g/cm³, while CCHGO has a density of 0.965 g/cm³, and water has a density of 1 g/cm³), as well as a decrease in viscosity (by 45–58%), which reduces the hysteresis stability of mineral – collector aggregates in a turbulent medium.

2. Selection of conditions for increasing the selectivity of luminophore attachment to diamonds and kimberlite mineral surfaces

To address the challenge of increasing the selectivity of luminophore attachment to diamond surface, we conducted a study involving agents from various groups, including polyphosphates, silicates, natural organic polymers, and lignosulfonates. These agents are known to hinder the fixation of apolar and weakly polar reagents on hydrophobic minerals [13, 14]. We also carried out experimental investigations to substantiate and select of parameters of the aqueous phase in the modifying agent emulsion (pH of the medium, mineralization, Eh) to facilitate the more selective fixation of apolar and weakly polar reagents on minerals [15, 16].

In the current research, the use of surfactants (alkyl sulfates, alkyl sulfonates) for dispersing the organic phase of the modifying agent is grounded in their mechanism of action on the properties of the diamond surface. According to principles in solution physicochemistry, heteropolar surfactant molecules adsorb at the interfaces of diamond-water and collector-water, aligning their apolar radicals with the hydrophobic phase and their polar groups with the aqueous phase. This results in a reduction of interfacial surface tension at both solid-liquid and water-collector interfaces. As per Young's equation [17] this leads to a decrease in the limiting wetting angle, indicating that the solid surface becomes better wetted by the surfactant solution compared to pure water. Experimental evidence supported this effect in the mineral – organic collector – aqueous phase system, where the additions of alkyl sulfonates was found to reduce the hydrophobicity of a mineral surface (Fig. 5, a) [18]. In contrast, for hydrophilic minerals, due to the reverse orientation of surfactant

Table 2

Variation of physicochemical characteristics and efficiency of organic collector attachment to diamonds with varying collector fractional composition

No.	BF fraction in compound collector	Limiting wetting angle, deg	Density, g/cm ³	Dynamic viscosity measured, mPa s, 24 °C	Average size of a drop on diamond, mm	Surface concentration of luminophore, %
1	0 (CCHGO only)	85	965.0	167.0	1.5	16.9
2	5	87.5	961.1	154.5	1.65	21.7
3	10	90.0	957.2	133.0	1.62	24.4
4	15	92.0	951.3	110.3	1.33	24.5
5	20	93.3	947.4	92.1	0.96	22.1
6	25	94.3	942.5	72.0	0.75	20.4
7	30	95.0	937.6	64.1	0.65	18.6
8	100	97.5	867.0	3.64	0.4	15.5

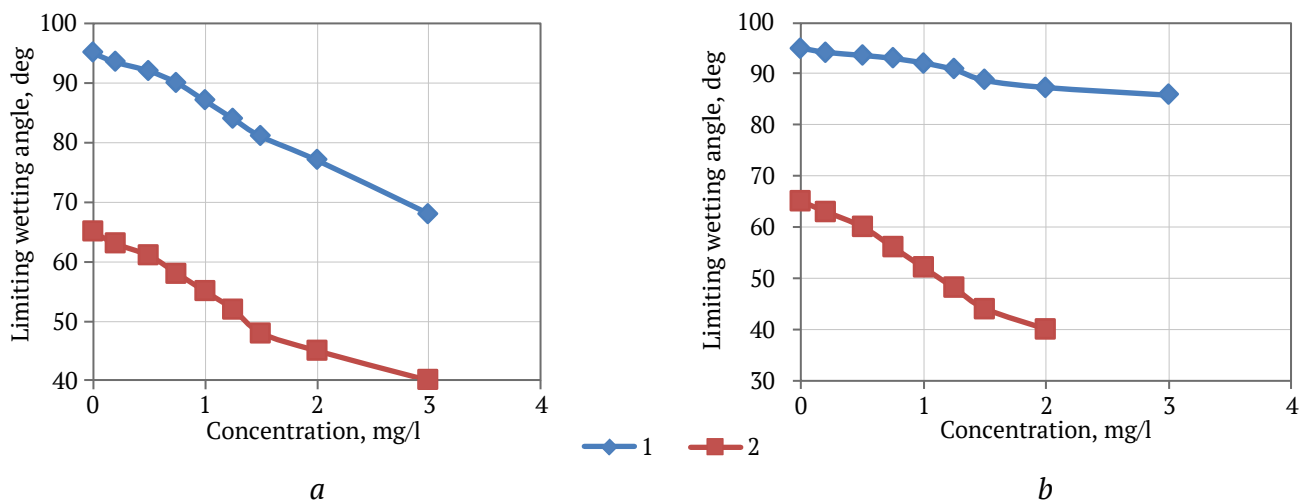


Fig. 5. Influence of alkyl sulfate (a) and hexametaphosphate (b) concentrations on limiting wetting angles of diamond (1) and phlogopite (2)

molecules, there is a possibility of surface hydrophobization [19]. This is a detrimental factor as it increases the oleophilicity of kimberlite minerals, thereby promoting the attachment of the luminophore-containing composition to them.

Polyphosphates exert a distinct influence on the mineral – aqueous phase – collector disperse system. The basis of polyphosphates action is their attachment to the surface of naturally hydrophilic minerals through a cation exchange mechanism, forming strong chemical bond with divalent cations (e. g., calcium, iron, magnesium) of a mineral [20, 21]. The effective action of sodium polyphosphate can also be attributed to the intensive adsorption of polyphosphate ions at the boundary of silicon-oxygen tetrahedra layers (e.g., natural hydrophobic layered aluminosilicates). This is due to the structural and size similarity between tripolyphosphate anions and the silicon-oxygen tetrahedra of clay minerals [22]. Additionally, polyphosphates enable the hydrophilization of phosphate mineral's surfaces.

The results of the studies revealed a fundamentally different effect of hexametaphosphate on the surface properties of minerals compared to alkyl sulfates. While there is a much smaller reduction in the value of the limiting wetting angle on diamonds, an intense hydrophilization of the phlogopite surface is observed instead (Fig. 5, b). Notably, the addition of hexametaphosphate does not lead to hydrophobization and an increase in oleophilicity of naturally hydrophilic kimberlite minerals (there is no detachment of organic liquid from the minerals).

Organic polymers, such as carboxymethylcellulose (CMC), exhibit significant over both diamond

surfaces and hydrophobic kimberlite minerals. This results in a substantial decrease in the limiting wetting angle (by 10–23°) on these minerals as the agent concentration increases to 3 g/L (Fig. 6, a). Chemical agents from the alkylphosphonate group show promise. Limiting wetting angle measurements indicate that within the concentration range of 0 to 1 g/L, these chemical agents (e.g., oxyethylene diphosphonic acid – OEDP) substantially reduce the hydrophobicity (oleophilicity) of phlogopite, with a relatively smaller change in the condition of the diamond surface (Fig. 6, b). This characteristic can be attributed in many ways to the formation of coordination bonds between the agent anions and Ca and Mg cations in the crystal lattice of the minerals.

The results obtained lead to the conclusion and confirmation on the feasibility of employing dispersing agents that lack a prominent apolar radical in their structure and interact with kimberlite minerals through the formation of chemical or coordination bonds.

Laboratory testing of the selected dispersing agents demonstrate their effectiveness. The optimal outcomes, marked by the highest selectivity of luminophore attachment at an agent consumption of 1.5 g/L, were achieved with oxyethylene diphosphonic acid (OEDP), hexametaphosphate, metasilicate, and sodium tripolyphosphate (Table 3).

The attachment selectivity was calculated using the following equation:

$$SLF_{DK} = \frac{C_{LD}}{15} - \frac{C_{LK}}{3}.$$

The designations of the variables in the equation are given in Table 3.

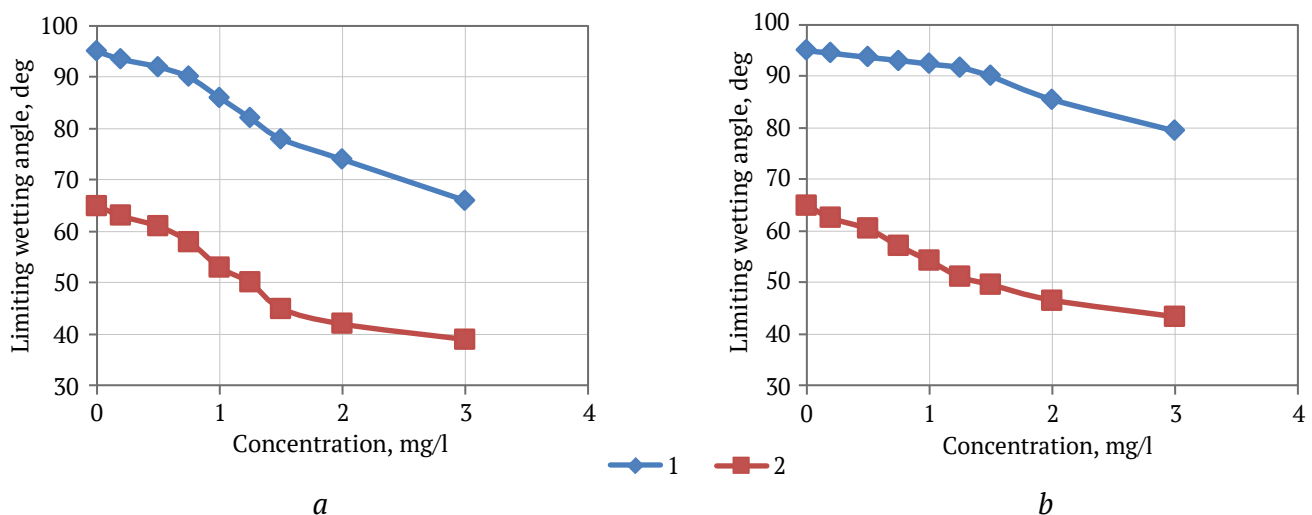


Fig. 6. Influence of CMC concentration (a) and OEDP concentration (b) on the limiting wetting angle of diamond (1) and phlogopite (2) in the aqueous phase of the modifying agent emulsion



3. Selection of temperature conditions for treating diamond-containing products with modifying agents

The temperature of the medium used in the process of preparing and treating diamond-containing material with modifying agent significantly influences the intensity and selectivity of luminophore attachment to the surfaces of both diamonds and kimberlite minerals. This influence is primary due to alterations in the physical and chemical properties of the complex composition organic liquids, which are petroleum-based products [23]. The medium's temperature impacts various aspects, including interface energy and wettability of minerals in dispersed systems, the viscosity properties of a collector, its ability to spread over surface, and the stability of attachment in turbulent media [24, 25].

In order to determine the optimal temperature conditions, studies were conducted involving the

treatment of diamond-bearing kimberlite products with emulsions of modifying agents, employing petroleum products of varying fractional composition as collectors.

The efficiency of luminophore attachment was assessed based on the surface concentration of the attached luminophors, which was determined using visiometric methods. Unlike the studies described in [17], the treated diamond-mineral product was subsequently subjected to X-ray luminescence separation using a "Polyus-M" separator. The study results confirmed that increasing the treatment temperature from 15 °C to 40 °C enhanced luminophore attachment to both diamonds and kimberlite minerals for all organic collector compositions (Table 4). However, it was observed that when the medium temperature exceeded 40 °C, the efficiency of luminophore attachment to diamonds slightly decreases.

Table 3

Impact of dispersing agents on surface concentration and selectivity of luminophore attachment to the surface of diamonds and kimberlite minerals

No.	Dispersing agent	Concentration of luminophore on diamond surface (C_{LD}), %		Concentration of luminophore on kimberlite mineral surface (C_{LK}), %		Attachment selectivity, SLF_{DK} , decimal quantity	
		Agent concentration, g/l					
		0	1.5	0	1.5	0	1.5
1	Tripolyphosphate	38	21.8	7.5	1.5	0.03	0.95
2	Hexametaphosphate	39.3	23.5	7	1.6	0.29	1.03
3	OEDP (etidronic acid)	38.3	25.5	7.1	1.9	0.19	1.07
4	Corn starch	38	20.4	6.9	2.2	0.23	0.63
5	CMC	37.4	18.5	6.7	1.8	0.26	0.63
6	Sulfonol	37.8	19.5	7.1	1.8	0.15	0.70
7	Sodium metasilicate	39.4	22.5	7.9	2.1	-0.01	0.80
8	Lignosulfonate	38.9	20.3	7.6	2.2	0.06	0.62

Table 4

Results of visiometric analysis of the temperature effect on the efficiency of luminophores attachment to the surface of diamonds and kimberlite minerals

No.	Composition of organic collector	Temperature, °C					
		20	25	30	35	40	45
		Covering of diamond surface with luminophore, %					
3	CCHGO (85%) BF (15%)	17.4	28.4	33	34.1	36.2	35.7
		Kimberlite minerals surface covering with luminophore, %					
6	CCHGO (85%) BF (15%)	2.4	2.6	2.8	2.9	3.2	3.5
		Attachment selectivity, conditional units.					
9	CCHGO (85%) BF (15%)	0.43	1.03	1.27	1.31	1.35	1.21
		Diamond recovery, %					
12	CCHGO (85%) BF (15%)	80	85	90	95	95	95
		Kimberlite recovery, %					
15	CCHGO (85%) BF (15%)	1.0	1.1	1.3	1.3	1.3	1.3

Notes: CCHGO is catalytic cracking heavy gas oil; BF is bunker fuel or technical grade diesel fraction.



The analysis of the data for calculating luminophore attachment selectivity indicates that the highest selectivity in attaching luminophore to both diamonds and kimberlite occurs when the treatment temperature ranges from 30 to 45 °C. The analysis of the results from X-ray fluorescence separation of the diamond-containing kimberlite product confirmed the findings from the visimetric analysis and demonstrated the feasibility of achieving maximum diamond recovery within the temperature range of 30 to 45 °C (see Table 4) without a significant increase in kimberlite recovery. Based on these results, it is recommended to conduct the treatment of diamond-containing products at elevated temperature.

4. Selecting the agent emulsion component composition for modifying spectral and kinetic characteristics of diamonds

The key technological parameters of the selective modification regimes for the spectral and kinetic characteristics of diamonds include the following characteristics of the modifying agent: the luminophore -to- collector ratio; the collector -to- aqueous phase ratio, and the concentration of the dispersing agent. Recognizing the potential interplay among these factors and the need to identify the optimal modifying agent composition, a second-order factorial experiment method was employed. The initial factorial experiment matrix (second-order orthogonal central composite design) was constructed following standard procedures, with the inclusion of zero and star points [26]. This experimental design encompassed 15 trials.

Mathematical analysis of experimental results, conducted in Excel, facilitated the determination of the region with optimal relationships between the components of the MLA-3 modifying agent within the emulsion process. A water : collector ratio of 90:1. Was chosen as optimal, alongside an optimal concentration of 1.5 g/L for HMF (Fig. 7). The collector-to-luminophore ratio was set at 9:1. These selected parameters closely align with values derived from prior laboratory studies and used as coordinates at the center of the matrix (60:1, 10:1, and 1.5 g/L).

The results demonstrated that the application of an aqueous emulsion of modifying agents, namely MLA-1 based on FL-530-G3-G5 luminophore and MLA-3 based on E-515-115-G5 luminophore, with the selected parameters for the component composition of the modifying agent emulsion using sodium hexametaphosphate as a dispersing agent, brings about the desired alterations in the spectral and kinetic characteristics of weakly and anomalously luminescent diamonds (Table 5).

The findings from tests carried out at a Polyus-M separator showed the high efficiency of the developed modifying agents and treatment protocols for diamond-kimberlite products. This allowed for the recovery of 80–95% of weakly and anomalously luminescent diamonds into the X-ray luminescence separation concentrate, without a significant increase in the recovery of kimberlite into the concentrate (see Table 5).

Thus, the research results validate the effectiveness of the chosen technology for preparing diamond-containing products for the XRF process and enable the determination of the optimal composition of a modifying agent and the parameters for the treatment of diamond-containing kimberlite products.

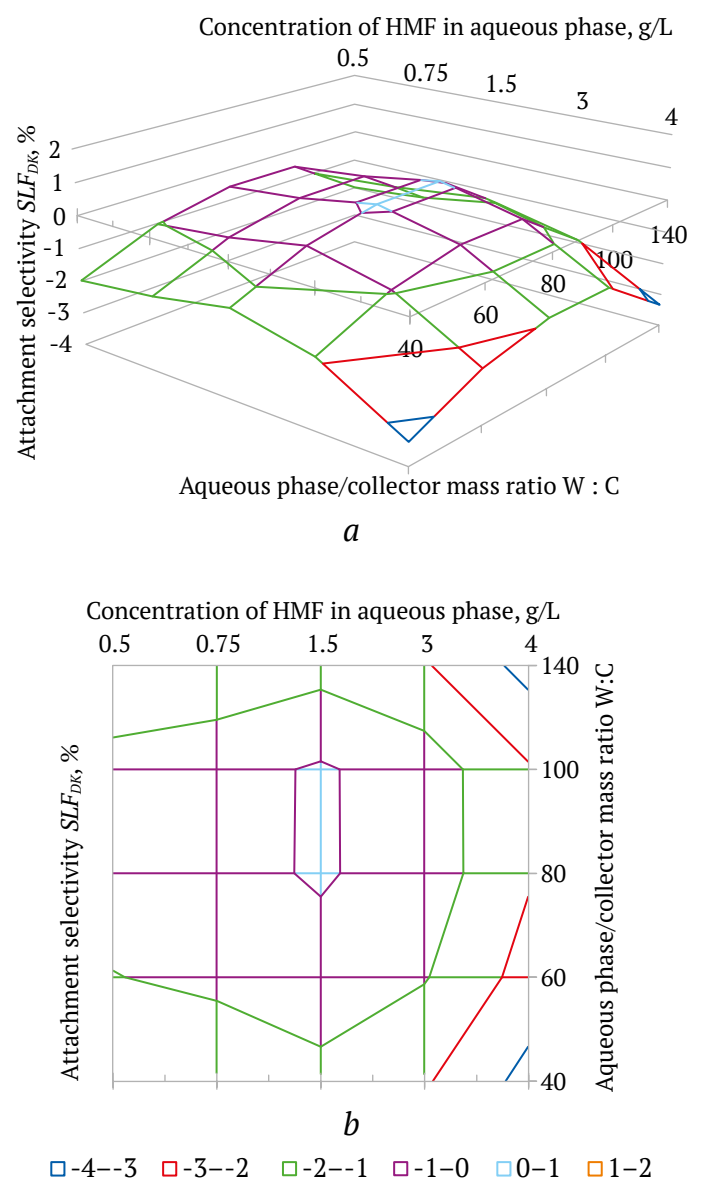


Fig. 7. 3D graphs (a) and cross-sections (b) depicting the relationships between selectivity of luminophore attachment (SLF_{DK}) and the mass ratio of aqueous phase to the collector (W:C) and hexametaphosphate (HMF) concentration



Table 5

Testing results of luminophore-based modifying agents FL-530 (MLA-1) and E-515-115 (MLA-3) for diamond-bearing kimberlite products

No.	Modifying agent composition	Mineral	Sv	τ_z , ms	A_{SC} , mV	$A_{FC} - A_{air}$, mV	K_A	Recovery, %
1	Without luminophores	Diamond (w)	0.15	4.3	120	564	5.7	40
		Diamond (an)	–	0.1	not measured	1,022	≥ 50	20
		Kimberlite	–	–	not measured	<50	–	0.75
2	MLA-1 (FL-530 + CCHGO + BF)	Diamond (w)	0.22	1.6	329	1,216	4.7	80
		Diamond (an)	0.17	0.6	275	1,469	6.3	90
		Kimberlite	–	–	not measured	<50	–	0.9
3	MLA-3 (E-515-115-G5 + CCHGO + BF)	Diamond (w)	0.26	2.3	258	1105	5.0	95
		Diamond (an)	0.18	0.5	168	1465	9.9	90
		Kimberlite	–	–	not measured	<50	–	0.5
4	Parameters of XRF selective regime	Diamond	0.1–1	0.1–10	More than 100	–	0.2–12	Recovery

Notes: w, an – are weakly and anomalously luminescent diamonds, respectively, A_F is amplitude of fast component of air X-ray luminescence signal (background); not measured – values were not measured.

Conclusions

The effective composition and application conditions of modifying agents in the preparation of diamond-containing material for X-ray luminescence separation have been determined based on the research findings.

The feasibility of purposeful modification of the spectral characteristics of weakly and anomalously luminescent diamonds, coexisting in diamond-containing material, has been established through the use of luminophores based on zinc orthosilicate and zinc sulfides (MLA-1 and MLA-3). These luminophores provide diamond crystals with spectral and kinetic characteristics that fall within the identification zone of the detection system.

The composition of the diamond collector (85% CCHGO and 15% BF) in the luminophore-containing compound, as well as the temperature treatment conditions (30–45 °C) for the diamond-containing product, were selected to ensure intensive and selective attachment of luminophores to the surface of diamond crystals.

The results of mathematical processing, using the criterion of luminophore-containing emulsion

attachment selectivity to diamonds and kimberlite minerals, calculated based on the measured surface concentrations of luminophores on these minerals, have allowed the determination of the optimal component ratios in the modifying agent emulsion. These ratios are as follows: water:collector = 90:1, collector:luminophore = 9:1, with a concentration of HMF at 1.5 g/l.

Dispersing agents (oxyethylene diphosphonic acid, hexametaphosphate, metasilicate, and sodium tripolyphosphate) were selected to ensure selective attachment of luminophores to diamonds through weakening the attachment of luminophores to the surface of kimberlite minerals.

The results from the tests carried out at a Polyus-M separator have confirmed the high efficiency of the modifying agents with the developed composition and application conditions for treating diamond-containing material. This process enables the recovery of low and anomalously luminescent diamonds into the X-ray luminescence separation concentrate at a level of 80–95%, without increasing the recovery of kimberlite minerals into the concentrate.

References

1. Mironov V.P. Optical spectroscopy of diamonds from concentrates and tailings of X-ray luminescence separation. *Nauka i Obrazovaniye*. 2006;(1)31–36. (In Russ.)
2. Martynovich E.F., Mironov V.P. X-ray luminescence of diamonds and its use in the diamond mining industry. *Izvestiya vuzov. Fizika*. 2009;52(12/3):202–210. (In Russ.)



3. Chanturia V.A., Dvoichenkova G.P., Morozov V.V. et al. Selective attachment of luminophore-bearing emulsion at diamonds-mechanism analysis and mode selection. *Journal of Mining Science*. 2020;56(1):96–103. <https://doi.org/10.1134/S1062739120016527> (Orig. ver.: Chanturia V.A., Dvoichenkova G.P., Morozov V.V. et al. Selective attachment of luminophore-bearing emulsion at diamonds-mechanism analysis and mode selection. *Fiziko-Tekhnicheskiye Problemy Pererabotki Poleznykh Iskopayemykh*. 2020;(1):104–113. (In Russ.) <https://doi.org/10.15372/FTPRPI20200111>)
4. Morozov V.V., Chanturia V.A., Dvoichenkova G.P., Chanturia E.L. hydrophobic interactions in the diamond–organic liquid–inorganic luminophore system in modification of spectral and kinetic characteristics of diamonds. *Journal of Mining Science*. 2022;58(2):257–266. <https://doi.org/10.1134/s1062739122020090> (Orig. ver.: Morozov V.V., Chanturia V.A., Dvoichenkova G.P., Chanturia E.L. hydrophobic interactions in the diamond–organic liquid–inorganic luminophore system in modification of spectral and kinetic characteristics of diamonds. *Fiziko-Tekhnicheskiye Problemy Pererabotki Poleznykh Iskopayemykh*. 2022;(2):94–104. (In Russ.) <https://doi.org/10.15372/FTPRPI20220209>)
5. Podkamennyi Yu.A., Makalin I.A. Substantiation of the collection of spectral-kinetic parameters of x-ray luminescent separators for selective extraction of diamond crystals. In: *Problems of Integrated and Environmentally Safe Processing of Natural and Technogenic Mineral Raw Materials (Plaksin Readings – 2021)*. Vladikavkaz: North Caucasus Mining and Metallurgical Institute (State Technological University); 2021. Pp. 341–345. (In Russ.)
6. Kondratyev S.A. Effect of Apolar Reagents and Surfactants on the Stability of a Flotation Complex *Journal of Mining Science*. 2000;36(4):399–407. <https://doi.org/10.1023/A:1026697811202>
7. Pentin Yu.A., Vilkov L.V. *Physical research methods in chemistry*. Moscow: Mir Publ. House; 2003. (In Russ.)
8. Gonzales R.C., Woods R.E., Eddins S.L. *Digital image processing using MATLAB*. Prentice Hall; 2004. (Transl. ver.: Gonzales R., Woods R., Eddins S. *Digital image processing using Matlab*. Moscow: Tekhnosfera; 2006. 616 p. (In Russ.))
9. Gorobets B.S., Rogozhin A.A. *Luminescence spectra of minerals*. Moscow: Publishing House of the All-Union Institute of Mineral Raw Materials; 2001. 316 p. (In Russ.)
10. Huhtamäki T., Tian X., Korhonen J.T., Ras R.H.A. Surface-wetting characterization using contact-angle measurements. *Nature Protocols*. 2018;13:1521–1538. <https://doi.org/10.1038/s41596-018-0003-z>
11. Separator “Polyus-M”. Passport and operating instructions. Saint Petersburg: JSC “Burevestnik”; 2015.
12. Mironov V.P., Emelyanov A.S., Shabalin S.A. et al. X-Ray luminescence in diamonds and its application in industry. In: *Luminescence and Laser Physics: XVII International Conference on Luminescence and Laser Physics – LLPh 2019*. 1–6 July, 2019. Irkutsk, Russia. 2021;2392(1):020010. <https://doi.org/10.1063/5.0061972>
13. Liu L., Cheng G., Yu W., Yang Ch. Flotation collector preparation and evaluation of oil shale. *Oil Shale*. 2018;35(3):242–251. <https://doi.org/10.3176/oil.2018.3.04>
14. Morozov V.V., Kovalenko E.G., Dvoichenkova G.P., Chut-Dy V.A. Selection of temperature regimes for conditioning and flotation of diamond-bearing kimberlite with compound collectors. *Mining Science and Technology (Russia)*. 2022;7(4):287–297. <https://doi.org/10.17073/2500-0632-2022-10-23>
15. Verkhoturova V., Elshin I., Nemarov A., Tolstoy M. et al. Scientific justification and optimum alternative selection to recover hydrophobic properties of diamond surface from “International” tube ore. *Proceedings of Irkutsk State Technical University*. 2014;(8):51–56. (In Russ.)
16. Avdokhin V.M., Chernysheva E.N. Modern technologies of diamond-containing kimberlites enrichment. *Mining Information and Analytical Bulletin*. 2010;(S1):465–477.
17. Adamson A.W. *Physical chemistry of surfaces*. New York: Wiley; 1976. 698 p. (Transl. ver.: Adamson A. *Physical chemistry of surfaces*. Moscow: Mir Publ. House; 1979. 568 p. (In Russ.))
18. Srdjan M. Bulatovic, in *Handbook of Flotation Reagents: Chemistry, Theory and Practice* i 2007. Elsevier, 458 p. <https://doi.org/10.15372/FTPRPI20230311>
19. Somasundaran P., Zhang L. Adsorption of surfactants on minerals for wettability control in improved oil recovery processes. *Journal of Petroleum Science and Engineering*. 2006;52(1–4):198–212. <https://doi.org/10.1016/J.PETROL.2006.03.022>
20. Lee H., Lim H.-K., Kim H. Hydration Thermodynamics of non-polar aromatic hydrocarbons: comparison of implicit and explicit solvation models. *Molecules*. 2018;23(11):2927. <https://doi.org/10.3390/molecules23112927>
21. Afanasova A.V., Aburova V.A., Prokhorova E.O., Lushina E.A. Investigation of the influence of depressors on flotation-active rock-forming minerals in sulphide gold-bearing ore flotation. *Mining Information and Analytical Bulletin*. 2022;(6–2):161–174. (In Russ.) https://doi.org/10.25018/0236_1493_2022_62_0_161



22. Chmielewská E., Hodossyová R., Kovaľáková M., Urík M. Comparable phosphate adsorption onto some natural aluminosilicates vs. Fe(III)oxihydroxide. *Desalination and Water Treatment*. 2016;(16):7387–7395. <https://doi.org/10.1080/19443994.2015.1017008>

23. Tumanyan B.P. *Scientific and applied aspects of the theory of oil dispersed systems*. Moscow: Technika; 2000. 336 p.

24. Polezhaeva N.I. *Physico-chemistry of petroleum dispersed systems. Thermodynamics and kinetics of phase transitions in petroleum dispersed systems*. Krasnoyarsk: Sibgau named after M.F. Reshetnev; 2021. 94 p. (In Russ.)

25. Zemtsov Yu.V., Mazaev V.V. *The current state of physico-chemical methods of increasing oil recovery: a literary and patent review*. Yekaterinburg: Publishing Solutions LLC; 2021. 240 p. (In Russ.)

26. Lunev V.A. *Mathematical modeling and experimental planning*. St. Petersburg: Publishing House of the Polytechnic University; 2012. 153 p. (In Russ.)

Information about the authors

Valentin A. Chanturiya – Dr. Sci. (Eng.), Professor, Academician of the Russian Academy of Sciences, Research Institute of Comprehensive Exploitation of Mineral Resources of the Russian Academy of Sciences, Moscow, Russian Federation; ORCID [0000-0002-4410-8182](https://orcid.org/0000-0002-4410-8182), Scopus ID [7004497128](https://scopus.com/authorid/7004497128); e-mail vchan@mail.ru

Valeriy V. Morozov – Dr. Sci. (Eng.), Professor of the Department of General and Inorganic Chemistry, Research Institute of Comprehensive Exploitation of Mineral Resources of the Russian Academy of Sciences, Moscow, Russian Federation; ORCID [0000-0003-4105-944X](https://orcid.org/0000-0003-4105-944X), Scopus ID [7402759618](https://scopus.com/authorid/7402759618)

Galina P. Dvoichenkova – Dr. Sci. (Eng.), Leading Researcher, Research Institute of Comprehensive Exploitation of Mineral Resources of the Russian Academy of Sciences, Moscow, Russian Federation; ORCID [0000-0003-3637-7929](https://orcid.org/0000-0003-3637-7929), Scopus ID [8837172700](https://scopus.com/authorid/8837172700); e-mail dvoigp@mail.ru

Yuri A. Podkamennyi – Dr. Sci. (Eng.), Researcher, Research Institute of Comprehensive Exploitation of Mineral Resources of the Russian Academy of Sciences, Moscow, Russian Federation; ORCID [0000-0002-4104-9113](https://orcid.org/0000-0002-4104-9113), Scopus ID [57209793744](https://scopus.com/authorid/57209793744)

Aleksandr S. Timofeev – Leading Researcher, Research Institute of Comprehensive Exploitation of Mineral Resources of the Russian Academy of Sciences, Moscow, Russian Federation; ORCID [0000-0002-3382-6007](https://orcid.org/0000-0002-3382-6007), Scopus ID [57191282007](https://scopus.com/authorid/57191282007)

Received 06.09.2023

Revised 16.09.2023

Accepted 10.10.2023



SAFETY IN MINING AND PROCESSING INDUSTRY AND ENVIRONMENTAL PROTECTION

Research paper

<https://doi.org/10.17073/2500-0632-2023-07-129>

УДК 502.3.7



Assessment of performance and environmental friendliness of a sorbent-based remediation method for heavy metal and metalloid contaminated soils

V. V. Yurak^{1,2}   , R. A. Apakashev¹  , M. S. Lebzina¹  , A. N. Malyshev¹  ¹ Ural State Mining University, Yekaterinburg, Russian Federation² Institute of Economics, Ural Branch of the Russian Academy of Sciences, Yekaterinburg, Russian Federation vera_yurak@mail.ru

Abstract

The contamination of natural ecosystems with heavy metals and metalloids (HMMs) primarily results from anthropogenic activities. Consequently, ongoing efforts are dedicated to the development of technologies aimed at restraining the mobility of HMMs and expediting chemical reactions that convert pollutants from mobile to immobile states. Addressing the reclamation issue always necessitates the selection of the most promising and effective type of reclamation work, as well as justification of land prioritization for reclamation purposes. In terms of performance and future potential, the sorbent-oriented approach, grounded in the concept of “green” utilization of man-made waste as a raw material for creating novel composite sorbents, is gaining traction for land reclamation in disturbed areas. In international practice, diverse environmental risk assessment methods are employed to substantiate the necessity for and prioritize reclamation efforts.

The aim of the present study is to evaluate established conventional methods for assessing the risks associated with environmental harm. Additionally, this research aims to assess the efficacy and ecological compatibility of the composite sorbents developed by the author. This evaluation will be conducted by assessing and comparing the levels of potential environmental risks or risks of environmental damage subsequent to the application of these sorbents.

The objectives of this study are as follows: 1) to explore the theoretical aspects of HMMs: including the formulation of a definition, investigation onto the origins of HMMs, examination of HMMs’ toxicity, and identification of prevalent methods for evaluating the environmental risks associated with HMMs; 2) to evaluate the effectiveness of established methods for assessing the environmental risks posed by HMMs; 3) to assess the efficacy and environmental sustainability of the composite sorbents developed by the author. This evaluation will involve an examination and comparison of the levels of potential environmental risks and the risks of environmental damage subsequent to the application of these sorbents.

The research subject: the mining allotment within the Levikhinskoye mine (classified as an environmental disaster site) is investigated as a disturbed land ecosystem, encompassing industrial waste dumps containing HMMs.

The research hypothesis aims to establish the viability of “green” waste utilization from industrial sources as a raw material for composite sorbents used in land reclamation, without escalating the environmental damage. The conducted experiments revealed that sorbents composed of peat/water treatment sludge (at a ratio of 20/80 wt. % with natural moisture content) and peat/diatomite/water treatment sludge (at a ratio of 5/15/80 wt. % with natural moisture content) exhibited the highest level of performance, surpassing an overall efficiency of 89%. A sorbent composed of peat/diatomite (at a ratio of 25/75 wt. % with natural moisture content) demonstrated an overall efficiency of 67.7%. The estimated environmental risks (*ER* and *ED*) after the application of the proprietary composite sorbents, which include water treatment sludge, exhibited an average reduction of 89.5% and 88%, respectively.

Keywords

sorbents, reclamation, disturbed lands, environmental risks, methods, assessment, “green” disposal, heavy metals and metalloids, biota, toxicity, environmental damage

Acknowledgments

The study was carried out at the expense of grant of the Russian Science Foundation No. 22-24-20102 with the financial support of the Government of the Sverdlovsk Region.

For citation

Yurak V.V., Apakashev R.A., Lebzina M.S., Malyshev A.N. Assessment of performance and environmental friendliness of a sorbent-based remediation method for heavy metal and metalloid contaminated soils. *Mining Science and Technology (Russia)*. 2023;8(4):327–340. <https://doi.org/10.17073/2500-0632-2023-07-129>



ТЕХНОЛОГИЧЕСКАЯ БЕЗОПАСНОСТЬ В МИНЕРАЛЬНО-СЫРЬЕВОМ КОМПЛЕКСЕ И ОХРАНА ОКРУЖАЮЩЕЙ СРЕДЫ

Научная статья

Оценка эффективности и экологичности сорбент-ориентированного метода восстановления загрязненных тяжелыми металлами и металлоидами почв

В. В. Юрак^{1,2}   , Р. А. Апакашев¹  , М. С. Лебзин¹  , А. Н. Малышев¹  

¹ Уральский государственный горный университет, г. Екатеринбург, Российская Федерация

² Институт экономики УрО РАН, г. Екатеринбург, Российская Федерация

 vera_yurak@mail.ru

Аннотация

Загрязнение природных экосистем тяжелыми металлами и металлоидами (НММ) – это главным образом результат антропогенной деятельности. Именно поэтому в настоящее время разрабатываются технологии, направленные на ограничение подвижности НММ и уменьшение сроков протекания химических реакций по переводу поллютантов из подвижной в неподвижную форму. Решение проблемы рекультивации всегда предполагает выбор наиболее перспективного и эффективного вида рекультивационных работ, а также обоснование приоритизации земель, подлежащих рекультивации. В части эффективности и перспективности популярность приобретает сорбент-ориентированный метод, основанный на принципе «зеленой» утилизации техногенных отходов в качестве сырья для создания композитных сорбентов нового типа в целях рекультивации нарушенных земель. Зарубежная практика в качестве обоснования необходимости и приоритизации рекультивационных работ использует различные методики оценки экологических рисков. **Цель** текущего исследования – апробировать имеющиеся распространенные методики оценки рисков причинения экологического ущерба и оценить эффективность и «экологичность» разрабатываемых авторских композитных сорбентов с позиции оценки и сравнения уровней возникновения потенциальных экологических рисков/рисков нанесения экологического ущерба после их (сорбентов) применения.

Задачи: 1) рассмотреть теоретические аспекты НММ: сформулировать определение, рассмотреть генезис НММ, исследовать вопрос токсичности НММ и выявить наиболее распространенные методики оценки экологических рисков НММ; 2) апробировать имеющиеся методики оценки экологических рисков НММ; 3) оценить эффективность и «экологичность» разрабатываемых авторских композитных сорбентов с позиции оценки и сравнения уровней возникновения потенциальных экологических рисков/рисков нанесения экологического ущерба после их (сорбентов) применения.

Объект исследования: горный отвод Левихинского рудника (зона экологического бедствия) как экосистема нарушенных земель, в составе которой присутствуют промышленные отвалы, содержащие НММ.

Гипотеза исследования: доказать возможность «зеленой утилизации» техногенных отходов в качестве сырья для композитных сорбентов, используемых для рекультивации нарушенных земель, без увеличения рисков причинения экологического ущерба природной среде. В результате проведенных экспериментов наибольшую эффективность продемонстрировали сорбенты торф/осадки водоподготовки (пропорция при естественной влажности: 20/80, %), торф/диатомит/осадки водоподготовки (пропорция при естественной влажности: 5/15/80, %), где суммарная эффективность превышала 89 %. У сорбента торф/диатомит (пропорция при естественной влажности: 25/75, %) наблюдается суммарная эффективность 67,7 %. Оцениваемые риски *ER* и *EH* после применения авторских композитных сорбентов, в состав которых входят осадки водоподготовки, снижались в среднем на 89,5 и 88 % соответственно.

Ключевые слова

сорбенты, рекультивация, нарушенные земли, экологические риски, методики, оценка, «зеленая» утилизация, тяжелые металлы и металлоиды, биота, токсичность, экологический ущерб

Благодарности

Исследование выполнено за счет гранта Российского научного фонда № 22-24-20102, при финансовой поддержке Правительства Свердловской области.

Для цитирования

Yurak V.V., Apakashev R.A., Lebzin M.S., Malyshev A.N. Assessment of performance and environmental friendliness of a sorbent-based remediation method for heavy metal and metalloid contaminated soils. *Mining Science and Technology (Russia)*. 2023;8(4):327–340. <https://doi.org/10.17073/2500-0632-2023-07-129>



Introduction

Human activity invariably exerts an impact on the natural environment, leading to the depletion of natural resources, environmental pollution, and disturbances of the Earth's surface and subsoil. This anthropogenic pressure on nature intensifies each year, with over 30 million tons of pollutants entering the atmosphere annually, and approximately 19% of wastewater being discharged into bodies of water without prior treatment. Nearly all regions experience soil degradation due to factors such as water and wind erosion, excessive moisture, flooding, and waterlogging. Desertification has affected more than 100 million hectares of land, with an additional 18 million hectares comprising ecological zones contaminated by industrial complexes. About 4 billion tons of production and consumption waste are generated annually, while authorized waste disposal facilities occupy around 4 million hectares of land. More than 30 million tons have already been accumulated, including over 400 thousand tons of highly toxic substances. The volume of non-recycled waste is also on the rise. According to expert assessment, the annual loss of Russia's GDP due to environmental degradation (excluding health-damage) falls within the range of 4% to 6%¹. The mining industry in Russia plays an important role in exacerbating environmental hazards. Although it may not rank highest in terms of industrial damage intensity, it impacts all components of the biosphere and facilitates the extraction and displacement of vast amounts of rock material. As indicated by a study [1], the quantity of waste rock extracted from subsoil exceeds that of minerals extracted by a factor ranging from 1.1 to 6.7 times. This waste rock is deposited on the Earth's surface, resulting in the expansion of disturbed land areas. In these areas, waste rock dumps (WRDs) and tailing storage facilities (TSFs) account for the largest portion of land allocation, ranging from 62% to 75% at iron ore mining operations and even more at copper ore producing enterprises [1].

According to data from the Federal State Statistics Service, the regions characterized by a substantial degree of land degradation encompass the Urals, Siberia, and the Far East, which are home to key mineral resource hubs in the Russian Federation. Consequently, disturbances stemming from mineral deposit development activities account for approximately 80% of the total extent of disturbed

land in these areas [2]. The open-pit mining method dominates the landscape, holding the largest share of disturbed land in Russia, and is widely prevalent. Disturbances extend to the subsoil as well, manifesting as the creation of man-made voids, both with and without surface access. In the former case, these voids pertain to open-pit excavations within active and exhausted mining pits and the collapse zones of operational and abandoned underground mines. In the latter case, they refer to underground man-made voids. Given that the rate of environmental change resulting from anthropogenic activities impacts significantly outpaces the natural restoration of the ecological balance, it becomes imperative to promptly address the aftermath of subsoil resource extraction. Consequently, reclamation work acquires primary importance and urgency.

Effectively resolving the reclamation challenge entails the selection of the most promising and efficient reclamation method, as well as substantiating the prioritization of lands slated for reclamation.

Regarding the selection of a promising and effective reclamation approach, it is important to note that studies [3–5] have identified two strategies for reclaiming disturbed lands: 1) a traditional approach, which involves a series of sequential reclamation, remediation, and recultivation measures. It encompasses a range of activities, starting from the cleaning and leveling of the reclaimed area, the application of an appropriate thickness of fertile soil, and concluding with the use of fertilizers and ameliorants, as well as the sowing or planting of vegetation; 2) an innovative approach, which is focused on methods and techniques that stimulate natural processes for the restoration and reclamation of disturbed ecosystems, particularly the process of soil formation. It achieves this through physical, chemical, and biological interventions on man-made substrates. Within the innovative approach, the author classifies four primary methods: algal, washing, bioremediation, and sorbent-oriented [6]. Of these, bioremediation and sorbent-oriented technologies, aimed at enhancing soil microflora, have garnered the most attention. Economic feasibility comparisons show that the sorbent-oriented method is the most promising when compared to bioremediation [7, 8]. A more detailed study of the sorbent-oriented method reveals that composite organo-mineral sorbents of natural origin are currently in focus due to their cost-effectiveness, performance, abundant reserves, and their capacity to function not only as sorbents but also as soil ameliorants [9–11]. Furthermore, a contemporary scientific trend involves the “green” disposal of waste materials from

¹ Project “Environmental Safety Strategy of the Russian Federation for the period up to 2025”, 2017; The Strategy of Environmental Safety of the Russian Federation for the Period up to 2025, approved by the Russian Federation. Decree of the President of the Russian Federation dated 19.04.2017 No. 176.



sectors such as woodworking, agriculture, housing and communal services, and other areas of economy. These waste materials are used as components in innovative composite sorbents-ameliorants [12–15].

When it comes to prioritization, for example, as of 2020, as stated by the Deputy Chief Prosecutor: “Over 350 sites of accumulated environmental damage in the Urals require reclamation”². In this scenario, the question arise of how to establish the order in which these sites should be reclaimed – first, second, and so forth (see Table 1). In foreign practice under similar circumstances, it is customary to employ legislative-level methods for assessing the risks associating with causing harm to the ecosystem [16–19].

Hence, the objective of the present study is to evaluate established methods for assessing the risks of environmental damage and to appraise the effectiveness and “environmental friendliness” of the author’s developed composite sorbents. This evaluation is framed within the context of assessing and comparing potential environmental risks and the risks of environmental damage following the application of these sorbents.

The specific objectives are as follows: 1) to consider the theoretical aspects of HMMs, which encompasses the formulation of a precise definition, an exploration of the origins of HMMs, an investigation into HMMs’ toxicity, and an identification of the most prevalent methods for evaluating the environmental risks linked to HMMs; 2) to conduct practical assessment of established methods for gauging

environmental risks associated with HMMs; 3) to assess the effectiveness and “environmental friendliness” of the author’s developed composite sorbents. This assessment involves an analysis and comparison of potential environmental risks and the risks of environmental damage following the application of these sorbents.

The research focuses on the mining area within the Levikhinskoye mine, an area designated as environmental disaster site. This mining allotment functions as a disturbed land ecosystem, encompassing industrial dumps containing HMMs.

The research hypothesis seeks to validate the feasibility of “green utilization” of man-made waste as a fundamental ingredient for composite sorbents used in the reclamation of disturbed lands. This approach is designed to minimize the potential for environmental damage.

On the nature of heavy metals: definition, origin, toxicity, and environmental risk assessment

The term “heavy metals” is currently a subject of complexity and controversy [21]. It is frequently used to refer to metals and metalloids that act as pollutants within biogeocenoses and are toxic to biota. This term has been defined in various ways, often based on the criteria of density in relation to atomic mass and atomic number. Such a variety of definitions has led to debates regarding the definitive list of heavy metals and metalloids – namely, which elements should be included in this category and which should not. For example, there is ongoing scientific discourse on whether to include the metalloid As and, indeed, the non-metal Se in the list of heavy metals and metalloids. Some even argue that this term has lost its meaning and should be abandoned altogether [21]. However, within the scope of

² More than 350 objects of accumulated environmental damage in the Urals require reclamation. ITAR-TASS. October 28, 2020. URL: https://news.rambler.ru/ecology/45113183-bolee-350-obektov-nakoplennoego-ekologicheskogo-vreda-naturala-trebuyut-rekultivatsii/?utm_source=copysharing&utm_medium=social

Table 1

Characteristics of mining allotments of deposits in the Sverdlovsk Region [20]

No.	Mining allotment (deposit)	Built-up area, km ²	Mining allotment area, km ²	Degree of disturbance	Characteristics
1	Levikhinskoye deposit	10.2	21	Highly disturbed	Environmental disaster area
2	Degtyarskoye deposit	19	2.2	Highly disturbed	Environmental disaster area
3	Berezovskoye deposit	33	15.1	Moderately disturbed	Densely built-up area
4	Bulanashskoye deposit	16.8	3.3	Highly disturbed	Zone of dangerous collapse and flooding
5	Pyshminsko-Klyuchevskoye deposit	20	Data not available	Moderately disturbed	Densely built-up area

the current study, we propose adopting a comprehensive interpretation of this term, one that is substantiated by numerous scientific studies by both domestic [22–24] and foreign researchers [25–26]. In this understanding, heavy metals and metalloids (HMM) are viewed as pollutants that resist biological and chemical degradation, possess the capacity to accumulate for a long time in the natural environment, and exhibit toxic properties affecting the biodiversity of ecosystems. According to a study [27, 28], the most commonly encountered HMMs in the natural environment include copper, zinc, chromium, nickel, lead, manganese, cadmium, and arsenic. The release of HMMs into the environment is primarily the result of rock weathering and anthropogenic activities, with the latter being a significant contri-

butor to environmental challenges. Consequently, a defining characteristic of HMMs is their toxicity. Even at relatively low concentrations, HMMs pose risks to soil, plants, living organisms, and, as a result, human health. The most highly toxic HMMs include chromium, cadmium, lead, zinc, copper, mercury, and arsenic [29, 30] (see Table 2). Table 2 presents values of HMMs' Maximum Permissible Concentrations (MPC), including both mobile water-soluble and non-mobile forms.

Table 2 illustrates the variations in maximum permissible concentration values for HMMs, and it is noteworthy that not every country or consortium of nations has adopted legislatively defined maximum permissible concentrations. For example, this omission is observed in the case of the European

Table 2

HMMs toxicity: MPC of HMMs, including mobile water-soluble and immobile forms

Country/ Organization	Land Category/Soil Type, UoM	Cr (VI)	Cd	Pb	Zn	Cu	Hg	As	S
United Nations [31]	Agricultural lands, ppm	0.1	0.003	0.1	n/a	n/a	0.08	n/a	n/a
China [31]	Agricultural lands, ppm	150–300	0.3–0.6	80	n/a	n/a	0.3–1.0	n/a	n/a
USA ¹	Agricultural lands, ppm	11	0.43	200	n/a	n/a	1.0	n/a	n/a
Italy ²	Residential area, mg/kg	2	2	100	150	120	1	20	n/a
	Industrial land, mg/kg	15	15	1,000	1,500	600	5	50	n/a
Finland ³ [32]	Threshold value, mg/kg	100	1	60	60	100	0.5	5	n/a
	Minimum value, mg/kg	200	10	200	200	150	2	50	n/a
	Maximum value, mg/kg	300	20	750	400	250	5	100	n/a
Canada ⁴	Agricultural land, mg/kg	250	3	200	n/a	n/a	0.8	n/a	n/a
Germany [33, 34]	Agricultural land, mg/kg	500	5	1,000	10–300	2–100	5	1–50	n/a
Spain ⁵	Acidic soils, mg/kg	100	1	50	150	1,000	1	5	n/a
	Alkaline soils, mg/kg	150	3	300	450	1,700	1.5	55	n/a
Russian Federation ⁶	Sandy and sandy loam, mg/kg	0.05	0.5	32.0	55.0	33.0	2.1	2.0	n/a
	Acidic (loamy and clayey), exchange soil acidity pH _{KCl} < 5.5, mg/kg	0.05	1.0	65.0	110.0	66.0	2.1	5.0	n/a
	Near-neutral, neutral (loamy and clayey) pH _{KCl} > 5.5, mg/kg	0.05	2.0	130.0	220.0	132.0	2.1	10.0	160

Note: N/A indicates that data is not available.

Source: The table was compiled by the authors using reference [28].

¹ New York state brownfield cleanup program. Development of soil cleanup objectives. Technical support document. Albany, NY, USA: New York State Department of Environmental Conservation and New York State Department of Health; 2006.

² Decreto Legislativo n. 152 del 3 aprile 2006 “Norme in materia ambientale”, Supplemento Ordinario alla “Gazzetta Ufficiale” n. 88 del 14 aprile 2006. URL: <https://www.camera.it/parlam/leggi/deleghe/06152dl.htm>

³ Government Decree on the Assessment of Soil Contamination and Remediation Needs 214/2007, 1 March 2007; Ministry of Environment: Helsinki, Finland, 2007 (the legally binding document is in Finnish or Swedish)

⁴ Soil, Ground Water and Sediment Standards for Use under Part XV.1 of the Environmental Protection Act. Toronto, ON, Canada: Canadian Ministry of the Environment (CME); 15 April 2011.

⁵ Real Decreto 1310/1990, de 29 de octubre, por el que se regula la utilización de los lodos de depuración en el sector agrario. URL: <https://www.boe.es/buscar/doc.php?id=BOE-A-1990-26490>

⁶ SanPiN 1.2.3685-21 “Hygienic Standards and Requirements for Ensuring the Safety and (or) Harmlessness of Environmental Factors for Humans”.



Union as a whole [28]. However, it is crucial to acknowledge that elevated concentrations of HMMs pose environmental risks to human health and overall quality of life (as depicted in Fig. 1). Concerning these risks, research practice offers methods for assessing environmental risks based on the level of soil and subsoil contamination with HMMs [16–19], with two widely recognized methods being:

1. HMMs’ potential environmental risk (*ER*) assessment methodology:

$$ER = I_t \times Z = I_t \times \frac{Z_m}{Z_a}, \quad (1)$$

where I_t is the toxicity level of HMMs and the biota’s sensitivity to these elements. This indicator is empirically determined and is treated as a specific constant for each elements: Cr, Ni, Cu, As, Cd, Pb, Zn, and S, with values of 2, 6, 5, 10, 30, 5, 5, 15, respectively. Z represents a microelement contamination coefficient, determined by the ratio of the measured concentration of an element in a subject (Z_m) to the background concentration (Z_a).

The *ER* calculation results categorize the soil or subsoil under investigation as follows: if $ER < 150$, the environmental risk from HMMs is considered low; if $150 \leq ER < 300$, it is categorized as medium; if $300 \leq ER < 600$, it is considered high; if $ER \geq 600$, it is classified as very high.

One limitation of this methodology is its reliance on the availability of data for the I_t indicator.

Chromium

Persistent forms that are toxic to humans: Cr(III) and Cr(VI). Cr(VI) is the most dangerous since it can more easily enter the human body through inhalation, ingestion, and skin contact. The human organs adversely affected include the liver, kidneys, spleen, and skeletal system. Diseases and manifestations caused by this heavy metal include ulcers, dermatitis, perforation of the nasal septum, and respiratory system cancers. When chromium enters a pedosphere, it can alter the structure of microbial communities and impede their growth.

Copper

Copper plays a crucial role in various biological processes, including oxidation, photosynthesis, and the metabolism of carbohydrates, proteins, and cell walls. High concentrations of copper can lead to cellular-level damage in human organs. The effects and symptoms associated with this heavy metal include nausea, vomiting, and abdominal pain. Prolonged exposure to copper can result in damage to the liver and kidneys. In the plant kingdom, copper tends to accumulate in the roots, leading to reduce growth and impaired absorption of other trace elements that are vital for healthy plant development.

Zinc

This element plays a significant role in the metabolism of nucleic acids and proteins, as well as in the growth, division, and overall functioning of cells. However, when present in high concentrations, zinc can induce symptoms such as vomiting, muscle cramps, and kidney damage in humans. In plants, elevated levels of zinc leads to a decrease in both growth and development, causing symptoms such as chlorosis and disruptions in metabolic processes.

Cadmium

Cadmium inhibits cell proliferation, differentiation, apoptosis, and DNA repair mechanism. Diseases and manifestations caused by this heavy metal include skeletal demineralization and issues with kidneys and liver function. In plants, excessive Cd accumulation can disrupt critical functions, including photosynthesis and respiration. This, in turn, hinders the transport and absorption of mineral nutrients, adversely affecting plant growth and development.

Lead

This microelement is swiftly absorbed into the bloodstream, resulting in damage to various systems, particularly the nervous and lymphatic systems. It has a detrimental impact on kidney function and the overall development of the human body.

Mercury

It is a highly toxic element capable of accumulating in various human body, tissues. It damages the brain, thyroid, pectoral muscle, myocardium, muscles, liver, kidneys, skin, and pancreas. Among these, the nervous system is the most severely affected. by mercury exposure.

Arsenic

This metalloid is known to cause a range of severe health issues. These include skin lesions as well as cancers affecting the lungs, bladder, liver, and kidneys. Arsenic exposure is also linked to coronary heart disease and can lead to impaired cognitive abilities, motor functions, and hormonal regulation.

Sulfur

Exposure to sulfur can lead to a range of adverse effects, including irritation of the mucous membranes of the eyes, excessive tearing, difficulty breathing, nausea and vomiting, headaches, increased fatigue, weakening of muscle strength, memory loss, slower cognitive perception, reduced heart function, changes in the bactericidal properties of the skin.

Fig. 1. Toxic effects of HMMs on biota



2. The second methodology aims to assess the risks of environmental damage (ED):

$$EH = \frac{Z_m}{Z_l}, \quad (2)$$

where Z_m similar to the formula (1), represents the measured concentration of an element in a subject, while Z_l , distinct from Z_a , denotes the maximum permissible concentration of an element established by current legislation.

The results of the environmental damage (ED) risk calculation indicate a low likelihood of adverse consequences if $ED < 1$. Conversely, if $ED > 1$, the probability of adverse events and environmental damage is high. This underscores the need for soil/subsoil remediation and reclamation.

Therefore, in both the first method for evaluating potential environmental risk from HMMs and the second method for assessing the risks of environmental damage, when the final indicators exhibit high values, soil/subsoil reclamation became necessary.

Materials for the study

The study used the following materials:

1. A composite sorbent comprising peat/water treatment sludge in a weight ratio of 20/80 at natural moisture. This composition was determined through numerous experiments and the construction of adsorption isotherms [35].

2. Another composite sorbent (peat/diatomite/water treatment sludge) containing peat, diatomite, and water treatment sludge in a weight ratio of 5/15/80 at natural moisture.

3. A composite peat/diatomite sorbent, consisting of peat and diatomite in a weight ratio of 25/75 at natural moisture.

Neutralized and fractionated high-moor peat (fraction 0–10). This peat had a moisture content ranging from 50 to 60%, a pH of the water extract between 5.5 to 6.0, and an ash content of less than 5 %. The main inorganic components of the peat included nitrogen up to 1.5% (wt.), and phosphorus, potassium, calcium (in total) up to 0.6%. The peat also contained 7.4–7.9% humic substances.

Diatomite from the Kamyshlovskoye deposit. This material is employed in the creation of silicate binder-fillers containing silicon, activated sorbents, construction and refractory materials, as well as for modifying the agrochemical properties of soils, among other uses.

Water treatment sludge originating from the Western Filtration Station in Yekaterinburg city. X-ray phase analysis revealed that over 70% of the

sludge consists of X-ray amorphous organic matter. The chemical composition of the sludge includes silicon, aluminum, and iron. The sludge's particle size distribution is polydisperse, with a wet sieve analysis indicating a dominance of particles smaller than 50 μm (21%) and particles larger than 100 μm (18%);

4. Man-made soil obtained from the waste rock dump of the Levikhinskoye group of copper-sulfide deposits (Levikha settlement, Sverdlovsk Region). This soil is comprised of loose terrigenous material consisting of angular grains. In the upper section of the dumps, it primarily includes psammite and psephite fractions (sand and crushed stone). In the lower section, there is a prevalence of the psephite fraction (blocks). The proportion of pelite fraction generally remains within the range of 5–10%. The waste rock comprises fragments of quartz-sericite and quartz-chlorite schists, sulphide ore, limonite, chalcedony, and quartz with vein and disseminated sulfides.

Methods and study algorithm

The samples gathered from the waste rock dumps of the Levikhinskoye group of copper-sulfide deposits (Levikha settlement, Sverdlovsk Region) were thoroughly blended in a single container. The rock mixture was not crushed to replicate the natural conditions of man-made areas. The grain-size distribution of the rock ranged from 12 cm to 1.5 mm.

Each container received 500 g (± 5 g) of rock measured on floor scales, creating a 2 cm-high layer of rock in the containers. A rectangular container with an 880 cm^3 volume for each test was partitioned by a plastic divider. In the first part of the container, the rock was first placed, and various sorbents were poured on top in separate containers:

1. Composite sorbent peat/water treatment sludge (P/S) in the ratio of 20/80 by weight at natural moisture.

2. Peat/diatomite/water treatment sludge. This composite sorbent, composed of peat/diatomite/water treatment sludge (P/D/S), was in the ratio of 5/15/80 by weight at natural moisture. Each sorbent sub-sample weighted 50 g (± 0.5 g), and the height of the sorbent layer varied from 0.4 to 0.6 cm based on the type of sorbent and the soil's looseness.

3. Peat/diatomite. This composite peat/diatomite sorbent (P/D) had a ratio of 25/75 by weight at natural moisture. Each sorbent sub-sample weighted 50 g (± 0.5 g), and the height of the sorbent layer varied from 0.4 to 0.6 cm depending on the type of sorbent and the soil's looseness.

Next, 500 ml of distilled water was evenly poured into the first part of each container containing the

rock and sorbents. This was done to establish a moist environment within the container to facilitate the free movement of HMMs ions in the aqueous solution with the immersed sorbent and rock, with the solution flowing into the second part of each container. Circulation of the solution between the two sections in the container occurred throughout the test, but the soil and sorbent did not migrate into the second part.

In order to minimize errors, prevent the entry of various dust particles, and reduce solution evaporation, the containers were sealed.

The testing solution was allowed to stand at room temperature for a minimum of 24 hours.

Subsequently, the solutions were filtered through medium-density paper filters to enable the quantitative and qualitative chemical composition of the solutions to be studied.

In order to analyze the quantitative chemical composition of the man-made soil and the author's sorbents and to determine the degree of heavy metal ions adsorption, atomic absorption and atomic emission spectrometry methods were employed. The corresponding analyses were carried out using an ICPE-9820 inductively coupled plasma parallel atomic emission spectrometer manufactured by Shimadzu (Japan) and a Kvant-2 flame atomization atomic absorption spectrometer. The tests were conducted in accordance with GOST ISO 22036–2014 Soil Quality. Determination of Microelements in Soil Extracts Using Inductively Coupled Plasma Atomic Emission Spectrometry (ICP-AES), and Environmental Regulatory Document (PND)

F 16.1:2:2.2:2.3.78-2013, titled “Quantitative Chemical Analysis of Soils”. Methodology for Measuring the Mass Fraction of Mobile Forms of Metals: Copper, Zinc, Lead, Cadmium, Manganese, Nickel, Cobalt, Chromium in Soil, Subsoil, Bottom Sediments, Sewage Sludge Samples by Flame Atomic Adsorption Spectrometry.

Findings

Assessment of ER and ED of man-made soil

The analyses of samples collected from the waste rock dumps of the Levikhinskoye group of copper-sulfide deposits were carried out in the laboratory [36]. The results of the studies are presented in Table 3.

The results of the studies³ have shown that the maximum concentrations of S, Cu, and Zn in the samples fall within the dangerous category of soil pollution according to the methodology proposed by the authors of the study. The primary source of pollution is sulfur, with copper and zinc playing a lesser role.

To determine the initial concentration of water-soluble HMMs ions in the man-made soil from the waste rock dumps of the Levikhinskoye group of copper-sulfide deposits, a similar test was conducted, but without the composite sorbent. As a result, HMMs ions were detected in the man-made soil, as presented in Table 4.

³ SanPiN 1.2.3685-21 “Hygienic Standards and Requirements for Ensuring the Safety and (or) Harmlessness of Environmental Factors for Humans”.

Table 3

Concentration (total) of HMMs ions in the waste rock dumps of the Levikhinskoye group of copper-sulfide deposits

Component	Grade, wt.% min/max	Content in sulphide sands, wt.%	MPC and APC*, wt.%	Factor Concentration min/max	Concentration factor in sulfide sands min/max
S	0.026/1.370	32.6	0.016	1.6/85.6	2037.5
Cu	0.005/0.1	0.16	0.0132	0.4/7.6	11.9
Zn	0.0097/0.0353	0.015	0.022	0.4/1.6	0.7

Note: * for the group of soils close to neutral and neutral (loamy and clayey), $pH_{KCl} > 5.5$.

Table 4

Concentration of water-soluble HMMs ions (mobile form) in the man-made soil from the waste rock dump of the Levikhinskoye group of copper-sulfide deposits and in a control sample

Sample	Cu, mg/l	Zn, mg/l	S, mg/l
Averaged (composite) sample from dumps (12 sampling points)	0.84427	0.61632	2.50000
Control sample (background contamination)	0.00500	0.00970	0.08900

The risk assessment, as per formulas (1) and (2), is provided in Table 5.

The *ER* values for all three HMMs are above 300, indicating that zinc and sulfur are ranked as high-risk, while copper is classified as very high-risk. However, the results for the *ED* indicator appear contradictory, as the risk of environmental damage for all three HMMs is below 1, signifying a low probability of negative consequences. This can be attributed to the fact that the sample was averaged (composited), and the long-term impact of surface precipitation on the environmental disaster area. Consequently, the concentrations of HMMs in the surface layer of soil are relatively low compared to the MPC but exceed background values. The arithmetic mean of the risk level indicators also reflects this pattern, with a high value for *ER* and a low value for *ED*.

Analysis of HMMs content in man-made soil after the application of the author’s sorbents

The data from Table 4, showing the concentrations of HMMs ions in man-made soil samples from the waste rock dumps of the Levikhinskoye group of copper-sulfide deposits (Levikha settlement, Sverdlovsk Region) are presented in Fig. 2.

The tests showed that the application of the proprietary sorbents resulted in a decrease in HMMs’ concentrations in the man-made soil. Fig. 3 presents the test results on the degree of water-soluble ions Cu (a), Zn (b), and S (c) extraction by the sorbents.

The sorbents, as depicted in Fig. 3, exhibit near-maximum performance in binding (adsorption) Cu, Zn, and S ions, with the exception of the

Table 5

Assessment of potential environmental risks from HMMs (ER) and risks of environmental damage (ED) based on the content of HMMs in man-made soil

HMM	Concentration, mg/l	Hazard Factor	Background, mg/l	MPC ¹ (mobile form, acidic soils, neutral regarding sulphur), mg/kg	Concentration, mg/kg	ER	EH
Cu	0.84427	5.00000	0.00500	3.00000	1.68854	844.27000	0.56285
Zn	0.61632	5.00000	0.00970	23.00000	1.23264	317.69072	0.05359
S	2.50000	15.00000	0.08900	160.00000	5.00000	421.34831	0.03125
Arithmetic Mean of HMMs Risk Level						527.76968	0.21590

¹ SanPiN 1.2.3685-21 “Hygienic Standards and Requirements for Ensuring the Safety and (or) Harmlessness of Environmental Factors for Humans”.

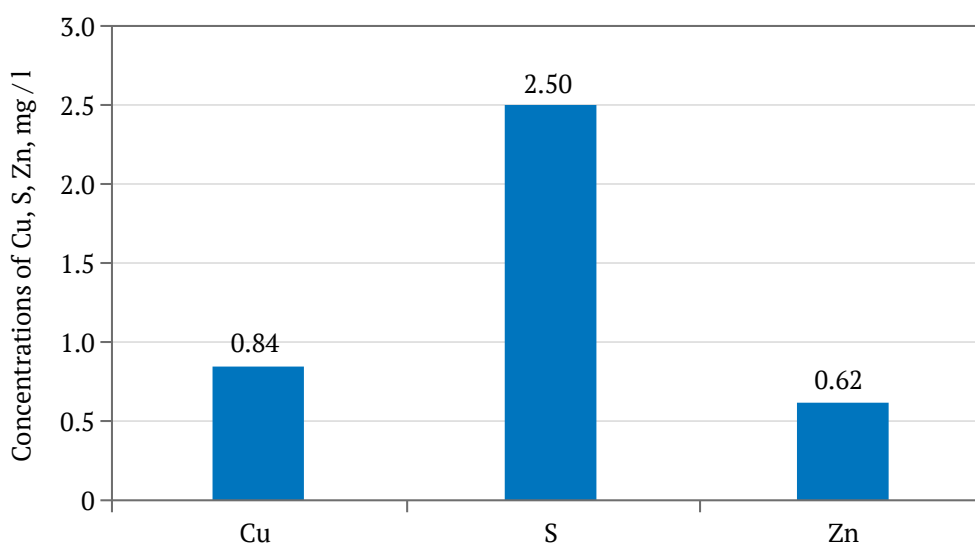


Fig. 2. Concentration of HMMs in the man-made soil from the waste rock dumps of the Levikhinskoye group of copper-sulfide deposits

peat/diatomite sorbent (at the ratio of 25/75, wt.%, at natural moisture), which shows moderate adsorption performance in relation to S.

The studies indicated that the adsorption of Cu ions was more efficient when the peat content in the sorbent exceeded 20 wt.% (at natural moisture). The addition of water treatment sludge significantly enhances the adsorption of Zn and S. It was not possible to evaluate the effect of the quantitative content of the water treatment sludge on adsorption

performance, as only one content of this man-made component was tested (80 wt.% at natural moisture). An increase in the weight percentage of diatomite in the composite sorbent negatively affects the adsorption of Zn and S.

The best performance was achieved by the peat/water treatment sludge sorbent (at a ratio of 20/80 wt.% at natural moisture) and the peat/diatomite/water treatment sludge sorbent (at a ratio of 5/15/80 wt.% at natural moisture), both of which

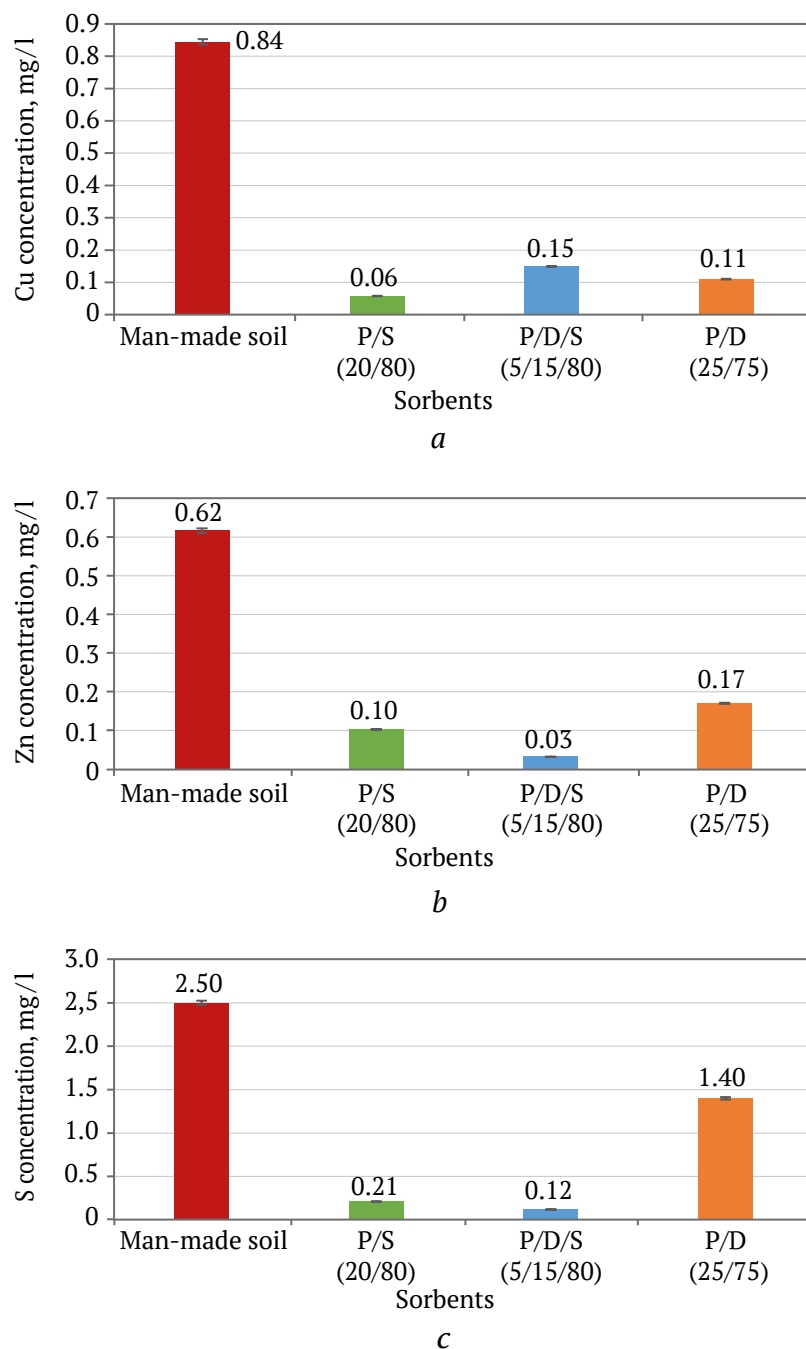


Fig. 3. Degree of Cu, Zn, S ions extraction by sorbents: peat/water treatment sludge (at the ratio of 20/80 wt.% at natural moisture), peat/diatomite/water treatment sludge (at the ratio of 5/15/80 wt.% at natural moisture) and peat/diatomite (at the ratio of 25/75 wt.% at natural moisture):

(a) degree of Cu ions extraction; (b) degree of Zn ions extraction; (c) degree of S ions extraction

exhibited an overall performance exceeding 89%. The peat/diatomite sorbent (at a ratio of 25/75 wt.% at natural moisture) demonstrated an overall performance of 67.7%.

Consequently, the results obtained after applying the authors' sorbents are presented in Tables 6–8.

After the application of the author's sorbents, the ED indicator decreased even further. The P/S (20/80) sorbent exhibited the highest performance in reducing the risks of environmental damage. Similarly, concerning the average value of the HMMs Potential Environmental Risk Index (ER), the P/S

(20/80) sorbent proved to be the most effective. However, in terms of ER for selective sorption of zinc and sulfur, the P/D/S (5/15/80) sorbent demonstrated the highest performance. The P/D (25/75) sorbent showed the least favorable results. The calculated data obtained support the hypothesis regarding the possibility and, moreover, the effectiveness of "green utilization" of man-made wastes for the reclamation of disturbed lands. This is evident as all sorbents, whether they included water treatment sludge selectively or comprehensively, exhibited maximum sorption performance (Table 9).

Table 6

Assessment of potential environmental risks from HMMs (ER) and risks of environmental damage (ED) based on the content of HMMs in man-made soil after applying P/S (20/80) sorbent

HMM	Concentration after applying P/S (20/80) sorbent, mg/l	Hazard Factor	Background, mg/l	MPC (mobile form, acidic soils), mg/kg	Concentration after applying P/S (20/80) sorbent, mg/kg	ER	EH
Cu	0.06000	5.00000	0.00500	3.00000	0.12000	60.00000	0.04000
Zn	0.10000	5.00000	0.00970	23.00000	0.20000	51.54639	0.00870
S	0.21000	15.00000	0.08900	160.00000	0.42000	35.39326	0.00263
Arithmetic Mean of HMMs Risk Level						48.97988	0.01711

Table 7

Assessment of potential environmental risks from HMMs (ER) and risks of environmental damage (ED) based on the content of HMMs in man-made soil after applying P/D/S (5/15/80) sorbent

HMM	Concentration after applying P/D/S (5/15/80) sorbent, mg/l	Hazard Factor	Background, mg/l	MPC (mobile form, acidic soils), mg/kg	Concentration after applying P/D/S (5/15/80) sorbent, mg/kg	ER	EH
Cu	0.15000	5.00000	0.00500	3.00000	0.30000	150.00000	0.10000
Zn	0.03000	5.00000	0.00970	23.00000	0.06000	15.46392	0.00261
S	0.12000	15.00000	0.08900	160.00000	0.24000	20.22472	0.00150
Arithmetic Mean of HMMs Risk Level						61.89621	0.03470

Table 8

Assessment of potential environmental risks from HMMs (ER) and risks of environmental damage (ED) based on the content of HMMs in man-made soil after applying P/D (25/75) sorbent

HMM	Concentration after applying P/D (25/75) sorbent, mg/l	Hazard Factor	Background, mg/l	MPC (mobile form, acidic soils), mg/kg	Concentration after applying P/D (25/75) sorbent, mg/kg	ER	EH
Cu	0.11000	5.00000	0.00500	3.00000	0.22000	110.00000	0.07333
Zn	0.17000	5.00000	0.00970	23.00000	0.34000	87.62887	0.01478
S	1.40000	15.00000	0.08900	160.00000	2.80000	235.95506	0.01750
Arithmetic Mean of HMMs Risk Level						144.52797	0.03521



Table 9

Assessment of changes in the established risk levels after applying the author’s sorbents

HMM Risk	Average for HMMs in man-made soil	Mean for HMMs after applying P/S (20/80) sorbent		HMMs average after applying P/D/S (5/15/80) sorbent		Mean for HMMs after applying P/D (25/75) sorbent		Mean changes after applying sorbents with Water Treatment Sludge (S), %
		Actual Performance	Changes as compared to mean value for HMMs in man-made soil, %	Actual Performance	Changes as compared to mean value for HMMs in man-made soil, %	Actual Performance	Changes as compared to mean value for HMMs in man-made soil, %	
ER	527.76968	48.97988	90.72	61.89621	88.27	144.52797	72.62	89.50
EH	0.21590	0.01711	92.08	0.03470	83.93	0.03521	83.69	88.00

Conclusions

The study successfully achieved its objective, which was to test the existing conventional methods for assessing environmental damage and to evaluate the effectiveness and “environmental friendliness” of the developed author’s composite sorbents. This evaluation was done by assessing and comparing the levels of potential environmental risks and risks of environmental damage after the application of these

sorbents. The results showed a significant reduction in estimated risks of ER and ED by an average of 89.5% and 88%, respectively, after applying the proprietary composite sorbents, which include water treatment sludge. This confirms the research hypothesis that “green utilization” of man-made waste as a raw material for composite sorbents used in land reclamation can be achieved without increasing the risks of environmental damage.

References

1. Chaplygin N.N., Galchenko Yu.P., Papichev V.I. et al. *Environmental Problems of Geotechnologies: New concepts, methods and solutions*. Moscow: Nauchtechlitzdat Publishing House LLC; 2009. 320 p. (In Russ.)
2. Naumov I.V. The study of spatial imbalances in the processes of disruption and land reclamation in Russia. *News of the Ural State Mining University*. 2019;(4):142–151. <https://doi.org/10.21440/2307-2091-2019-4-143-152> (In Russ.)
3. Chiampo F., Zacchini M. Environmental restoration of metal-contaminated soils. *Applied Sciences*. 2021;11(22):10805. <https://doi.org/10.3390/app112210805>
4. Voronchikhina E.A. *Reclamation of disturbed landscapes: theory, technologies, regional aspects*: monograph. Perm; 2010. 165 p. (In Russ.)
5. Zhu J., Wang P., Lei M.-J., Zhang W.-L. Polyhydroxyl-aluminum pillaring improved adsorption capacities of Pb²⁺ and Cd²⁺ onto diatomite. *Journal of Central South University*. 2014;21:2359–2365. <https://doi.org/10.1007/s11771-014-2188-9>
6. Yurak V.V., Usmanov A.I. Approaches to the restoration of lands disturbed by the mining and metallurgical complex. *Sustainable Development of Mountain Territories*. 2023. In print.
7. Mishra M., Mohan D. Bioremediation of contaminated soils: an overview. In: Rakshit A., Abhilash P., Singh H., Ghosh S. (eds) *Adaptive Soil Management: From Theory to Practices*. Springer, Singapore; 2017. https://doi.org/10.1007/978-981-10-3638-5_16
8. Singh A., Prasad S.M. Remediation of heavy metal contaminated ecosystem: an overview on technology advancement. *International Journal of Environmental Science and Technology*. 2015;12:353–366. <https://doi.org/10.1007/s13762-014-0542-y>
9. Ignatyeva M., Yurak V., Pustokhina N. Recultivation of post-mining disturbed land: review of content and comparative law and feasibility study. *Resources*. 2020;9(6):73. <https://doi.org/10.3390/resources9060073>
10. Ermakov A.S., Ermakova A.Ya. Restoration of soil cover disturbed due to adverse impact from industrial enterprises. *Nauchnyy Vestnik MGGU*. 2014;(1):24–29. (In Russ.)
11. Marques J.P., Rodrigues V.G.S., Raimondi I.M., Lima J.Z. Increase in Pb and Cd Adsorption by the application of peat in a tropical soil. *Water, Air, & Soil Pollution*. 2020;231:136. <https://doi.org/10.1007/s11270-020-04507-z>



12. Yakonovskaya T.B., Zhigul'skaya A.I. Features of evaluating the economic security of peat industry enterprises in the Tver Region of Russia (the industry review). *Mining Science and Technology (Russia)*. 2021;6(1):5–15. <https://doi.org/10.17073/2500-0632-2021-1-5-15>
13. Ignatyeva M.N., Yurak V.V., Dushin A.V., Strovsky V.E. Technogenic mineral accumulations: problems of transition to circular economy. *Mining Science and Technology (Russia)*. 2021;6(2):73–89. <https://doi.org/10.17073/2500-0632-2021-2-73-89>
14. Apakshv R.A., Malyshev A.N., Lebzin M.S. Study of the physicochemical properties of water treatment residuals for “green” soil utilization. *News of the Ural State Mining University*. 2022;(3):117–124. (In Russ.)
15. Bukin A.V., Motorin A.S., Iglovikov A.V. Creation of a reclamation mixture based on water treatment sludge (from the Nyagan State District Power Plant) and peat. *Agroprodoval'stvennaya politika Rossii*. 2016;(12):70–75. (In Russ.)
16. Håkanson L. An ecological risk index for aquatic pollution control. A sedimentological approach. *Water Research*. 1980;14(8):975–1001. [https://doi.org/10.1016/0043-1354\(80\)90143-8](https://doi.org/10.1016/0043-1354(80)90143-8)
17. Baran A., Wiczczyk J., Mazurek R. et al. Potential ecological risk assessment and predicting zinc accumulation in soils. *Environmental Geochemistry and Health*. 2018;40:435–450. <https://doi.org/10.1007/s10653-017-9924-7>
18. Wu Q., Leung J.Y.S., Geng X. et al. Heavy metal contamination of soil and water in the vicinity of an abandoned e-waste recycling site: Implications for dissemination of heavy metals. *Science of the Total Environment*. 2015;506–507:217–225. <https://doi.org/10.1016/j.scitotenv.2014.10.121>
19. Pan X.-D., Wu P.-G., Jiang X.-G. Levels and potential health risk of heavy metals in marketed vegetables in Zhejiang, China. *Scientific Reports*. 2016;6:20317. <https://doi.org/10.1038/srep20317>
20. Staritsyn I.A., Belichev A.A. Analysis of the Sverdlovsk region' disturbed lands use. *Agrarian Bulletin of the Urals*. 2018;4:31–36. (In Russ.)
21. Ali H., Khan E. What are heavy metals? Long-standing controversy over the scientific use of the term ‘heavy metals’ – Proposal of a comprehensive definition. *Toxicological & Environmental Chemistry*. 2018;100:6–19. <https://doi.org/10.1080/02772248.2017.1413652>
22. Seleznev A.A., Klimshin A.V. Heavy metals in urban grounds in Ekaterinburg (Russia). *News of the Ural State Mining University*. 2020;(1):96–104. <https://doi.org/10.21440/2307-2091-2020-1-96-104>
23. Semyenov A.I., Koksharov A.V., Pogodin Yu.I. The content of heavy metals in Chelyabinsk soils. *Occupational Medicine and Human Ecology*. 2015;(3):184–191.
24. Pisareva A.V., Belopukhov S.L., Savich V.I. et al. Migration of heavy metals from the source of pollution depending on the interconnections in a landscape. *Vestnik Tekhnologicheskogo Universiteta*. 2017;20(6):160–163. (In Russ.)
25. Bou Kheir R., Greve M., Greve M. et al. Comparative GIS tree–pollution analysis between arsenic, chromium, mercury, and uranium contents in soils of urban and industrial regions in Qatar. *Euro-Mediterranean Journal for Environmental Integration*. 2019;4:10. <https://doi.org/10.1007/s41207-019-0099-8>
26. Mikkonen H.G., Dasika G., Drake J.A. et al. Evaluation of environmental and anthropogenic influences on ambient background metal and metalloid concentration in soil. *Science of the Total Environment*. 2018;624:599–610. <https://doi.org/10.1016/j.scitotenv.2017.12.131>
27. Ali H., Khan E., Ilahi I. Environmental chemistry and ecotoxicology of hazardous heavy metals: environmental persistence, toxicity, and bioaccumulation. *Journal of Chemistry*. 2019;2019:6730305. <https://doi.org/10.1155/2019/6730305>
28. Raffa C.M., Chiampo F., Shanthakumar S. Remediation of metal/metalloid-polluted soils: a short review. *Applied Sciences*. 2021;11:4134. <https://doi.org/10.3390/app11094134>
29. Wuana R.A., Okieimen F.E. Heavy metals in contaminated soils: a review of sources, chemistry, risks and best available strategies for remediation. *International Scholarly Research Network*. 2011;2011:402647. <https://doi.org/10.5402/2011/402647>
30. Dutta S., Mitra M., Agarwal P. et al. Oxidative and genotoxic damages in plants in response to heavy metal stress and maintenance of genome stability. *Plant Signaling & Behavior*. 2018;13(8):e1460048. <https://doi.org/10.1080/15592324.2018.1460048>
31. Kinuthia G.K., Ngunjiri V., Beti D. et al. Levels of heavy metals in wastewater and soil samples from open drainage channels in Nairobi, Kenya: Community health implication. *Scientific Reports*. 2020;10:8434. <https://doi.org/10.1038/s41598-020-65359-5>
32. Carlon C. (Ed.) *Derivation methods of soil screening values in Europe. A review and evaluation of national procedures towards harmonization*. Ispra: European Commission, Joint Research Centre; 2007. 306 p.



33. He Z., Shentu J., Yang X. et al. Heavy Metal Contamination of Soil: Sources, Indicators, and Assessment. *Journal of Environmental Indicators*. 2015;9:17–18.

34. Kasyanenko A.A. *Environmental quality control*. Moscow: Peoples' Friendship University of Russia; 1992. 136 p. (In Russ.)

35. Apakashev R.A., Lebzin M.S., Yurak V.V., Malyshev A.N. Hybrid sorbents – meliorants for recultivation of arsenic-contaminated soils. *Mining Informational and Analytical Bulletin*. 2022;(11–1):18–28. (In Russ.) https://doi.org/10.25018/0236_1493_2022_111_0_18

36. Fedorov S., Zavyalov S., Yurak V. Ore minerals in technogenic wastes of the levikhinsky mine (Middle Urals) In: *IOP Conference Series: Earth and Environmental Science. International Science and Technology Conference "Earth Science", ISTC EarthScience 2022*. 2022;988(2):032088. <https://doi.org/10.1088/1755-1315/988/3/032088>

Information about the authors

Vera V. Yurak – Dr. Sci. (Econ.), Associate Professor, Department of Economics and Management, Head of the Research Laboratory for Reclamation of Disturbed Lands and Technogenic Objects, Ural State Mining University, Yekaterinburg, Russian Federation; Senior Researcher, Institute of Economics of the Ural Branch of Russian Academy of Sciences, Yekaterinburg, Russian Federation; ORCID [0000-0003-1529-3865](https://orcid.org/0000-0003-1529-3865), Scopus ID [57190411535](https://scopus.com/authorid/57190411535), ResearcherID [J-7228-2017](https://orcid.org/J-7228-2017); e-mail vera_yurak@mail.ru

Rafail A. Apakashev – Dr. Sci. (Chem.), Professor, Vice-Rector for Research, Ural State Mining University, Yekaterinburg, Russian Federation; ORCID [0000-0002-9006-3667](https://orcid.org/0000-0002-9006-3667), Scopus ID [6603092433](https://scopus.com/authorid/6603092433); e-mail Apakashev.R@m.ursmu.ru

Maxim S. Lebzin – Junior Researcher, Research Laboratory for the Reclamation of Disturbed Lands and Technogenic Objects, Yekaterinburg, Russian Federation; ORCID [0000-0001-5959-135X](https://orcid.org/0000-0001-5959-135X), Scopus ID [57218647741](https://scopus.com/authorid/57218647741); e-mail science@ursmu.ru

Alexander N. Malyshev – Research Assistant, Research Laboratory for the Reclamation of Disturbed Lands and Technogenic Objects, Yekaterinburg, Russian Federation; ORCID [0000-0002-3104-1687](https://orcid.org/0000-0002-3104-1687), Scopus ID [57223099993](https://scopus.com/authorid/57223099993); e-mail malyshev.k1b@gmail.com

Received 07.07.2023

Revised 28.07.2023

Accepted 15.09.2023



SAFETY IN MINING AND PROCESSING INDUSTRY AND ENVIRONMENTAL PROTECTION

Research paper

<https://doi.org/10.17073/2500-0632-2023-02-79>

УДК 622:331.45

**Chemical additive based on sodium oleate and linseed oil
for preparation coal dust suppression composition**V. A. Golubkov¹ , G. A. Gorenkova² , E. P. Vorozhtsov² , M. A. Bespalova² , S. V. Bortnikov² ¹ Institute of Chemistry and Chemical Technology of the Siberian Branch of the RAS, Krasnoyarsk, Russian Federation² Khakassian State University named after N. F. Katanov, Abakan, Russian Federation golubkov.va@icct.krasn.ru**Abstract**

The mining, transportation, and processing of coal involve the formation and emission of significant amounts of particulate matter, which includes coal dust. The most commonly employed method for controlling coal dust in an air is water spray dust suppression (hydrodedusting). This method is founded on water's capacity to moisten dust particles and bond them to both each other and the surfaces where the dust settles. One notable limitation of this method is the coal's hydrophobic nature, which hinders water from wetting coal dust particles. In order to overcome this, surfactants are introduced into the water to increase the wettability of the hydrophobic coal particle surface. In this paper, we proposed a dust suppressant composition consisting of oleic acid, sodium hydroxide, and linseed oil in water. We examine its properties and evaluated its ability to enhance the wettability of coal dust. We have identified the most effective concentration, resulting in a working solution that improves the wettability of coal dust by 87 % compared to water, surpassing the wettability of most known reagents. The proposed composition contains 140 mg/L oleic acid, 100 mg/L sodium hydroxide, and 70 mg/L linseed oil in water. The simplicity of this composition, its minimal impact on the environment and human health, and its negligible influence on the further use of coal raw materials make this wetting agent composition highly promising for application in coal industry technologies of water spray dust suppression.

Keywords

coal dust, dust suppression, hydrodedusting, wettability, surfactants, sodium oleate, linseed oil

Acknowledgments

The research was carried out at the expense of a grant of the Ministry of Education and Science of the Republic of Khakassia (Agreement No. 93 of 13.12.2022).

For citation

Golubkov V. A., Gorenkova G. A., Vorozhtsov E. P., Bespalova M. A., Bortnikov S. V. Chemical additive based on sodium oleate and linseed oil for preparation coal dust suppression composition. *Mining Science and Technology (Russia)*. 2023;8(4):341–349. <https://doi.org/10.17073/2500-0632-2023-02-79>

**ТЕХНОЛОГИЧЕСКАЯ БЕЗОПАСНОСТЬ В МИНЕРАЛЬНО-СЫРЬЕВОМ КОМПЛЕКСЕ
И ОХРАНА ОКРУЖАЮЩЕЙ СРЕДЫ**

Научная статья

**Добавка на основе олеата натрия и льняного масла
для углепылеподавляющих растворов**В. А. Голубков¹ , Г. А. Горенкова² , Е. П. Ворожцов² , М. А. Беспалова² , С. В. Бортников² ¹ Институт химии и химической технологии СО РАН, г. Красноярск, Российская Федерация² Хакасский государственный университет им. Н. Ф. Катанова, г. Абакан, Российская Федерация golubkov.va@icct.krasn.ru**Аннотация**

Добыча угля, его транспортировка и переработка сопровождаются образованием и поступлением в воздушную среду значительных объемов твердых частиц, в том числе угольной пыли. Наиболее распространенной технологией борьбы с угольной пылью в воздухе является гидрообеспыливание. Эта технология основана на способности воды смачивать пылевые частицы и связывать их между собой и с поверхностями, на которые осаждаются пыль. Существенное ограничение данной технологии заключается в гидрофобности поверхности угля, которая препятствует смачиванию водой частиц угольной



пыли. Для увеличения смачиваемости гидрофобной поверхности угольных частиц в воду добавляют поверхностно-активные вещества. В настоящей работе нами предложен состав для пылеподавления на основе олеиновой кислоты, гидроксида натрия и льняного масла в воде, изучены его свойства и оценена способность улучшать смачиваемость угольной пыли. Найдена наиболее эффективная концентрация, которая позволяет рабочему раствору улучшить смачиваемость угольной пыли на 187 % относительно воды, что превышает смачивающую способность большинства известных реагентов. Предлагаемый состав содержит 140 мг/л олеиновой кислоты, 100 мг/л гидроксида натрия, 70 мг/л льняного масла в воде. Простота состава, отсутствие вредности для окружающей среды и человека, незначительное влияние на дальнейшую эксплуатацию угольного сырья делают предлагаемый состав смачивателя перспективным для применения в технологиях гидрообеспыливания в угольной промышленности.

Ключевые слова

угольная пыль, пылеподавление, гидрообеспыливание, смачиваемость, поверхностно-активные вещества, олеат натрия, льняное масло

Благодарности

Исследование выполнено за счет гранта Министерства образования и науки Республики Хакасия (Соглашение № 93 от 13.12.2022).

Для цитирования

Golubkov V.A., Gorenkova G.A., Vorozhtsov E.P., Bepalova M.A., Bortnikov S.V. Chemical additive based on sodium oleate and linseed oil for preparation coal dust suppression composition. *Mining Science and Technology (Russia)*. 2023;8(4):341–349. <https://doi.org/10.17073/2500-0632-2023-02-79>

Introduction

The development of coal deposits, coal transportation, and processing results in the release of significant amounts of particulate matter, including coal dust into the air.

Prolonged exposure to coal dust can lead to preventable but incurable lung diseases, such as pneumoconiosis, chronic obstructive pulmonary disease, tuberculosis, chronic bronchitis, emphysema, and more, some of which can be fatal [1–4]. Workers and engineers in coal mines, open pits, coal transfer stations, coal preparation shops, and those involved in coal transportation are most susceptible to these diseases. Additionally, high concentrations of coal dust mixed with oxygen in the air pose a fire and explosion hazard [5]. These pressing issues highlight the necessity for effective technologies for removing coal dust from the air while minimizing of aerological risks [6].

In order to prevent dust formation during the crushing, processing, and transportation of dusty materials and suppress generated dust at mining and processing facilities, measures such as dampening rock masses and capturing flying dust are implemented. These methods, which focus on reducing the dust load by wetting of particles with water, are collectively referred to as water spray dust suppression or hydrodedusting [7]. Hydrodedusting relies on water's ability to wet dust particles, bind them together, and settle them. A significant challenge of this method is the hydrophobicity of coal surfaces, which prevents water from wetting coal dust particles. To overcome this, it is necessary to modify the particle surfaces to make it hydrophilic.

Extensive research has been conducted in the development of coal dust control technologies. One

of the most effective approaches is dust suppression through spraying water with the addition of surfactants [8]. This technology's development began in the early 20th century and gained particular importance after the 1970s due to the mechanization and intensification of coal mining [9, 10].

Surfactants, due to their diphilic nature, efficiently adsorb to the water-coal interface, rendering the surface of coal particles hydrophilic. This adsorption process reduces the free surface energy of coal dust and expedites the wetting process [11, 12].

Common wetting agents for coal dust suppression generally contain various surfactants as the main component to improve dust particles wetting. For example, in [13], authors propose using a combination of the sodium salt of alkylbenzenesulfonic acid and oxyethylated alkylphenol (neonol), and in [14], the sodium salt of carboxymethylcellulose. Apart from surfactants, these wetting agents contain other components, comprising 0.2–2.0 wt.% of the total composition, such as urea, inorganic salts, alcohols and polyols. While many dust suppression formulations are known, the search for new, more effective, and environmentally friendly alternatives remains an urgent task.

The objective of this study was to improve the coal dust suppression process through hydrodedusting by developing a novel formulation of wetting agent. The criteria for selecting reagents in this work included:

- the reagent's performance in dust suppression, supported by at least indirect methods;
- the simplicity and cost-effectiveness of the proposed technology;
- the environmental friendliness of the reagent.

In this context, it was deemed appropriate to explore the use of a naturally derived substance with surface activity, namely, the sodium salt of oleic acid.

Oleic acid is an anionic surfactant that reduces the adhesion of non-polar substances in a “solid non-polar surface: polar liquid” surface system. Additionally, sodium oleate significantly reduces the explosion potential of coal dust [15].

Sodium hydroxide is a reagent that, when combined with oleic acid, forms water-soluble sodium oleate.

Linseed oil is a reagent capable of inducing particle adhesion through the affinity of the oil and coal particle polarity. Furthermore, fatty unsaturated acids with long alkyl chains can polymerize to create a monolayer on a surface [16].

We have proposed a composition [17] for use in hydrodedusting processes and have determined the optimum concentrations to enhance dust suppression efficiency through the application of various physicochemical methods.

Research Materials and Techniques

Reagent preparation

The reagents were prepared as follows: a combination of 30 mL of water and 6 g (~150 mmol) of sodium hydroxide were merged with 8 g (~28 mmol) of oleic acid. The resulting mixture was heated

to 89–95°C. Subsequent to cooling, water was added to achieve a final volume of 1 L. To the resulting solution. We then added weighed portions of linseed oil while stirring to attain concentrations of 1, 4, 8, and 20 g/L.

The wettability study of coal dust was carried out using samples collected from the Chernogorsky deposit within the Minusinsk coal basin. In accordance with the genetic classification by S.I. Arbuzov [18], it was determined that the coal from the Chernogorskoye deposit falls into the category of humus coal of D grade, commonly referred to as “candle coal”. The macrocomponent composition of the coal includes vitrinite (67–74%), semivitrinite (1–4%), fusinite (17–27%), and liptinite (2–8%), with varying percentages for each individual seam. The coal from this deposit is mid-ash coal, with ash content ranging from 2.8% to 30%. The average volatile-matter yield is within the range of 36–43%, and the lower calorific value is 4830 kcal/kg. Coal dust was obtained by grinding coal from the Chernogorsky coal deposit in a porcelain jar; averaging was carried out by the envelope method, and the powder was sieved through a 0.5 mm sieve. According to particle size analysis performed on a laser particle size analyzer Laska TD (Russia), the share of particles with sizes 0.5–5 μm is less than 0.05%; 5–20 μm, 56.0%; 20–50 μm, 43.5%; 50–100 μm, 0.5%.

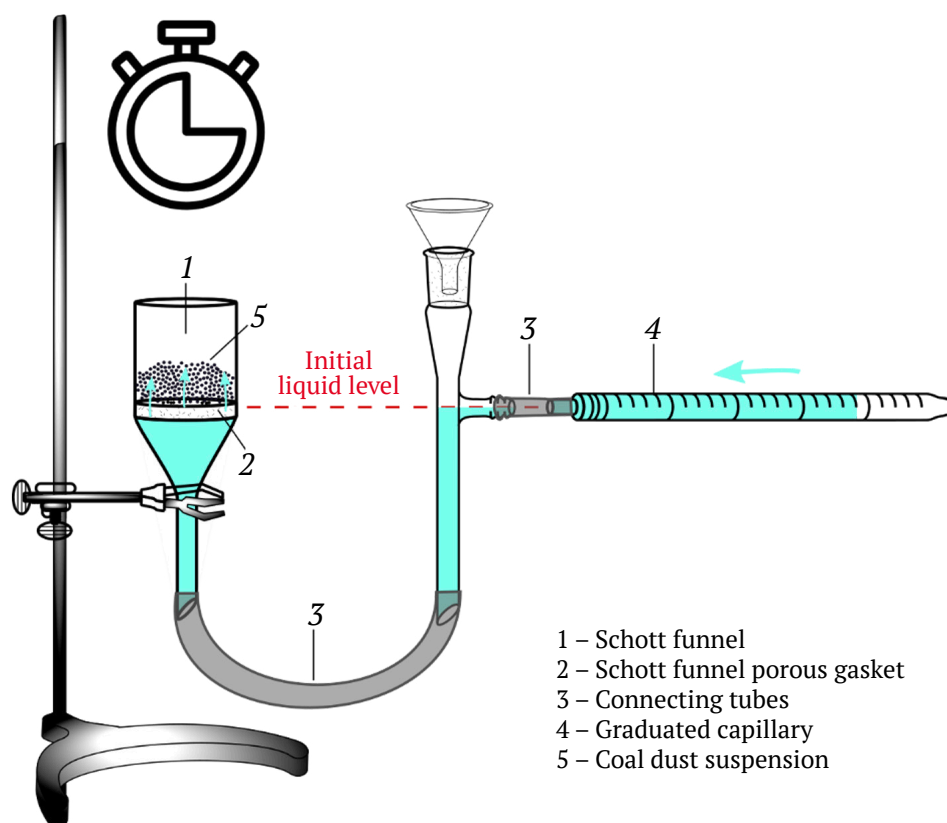


Fig. 1. Experimental set-up for wettability determination

Capillary soaking method

The wetting assessment of coal particle surfaces with aqueous solutions of various compositions was conducted using the established capillary soaking (absorption) method [19], as depicted in Fig. 1. A 1 g weighted portion of coal dust was placed in a Schott funnel (POR 100 class) with a porosity ranging from 0.04 to 0.1 mm. The room temperature was 21°C, and the maximum exposure time was 180 s. Wettability, which represents the maximum absorption of the solution, was determined as the ratio of the volume of absorbed liquid to the mass of coal, expressed as a percentage.

Film flotation method

The determination of the mass of coal particles applied to the surface of a liquid and their settling over time was carried out using VT-500 torsion scales. Specifically, 1 g of coal was applied to the surface of either water or reagent solution, and the weight of the settled particles after 1 and 3 min was measured.

Method of continuous weighing of settling particles

Sedimentation curves, which depict the weight of settling coal particles as a function of settling time, were obtained for coal particles in both water and reagent solutions using VT-500 torsion scales. This involved dispersing 1 g of coal was in 300 mL of a solution, and the weight of settling particles over time was recorded.

Measurement of electrokinetic potential

The measurements of particle distribution by hydrodynamic diameter using dynamic light scattering (DLS) and particle distribution by electrokinetic potential using electrophoretic mobility were

carried out using a Zetasizer Nano ZS instrument (Malvern Instruments, UK). The instrument specifications include a 633 nm laser, backscattering mode at an angle of 173°, a polycarbonate cell with Pd electrodes, and a measurement temperature of 25°C. All measurements of coal colloids were performed at pH 11±0.1 and autogenous ionic strength. Micelles of the initial reagent were measured at autogenous pH and ionic strength.

A coal colloid for electrokinetic potential measurements was obtained by subjecting 1 g of coal to ultrasonic treatment in 50 ml of deionized water for 15 min (100 kJ) using a SONOPULSmini20 ultrasonic homogenizer (Bandelin, Germany). This suspension was allowed to stand for 24 h at room temperature, and then a top layer was sampled. The particles in this top layer were used as a model for coal dust particles.

The Findings and Discussion

Wettability measurement and formulation optimization

The wettability of coal dust was found to vary depending on the wetting agent used. When the dust was treated with distilled water, the wettability index was 39%. In order to enhance the wettability of dust particles, sodium oleate, a sodium salt of oleic acid, was introduced. This resulted in an increased wettability of 54%. Notably, a more significant increase in wettability (up to 64%) was observed when using a sodium oleate solution with the addition of linseed oil. Linseed oil was added to the working solution in amounts of 1, 4, 8, 20 g/L. The optimum concentration of linseed oil in the solution was found to be 4 g/L (Fig. 2).

Synthesis of optimal dust suppression reagent composition and its characteristics

Based on experimental data, the most effective reagent composition was selected, consisting of 8 g/L oleic acid, 6 g/L sodium hydroxide, and 4 g/L linseed oil. The resulting reagent is a transparent liquid with a light yellow color, a pH of 12.85, and a conductivity of 22 mS/cm.

The reagent forms a dispersed system due to the surfactant concentration exceeding the critical micelle concentration. The size distribution of the dispersed phase exhibits two modes: Mode 1, likely comprising micelles with an average size of 7.5 nm, and Mode 2, with an average size of 150 nm (Fig. 3). The larger particles are believed to be aggregates of the surfactant micelles, and with sufficient dilution, both modes will dissolve. Therefore, this formulation aligns well with the requirements for wetting agents for dust suppression for coal and mining industries [20].

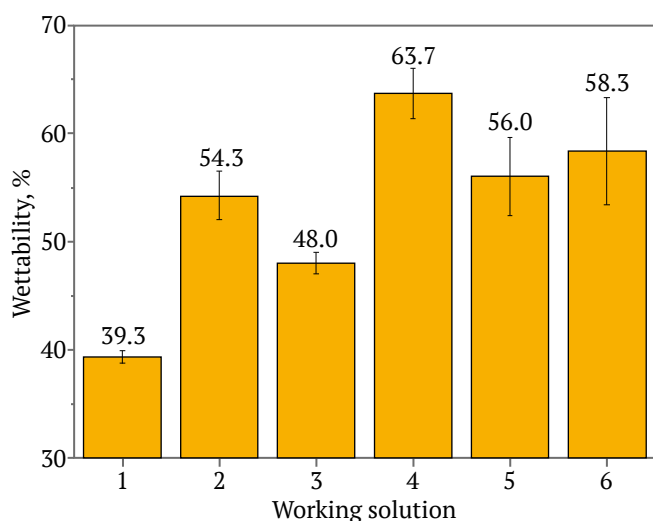


Fig. 2. Wettability of coal dust with working solutions: 1) distilled water; 2) sodium oleate (SO); 3) SO with linseed oil 1 g/L; 4) SO with linseed oil 4 g/L; 5) SO with linseed oil 8 g/L; 6) SO with linseed oil 20 g/L

Selecting the optimal reagent dilution level

Using a reagent with a high concentration in hydrodedusting is economically inefficient, comes with technical and engineering challenges, and can even have a negative impact on the environment. Therefore, it is crucial to determine the optimum degree of dilution. The influence of reagent concentration on the wettability of coal dust was investigated using capillary soaking method. Pure water exhibited low wetting efficiency, at 39%, whereas the initial reagent demonstrated significantly higher efficiency at 64%. Dilution of the reagent led to an improvement in coal wettability: a 10% solution showed a wettability of 68%, a 3.3% solution reached 69%, and a 1.7% solution achieved 73% (Fig. 4).

In order to estimate the added wetting performance when surfactants are used, the following formula is employed:

$$E_r = \frac{E_w P_r}{P_w}$$

where E_r represents wetting agent performance, %, E_w is water performance (100%), P_r is wetting agent performance in an experiment, %, (i.e. wettability), in this case, and P_w is water performance in an experiment.

In studies involving different additives, the relative efficiency ranged from 100% (equal to the effect of pure water) to 193% (exceeding the efficiency of water by nearly 2 times) [8]. The proposed composition demonstrates maximum efficiency in wetting coal dust at a dilution of up to 1.7% (140 mg/L oleic acid, 100 mg/L sodium hydroxide, 70 mg/L linseed oil in water). Its efficiency relative to pure water was 187%. Considering the availability and affordability of the components and their low potential environmental impact, this version of the reagent is recommended for further research.

It is important to note that not only wettability but also the wetting rate depends on the composition used. Water exhibited a lower initial wetting rate, whereas hydrodedusting reagent solutions demonstrated significantly higher rates. However, the initial settling rate remained independent of surfactant concentration in the system (Fig. 5).

Particle immersion tests in surfactant solutions, including methods like the film flotation method and sedimentation analysis, are conventional approaches for assessing the wetting efficiency of coal dust using working solutions [8, 21]. The rate at which particles immerse from the solution's surface is a key determinant of wetting efficiency. With an increase in concentration up to 3.3%, there is an observable increase in the mass of settled particles. This suggests

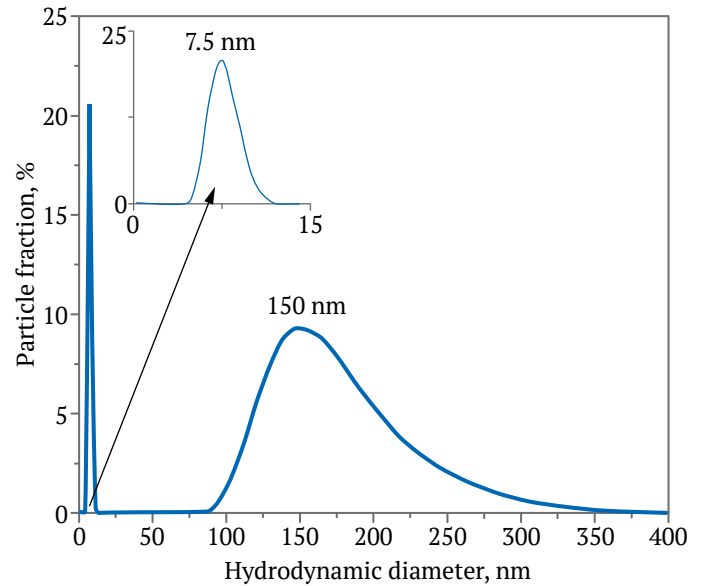


Fig. 3. Micelles and floccule size distribution in the initial reagent

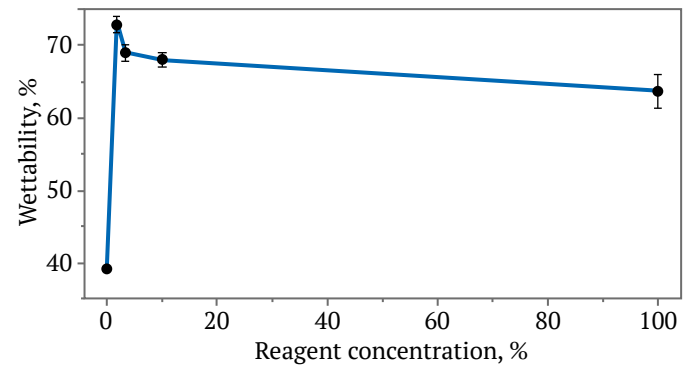


Fig. 4. Wettability of coal with reagent solutions of different concentrations

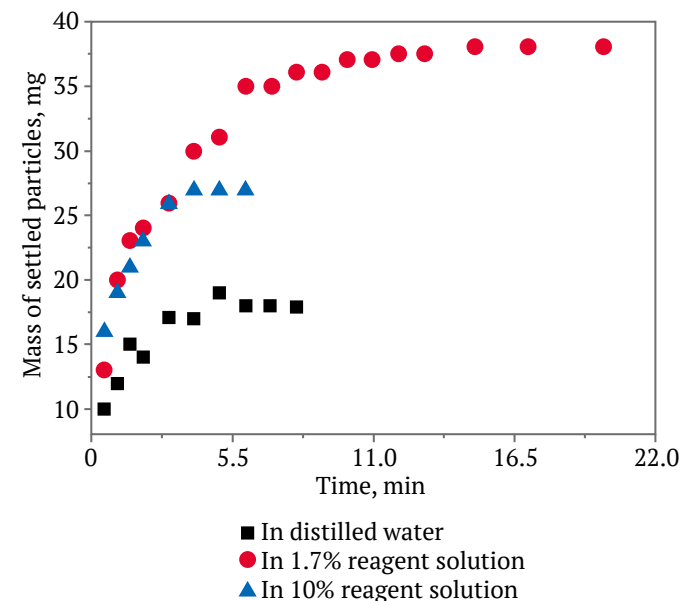


Fig. 5. Coal dust particle sedimentation rate in wetting reagent solutions

an improved wetting of the particles, making it easier for them to pass through the liquid surface. However, when the reagent concentration exceeds 5%, the mass of settling particles over time significantly decreases, sometimes even falling below that of pure water. In such cases, the settling process is limited not by the particle's penetration from the liquid surface into the solution volume, but by the aggregative stability of

the particles. Naturally, the adsorption of an anionic surfactant leads in an increase in the surface charge of the particles, resulting in greater electrostatic repulsion between them.

In order to confirm the established patterns, the distributions of hydrodynamic radii and electrokinetic potentials of coal colloids were measured (Fig. 7).

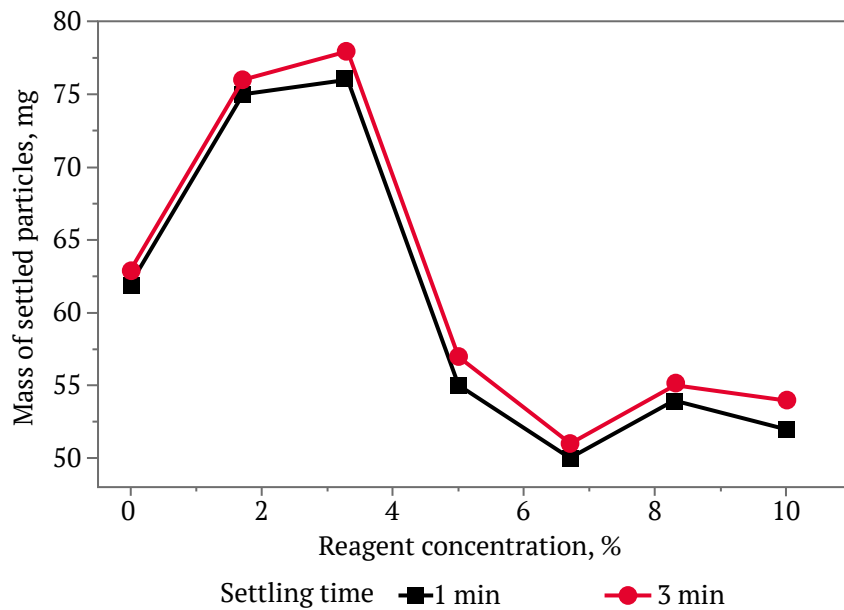


Fig. 6. Dependence of settled particle mass on reagent concentration

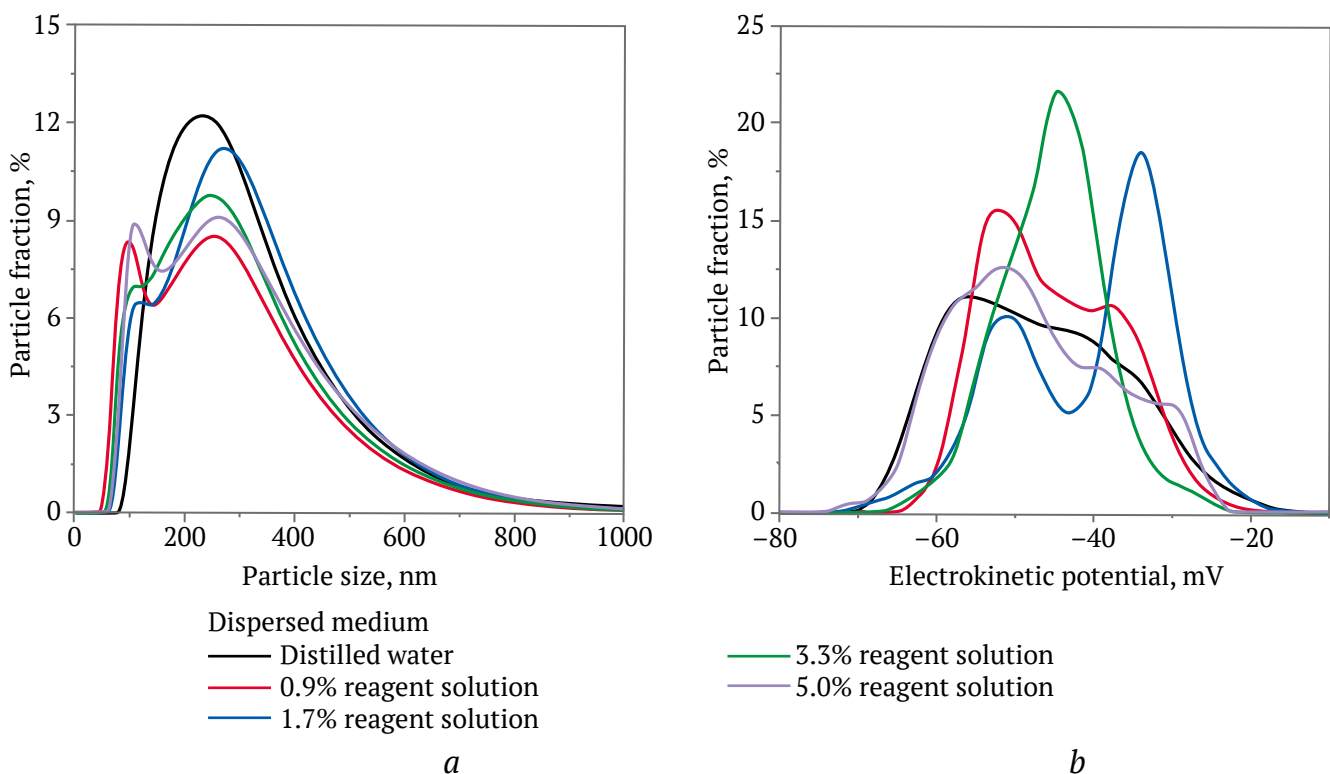


Fig. 7. Colloidal particle size (a) and electrokinetic potential (b) distribution with dust suppression reagent additives

In water, the particle distribution is monomodal, with an average size of 230 nm. However, upon the addition of a surfactant, we observe the emergence of two modes in the size distribution across all reagent concentrations. A significant portion of the particles experience size reduction, forming a mode with an average size of 100–110 nm. This phenomenon represents particle disaggregation or disagglomeration resulting from electrostatic repulsion, a well-known phenomenon [22]. It is worth noting that the use of sodium oleate for dispersing carbon black is also known to lead to particle size reduction [23].

At a pH of 11, a coal colloid exhibits a strongly negative charge, with an average ζ potential of -46 mV. The introduction of a surfactant and its adsorption on the particle surfaces result in alterations to the charge distribution of the particles (Fig. 7, b). This surfactant adsorption involves two concurrent processes: the suppression of surface acid group dissociation in coal and the emergence of new ionization centers through dissociated adsorbate molecules [24]. At lower surfactant concentrations (0.9% reagent solution), both factors exert a weak influence, and at the highest surfactant concentration (5% reagent solution), the particle charge distribution remains similar to that of coal in water, signifying a compensation of these factors. However, the most intriguing results are observed at reagent concentrations of 1.7 and 3.3%. In these cases, there is a narrowing of the particle distribution in ζ potential and a shift towards

lower charges. These formulations also yield better results in wettability measurement and particle immersion experiments.

Upon contact between coal particles and atomized drops of surfactant solution, effective wetting of coal particles occurs, in contrast to pure water drops. Fig. 8 graphically illustrates the action of the anionic surfactant additives in the water spray dust suppression process. In the initial stages (processes I and II), dust particles and droplets collide, which are largely independent of solution properties. When a hydrophobic coal dust particle interacts with pure water, it exhibits a limiting wetting angle $\theta > 90^\circ$, preventing droplets from capturing coal dust and depositing it (process III). However, the adsorption of sodium oleate from drops of surfactant solution renders the surface of coal particles more hydrophilic. In this scenario, the interaction of solute, solid particle, and water allows water to spread over the initially hydrophobic surface, with a limiting wetting angle $\theta < 90^\circ$ (process III). This altered liquid-solid interaction pattern leads to particle aggregation through particle absorption by droplets (process IV), which proliferates [12]. Nevertheless, excessive adsorption and correspondingly high surface charge on the particles can slow or even stop the particle immersion due to electrostatic repulsion. This explains the observed extreme dependence of wetting performance on surfactant concentration and justifies the selection of the reagent concentration required for high coal dust wetting performance.

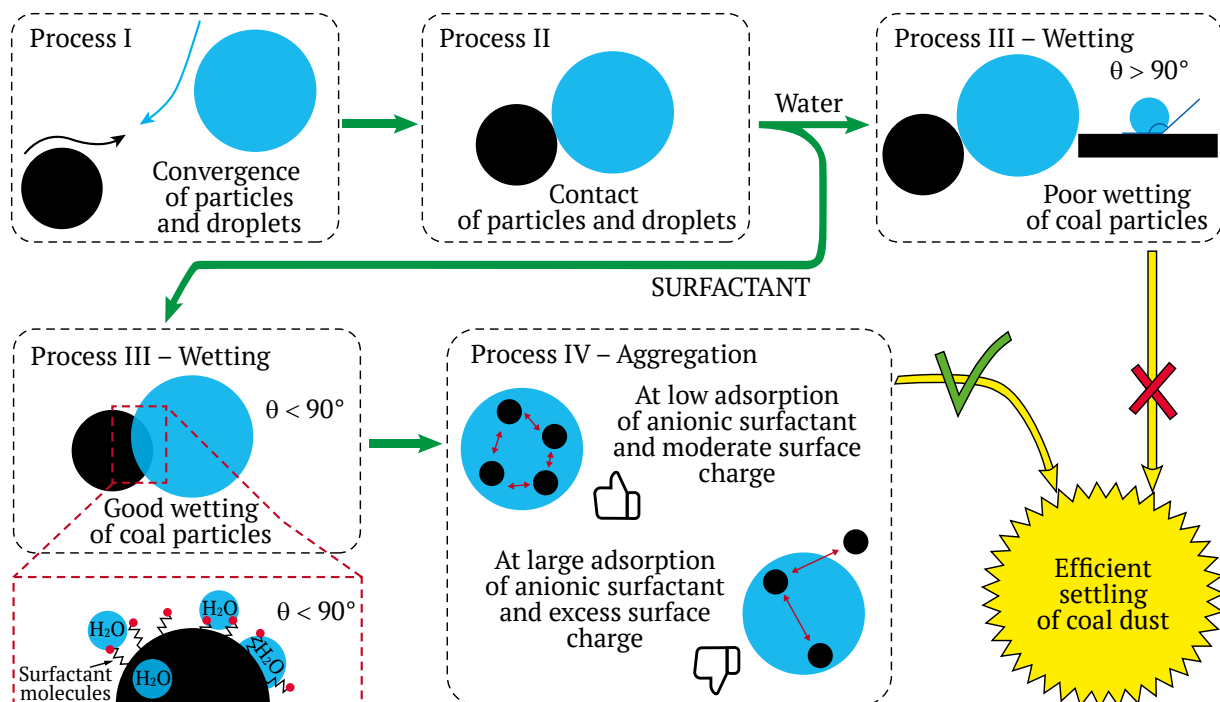


Fig. 8. Scheme of action of anionic surfactant additives in the process of water spray dust suppression



Conclusion

We have introduced a wetting agent composition for coal dust suppression [17], thoroughly studied its properties, and evaluated its ability to improve the wettability of hydrophobic surface. Through physico-chemical methods, we determined the most effective concentration for water spray dust suppression. The optimal composition for hydrodedusting was found to be a 1.7% aqueous solution of the reagent, consisting of 140 mg/L oleic acid, 100 mg/l sodium hydroxide, and 70 mg/L linseed oil in water). This solution

demonstrated remarkable efficiency in coal dust wetting experiments, achieving a performance level of 187% compared to pure water (set at 100%). This places it on par with the most effective dust suppression formulations reported in research publications in this field. The findings clearly illustrate that the components of the working solutions have a positive impact on coal wettability and wetting speed. One notable advantage of this composition is the safety of the surfactants used - oleic acid and linseed oil – both derived from renewable vegetable sources.

References

1. Ayoglu F.N., Acikgoz B., Tutkun E., Gebedek S. Descriptive characteristics of coal workers' pneumoconiosis cases in Turkey. *Iranian Journal of Public Health*. 2014;43(3):389. URL: <https://ijph.tums.ac.ir/index.php/ijph/article/view/4162>
2. Pollock D., Potts J.D., Joy G. Investigation into dust exposures and mining practices in mines in the southern Appalachian Region. *Mining Engineering*. 2010;62:44.
3. Ross M., Murray J. Occupational respiratory disease in mining. *Occupational Medicine*. 2004;54(5):304–310. <https://doi.org/10.1093/occmed/kqh073>
4. Perret J. L., Plush B., Lachapelle P. et al. Coal mine dust lung disease in the modern era. *Respirology*. 2017;22(4):662–670. <https://doi.org/10.1111/resp.13034>
5. Cao W., Gao W., Peng Y., Liang J., Pan F., Xu S. Experimental and numerical study on flame propagation behaviors in coal dust explosions. *Powder Technology*. 2014;266:456–462. <https://doi.org/10.1016/j.powtec.2014.06.063>
6. Balovtsev S. Higher rank aerological risks in coal mines. *Mining Science and Technology (Russia)*. 2022;7(4):310–319. <https://doi.org/10.17073/2500-0632-2022-08-18>
7. Letuyev K., Kovshov S., Gridina E. The Technology of Hydrodedusting of coal pits' auto roads using purified wastewater and drainage water. *Ecology and Industry of Russia*. 2020;24(1):30–33. (In Russ.) <https://doi.org/10.18412/1816-0395-2020-1-30-33>
8. Xu G., Chen Y., Eksteen J., Xu J. Surfactant-aided coal dust suppression: A review of evaluation methods and influencing factors. *Science of The Total Environment*. 2018;639:1060–1076. <https://doi.org/10.1016/j.scitotenv.2018.05.182>
9. Hartmann I., Greenwald H.P. *Use of wetting agents for allaying coal dust in mines*. US Department of the Interior, Bureau of Mines; 1940.
10. Harrold R. Surfactants vs. dust – do they work? *Coal Age*. 1979;84(6):102–105.
11. Liu H., Sun D., Hao J. *Colloid and interface chemistry*. Chemical Industry Press, Peking, China; 2016.
12. Li S., Zhao B., Lin H. et al. Review and prospects of surfactant-enhanced spray dust suppression: Mechanisms and effectiveness. *Process Safety and Environmental Protection*. 2021;154:410–424. <https://doi.org/10.1016/j.psep.2021.08.037>
13. Glebov A.F. *Penetrating agent for coal dust suppression*. RU2495250C1 (Patent). 2013.
14. Kovshov S.V., Kovshov V.P., Erzin A.Kh., Safina A.M. *Method of dust suppression in opened coal storages*. RU2532939. Patent. 2013.
15. Huang Q., Honaker R.Q., Perry K.A., Lusk B. Surface chemistry modification of rock dust for improved dispersion and coal dust explosion prevention. In: *Proceedings of the 2015 SME Annual Conference and Expo and CMA 117th National Western Mining Conference – Mining: Navigating the Global Waters*. 2015. Pp. 245–251.
16. Osman M.A., Suter U.W. Surface treatment of calcite with fatty acids: structure and properties of the organic monolayer. *Chemistry of Materials*. 2002;14(10):4408–4415. <https://doi.org/10.1021/cm021222u>
17. Bortnikov S.V., Gorenkova G.A. *Wetting agent for the suppression of coal dust*. RU2689469 C1 Patent. 2019.
18. Arbuzov S.I., Ershov V.V. *Geochemistry of rare elements in Siberian coals*. Tomsk: D-Print Publ.; 2007, 468 p. (In Russ.)
19. Kouzov P.A., Skryabin L. Ya. *Methods of determination of physical and chemical properties of industrial dusts*. Leningrad: Khimiya Publ.; 1983. (In Russ.)



20. Pozdnyakov G., Tretyakov A., Garavin V., Novoseltsev A. Requirements for wetting agents for dust suppression in coal and mining industries. *Occupational Safety in Industry*. 2013;(10):36–39. (In Russ.)

21. Walker P., Petersen E., Wright C. Surface active agent phenomena in dust abatement. *Industrial & Engineering Chemistry*. 1952;44(10):2389–2393. <https://doi.org/10.1021/ie50514a032>

22. Knyazheva O., Baklanova O., Lavrenov A. et al. The effect of ultrasonic exfoliation and the introduction of a surfactant on particle size and aggregative stability water dispersions of carbon black. In: *Oil and Gas Engineering (OGE-2018)*. 26 February – 2 March 2018, Omsk, Russia. 2018;2007(1):020016. <https://doi.org/10.1063/1.5051855>

23. Sis H., Birinci M. Effect of nonionic and ionic surfactants on zeta potential and dispersion properties of carbon black powders. *Colloids and Surfaces A: Physicochemical and Engineering Aspects*. 2009;341(1–3):60–67. <https://doi.org/10.1016/j.colsurfa.2009.03.039>

24. Maršálek R. The influence of surfactants on the zeta potential of coals. *Energy Sources, Part A: Recovery, Utilization, and Environmental Effects*. 2008;31(1):66–75. <https://doi.org/10.1080/15567030701468142>

Information about the authors

Viktor A. Golubkov – Ph.D.-Student, Junior Researcher, Laboratory of Catalytic Transformations of Renewable Resources, Institute of Chemistry and Chemical Technology of the Siberian Branch of the RAS, Krasnoyarsk, Russian Federation; ORCID [0000-0002-1518-790X](https://orcid.org/0000-0002-1518-790X), Scopus ID [57391926200](https://scopus.com/authorid/57391926200); e-mail golubkov.va@icct.krasn.ru

Galina A. Gorenkova – Cand. Sci. (Chem.), Associate Professor, Department of Chemistry and Geoecology, Khakassian State University named after N.F. Katanov, Abakan, Russian Federation; ORCID [0000-0003-3412-6384](https://orcid.org/0000-0003-3412-6384); e-mail gorenkovagala@mail.ru

Evgeniy P. Vorozhtsov – Student, Department of Chemistry and Geoecology, Khakassian State University named after N.F. Katanov, Abakan, Russian Federation; ORCID [0000-0001-8388-1330](https://orcid.org/0000-0001-8388-1330); e-mail vorozhcov2001@mail.ru

Mariya A. Bespalova – Student, Department of Chemistry and Geoecology, Khakassian State University named after N.F. Katanov, Abakan, Russian Federation; ORCID [0009-0001-5377-3715](https://orcid.org/0009-0001-5377-3715); e-mail bespalova.mariya.1307@mail.ru

Sergey V. Bortnikov – Cand. Sci. (Chem.), Head of the Department of Chemistry and Geoecology, Khakassian State University named after N.F. Katanov, Abakan, Russian Federation; ORCID [0000-0002-4583-0118](https://orcid.org/0000-0002-4583-0118); e-mail svb@khsu.ru

Received 04.02.2023

Revised 28.06.2023

Accepted 30.06.2023



SAFETY IN MINING AND PROCESSING INDUSTRY AND ENVIRONMENTAL PROTECTION

Research paper

<https://doi.org/10.17073/2500-0632-2023-10-163>

УДК 622.4:622.8



Monitoring of aerological risks of accidents in coal mines

S. V. Balovtsev   

National University of Science and Technology MISIS, Moscow, Russian Federation

 balovtsev@yandex.ru

Abstract

The assessment and management of aerological risks in coal mine accidents are based on the development of a data analytics system that hosts design values for various parameters and subsystems related to coal mines, as well as the real-time monitoring of operational parameters through various sensors and devices. This study presents the methodology for monitoring aerological risks. It utilizes mining, geological, and geotechnical conditions for seam extraction, along with statistical data concerning elements of coal mine ventilation and gas drainage systems, to assess aerological risks at individual coal mine functionality levels and individual risk factors. Eight coal mines have been ranked according to their aerological risk level. For rank I, the minimum aerological risk is 0.0769, while the maximum is 0.5698. Rank II is associated with category II mines. Aerological risk for this rank is the lowest and ranges from 0,1135 to 0,3873. In the case of rank III, the minimum aerological risk is 0.057, with a maximum of 0.595. This ranking of coal mines by aerological risk level allows to identify potentially unsafe mines in terms of aerology, and enables us to determine aerological risk mitigation measures (technical, technological, and organizational) for each mine to enhance aerological safety.

Keywords

coal mine, data analytics system, aerological system, aerological risk monitoring, vulnerability of ventilation schemes and types

For citation

Balovtsev S.V. Monitoring of aerological risks of accidents in coal mines. *Mining Science and Technology (Russia)*. 2023;8(4):350–359. <https://doi.org/10.17073/2500-0632-2023-10-163>

ТЕХНОЛОГИЧЕСКАЯ БЕЗОПАСНОСТЬ В МИНЕРАЛЬНО-СЫРЬЕВОМ КОМПЛЕКСЕ И ОХРАНА ОКРУЖАЮЩЕЙ СРЕДЫ

Научная статья

Мониторинг аэрологических рисков аварий на угольных шахтах

С. В. Баловцев   

Университет науки и технологий МИСИС, г. Москва, Российская Федерация

 balovtsev@yandex.ru

Аннотация

Оценка и управление аэрологическими рисками аварий в угольных шахтах основываются на создании информационно-аналитической системы данных, включающей в себя проектные значения показателей разных уровней и подсистем угольных шахт, эксплуатационные значения показателей, отслеживаемых системой мониторинга в реальном времени с использованием различных датчиков и устройств. В настоящем исследовании представлена методология мониторинга аэрологических рисков. На основании горно-геологических и горнотехнических условий отработки пластов, статистических данных по элементам вентиляционных и дегазационных систем угольных шахт приведены результаты оценки аэрологических рисков по отдельным уровням функциональной структуры угольных шахт, а также по отдельным факторам риска. По уровням аэрологических рисков выполнено ранжирование восьми угольных шахт. Установлено, что минимальное значение аэрологического риска I ранга составляет 0,0769, максимальное – 0,5698. Наименьшие значения аэрологического риска II ранга (0,1135–0,3873) относятся к шахтам II категории. Минимальное значение аэрологического риска III ранга составляет



0,057, максимальное – 0,595. Ранжирование угольных шахт по уровням аэрологических рисков позволяет выявить шахты с низким уровнем аэрологической безопасности и для каждой шахты определить направления технических, технологических и организационно-технических мероприятий по повышению аэрологической безопасности.

Ключевые слова

угольная шахта, информационно-аналитическая система, аэрологическая безопасность, мониторинг аэрологических рисков, уязвимость схем и способов вентиляции

Для цитирования

Balovtsev S.V. Monitoring of aerological risks of accidents in coal mines. *Mining Science and Technology (Russia)*. 2023;8(4):350–359. <https://doi.org/10.17073/2500-0632-2023-10-163>

Introduction

The trend towards intensified mining and increased underground coal mining in increasingly complex geological, geotechnical, and mining conditions requires a focused and systematic approach to HSE (Health, Safety, and Environment) issues, with aerological safety being a major concern.

Failures in the aerological safety system may result from an unfavourable combination of various factors. These factors include fluctuating gas emissions from the seam under development, worked-out space, unsteady gas dynamic processes [1, 2], fluctuations in air discharge, unplanned change in the resistance of workings, and failing ventilation systems [3, 4], fluctuations in mining, geotechnical, and geological conditions, as well as changing physical and technical properties of the formation (such as gas content, gas permeability, gas recovery factor, formation porosity and permeability, and dust generation capacity), geological disturbances, and more [5, 6]. When investigating the regularity of aerological safety system failures, some of the above-mentioned parameters are often treated as continuous random variables, rather than discrete ones, which can take any value within a given range, and are not known in advance.

Unsteady dynamic processes (involving gas-dust-heat emissions) in mines are the primary causes of the loss of operability in aerological safety management systems. Changes in mining, geological, and geotechnical conditions during the development of coal seams can lead to risk of explosions, ignitions of dust-gas mixtures, fires, rock bumps, spontaneous coal ignition, and other types of accidents [7, 8].

The properties and conditions of coal seams and host rocks determine the sources and locations of gas emissions, dust formation, sudden outbursts of coal, rocks, and gas, spontaneous coal ignition, and rock bumps [9, 10]. Therefore, a thorough study of the processes in coal formations is necessary to select an appropriate technical solution for the aerological safety management system. The effectiveness of such technical solutions directly depends on the

reliability of and prompt access to data that characterize many technological processes [11, 12]. Knowledge of process patterns helps assess the importance and weighting factors of safety system mitigation measures. For example, gas drainage (early preventive, preliminary, in-seam) is crucial when mining coal seams with high gas concentration that are prone to dust explosions. [13, 14]. The order in which seams are mined in the formation is also important, followed by the selection of ventilation schemes, ventilation with gas-suction units, and more [15, 16].

As coal seams are mined deeper, roof-to-floor convergence intensifies, leading to aerodynamic aging of workings that impacts the performance of the aerological safety system [17, 18].

The management of gas emissions plays an important role in aerological safety and involves a series of measures to redistribute or alter gas emission flows. The purpose of gas emission management is to enhance the ventilation of mine workings, improve the ventilation of working areas, preparatory workings, and the mine as a whole.

Key measures in gas emission management include changing ventilation schemes, modifying the aerodynamic resistance of mine workings using ventilation facilities and devices, selecting the appropriate order for mining seams in the formation and mining systems; implementing special ventilation for mined-out space, using gas-suction units, degassing mine workings and seams, gas-draining mine workings and holes, and more.

To study the interaction between gas and coal and the mechanism of spontaneous ignition in the mined-out space, numerical simulation of gas explosion risks can be applied [19, 20].

Methodology for monitoring aerological risks

The assessment of aerological safety system performance can be achieved through the evaluation of aerological risks at various levels and subsystems within coal mines. This includes risks categorized as I, II, and III-rank risks, risks of high gas concentration,



risks of reusing mine workings, risks linked to the impact of heavy hydrocarbons (HCs), as well as composite and expected estimated risk factors (Table 1). Accident-related aerological risk monitoring at coal mines can be effectively carried out using predictive analytics based on available data.

Predictive analytics uses collected, processed, and structured data to create scenarios for the further development of events of interest. Consequently, the primary challenge in this regard pertains to data retrieval, processing, scenario development, and the interpretation of obtained results to make informed management decisions related to aerological safety.

Data collection can be quite complex and relies on personnel involvement, and manual work, which is still not highly reliable and carries a high risk of errors. [21, 22]. To improve the reliability of the obtained solutions, ensemble methods, comparing basic individual solutions, are applied [23, 24].

There are four types of data analytics:

1. Descriptive analytics, which involves collecting data over the monitoring of the object (target). The gathered data are analyzed to address the question, “What has happened?” In the context of coal mines, descriptive analytics may be employed to collect the data pertaining to accidents in coal mines, including their causes, extent of damage, mining, geological, and geotechnical conditions at the time of the accident, and accident investigation data, etc. [25, 26].

2. Diagnostic analytics involves diagnosing the causes of the event under study using statistical analysis. All collected data can be categorized into separate groups and subgroups, with an analysis of data correlation. Significant factors influencing the outcome of the event are identified. Diagnostic analytics can group statistical data based on seam properties, coal grades, mining depth, methane

Table 1

Operational parameters of aerological risks

Rank of aerological risk	Operational parameters of aerological risks	Notes
I	Rank I aerological risk $R_{a,m}$	Depends on specific dust emission, relative gas content, mine ventilation scheme and method, vulnerability of main ventilators
II	Rank II aerological risk $R_{a,mw}$	Depends on specific dust emission, relative gas content, scheme and method of mine wing ventilation, vulnerability of ventilation structures
II	Rank III aerological risk R_a	Depends on specific dust emission, relative gas content, vulnerability of working area
	Aerological risk of accidents R_{hHCwa} in working areas induced by heavy HCs impact	Depends on heavy HCs content in residual coal gases (grades D, G, DG, GZh, Zh, KZh, K, KS, OS), methane concentration in coal seams, specific dust emission, mining depth and technological vulnerability of working area
	Estimated composite aerological risk Q_{es}	Depends on specific dust emission, relative gas content, vulnerability of working area; accounts for seam ignitibility and susceptibility to rock bump, application of gas drainage, gas sucking units and gas draining drive
	Risk of high gas concentration in the working area R_{hgca}	Takes into account average statistical data of failure rates in mine workings and the working area ventilation scheme
	Risk of high gas concentration in the reused working area $R_{hgca, day^{-1}}$	Takes into account average statistical data of failure rates in mine workings, the working area ventilation scheme, and workings reuse
	Aerological risk of accidents in preparatory workings induced by heavy HCs impact R_a	Depends on specific dust emission, relative gas content, vulnerability of preparatory workings
	Aerological risk of accidents R_{hHCwa} in preparatory workings induced by heavy HCs impact	Depends on heavy HCs content in residual coal gases (grades D, G, DG, GZh, Zh, KZh, K, KS, OS), methane concentration in coal seams, specific dust emission, mining depth, and technological vulnerability of preparatory workings
Estimated aerological risk of accidents in preparatory workings Q_{es}	Depends on specific dust emission, relative gas content, vulnerability of preparatory workings; accounts for seam ignitibility and susceptibility to rock bump, gas draining	



concentrations in seams, dust hazard factor, load on the mine face, absolute methane-bearing capacity of mines, the rate of face advance, ventilation schemes and types in mines and working areas, parameters of the main and local fans, and more.

3. Predictive analytics predicts the further development of events based on pre-processed data obtained through descriptive and diagnostic analytics. For example, predictive analytics can analyze the aging of mine workings, allowing for the properly scheduling of preventive maintenance in the workings, thereby reducing aerological risks in mine ventilation systems [4, 27].

4. This type of analytics enables the understanding and justification of steps to be taken to prevent undesirable events. One can call it prescriptive analytic. In the context of the aerological safety system, these steps encompass technical solutions aimed at managing coal seam properties and condition (such as pre-moistening, advance, preliminary, in-seam gas drainage, and emergency shut-down system parameters, etc.), as well as technical and technological measures.

Therefore, in order to assess the performance of the aerological risk management system, a comprehensive statistical dataset is required, relating to ventilation system components (main fans, gas-sucking units, local site fans, vent doors, and airlocks, crossings, main downcast and air shafts, longwalls, gas-intake pipelines, ACS, etc.), as well as mining and geotechnical conditions (longwall productivity, seam thickness, rock strength, workings protection technology, mining depth, mining system, etc.) (Table 2).

Results and discussion

Table 3 presents the computed results for aerological risk of all three ranks (I – for the entire mine, II – for the mine wing, III – for working areas and preparatory workings). The additional risks estimates were made for the working areas, including the risk of high gas concentrations in the areas due to their ventilation scheme, the risk of high gas concentrations of the working reuse, as well as the risk of accidents induced by heavy HCs (based on coal grades). An expected composite aerological risk was also calculated for the working areas, assuming gas drainage is applied. These estimations were made for the case of maximum mining depth. It's important to note that the expected risk considered seam ignitability and susceptibility to rock bursts. For mines No. 2 and 8, gas drainage efficiency was 0.95 and 0.9, respectively, while the average gas drainage efficiency of 0.6 was used for the rest of the mines.

For the preparatory workings, estimates were made for the accident risk caused by heavy HCs and the aerological risk, assuming gas drainage measures are implemented.

In the study of eight analyzed mines, three mines are categorized as methane hazard category II, while five mines are super-category. The analysis of the data presented in Table 3 reveals the following findings: for I rank aerological risk, the minimum risk is 0.0769, and the maximum is 0.5698, representing a 7.4-fold difference between the two extremes. The minimum risk is observed in category II mines (No. 3, 4, 5), indicating low risk, with the threshold for safe operations set at a maximum of 0.15.

In the study of eight analyzed mines, three mines are categorized as methane hazard category II, while five mines are super-category. The analysis of the data presented in Table 3 reveals the following findings: for I rank aerological risk, the minimum risk is 0.0769, and the maximum is 0.5698, representing a 7.4-fold difference between the two extremes. The minimum risk is observed in category II mines (No. 3, 4, 5), indicating low risk, with the threshold for safe operations set at a maximum of 0.15.

Among the super-category mines, the risks vary significantly. Two mines (No. 1 and 6) exhibit moderate risk (reduced operational safety with a risk range of 0.15–0.3), two mines (No. 7 and 8) show high risk (poor operational safety level with a risk higher than 0.3 but lower than 0.5, and one mine (No. 2) faces an emergency-level risk, which could potentially lead to an accident, with a risk exceeding 0.5.

The analyzed geological, geotechnical, and mining factors (as detailed in Table 2) reveal that rank I risks are less affected by the scheme and method of mine ventilation, air supply availability in mines, external and internal air leakage, but more affected by the absolute methane content in mines and main fans pressure. For Mine No. 8, these values are particularly high, with an absolute methane content of 239 m³/min and a main fan pressure of 820 daPa. Notably, this mine has the largest number of ventilation facilities compared to others (190).

The estimated rank II aerological risk shows a range of conditions, from the best (low depression of haulage and ventilation drifts, ventilation stability in the mine wing, low impact of thermal depression in inclined workings, low impact of ventilation method on gas concentration in the workings at the main fan emergency shut-down, low impact of ventilation facilities on ventilation stability) to the worst. In the worst conditions, the factors listed in brackets above have a more significant impact on the vulnerability of ventilation schemes, methods, and facilities in mine's wings.



Table 2

Aerological risk factors

Aerological risk factor	Coal mine No							
	1	2	3	4	5	6	7	8
Gas hazard category	Super-category	Super-category	CategoryII	CategoryII	Category II	Super-category	Super-category	Super-category
Seam susceptibility or rock burst	Yes	Yes	Yes	Yes	Yes	Yes	Yes	Yes
Seam ignitibility	Yes	Yes	Yes	Yes	Yes	Yes	Yes	Yes
Dust hazard	Yes	Yes	Yes	Yes	Yes	Yes	Yes	Yes
Coal grade	G	G, GZh	D, DG	D	D, DG	D, DG	D, DG	G
Methane content in coal seams, m ³ /t	10–15	13–15 17–20	4–6 4–9		0–5	0–5 0–6	10–15	14–20
Mining depth, m	130–480	420–660	400	400	240–290	540	350–440	540
Mine ventilation pressure, daPa	292	820	290	220	295	265	306	320
Mine ventilation stability	Category II	Category II	Category II	Category II	Category II	Category II	Category II	Category II
Mine ventilation scheme	Combined	Radical	Combined	Radical	Combined	Combined	Combined	Combined
Mine ventilation method	Blowing	Combined	Combined	Combined	Blowing	Blowing	Blowing	Combined
Stability of combined operation of main fans	Low vulnerable	Highly vulnerable	Low vulnerable	Low vulnerable	Low vulnerable	Low vulnerable	Highly vulnerable	Highly vulnerable
Mine air availability	1.33	1.47	1.2	1.17	1.27	1.13	1.05	1.46
External air leakage (estimated), %	13.14	13.45	14	14	10	10		12.9
External air leakage (actual), %	16.69	8.43	11	9.8	5	6	5.77	12.9
Stability of mine wing ventilation	Category II	Category II	Category II	Category II	Category II	Category II	Category II	Category II
Scheme of mine wing ventilation	Central-dual	Radical	Central-dual	Radical	Central-dual	Central-dual	Central-dual	Central-dual
Method of mine wing ventilation	Blowing	Blowing	Blowing	Blowing	Blowing	Blowing	Blowing	Blowing
Impact of ventilation structures on ventilation stability	Low vulnerable	Highly vulnerable	Low vulnerable	Low vulnerable				
Per face output t/day	6300	13500	13300	10900	7500	13400	20900	6600
Absolute methane content in mine, m ³ /min	109	239	28.34	32	17	16.6	181	108
Face performance rate, m/day	7	7 9.5	9 9.5	5	7.2	5.2	8.3	5.73
Face length, m	230	365 365	300 300	350	300	410	400	300
Extraction panel length, m	1960	2100 2550	2850 2800	2850	2500	2300	3000	2100
Gas drainage	No	Yes	Yes	Yes	No	No	Yes	Yes
Number of stopes	1	2	2	1	1	1	1	1



Table 3

Estimated aerological risks

Aerological risk parameter	Coal mine No							
	1	2	3	4	5	6	7	8
Rank I aerological risk R_{am}	0.2074	0.5698	0.0974	0.0769	0.1159	0.2134	0.3831	0.3532
Rank II aerological risk R_{awm}	0.2457–0.6931	0.2125–0.6166	0.1373–0.3873	0.1135–0.3322	0.1373–0.3873	0.2457 0.6931	0.2457 0.6931	0.2457 0.6931
Rank III aerological risk R_a	0.425	0.272; 0.272	0.3325; 0.3325	0.057	0.3325	0.595	0.595	0.255
Aerological risk of accidents R_{hHCwa} in working areas induced by heavy HCs impact	0.5464–0.9255	0.5551–0.94; 0.5813–0.9846	0.3026–0.6548	0.2858–0.7317	0.2385–0.5297	0.2628–0.5547	0.5372–0.9256	0.5551–0.94
Estimated composite aerological risk Q_{es}	0.4675	0.2346; 0.2346	0.3358; 0.3358	0.0576	0.3857	0.6902	0.6009	0.2231
Risk of high gas concentration in the working area R_{hgca}	0.189	0.065 0.065	0.189 0.189	0.097	0.189	0.189	0.189	0.097
Risk of high gas concentration in the reused working area R_{hgca} day ⁻¹	0.2403	0.1244 0.1244	0.2403 0.2403	0.155	0.2403	0.2403	0.2403	0.1244
Aerological risk of accidents in preparatory workings R_a	0.17–0.85	0.17–0.85	0.095–0.475	0.095–0.475	0.095–0.475	0.17–0.85	0.17–0.85	0.17–0.85
Aerological risk of accidents $R_{hHC pw}$ in preparatory workings induced by heavy HCs impact	0.0696–0.9846	0.0696–0.9846	0.0454–0.8185	0.0454–0.9692	0.0432–0.7996	0.0476–0.8373	0.0675–0.9692	0.0696–0.9846
Estimated aerological risk in preparatory workings Q_{es}	0.187–0.935	0.1466–0.7331	0.096–0.4798	0.096–0.4798	0.1102–0.551	0.1972–0.986	0.1717–0.8585	0.1488–0.7438



The lowest rank II aerological risk corresponds to category II mines and is 1.78 times lower for both the best and the worst conditions.

The minimum rank III aerological risk is 0.057, and the maximum is 0.595, which is 10.4 times higher than the minimum. The minimum risk refers to the category II mine No. 4 and is classified as a low risk.

Two mines (No. 2 and 8) have estimated moderate risk, two mines (No. 1 and 5) exhibit high risk, and two mines (No. 6 and 7) have an emergency-level risk, potentially leading to accidents due to a U-ventilation in the working areas with partial dilution of harmful agents at the emission sources. The ventilation scheme in mines No. 6 and 7 is quite intricate because of a diagonal connection, which can lead to air flow-back under specific conditions.

Aerological risks of accidents in working areas, induced by heavy HCs in coal residual gases, are more likely when mining coal seams of grades D, G, DG, GZh, Zh, KZh, K, KS, or OS, particularly with a high load on the mining face at a high mining face advance rate. The highest heavy HCs-related risk of accidents was observed in mine No. 2, which is developing a GZh gradeseam [28].

The expected composite aerological risk takes into account additional hazards, such as coal seam susceptibility to rock bumps and spontaneous igni-

tion, as well as gas release management measures like degassing, gas-draining workings, and gas-suction units. Depending on the mining, geotechnical, and geological conditions, the value of the expected composite risk may increase or decrease. Generally, the expected risk has slightly increased for all mines, except for mines No. 2 and 8, which develop formations not prone to spontaneous ignition.

Histograms for five types of risks in the analyzed mines (Fig. 1) were plotted based on the data provided by Table 3. These histograms demonstrate that three of the mines (No. 3, 4, 5) exhibit low aerological risks, falling within the normal safety range, even though the risks in their working areas slightly exceed this range. There is a return-flow ventilation scheme with diagonal connections there, but due to the low absolute gas content (from 17 to 28.4 m³/t), these risks are not very dangerous. In general, all the three mines are characterized by low aerological risks.

The data from Table 3 was used to generate histograms representing five types of risks for the examined mines (Fig. 1). Analysis of the data reveals that three of these mines (No. 3, No. 4, No. 5) exhibit low aerological risks that fall within the acceptable safety range. Slight elevation of risks is observed in their working areas, attributed to their use of

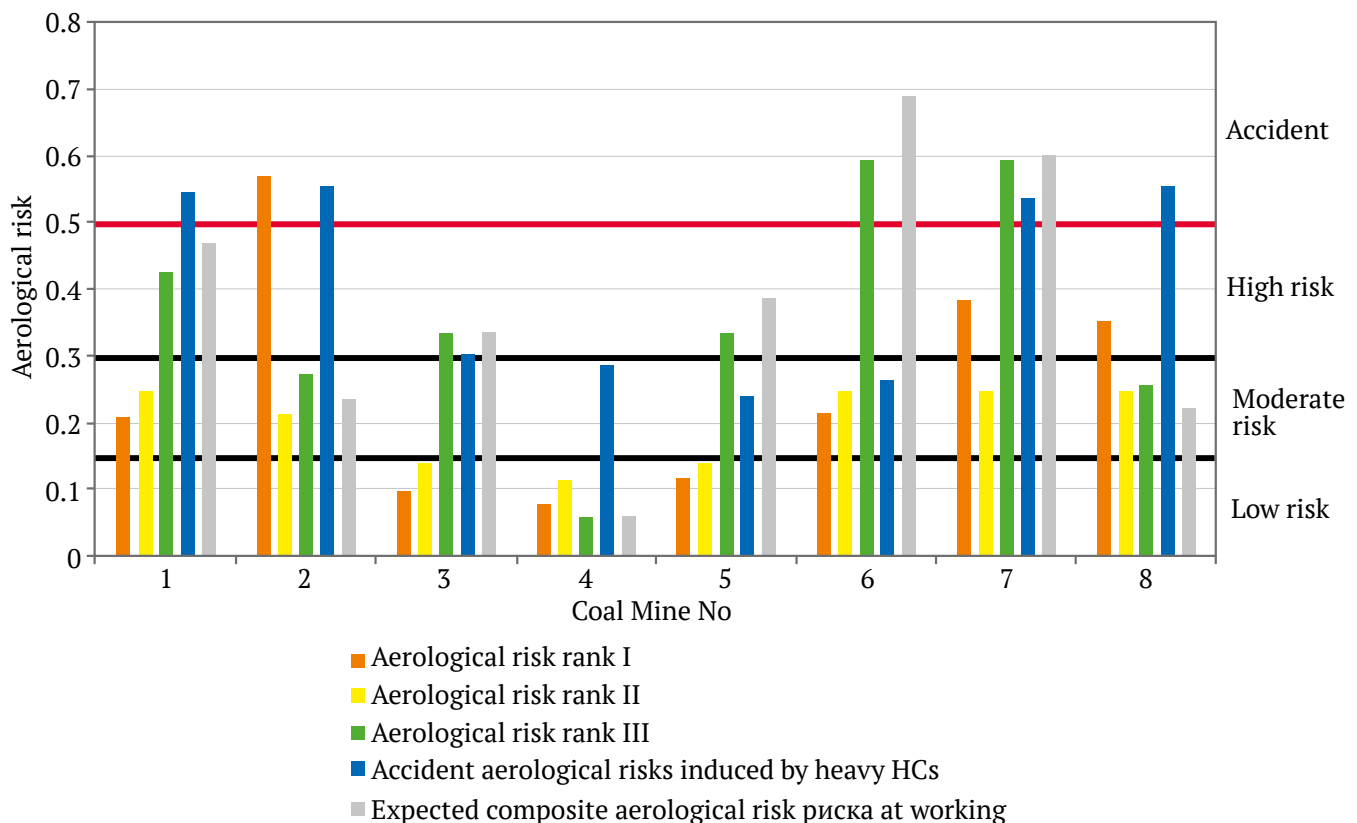


Fig. 1. Comparative assessment of aerological risks in coal mines



return-flow ventilation schemes with diagonal connections. However, the absolute gas content in these areas is low (ranging from 17 to 28.4 m³/t), making these risks relatively insignificant. In summary, these three mines can be classified as having low aerological risks.

The analysis of the remaining five mines, which are categorized as super-category mines, revealed high risks. These risks primarily result from the development of seams containing heavy HCs in residual coal gasses, which are prone to spontaneous ignition and rock bursts. These risks are exacerbated by vulnerable ventilation schemes that fail to ensure complete dilution of harmful agents at their emission sources (mines No. 6, 7). For mine No. 2, while the risks in working areas are low, the risks of the highest rank are of emergency level for the mine as a whole, indicating an urgent need for technical solutions in the mine ventilation scheme. The lowest aerological risks, of moderate degree, are characteristic of mines No. 8 and 1, signifying a reduced safety level and the necessity for ongoing monitoring of geological, geotechnical, and mining parameters that are crucial for the mine's aerological safety system.

Conclusion

The data analytics system for coalmines plays a pivotal role in assessing aerological risks and aerological safety system. The system's database should contain both the design values of various parameters of coalmine subsystems and the real-time operational values monitored by various sensors and devices [29, 30]. Aerological safety can be achieved through an analytical tool that assesses aerological risk for individual levels of the coal mine's functional structure and individual risk factors. These factors include the risks associated with high gas concentration at the working site and in reused workings, as well as the risk of heavy HCs impact, among others.

The final stage of aerological risk assessment involves computing expected values, considering technical and technological measures to eliminate or mitigate the identified negative factors, as well as accounting for hazards like rock bursts and spontaneous coal ignition. Ranking coal mines by their aerological risk levels enables the identification of mines with poor aerological safety and the development of organizational and technological measures to improve aerological safety.

References

1. Tarasenko I.A., Kulikova A.A., Kovaleva A.M. On the issue of assessing the automation of control of the parameters of the methane-air mixture. *Ugol'*. 2022;(11):84–88. (In Russ.) <https://doi.org/10.18796/0041-5790-2022-11-84-88>
2. Martirosyan A.V., Ilyushin Yu.V. The development of the toxic and flammable gases concentration monitoring system for coalmines. *Energies*. 2022;15(23):8917. <https://doi.org/10.3390/en15238917>
3. Bosikov I.I., Martyushev N.V., Klyuev R.V. et al. Modeling and complex analysis of the topology parameters of ventilation networks when ensuring fire safety while developing coal and gas deposits. *Fire*. 2023;6(3):95. <https://doi.org/10.3390/fire6030095>
4. Skopintseva O.V. Preventive repair of mining works as a method for preventing failures in the gas control system. *Mining Informational and Analytical Bulletin*. 2021;(2–1):54–63. (In Russ.) <https://doi.org/10.25018/0236-1493-2021-21-0-54-63>
5. Kobylkin S.S., Pugach A.S. Rock burst forecasting technique and selecting a safe coal face advance direction. *Mining Science and Technology (Russia)*. 2022;7(2):126–136. <https://doi.org/10.17073/2500-0632-2022-2-126-136>
6. Bosikov I.I., Klyuev R.V., Khetagurov V.N. Analysis and comprehensive evaluation of gas-dynamic processes in coal mines using the methods of the theory of probability and math statistics analysis. *Sustainable Development of Mountain Territories*. 2022;14(3):461–467. (In Russ.) <https://doi.org/10.21177/1998-4502-2022-14-3-461-467>
7. Rodionov V., Tumanov M., Skripnik I. et al. Analysis of the fractional composition of coal dust and its effect on the explosion hazard of the air in coal mines. In: *IOP Conference Series: Earth and Environmental Science, Volume 981, Information Technologies, Automation Engineering and Digitization of Agriculture*. 2022;981(3):032024. <https://doi.org/10.1088/1755-1315/981/3/032024>
8. Kobylkin A.S. Dust distribution at a coal shearer in the face area. *Mining Informational and Analytical Bulletin*. 2020;(6–1):65–73. (In Russ.) <https://doi.org/10.25018/0236-1493-2020-61-0-65-73>
9. Gao L., Kang X., Tang M. et al. Study on prediction of outburst risk of excavation face by initial gas emission. *Geofluids*. 2022;2022:4866805. <https://doi.org/10.1155/2022/4866805>



10. Kornev A.V., Spitsyn A.A., Korshunov G.I., Bazhenova V.A. Preventing dust explosions in coal mines: Methods and current trends. *Mining Informational and Analytical Bulletin*. 2023;(3):133–149. (In Russ.) https://doi.org/10.25018/0236_1493_2023_3_0_133
11. Kim M.L., Pevzner L.D., Temkin I.O. Development of automatic system for Unmanned Aerial Vehicle (UAV) motion control for mine conditions. *Mining Science and Technology (Russia)*. 2021;6(3):203–210. <https://doi.org/10.17073/2500-0632-2021-3-203-210>
12. Zhu Z., Wang H., Zhou J. Monitoring and control model for coal mine gas and coal dust. *Chemistry and Technology of Fuels and Oils*. 2020;56:504–515. <https://doi.org/10.1007/s10553-020-01161-3>
13. Tyuleneva T., Kabanov E., Moldazhanov M., Plotnikov E. Improving the professional risk management system for methane and coal dust explosions using a risk-based approach. In: *E3S Web of Conferences. The Second Interregional Conference “Sustainable Development of Eurasian Mining Regions (SDEMR-2021)”*. 2021;278:01027. <https://doi.org/10.1051/e3sconf/202127801027>
14. Li F., He X., Zhang Yu. et al. Superposition risk assessment of the working position of gas explosions in chinese coal mines. *Process Safety and Environmental Protection*. 2022;167:274–283. <https://doi.org/10.1016/j.psep.2022.09.017>
15. Kazanin O., Sidorenko A., Drebenstedt C. Intensive underground mining technologies: Challenges and prospects for the coal mines in Russia. *Acta Montanistica Slovaca*. 2021;26(1):60–69. <https://doi.org/10.46544/AMS.v26i1.05>
16. Álvarez-Fernández M.-I., Prendes-Gero M.-B., Peñas-Espinosa J.-C., González-Nicieza C. Innovative techniques in underground mining for the prevention of gas dynamic phenomena. *Energies*. 2021;14(16):5205. <https://doi.org/10.3390/en14165205>
17. Kulikova E. Yu., Konyukhov D. S. Accident risk monitoring in underground space development. *Mining Informational and Analytical Bulletin*. 2022;(1):97–103. (In Russ.) https://doi.org/10.25018/0236_1493_2022_1_0_97
18. Mitra S., Kumar D., Chaulya S. K., Kumar Ch. Prediction of strata monitoring system in underground coal mines using IoT. *Journal of the Geological Society of India*. 2022;98:232–236. <https://doi.org/10.1007/s12594-022-1963-8>
19. Li Y., Su H., Ji H., Cheng W. Numerical simulation to determine the gas explosion risk in longwall goaf areas: A case study of Xutuan Colliery. *International Journal of Mining Science and Technology*. 2020;30(6):875–882. <https://doi.org/10.1016/j.ijmst.2020.07.007>
20. Feng X., Ai Z., Zhang X. et al. Numerical investigation of the evolution of gas and coal spontaneously burned composite disaster in the goaf of steeply inclined coal seam. *Sustainability*. 2023;15(12):9246. <https://doi.org/10.3390/su15129246>
21. Tang C., Gao E., Li Y. et al. Inspection robot and wall surface detection method for coal mine wind shaft. *Applied Sciences*. 2023;13(9):5662. <https://doi.org/10.3390/app13095662>
22. Niu L., Zhao J., Yang J. Risk assessment of unsafe acts in coal mine gas explosion accidents based on HFACS-GE and Bayesian networks. *Processes*. 2023;11(2):554. <https://doi.org/10.3390/pr11020554>
23. Wang G., Ren H., Zhao G. et al. Research and practice of intelligent coal mine technology systems in China. *International Journal of Coal Science & Technology*. 2022;9:24. <https://doi.org/10.1007/s40789-022-00491-3>
24. Bukhtoyarov V.V., Tynchenko V.S., Nelyub V.A. et al. A study on a probabilistic method for designing artificial neural networks for the formation of intelligent technology assemblies with high variability. *Electronics*. 2023;12(1):215. <https://doi.org/10.3390/electronics12010215>
25. Shareef Sk.Kh., Kumar B.A., Suwarna G., Swathi M. Coal miners safety monitoring system. *International Journal of Innovative Technology and Exploring Engineering (IJITEE)*. 2019;8(12):3202–3204. <https://doi.org/10.35940/ijitee.L3246.1081219>
26. Tripathi A.K., Aruna M., Prasad S. et al. New approach for monitoring the underground coal mines atmosphere using IoT technology. *Instrumentation Mesure Métrologie*. 2023;22(1):29–34. <https://doi.org/10.18280/i2m.220104>
27. Diaz J., Agioutantis Z., Hristopoulos D.T. et al. Forecasting of methane gas in underground coal mines: univariate versus multivariate time series modeling. *Stochastic Environmental Research and Risk Assessment*. 2023;37(12):2099–2115. <https://doi.org/10.1007/s00477-023-02382-8>
28. Ganova S.D., Skopintseva O.V., Isaev O.N. On the issue of studying the composition of hydrocarbon gases of coals and dust to predict their potential hazard. *Bulletin of the Tomsk Polytechnic University. Geo Assets Engineering*. 2019;330(6):109–115. (In Russ.) <https://doi.org/10.18799/24131830/2019/6/2132>



29. Yang J., Zhao J., Shao L. Risk assessment of coal mine gas explosion based on fault tree analysis and fuzzy polymorphic Bayesian network: a case study of Wangzhuang Coal Mine. *Processes*. 2023;11(9):2619. <https://doi.org/10.3390/pr11092619>

30. Srivalli Dr.G., Ujwala S.V., Sahithi G. et al. Study on coal mine safety monitoring and alerting system using IOT. *International Journal for Research in Applied Science & Engineering Technology (IJRAS)*. 2023;11(6):3781–3786. <https://doi.org/10.22214/ijraset.2023.54194>

Information about the author

Sergey V. Balovtsev – Cand. Sci. (Eng.), Associate Professor, National University of Science and Technology MISIS, Moscow, Russian Federation; ORCID [0000-0002-0961-6050](https://orcid.org/0000-0002-0961-6050), Scopus ID [56780405300](https://scopus.com/authid/detail.url?authorID=56780405300); e-mail balovtsev@yandex.ru

Received 09.10.2023

Revised 23.10.2023

Accepted 25.10.2023



MINING MACHINERY, TRANSPORT, AND MECHANICAL ENGINEERING

Research paper

<https://doi.org/10.17073/2500-0632-2022-12-67>

УДК 621.23.05

**Justification of the air distribution system of a down-the-hole hammer with an efficient operating cycle**P. N. Tambovtsev   , E. P. Rusin  

N.A. Chinakal Institute of Mining of the Siberian Branch of the RAS, Novosibirsk, Russian Federation

 tambovskiyp@mail.ru**Abstract**

One method for conserving energy in the mining industry and ensuring the required pressure of compressed air in underground mining networks is to decrease the specific energy carrier consumption, particularly in the case of down-the-hole hammers. The objective of this study is to substantiate the air distribution system of an air hammer, aimed at reducing the specific consumption of compressed air. We propose a system consisting of two chambers with a constant supply of compressed air, two controllable chambers, two elastic valves on the hammer, and a valve for cutting off the supply of compressed air to the forward stroke chamber, which is controlled by the hammer's position. This proposed configuration was employed to create two different designs for the air hammer. The operational cycle of the designed device has been numerically examined using SimulationX software and validated through experimental testing on a laboratory bench. Our calculations reveal that the suggested air distribution system, featuring controlled inlet to the backward stroke chamber, successfully achieves the stated objective. In comparison to the standard M29T hammer with nearly identical dimensions, striking power, and compressed air consumption for cleaning the borehole, the designed hammer exhibits a 53% reduction in specific energy consumption, and its electrical power usage for compressed air supply is halved. These design specifications align with both experimental results and data derived from the existing literature, confirming the accuracy of our calculation.

Keywords

energy consumption, down-the-hole hammer, air distribution system, specific consumption, percussion power, bottomhole purging, numerical simulation, operating cycle parameters, bench experiments

For citation

Tambovtsev P.N., Rusin E.P. Justification of the air distribution system of a down-the-hole hammer with an efficient operating cycle. *Mining Science and Technology (Russia)*. 2023;8(4):360–376. <https://doi.org/10.17073/2500-0632-2022-12-67>

ГОРНЫЕ МАШИНЫ, ТРАНСПОРТ И МАШИНОСТРОЕНИЕ

Научная статья

Обоснование системы воздухораспределения погружного пневмоударника с экономичным рабочим цикломП. Н. Тамбовцев   , Е. П. Русин  

Институт горного дела им. Н. А. Чинакала СО РАН (ИГД СО РАН), г. Новосибирск, Российская Федерация

 tambovskiyp@mail.ru**Аннотация**

Одним из способов экономии энергии в горной промышленности и обеспечения необходимой величины давления сжатого воздуха в воздухопроводных сетях подземных добычных предприятий является уменьшение удельного расхода энергоносителя потребителями, в частности, погружными пневмоударниками. Цель настоящей работы – обоснование системы воздухораспределения пневмоударника, обеспечивающей снижение удельного расхода сжатого воздуха. Предложена система, включающая две камеры с постоянной подачей сжатого воздуха, две управляемые камеры, два упругих клапана на ударнике и клапан для отсечки подачи сжатого воздуха в камеру прямого хода, управляемые от положения ударника. На основе предложенной конфигурации разработаны два варианта конструкции пневмоударника. Рабочий цикл разработанного устройства исследован численно с привлечением программно-



го обеспечения SimulationX и экспериментально на лабораторном стенде. Расчеты показали, что предложенная система воздухораспределения в версии с управляемым впуском в камеру обратного хода обеспечивает достижение поставленной цели. По сравнению с серийным пневмоударником M29T, при практически одинаковых с ним габаритах, ударной мощности, расходе сжатого воздуха на продувку забоя скважины, разработанный пневмоударник имеет удельный расход энергоносителя на 53 % меньше, а потребление электрической мощности на его питание сжатым воздухом в 2 раза ниже. Расчетные данные соответствуют опытным, полученным в эксперименте и из литературных источников, что подтверждает корректность результатов расчета.

Ключевые слова

энергопотребление, погружной пневмоударник, система воздухораспределения, удельный расход, ударная мощность, продувка забоя скважины, численное моделирование, показатели рабочего цикла, стендовые эксперименты

Для цитирования

Tambovtsev P.N., Rusin E.P. Justification of the air distribution system of a down-the-hole hammer with an efficient operating cycle. *Mining Science and Technology (Russia)*. 2023;8(4):360–376. <https://doi.org/10.17073/2500-0632-2022-12-67>

Introduction

The mining industry stands as one of the primary consumers of energy resources. Therefore, the conservation of energy during various operational processes within the industry holds significant importance. Moreover, energy management efforts should be directed towards diminishing energy intensity [1]. This notion is particularly relevant to one of the fundamental processes in mining, which is drilling. Thus, there arises a need to enhance the energy efficiency of air percussion drilling in domestic mines [2–4].

It is imperative to note that the majority of underground mines and shafts operating in Russia currently fail to maintain the required level of compressed air pressure within their air networks. One of the contributing factors to this issue is the excessive energy consumption of pneumatic mining equipment, surpassing the technical capabilities of compressor stations. Consequently, the air network's pressure drops below 0.5 MPa, negatively impacting the efficiency of operational processes [5], including drilling activities.

One effective approach to address these challenges involves the reduction of specific compressed air consumption in down-the-hole hammers (DTH hammers). In the context of DTH hammers, specific consumption pertains to the volume of compressed air needed to generate one unit of percussion energy. Table 1 compiles the principal technical data concerning domestic DTH hammers. Most widely known, mass-produced machines feature either a valve or spoolless type of air distribution, resulting in specific consumption rates of $(37.0–49.4) \times 10^{-6} \text{ m}^3/\text{J}$. Some spoolless-type air hammers, like the PV-170, allow for a slight reduction in specific consumption while maintaining high percussion energy. Nevertheless, this reduction comes at the cost of a significant decrease in percussion frequency and overall percus-

sion¹ [6]. Notably, commercially available down-the-hole hammers with a spool-operated air distribution system are conspicuously absent. Prototypes featuring a combined air distribution system, such as the P105-1K, P105-2K², P-110-3,5, and P110-EN³, were developed at the Institute of Mining of the Siberian Branch of the Russian Academy of Sciences. These prototypes have exhibited notable improvements in their technical characteristics [7, 8].

Internationally, DTH hammers are manufactured in several countries, including Sweden (Atlas Copco⁴ [12], Sandvik⁵), USA (Rockmore International⁶), Great Britain (Halco Rock Tools⁷), China (Change ENYU Engineering Equipment Co. Ltd.⁸), India (SVE

¹ Alexeyev S.E. Down-the-hole pneumatic percussion mechanism. 2090730 (RF Patent), published in Bulletin of Inventions No. 26, 1997.

² Gaun V.A. Pneumatic percussion mechanism. Patent 998740 (USSR certificate of authorship). Published in Bulletin of Inventions No. 7, 1983.

³ Lipin A.A., Belousov A.V., Zabolotskaya N.N. Down-the-hole hammer. 2252996 (RF Patent). Published in Bulletin of Inventions No. 15, 2005.

⁴ Secoroc Rock Drilling Tools. Product catalogue – DTH equipment. Atlas Copco. URL: https://atlas-co.ru/files/pdf/core_drilling/9851%206545%2001_L.pdf; Atlas Copco Secoroc. Technical specifications DTH Hammers. URL: <https://disk.yandex.ru/i/DgE7PG25o11AXA/>

⁵ Sandvik RH560 3.5", 4", 5" and 6" DTH Hammers. URL: <https://www.rocktechnology.sandvik/en/products/rock-tools/down-the-hole-drilling-tools/down-the-hole-hammers/rh560-down-the-hole-hammers/>

⁶ Down-the-hole hammers. RockMore International. URL: <https://www.rockmore-intl.com/download/61/dth-product-information-downloads/816/dth-hammers-catalog-section-4.pdf>

⁷ Halco Rock Tools. Hammers (Unite Kingdom, Halco Brighthouse Ltd). URL: <https://www.halco.uk/hammers/>

⁸ Changsha ENYU Engineering Equipments Co. Ltd (China). DTH hammer. URL: [http://www.enyudrill.com/pclass/?classa=1&classb=1](http://www.enyudrill.com/pclass=?classa=1&classb=1)



Drilling Tools Pvt. Ltd.⁹), and others. majority of foreign prototypes feature spoolless air distribution, extended percussion components (piston, bit), and are pressure-operated (1.0–2.5 MPa). The key technical data for DTH hammers produced abroad is presented

⁹ SVE Drilling Tools Pvt. Ltd. DH 01 Hammers (India). URL: <http://www.svedrillingtools.in/dh01-hammers.php>

in Table 2. Atlas Copco and Sandvik air hammers are industry leaders, outperforming their Russian counterparts in terms of percussion power. However, it's important to note that they operate at higher pressures (1.0–2.5 MPa), which may not be suitable for the conditions prevalent in most Russian mining enterprises.

Table 1

Specifications of domestic air hammers

Parameters	Domestic air hammers						
	M29T [9] / (P85-2)	M48 (P105PMK) ¹ [9]	P155 (M32k) [10]	P105K [11]	P125 [11] / (P130-4m)	P105-1K [7]	P105-2k (M74u) ² [7]
Air distribution type	Valve-operated			Spoolless		Combined	
Pressure <i>p</i> , MPa	0,5 / 0,7	0.5	0.5	0.5	0.5 / 0.7	0.5	0.5
Percussion energy <i>A</i> , J	54 / 91	93	178	96	150 / 182	194	206
Percussion frequency <i>f</i> , Hz	25 / 22	28.3	23	26.7	20,8 / 22	16.3	16.1
Total air consumption <i>Q</i> , m ³ /min	4.0 / 4.8	7.0	9.7	5.7	7.0 / 8.8	6.4	6.6
Percussion power <i>N</i> , kW	1.35 / 2.0	2.63	4.1	2.56	3.12 / 4.0	3.17	3.32
Hammer mass <i>m</i> , kg	1.75 / –	2.80	5.5	3.0	5.6 / –	4.45	4.45
Machine mass <i>M</i> , kg	10 / 15	16.1	35.5	21.0	31.0 / 33.2	18.2	18.2
Specific power, W/kg	135 / 134	160	120	120	101 / 120	174	182
Dimensions (without bit):							
length, mm	549 / 622	(470)	459	615	(566) / 657	594	594
diameter, mm	70 / 80	92	140	92	110 / 116	96	96
Bit diameter, mm	85 / 85	105	155	105	125 / 130	105	105
Specific air consumption <i>q</i> , m ³ /J* (×10 ⁻⁶)	49.4 / 40	45	39	37	37 / 37	34	33

* The specific consumption of the air hammer is given with account of compressed air intake for borehole purging.

¹ Zinovyev A.A., Semenov L.I. Drill hammer. Patent 112867 (USSR certificate of authorship). 1958.

² Gaun V.A. Pneumatic percussion mechanism. Patent 998740 (USSR certificate of authorship). Published in Bulletin of Inventions No. 7, 1983.

Table 2

Specifications of foreign air hammers

Parameters	Model					
	USA		Sweden			
	(Rockmore International)		Sandvik		Atlas Copco (Secoroc)	
	ROK 2LT	ROK-3	RH560 3,5"	RH560 g4"	COP-34	COP-44
Air distribution type	–		–		Spoolless	
Pressure <i>p</i> , MPa	0.6 / 1.04	0.6 / 2.4	1.0 / 1.8 / 2.4	1.0 / 1.8 / 2.4	1.05 / 2.5	1.05 / 2.5
Percussion energy <i>A</i> , J	–	–	–	–	154 / 317	296 / 514
Percussion frequency <i>f</i> , Hz	–	–	–	–	26 / 41	23.7 / 35
Air consumption <i>Q</i> , m ³ /min	2.0 / 3.8	3.1 / 14.5	4,5 / 8.3 / 11.1	6.7 / 12.5 / 16.9	4.8 / 15.0	5.46 / 16.9
Power <i>N</i> , kW	–	–	–	–	4.0 / 13.0	7.0 / 18.0
Hammer mass <i>m</i> , kg	–	–	5.3	8.5	4.8	7.1
Hammer diameter <i>d</i> , mm	–	–	–	–	–	78
Machine mass <i>M</i> , kg (w/o bit)	(13)	(22)	(29)	(48)	27	38
Specific power, W/kg	–	–	–	–	148 / 481	184 / 474
Dimensions:						
length, mm (w/o bit)	(840)	(750)	1004 (914)	1140 (1016)	1025	1034
diameter, mm (w/o bit)	(62)	(82)	85	105	(83.5)	(98)
Bit diameter, mm	70, 76	85, 105	85	105	105	110, 125
Specific air <i>q</i> , m ³ /J (×10 ⁻⁶)	–	–	–	–	20.0 / 19.2	13.0 / 15.6



Research Aim, Objectives, and Methods

The aim of this study is to substantiate the air distribution system of an air hammer, with the goal of reducing the specific consumption of compressed air.

Research objectives:

- conducting a numerical investigation into the dynamics of working processes in typical air percussion systems, performing a comparative analysis of their efficiency for light-type DTH hammers, and identifying factors that hinder their efficiency;
- selecting an air distribution system and structural layout capable of mitigating the factors that negatively impact the consumption parameters of DTH hammers;
- developing the design of the air hammer, with the determination of its key dimensions;
- employing simulation modeling to explore the working process of a new DTH hammer and selecting the most suitable combination of design parameters to ensure the realization of the operating cycle with reduced specific consumption;
- estimating the compressed air consumption required for cleaning the bottomhole;
- experimentally verifying the reliability of the results obtained from numerical simulations of the air hammer;
- summarizing and evaluating the findings of the research.

Numerical (simulation) modeling of the working process within the air systems of DTH hammers was conducted using the SimulationX software¹⁰. The software's calculation module relies on a mathematical model [13, 14] that characterizes the dynamics of the percussion system. This model has demonstrated its adequacy and effectiveness in the analysis of a broad spectrum of air percussion devices [3]. The design diagram of the air percussion system encompasses generalized depictions of air connections and mechanical connections. The air connections diagram delineates the architecture of the air component, including the number of chambers, the interconnecting channels, and the presence of moving components that interact with these chambers. Channels connecting the chambers are specified by the flow cross-sectional area. Adjustable channels are characterized by diagrams illustrating changes in flow area. The mechanical connections diagram illustrates the nature of power interactions, which may involve elastic couplings, friction, and other relevant factors. Additionally, it accounts for percussion interactions between moving components, assuming them to be instantaneous

and describing them based on the concept of velocity recovery coefficients. The software utilizes the given initial conditions to calculate displacements and velocities of the moving components, along with pressure and temperature within the chambers, and the instantaneous mass flow rate of compressed air. The outcomes are presented in the form of operational cycle diagrams, showcasing factors such as chamber pressure, velocity and displacement of moving components, and the rate of compressed air flow within channels. Specific characteristics of the calculations are elucidated below.

A comparative analysis of the efficiency of air percussion systems for lightweight DTH hammers with similar dimensions and percussion power involves identifying the system with the lowest specific consumption of compressed air.

Physical experiments are carried out using a laboratory prototype of an air hammer. These experiments make use of measurement equipment, including a laboratory bench and an array of recording devices. Further details regarding this equipment and the methodology for conducting experimental work are expounded upon in the relevant section below.

Numerical Study of the Working Process Dynamics in Typical Air Percussion Systems for Lightweight DTH Hammers

The objective of this study is to assess the efficiency of typical air percussion systems in terms of specific energy consumption and percussion power for DTH hammers with a body diameter of 70 mm, categorizing them as lightweight models.

The investigation considered three primary types of air distribution systems commonly used in the design of air percussion devices [9, 10]: valve-operated (M29T), spoolless (P125), and spool-operated (PN-1300). As a baseline for comparison, a commercially available valve-type lightweight DTH hammer, the M29T, was selected. The two other systems, spoolless and spool-operated, were configured as air hammers with geometric and mass-dimension parameters scaled down to match those of the baseline. Consequently, identical values for the key parameters were established for all three selected air percussion mechanisms: L (the length of the air hammer), D (the outer diameter of the body or cylinder), m_1 (the mass of the hammer), S (the effective area of the hammer), H_o (the overall stroke of the hammer), and p_m (the operating pressure in the main line). Variations in other parameters, encompassing the volumes of working chambers, cross-sectional areas of air passages, and air distribution coordinates, were systematically adjusted to ensure the congruence of the

¹⁰ ESI Group. System Simulation Software. SimulationX. URL: <https://www.esi-group.com/products/system-simulation>

operational cycle diagrams of the DTH hammer’s typical air percussion mechanisms with those observed in actual machines. In the subsequent sections, the working chambers are referred to as follows: the forward stroke chamber – FSC and the backward stroke chamber – BSC.

The designs of the considered models of down-the-hole air hammers with typical air percussion systems are presented in Fig. 1, and their operating principle and working process features are described in [11, 13, 17]. Construction diagrams (Fig. 1, a, b, c) illustrate the moving components of these systems, set at the origin of coordinates (hammer at the

moment of percussion). In this configuration, the initial chamber volumes, air distribution window coordinates, and the range of movement for these components are all ascertained.

In Fig. 2 the generalized design diagrams of typical air percussion systems are demonstrated. Each chamber and its associated moving mass are designated with a serial number, such as chamber V_i , mass m_i . The clear area between chamber 1 and chamber 2 is conventionally labeled by J_{12} , while the effective area of the moving components, like hammer m_1 on the side of chamber V_2 , is represented by S_{21} . The modifications in flow cross-sections

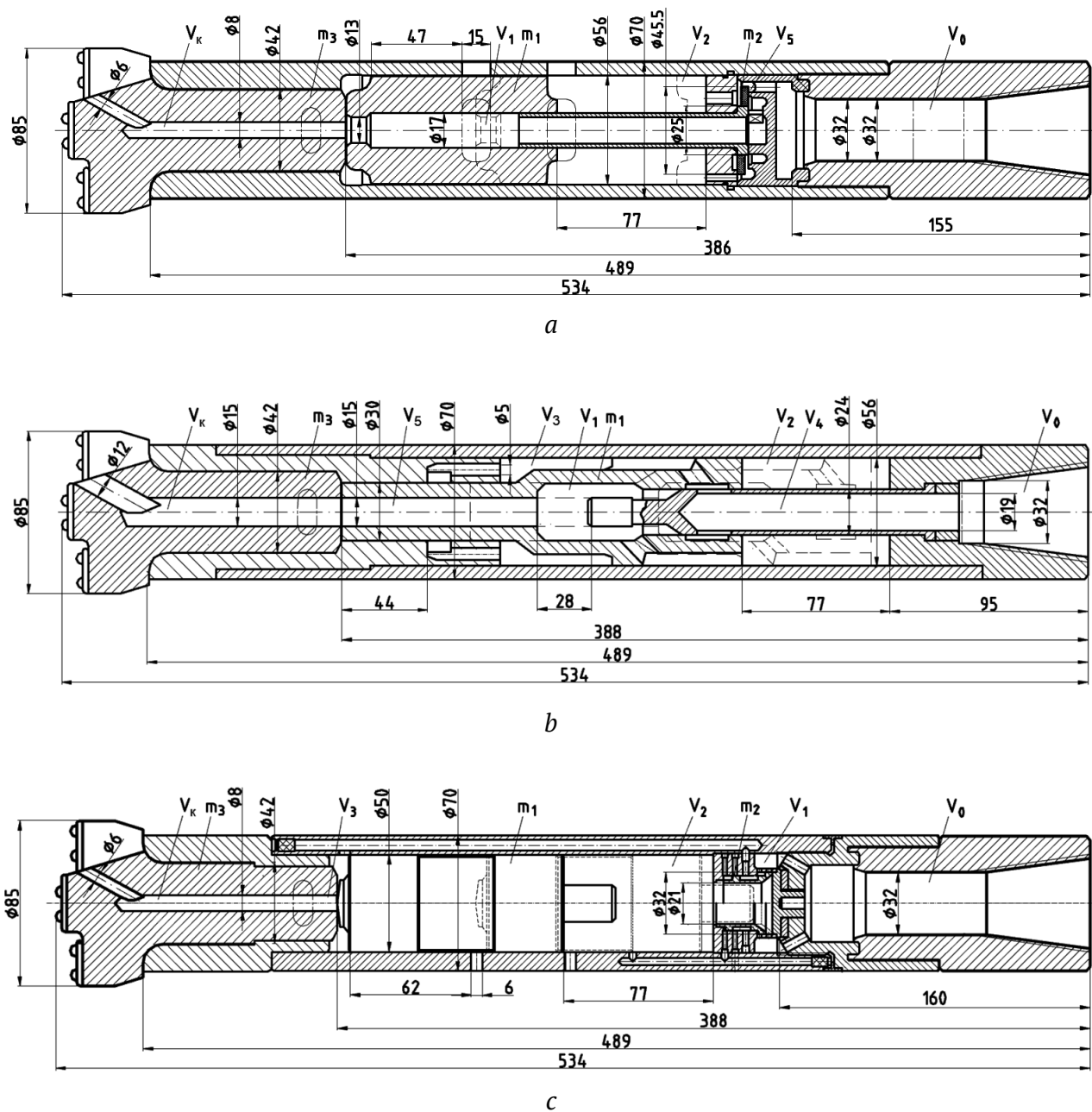


Fig. 1. Layout and main structural dimensions of air hammers with typical air distribution systems: a – valve-operated (M29T [9]), b – spoolless (P125 [11]), c – spool-operated (PN-1300 [11, 15])

that correspond to the positions of hammer 1 and the distributing components (valve or spool) are described in a similar fashion [14]. The pneumatic resistances within the channels are accounted for using flow coefficients ($k_f = 0.4...0.6$). The essential design parameters, initial pressures in the chambers, and velocity recovery coefficients have been incorporated into the design model. The evaluation of the working process is based on the structure of the operating cycle diagrams and the values of output indicators, encompassing parameters such as the energy and frequency of percussions, compressed air consumption, and their respective derived values, as well as the working stroke of the hammer. The pursuit of optimal configurations for air distribution systems was carried out with the objective of minimizing specific compressed air consumption. This involved

adjusting the working volumes of chambers, the areas of air passage cross-sections, the coordinates where moving components interact, and the masses of valves, guided by this criterion.

Design diagrams of typical air percussion systems are presented in Fig. 3, depicting pressure, displacement, and velocity of moving components, the instantaneous mass flow rate. These diagrams correspond to the design parameter values and initial calculation conditions outlined in Table 3. The calculations reveal that the hammer is provided the percussion velocity within permissible limits, reaching up to 8.43 m/s, along with the necessary operating stroke of the hammer (65–68 mm) and a suitably high frequency of percussions (22.2–27.8 Hz). Table 3 presents the design output indicators for typical air percussion systems.

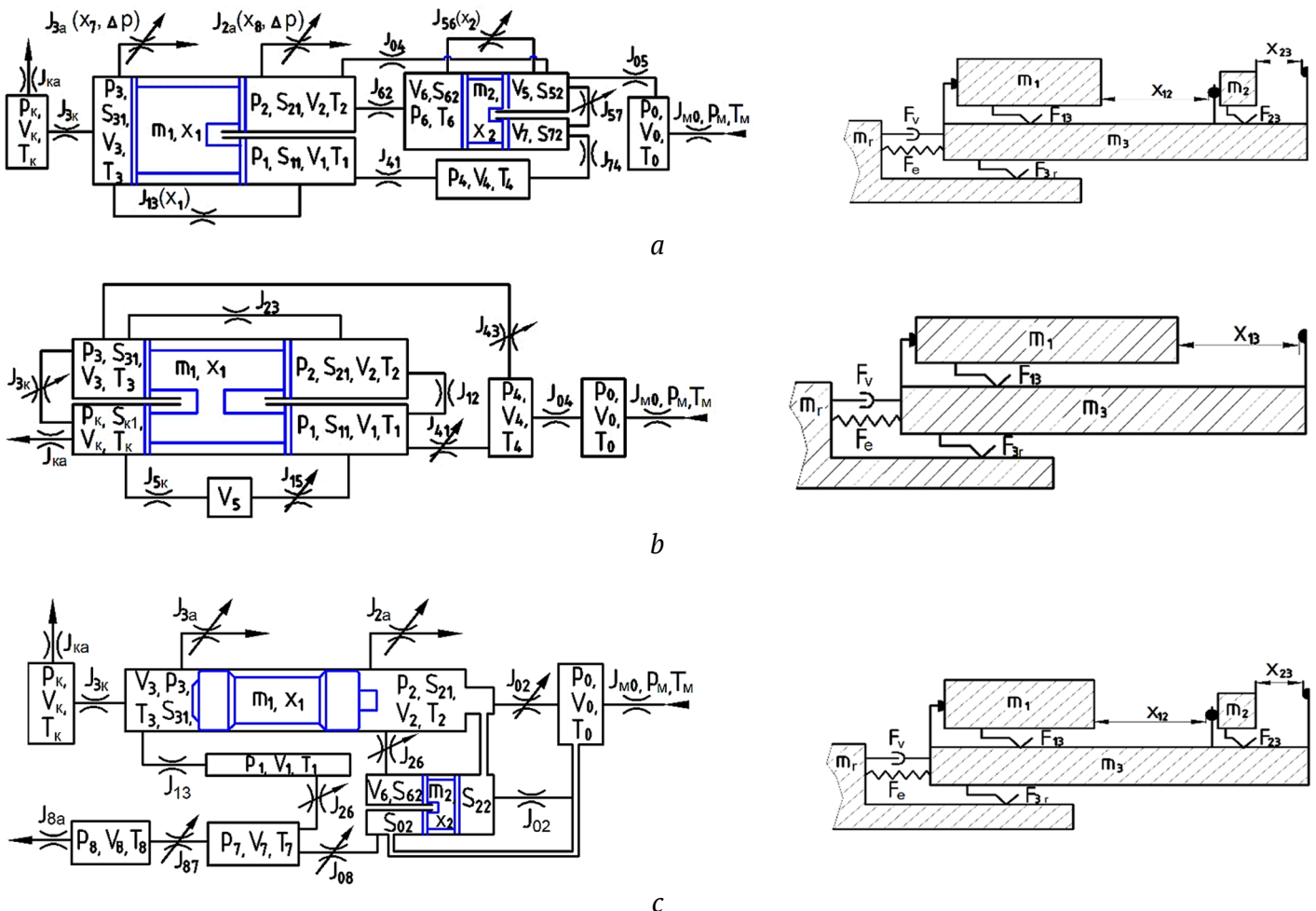


Fig. 2. Generalized design diagrams (pneumatic, mechanical) of typical air percussion systems: *a* – valve-operated (prototype M29T); *b* – spoolless (P125); *c* – spool-operated (PN-1300): V_i – volumes of chambers; J_{m0} – area of the air passage cross-section of the main line; J_{ij}, J_{ia} – areas of air passage cross-sections between the *i*-th and *j*-th chambers, between the *i*-th chamber and atmosphere; m_i, x_i – masses and coordinates of moving components (hammer, valves, m_r – rock); S_{ij} – effective areas of components m_i from the side of the *j*-th chamber; T_i, T_m – absolute temperature of compressed air in the *i*-th chamber and in the main line; p_m, p_i, p_a – absolute pressure of compressed air in the main line, *i*-th chamber and in the atmosphere; F_e, F_v – forces of elastic-damping connection of the air hammer with the rock; F_{13}, F_{5r}, F_{23} – friction forces: hammer – body, body – rock, valve – body

The simulation demonstrates that all models of air hammers with typical air distribution systems operate stably at two main pressure values of 0.5/0.6 MPa. With similar mass-dimensional characteristics, the valve system (M29T) yields percussion power of 1.42/1.63 kW, while the valveless system provides 0.96/1.19 kW, and the spool system delivers 1.13/1.48 kW. Notably, the maximum percussion energy is achieved by the valve (54.0/60.0 J) and spool (51.2/60.2 J) systems, whereas the valveless system exhibits the lowest percussion energy at 36.4/42.8 J. In terms of specific consumption, the operating cycles of air hammers with spool and valveless types of air distribution systems ($29.3/32.0 \times 10^{-6} \text{ m}^3/\text{J}$) are the most efficient. The specific consumption of the batch-produced air hammer M29T is 1.4/1.7 times higher than that of the other two typical systems.

Let us analyze the operating cycles of typical air percussion mechanisms using diagrams (see Fig. 3) and calculated output indicators (Table 3).

Regarding the valve-operated air hammer M29T, the actuation of the cross-over valve at specific intervals connects the main line to the atmosphere through channels, leading direct air leakage. In the FSC, just before the beginning of exhaust, there is elevated pressure (0.37 MPa). Prior to percussion, a pressure pulse occurs in the BSC, which reduces the percussion energy. These factors contribute to high specific compressed air consumption ($q = 44.7 / 50.6 \times 10^{-6} \text{ m}^3/\text{J}$).

The spoolless air hammer, as depicted in the P125 diagram, introduces air into the working chambers through controllable channels, that are manipulated by the hammer's actions. It is evident from the diagrams (see Fig. 3, b) that the percussion power of the device decreases, and air consumption increases due to several factors: relatively high pressure in the FSC just before exhaust (0.43 MPa), a substantial initial volume of the BSC, and a notable pressure pulse in the BSC, which diminishes the kinetic energy of the hammer during the forward stroke. This air

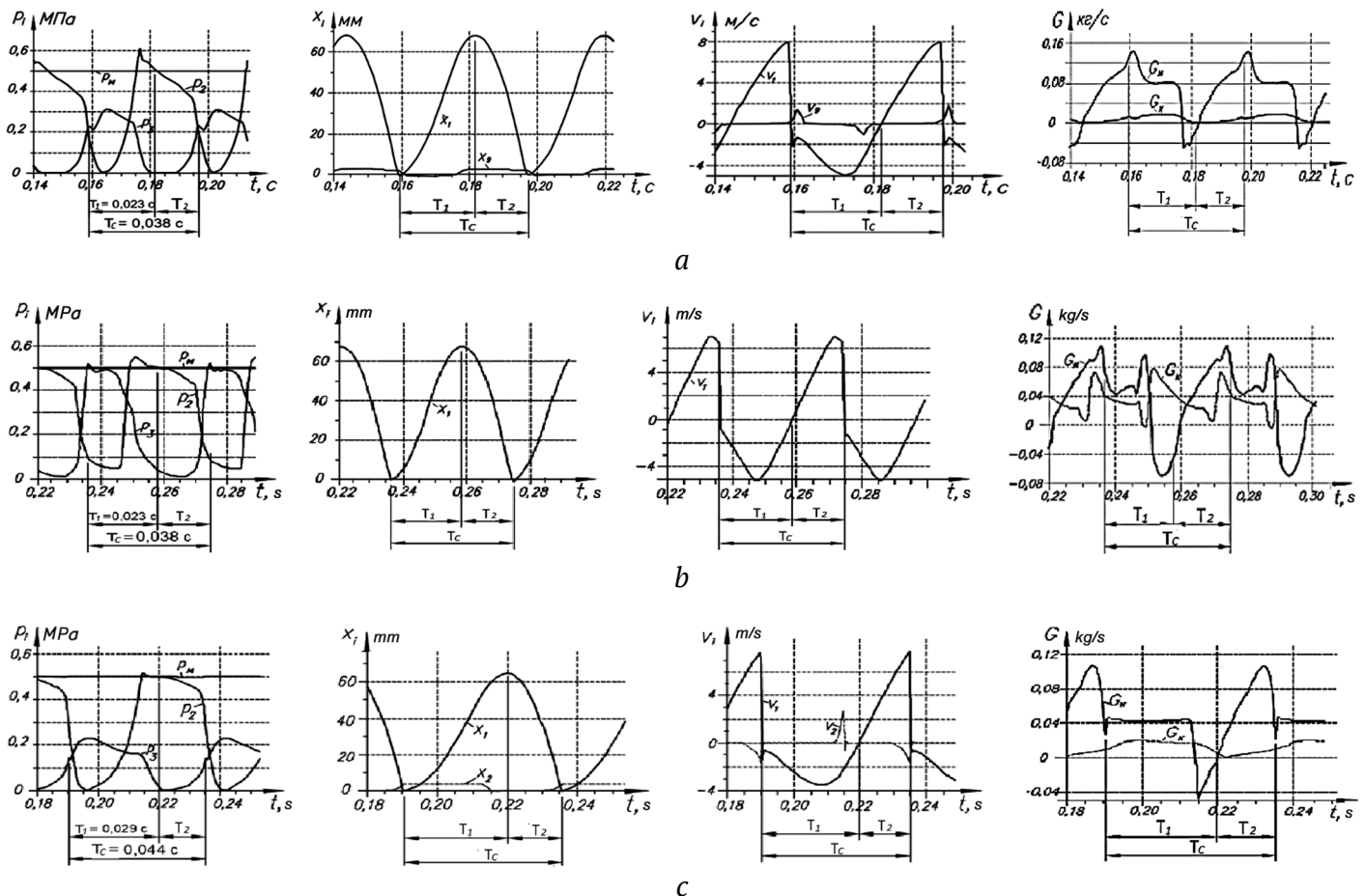


Fig. 4. Design diagrams of operating cycles (changes in compressed air pressure in time $p_i(t)$ in the i -th chambers; displacement of hammer x_1 , valve and spool x_2 ; velocity of hammer v_1 , valve and spool v_2 , the instantaneous mass flow rate of compressed air G) of the air hammer models with typical air distribution systems: a – valve-operated (M29T), b – spoolless (P125), c – spool-operated (PN-1300): v_1, v_2 – velocity of the hammer, valve / spool respectively, m/s; x_1, x_2 – displacement of the hammer, valve / spool respectively, m/s; G_m – flow rate through the main channel j_{m0} ; G_c – flow rate through the channel j_{cha} in the bit t – time, s; T_c – cycle period; T_1, T_2 – periods of backward and forward strokes



hammer delivers a percussion power of 0.96 / 1.19 kW, a percussion energy of 36.4 / 42.8 J, and a specific consumption of 32.0 / 31.1 × 10⁻⁶ m³/J.

The *spool-operated air hammer according to the basic flow diagram of the PN-1300 air percussion machine* provides compressed air to the working chambers through channels in the body, with opening and closing managed by a spool. The spool's movement depends on the pressure within the working chambers and the pre-spool chamber. Notably, the BSC of this device holds the smallest volume (0.0134 dm³) as compared to 0.0950 dm³ in the spoolless system and 0.0162 dm³ in the valve-operated one. The maximum pressure in the BSC (0.23 MPa) also stands as the lowest (as opposed to 0.5 MPa in the spoolless system and 0.31 MPa in the valve-operated one), and the pressure just before exhaust registers at 0.16 MPa (versus 0.43 MPa in the spoolless system and 0.24 MPa in the

valve-operated one). These characteristics contribute to a reduction in compressed air consumption by the spool-operated air hammer.

During the direct stroke of the hammer, there is notably high average pressure (0.52–0.53 MPa) in the period preceding the beginning of exhaust from the FSC, while the pressure pulse in the BSC is reduced (with the pressure in the BSC at the moment of percussion not exceeded 1.4 MPa). Although the effective area of the hammer is smaller, this configuration results in higher percussion energy. However, concurrently, the high pressure in the FSC just before exhaust (0.43 MPa) and the large volume of the FSC lead to losses in the internal energy of compressed air. Among the three considered pneumatic percussion mechanisms, this specific consumption is the lowest ($q = 31.7 / 29.3 \times 10^{-6}$ m³/J), suggesting a significant margin for its further reduction.

Table 3

Design parameters of typical air percussion systems for light-weight DTH hammers

Prototype machine	M29T					
	M29T		P125		PN-1300	
Air percussion system diagram	M29T		P125		PN-1300	
Air distribution type	Valve-operated		Spoolless		Spool-operated	
Specified parameters						
Overpressure p , MPa	0.5	0.6	0.5	0.6	0.5	0.6
Bit diameter, mm	85		85		85	
Outer diameter of the body (cylinder), mm	70		70		70	
Total length of air hammer with bit L , mm	534		534		534	
Internal diameter of cylinder, mm	56		56		50	
Hammer mass m , kg	1.75		1.75		1.75	
Valve mass m_2 (spool m ²), kg	0.035		–		(0.036)	
Effective area of hammer (BSC/FSC) S_{ij} , cm ²	22.3 / 22.3		17.5 / 22.8		19.6 / 19.6	
Ratio of hammer effective area to cross-section area of body with a diameter of 70 mm	0.58		0.59		0.51	
Overall stroke H_d , mm	77		77		77	
Flow rate coefficient k_f	0.5–0.6		0.5–0.6		0.5–0.6	
Velocity recovery coefficient k_r	0.10–0.15		0.10–0.15		0.10–0.15	
Stroke before exhaust from BSC, mm	47		38		62	
Chamber initial volumes: V_1 , dm ³ ; V_2 , dm ³ ; V_3 , dm ³ ; V_4 , dm ³	0.0204; 0.1810; 0.0162; 0.0196		0.0280; 0.1600; 0.0950; 0.0410		0.0270; 0.1570; 0.0134; 0.0267	
Main line channel area J_{m0} , cm ²	8.04		8.04		8.04	
Hammer/cylinder clearance area, cm ²	0.04		0.04		0.04	
Area of channel in bit J_{cha} , cm ²	0.502		2.010		0.502	
Output indicators						
Stroke velocity v , m/s	7.86	8.28	6.45	7.00	7.65	8.43
Operating stroke H_o , mm	67	68	67	68	65	66
Percussion energy A , J	54.0	60.0	36.4	42.8	51.2	62.2
Percussion frequency f , Hz	26.3	27.1	26.3	27.8	22.2	23.8
Cycle period T_c , s	0.038	0.037	0.038	0.036	0.044	0.042
Percussion power N , kW	1.42	1.626	0.96	1.19	1.13	1.48
Total air consumption Q , m ³ /min	3.81	4.94	1.84	2.22	2.16	2.60
Air flow rate through bit channel Q_b , m ³ /min	0.69	0.78	1.84	2.22	0.62	0.69
Specific air consumption q , m ³ /J (×10 ⁻⁶)	44.7	50.6	32.0	31.1	31.7	29.3



Selection of air distribution systems and design diagrams of DTH hammers

Table 4 summarizes the main advantages and disadvantages of typical air percussion mechanisms, along with the factors that contribute to increased specific consumption and the methods identified through numerical simulation to reduce it.

Analysis of the operating cycles of typical air percussion systems has led to the establishment, that an effective air percussion system should fulfill:

1. Avoid continuous compressed air supply to working chambers; instead, control the compressed air inlet and exhaust.
2. Ensure that the effective area of the hammer on the FSC side is not less than 0.6 times the cross-sectional area of the air hammer.
3. Minimize resistance to the hammer’s movement caused by air pressure from the respective working chambers.
4. Cut-off of compressed air supply to the working chambers before exhaust and provision of increased rate of compressed air expansion.
5. Keep the initial volume of the BSC relatively small.
6. Maintain a design simplicity.

From the above conditions, it becomes evident that reducing the specific compressed air consumption by an air hammer is achievable by eliminating resistance during both the forward and backward strokes of the hammer caused by air compression in the controllable working chambers

and by ensuring a greater degree of air expansion. One of the most effective and structurally simple components for meeting these requirements is the elastic valve¹¹ [7, 16], which was initially proposed by V.A. Gaun at the Institute of Mining of the Siberian Branch of the USSR Academy of Sciences. The use of elastic valves has led in a doubling of percussion energy and a 30% increase in percussion power for air hammers with the same diameter and compressed air consumption. Elastic valves offer several advantages due to their ease of integration into the machine design and their ability to provide a large air passage cross-section. These valves consist of a ring made of elastic material, such as rubber or plastic, placed in a groove on the hammer or the body of the air percussion mechanism. The ring can open or close the gap along the outer or inner diameter, depending on the pressure in the chambers communicating through this gap, ensuring the sealing of the working chamber or its connection with the atmosphere.

For the timely inlet and cut-off of compressed air supply to the FSC, an annular step inelastic valve, controlled by the hammer, can be employed. This valve allows for almost instantaneous full opening of the inlet cross-section to the chamber, just before the hammer changes direction. The efficiency of this solution has been confirmed through experimental studies [17].

¹¹ Gaun V.A. Pneumatic percussion mechanism. Patent 998740 (USSR certificate of authorship). Published in Bulletin of Inventions No 7, 1983.

Table 4

Comparative analysis of typical air percussion mechanisms

Air distribution system	Specific consumption (×10 ⁻⁶) m ³ /J	Advantages	Disadvantages	Main factors improving specific consumption	Ways to reduce the specific consumption and improve the design
Valve-operated (M29T)	44.7	High specific percussion power (W/kg), high frequency of percussions, design simplicity	High specific consumption	Inevitable direct overflow of compressed air from the main line to the atmosphere to activate the cross-over valve	Cut-off of compressed air supply to working chambers before exhaust; increase of the compressed air expansion rate in the chambers.
Spoolless (P125)	32.0	High percussion frequency, simple design	High specific consumption, low percussion energy; design complexity, low hammer durability and strength	Large initial volume of BSC, losses of internal energy with exhaust, resistance to hammer movement from air compression in the BSC, resistance in the FSC.	Elimination of constant supply of compressed air to the FSC; increase in the degree of expansion of compressed air in the BSC; elimination of stress concentrators in the hammer.
Spool-operated (PN-1300)	31.7	High percussion energy, integral hammer, reliable operation; no uncontrollable working chambers, reduced resistance to hammer stroke.	High specific consumption; complexity of manufacturing of the body (cylinder with channels).	Resistance to hammer movement from air compression in the FSC and BSC, low rate of expansion of compressed air in working chambers and losses of internal energy during exhaust; small working area of the hammer.	Elimination of internal energy losses of compressed air with exhaust; simplification of body design, elimination of resistance to hammer stroke from air compression in the BSC at the end of the hammer forward stroke

Controlling the supply of compressed air to the BSC can be more easily achieved by using a channel in the hammer controlled by its position. An alternative, simpler approach is to maintain a constant air inlet to the BSC through a throttle hole in the hammer.

Typical air percussion systems do not fully realize the proposed methods for reducing specific consumption (see Table 4). Therefore, we use combined air hammer diagrams that incorporate elastic ring valves (Fig. 4). The starting point is the diagram of the two-valve air hammer P105-2K¹² [7] (Fig. 4, a), which has twice the percussion energy compared to analogs with the same compressed air consumption. This diagram's distinct feature is that during the backward stroke, elastic valves m_4 and m_5 connect the BSC with the atmosphere, effectively eliminating resistance to the hammer's movement¹³.

¹² Gaun V.A. Pneumatic percussion mechanism. Patent 998740 (USSR certificate of authorship). Published in Bulletin of Inventions No 7, 1983.

¹³ I bid.

Figs. 4, b, and c provide new diagrams that allow for the implementation of the proposed methods to reduce specific consumption (see Table 4). In these diagrams, in contrast to the P105-2K diagram (Fig. 4, a), the use of two elastic valves (m_4, m_5) on the hammer (m_1) eliminates pneumatic resistance during not only the backward but also the forward stroke.

The air hammer shown in Fig. 4, b employs air distribution system K1 (valve-spoolless) with a controllable channel in the hammer. In Fig. 4, c, it utilizes system K2 (valve-throttle-operated) with a throttle channel in the hammer. The air inlet to chamber V_2 from main line V_0 occurs at the end of the backward stroke of hammer m_1 when valve m_2 is actuated, overriding its displacement by the hammer. Exhaust from chamber V_2 takes place at the end of the forward stroke through exhaust windows in the cylinder. Compressed air is introduced into the chamber V_3 through channel V_4 in the nozzle, chamber V_1 , the channel

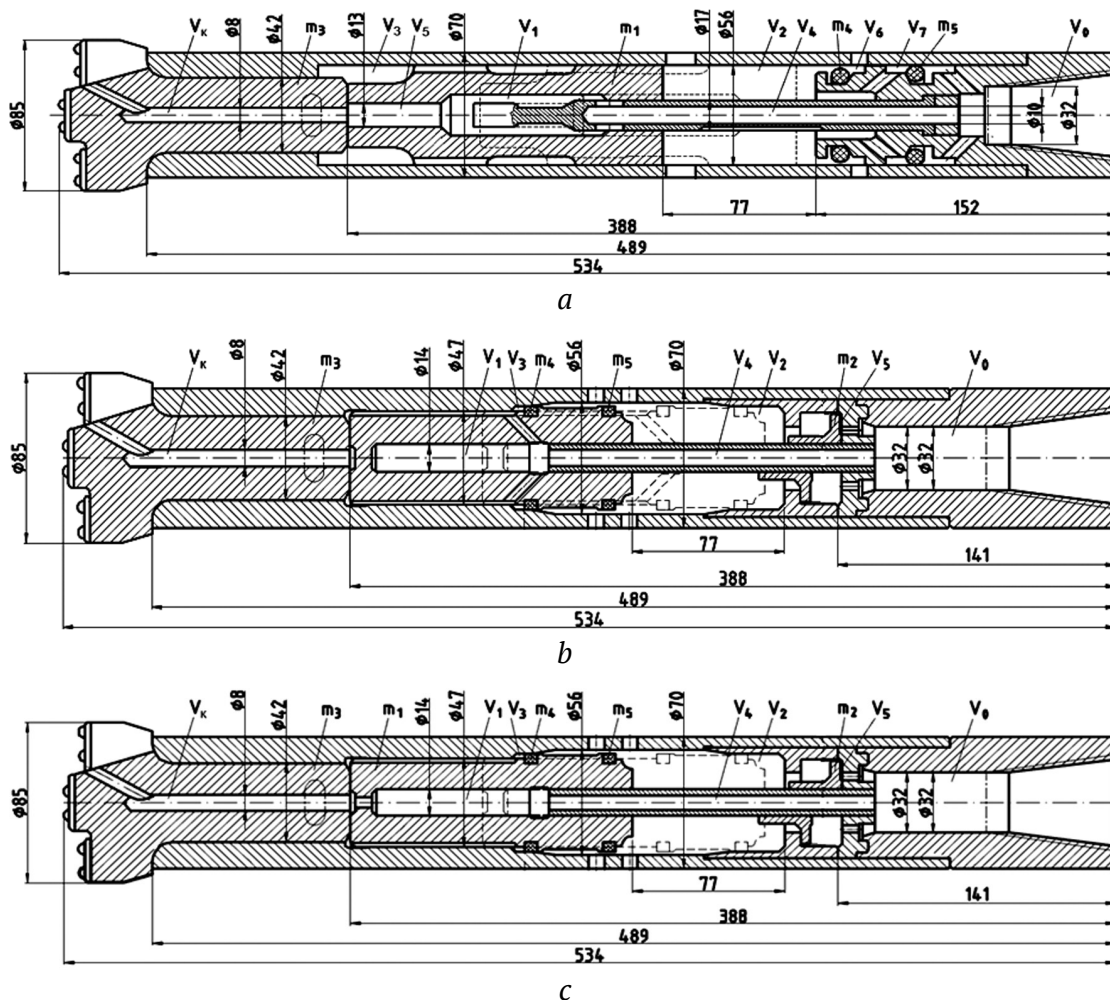


Fig. 4. Diagrams and main structural dimensions of air hammers with components designations: a – air hammer according to the P105-2K diagram; b – air hammer K1 with controllable inlet to the BSC (V_3); c – air hammer K2 with permanent throttled inlet to the BSC: V_i – chamber volumes; m_i – masses of moving components (hammer, valves)



in the hammer, and exhaust is conducted through side windows in the cylinder and channel V_b in the bit. Valve m_4 seals working chamber V_3 during the backward stroke of the hammer, and valve m_5 seals chamber V_2 during the forward stroke. Valve m_2 increases the reliability of the air percussion mechanism by ensuring stable air inlet into the controllable forward stroke chamber V_2 at the end of the hammer's backward stroke, thus facilitating a smooth transition from the backward stroke to the forward stroke.

To quantitatively assess the capabilities of air hammers with combined air distribution systems (see Fig. 4), a numerical analysis of their operating cycles was performed. Similar to the study of typical air distribution diagrams presented above, the design dimensions of all three air hammers were standardized to the same size as a DTH hammer with an outer body diameter of 70 mm.

Results of simulation modeling of the operating cycle of DTH hammer designs with combined air distribution systems

The numerical study and the search for optimal settings of DTH hammer parameters were conducted using the methodology described earlier. For a more detailed examination of the mechanical diagram of the ring elastic valve integrated into the comprehensive computational model of the air percussion machine, additional information can be found in [18]. Table 5 provides the initial calculation conditions, design parameter values, and output design parameters of the air hammers. The diagrams illustrating the operating cycle can be referred to in Fig. 5.

The results of simulating air hammers with elastic valves (P105-2K, K1, K2 diagrams) have demonstrated the stable operation of these devices, with the valves effectively fulfilling their functions. In all air distribution systems employing elastic valves,

Table 5

Design parameters of combined air percussion systems for lightweight DTH hammers

Prototype machine	M29T					
	P105-2K		K1		K2	
Air percussion system diagram						
Air distribution type	Valve-spoolless		Valve-spoolless		Valve-throttle	
Specified parameters						
Overpressure in the main line p_m , MPa	0.5	0.6	0.5	0.6	0.5	0.6
Bit diameter, mm	85		85		85	
Outer diameter of the body (cylinder), mm	70		70		70	
Inner diameter of the body (max / min), mm	56 / 56		56 / 47		56 / 47	
Total length of air hammer with bit L , mm	534		534		534	
Hammer mass m_1 , kg	1.75		1.75		1.75	
Effective area of hammer (BSC/FSC) S_{ij} , cm ²	23.3 / 23,3		24.1 / 23.3		24.1 / 23.3	
Ratio of effective area (FSC) of hammer to cross-section area of body with a diameter of 70 mm	0.61		0.61		0.61	
Dimensional stroke H_d , mm	77		77		77	
Flow rate coefficient k_f	0.5–0.6		0.5–0.6		0.5–0.6	
Velocity recovery coefficient k_v	1.10–0.15		0.10–0.15		0.10–0.15	
Stroke before exhaust from BSC, mm	46		32		32	
Chamber initial volumes: V_1 , dm ³ ; V_2 , dm ³ ; V_3 , dm ³ ; V_4 , dm ³	0.0380; 0.1750; 0.1100; 0.0220		0.0146; 0.1620; 0.0230; 0.0080		0.0146; 0.1620; 0.0230; 0.0080	
Main line channel area J_{m0} , cm ²	8.04		8.04		8.04	
Area of throttle channel in hammer J_{13} , cm ²	–		–		0.25	
Hammer/cylinder clearance area, cm ²	0.04		0.04		0.04	
Area of channel in bit J_{cha} , cm ²	0.502		0.502		0.502	
Output indicators						
Stroke velocity v , m/s	8.26	9.03	7.58	8.16	7.40	8.06
Operating stroke H_o , mm	67	66	69	69	69	69
Percussion energy A , J	59.7	70.9	50.3	58.3	47.9	56.8
Percussion frequency f , Hz	25.64	27.77	23.8	25.6	22.7	24.4
Cycle period T_c , s	0.039	0.036	0.042	0.039	0.044	0.041
Percussion power N , kW	1.530	1.968	1.196	1.494	1.087	1.386
Total air consumption Q , m ³ /min	3.14	3.72	1.35	1.47	2.51	3.08
Air flow rate through bit channel Q_b , m ³ /min	0.52	0.53	0.24	0.28	0.37	0.42
Specific air consumption q , m ³ /J, ($\times 10^{-6}$)	34.2	31.5	18.8	16.4	38.5	37.0

the pre-percussion pressure impulse that resists the hammer's movement is notably reduced (see Fig. 5) compared to the M29T system (as shown in Fig. 3, a) with a cross-over valve. This reduction results in decreased kinetic energy losses of the hammer before percussion, leading to improved machine efficiency.

The air hammer following the P105-2K diagram offers the advantage of increased energy (59.7 J at $p_m = 0.5$ MPa) and a higher percussion frequency (25.64 Hz). However, this air hammer features elevated average pressure in the forward stroke chamber (FSC) at 0.46 MPa (as seen in Fig. 5, a), and the pressure just before exhaust is 0.43 MPa. Consequently, there is a limited degree of compressed air expansion in the FSC, leading to significant losses of its energy during exhaust. As a result, this air hammer exhibits increased consumption (specific consumption of $34.2 \times 10^{-6} \text{ m}^3/\text{J}$ absolute consumption $3.14 \text{ m}^3/\text{min}$, as shown in Table 3).

The diagrams for the K1 scheme (Fig. 5, b) reveal closely aligns with the optimal mode. In this configuration, the hammer is supplied with the specified kinetic energy, resulting in a percussion energy of 50.3 J and a percussion velocity of 7.58 m/s. The percussion frequency is maintained at 23.8 Hz, and the necessary working stroke of the hammer, measuring 69 mm, is achieved. Additionally, this scheme effectively reduces resistance to the hammer's movement due to air compression and ensures a higher degree of air expansion, enhancing overall efficiency.

The decrease in percussion power by 21.8% in comparison with the P105-2K diagram is attributed to a reduction in the average pressure in the FSC during the working stroke, while the air hammer of the K1 diagram exhibits a 45% lower specific consumption ($18.8 \times 10^{-6} \text{ m}^3/\text{J}$) When compared with the output indicators of the M29T air hammer, the air hammer of K1 diagram demonstrates an 8% lower percussion

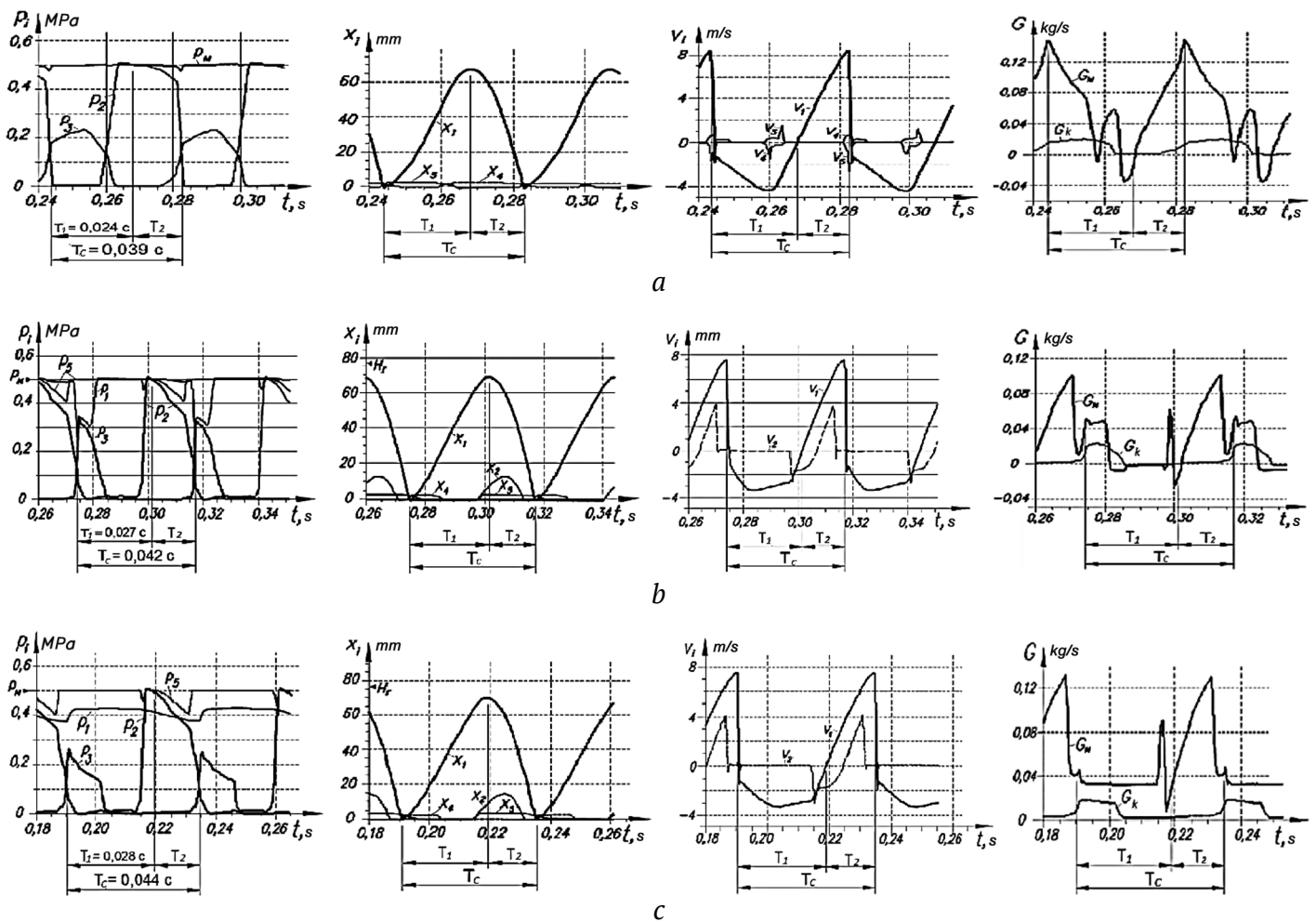


Fig. 5. Design diagrams of operating cycles of air hammer models with combined air distribution systems (variations in compressed air pressure in time $p_i(t)$ in the i -th chambers; displacement of hammer x_i and elastic valves x_4, x_5 ; velocity of hammer v_i and valves v_4, v_5 ; the instantaneous mass flow rate G : G_m – instantaneous flow rate through the main channel j_{m0} ; G_{ch} – instantaneous flow rate through channel j_{cha} in the bit): a – air hammer according to the P105-2K diagram; b – according to the K1 diagram; c – according to the K2 diagram: t – time, s; T_c – cycle period; T_1, T_2 – periods of backward and forward strokes

power due to a decrease in the frequency of percussions (23.8 Hz), while the specific consumption of K1 is 65% lower.

Simulation results confirm the operational functionality and the lowest specific air consumption for the K1 DTH hammer among the considered devices (refer to Table 5).

The results of simulating the air hammer as per the K2 diagram (Fig. 5, c) demonstrate that the model of the air hammer operates effectively with a cross-sectional area of the throttle channel $J_{13} \approx 0.25 \text{ cm}^2$, and with a smaller area ($J_{13} \leq 0.15 \text{ cm}^2$), it does not achieve the required value for the hammer's backward stroke. Key characteristics of the operating cycle are provided in Table 5. In comparison with the K1 diagram, only the diagrams of the instantaneous consumption noticeably differ (as seen in Fig. 5, b, c). The total absolute and specific consumption of the air hammer following the K2 diagram is higher than that of the device adhering to the K1 diagram (see Table 5). Therefore, with the same percussion power, the controllability of channel J_{13} in the K1 hammer leads to a 2.04-fold reduction in air consumption compared to the K2 hammer. Consequently, it is more advisable to develop air hammers based on the K1 diagram.

In practical applications, it is preferable to utilize the K1 percussion system at a main pressure of

$p_m = 0.6 \text{ MPa}$, as in this scenario, its percussion power exceeds the design percussion power of the air hammer M29T by 14.9%. However, at $p_m = 0.5 \text{ MPa}$, the percussion power of K1 is 8% lower.

Diagrams of the operating cycle of the model K1 at $p_m = 0.6 \text{ MPa}$ are depicted in Fig. 6. Fig. 6, a presents characteristic sections of the diagrams illustrating hammer displacement $x_1(t)$ and pressure $p_i(t)$ during the period of compressed air operation in the forward and backward chambers: 1–2 represents the section of air displacement from the FSC by the hammer during its backward stroke, 2–3 is the period of compressed air intake to the FSC, 3–4 illustrates the air's function in the FSC for expansion before the beginning of exhaust (point 4), 5–6 signifies the period of compressed air intake to the BSC, 6–7 depicts air operation in the BSC for expansion before the beginning of exhaust (point 7).

Estimation of the compressed air minimum consumption required for bottomhole cleaning

Let us calculate the compressed air consumption, m^3/min , required for cuttings removal, supplied to the bottomhole through the bit channel [21]:

$$Q_b = \frac{0.785 \gamma_r d^2 v_d}{\gamma_a \mu}, \quad (1)$$

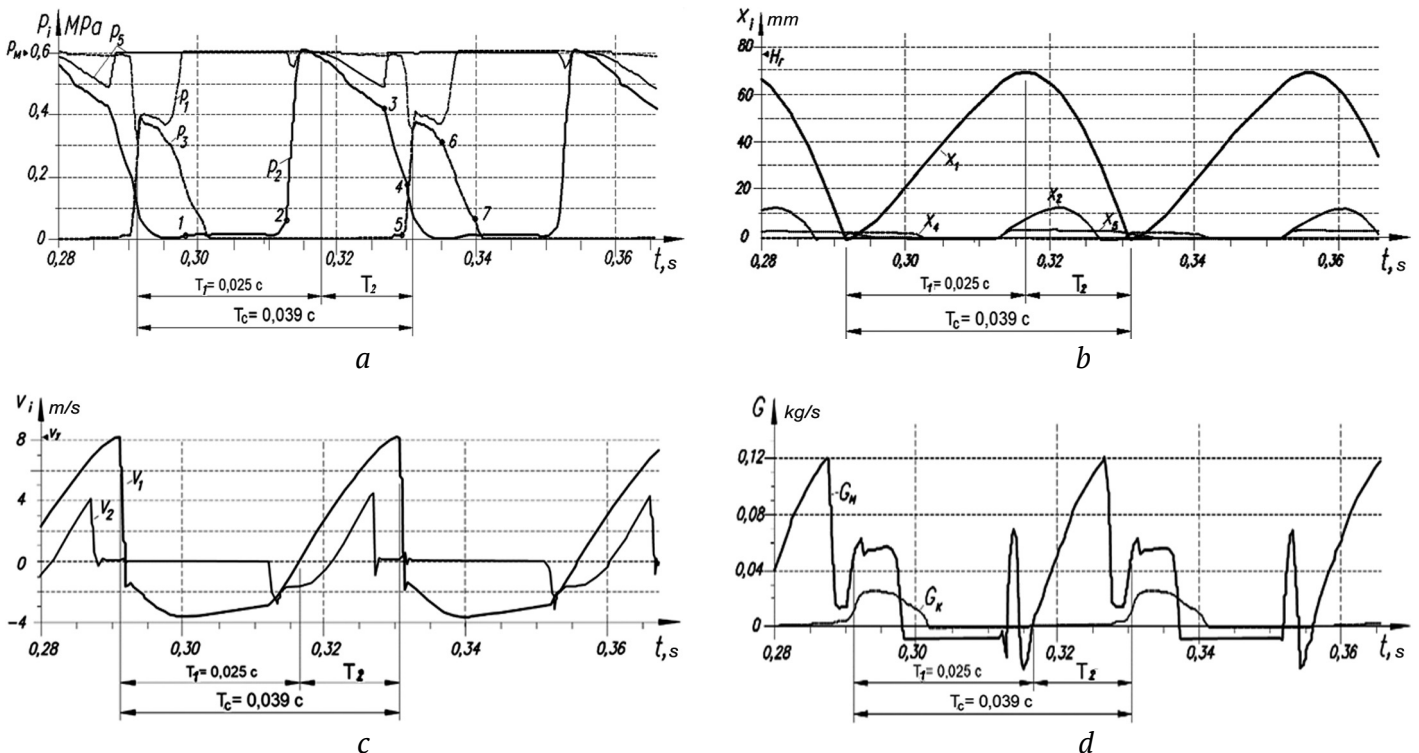


Fig. 6. Design diagrams of operating cycles of model K1 air hammer at the main line pressure of 0.6 MPa: a – changes in compressed air pressure in time $p_i(t)$ in the i -th chambers (points 1–7 characteristic sections of the diagram); b – displacements of hammer $x_1(t)$ and valves $x_2(t)$, $x_4(t)$, $x_5(t)$; c – variations in the hammer velocity $v_1(t)$ and valve velocity $v_2(t)$; d – instantaneous mass flow rate of compressed air $G(t)$; t – time, s; T_c – cycle period; T_1 , T_2 – backward and forward periods; G_m – flow rate through main line channel j_{m0} ; G_k – flow rate through channel j_{cha} in the bit



where γ_r is the density of the drilled rock, kg/m³, d is the diameter of the borehole (bit), m, v_d is the mechanical drilling speed, m/min, γ_a is the air density, kg/m³ (1.2041 kg/m³ at 20°C), μ is the weight concentration of a mixture of fracture products and air ($\mu = 6$ [19]).

The mechanical drilling speed, m/min, can be determined by formula [10]:

$$v_b = \frac{80An}{d^2f} \cdot \frac{60}{10^6 \cdot 10^3} = 4.8 \cdot 10^{-6} \frac{An}{d^2f}, \quad (2)$$

where A is the percussion energy, J; n is the percussion frequency, Hz; f is the rock hardness coefficient; d is the borehole (bit) diameter, m; $4.8 \cdot 10^{-6}$ is the dimensional coefficient.

Substituting (2) into (1), we obtain, m³/min:

$$Q_b = 3.768 \cdot 10^{-6} \frac{\gamma_r An}{\gamma_a \mu f}. \quad (3)$$

From (3), we can determine the coefficient of the compressed air consumption, m³/min/W, required for bottomhole purging:

$$\psi_b = \frac{Q_b}{An} = 3.768 \cdot 10^{-6} \frac{\gamma_r}{\gamma_a \mu f}. \quad (4)$$

The values of the coefficient ψ_b , calculated by formula (4), are as follows: for basalt ($f = 20$, $\gamma_r = 2600$ kg/m³) $\psi_b = 63 \cdot 10^{-6}$ m³/min/W, for granite and marble ($f = 10$, $\gamma_r = 2600$ kg/m³) $\psi_b = 125 \cdot 10^{-6}$ m³/min/W, for iron ore ($f = 6$, $\gamma_r = 3440$ kg/m³) $\psi_b = 276 \cdot 10^{-6}$ m³/min/W.

The air hammer (K1) with a percussion power of 1.494 kW, when drilling rock of medium hardness ($f = 6$, $\gamma_r = 3440$ kg/m³), should provide a minimum flow rate through the channel in the bit, $Q_b = 0.41$ m³/min. In harder rocks ($f = 10$, $\gamma_r = 2600$ kg/m³), the minimum flow rate is $Q_b = 0.1$ m³/min, and at $f = 20$, $\gamma_r = 2600$ kg/m³, the minimum flow rate through the bit channel is $Q_b = 0.09$ m³/min.

The calculation results indicate that air hammer K, at $p_m = 0.6$ MPa and the rock hardness coefficient of $f = 10-20$, provides a compressed air flow rate through the bit channel of $Q_b = 0.28$ m³/min, sufficient for cleaning the bottomhole. For rocks with $f = 6$, the compressed air intake for borehole purging through the bit channel should be increased by 0.13 m³/min. For reliable bottomhole purging, it is advisable to provide a flow rate through the bit of $Q_b = 0.69$ m³/min in air hammer K1, similar to the batch-produced machine M29T. In this case, the total consumption Q for K1 will be 1.88 m³/min, and the total specific consumption is $q = 21.0 \cdot 10^{-6}$ m³/J, which is 51% and 57% lower, respectively, than that of air distribution system M29T.

Assessment of energy efficiency of a new air hammer

To comparatively assess the energy efficiency of batch-produced M29T and the new K1 air hammers, let us determine the necessary electric power consumed by the compressor when using them:

$$N_c = nQ, \quad (5)$$

where n is the specific power of the compressor, kW/(m³/min), Q is the compressed air consumption of the air hammer, m³/min.

Given the average value of $n \approx 5.48$ kW/(m³/min)¹⁴, we obtain the following values of the required electrical power:

- for air hammer M29T: $N_c = 20.9$ kW;
- for air hammer K1: $N_c = 10.3$ kW.

Thus, the new air hammer K1 consumes 2.03 times less power than the batch-produced M29T during operation.

Experimental study of the air percussion mechanism.

Assessment of the design models' adequacy

The purpose of the experiments was to obtain experimental data for assessing the adequacy of design models by comparing the indicators of the operating cycle of the air percussion mechanism obtained through physical and numerical simulation. The objectives of the experiments were to record pressure diagrams in the chambers of the device and measure the compressed air consumption. Experimental studies were conducted on a laboratory bench, the diagram and appearance of which are shown in Fig. 7, a, b. The available prototype of the air percussion mechanism of model PM-K2, designed according to the K2 diagram, was used as the research object (see Fig. 4, c).

The percussion device was installed between the work absorber and the power delivery mechanism to balance the recoil of the air percussion mechanism body during its operation. Piezosensors were used to register pressure in the chambers and in the main line. Before each series of experiments, their calibration was performed. The pressure was controlled by a manometer, and the instantaneous flow rate G of compressed air during the cycles was registered by a flow sensor. The average flow rate of the device was determined by its readings.

In the process of analyzing the experiment results, the percussion energy A , J, was determined according to the method [20]. The specific compressed

¹⁴ Atlas Copco screw compressors of GA/GA+ series (160–315 kW). URL: https://aerocompressors.ru/katalog_produkcii/kompressori/vintovye_elektricheskie_kompressory/kompressory_atlas_copco/kompressor_atlas_copco_ga_160-315_kv/

air consumption q , m^3/J , was calculated using the formula

$$q = \frac{Q}{60fA}, \quad (6)$$

where Q is the compressed air consumption, m^3/min ; f is the frequency of percussions, Hz, and A is the percussion energy, Hz.

The experiments demonstrated the stable operation of the laboratory prototype PM-K2, and experimental pressure diagrams are presented in Fig. 7, *c*, *Experimental*. The following parameters of the operating cycle were established: percussion energy – 630 J, percussion frequency – 8.6 Hz, air consumption – 7.57 m^3/min , percussion power $N = 5418$ W, and specific consumption $23.3 \cdot 10^{-6} m^3/J$.

Under identical experimental conditions, the operating cycle of the PM-K2 was also investigated using the simulation model. A comparison of the experimental data (see Fig. 7, *c*, *Experimental*) and the simulation results (Fig. 7, *c*, *Calculated*) shows that they are nearly identical, sharing the same qualitative and quantitative characteristics. The pressure diagrams (p_2 , p_3 , as seen in Fig. 7) illustrate a significant degree of air

expansion in the working chambers: the pressures before exhaust in the experiment are $p_2 = 0.35–0.41$ MPa, and $p_3 = 0.2$ MPa, while in the simulation, they are $p_2 = 0.25–0.30$ MPa and $p_3 = 0.15$ MPa. The pressure curves for p_0 and p_5 indicate that the cut-off valve is activated before exhaust, preventing air leakage from the main line into the atmosphere.

To further confirm the adequacy of the design models, experimental data for the M29T air hammer were also used, which were obtained from publications [10, 11]. The technical parameters of air percussion mechanisms M29T and PM-K2 are summarized in Table 6.

The data presented in Table 6 demonstrate that the deviations between the calculated values and the experimental ones are within an acceptable range, with deviations of up to 6% for percussion frequency, 1% for percussion energy, 5% for total compressed air consumption, and 8% for specific compressed air consumption. These comparison results affirm the alignment of the calculated and experimental operating cycles of the air percussion devices being studied. Consequently, the adequacy of the calculation models employed in this research has been validated.

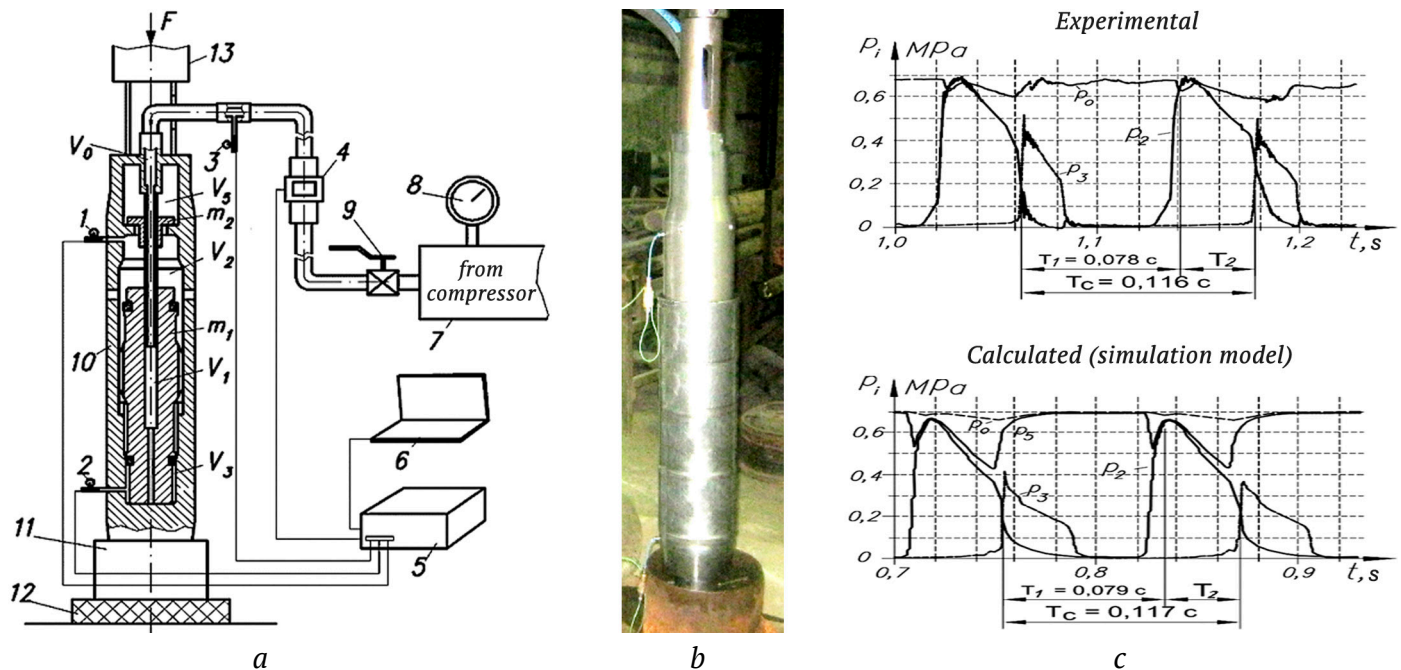


Fig. 7. Measurement of pressure in working chambers of air percussion mechanism PM-K2 with two elastic valves on the hammer and compressed air supply cut-off valve to the controllable FSC: *a* – pressure sensors, flow meters, and measuring equipment installation diagram; *b* – laboratory prototype’s appearance with pressure sensors installed, *c* – diagrams of pressure (Experimental, Calculated) in chambers of the laboratory prototype at a pressure in the main line of 0.7 MPa: 1, 2 – pressure sensors (piezosensor of the Kistler instrumente AG company type 701A) in the working and backward stroke chamber; 3 – pressure sensor in the main line; 4 – flow meter (Digital flow switch PF2A706H), 5 – ADC (analog-to-digital converter), 6 – PC (personal computer), 7 – receiver, 8 – pressure gauge, 9 – main line valve, 10 – percussion unit, 11 – adapter, 12 – work absorber, 13 – power delivery mechanism; F – delivery force, V_i – working chambers, m_i – moving components (hammer, cut-off valve); p_2 – pressure in the controllable FSC, p_3 – pressure in the BSC, p_0 – pressure in the main FSC, p_5 – pressure in chamber V_5



Table 6

Comparison of experimental and design technical indicators of air percussion machines

Indicator	M29T				PM-K2		
	Designed	Experimental		Deviation, % (from [11])	Designed	Experimental	Deviation, %
		[11]	[10]				
Main line pressure (g) design p_m , MPa	0.5	0.5	0.5	–	0.7	0.7	–
Hammer mass m_1 , kg	1.75	1.75	1.60	–	34.5	34.5	–
Bit channel J_{cha} , cm ²	0.502			–	0	–	–
Channel area J_{13} , cm ²	–	–	–	–	–	0.453	–
Cycle period T_c , s	0.038	0.040	0.035	–5.0	0.117	0.116	+0.9
Period of backward stroke T_1 , s	0.023	–	–	–	0.079	–	–
Period of forward stroke T_2 , s	0.015	–	–	–	0.039	–	–
Operating stroke of hammer H_0 , mm	67	–	–	–	134	–	–
Stroke velocity v , m/s	7.86	7.86	7.83	0.0	6.02	6.05	–0.5
Percussion energy A , J	54.0	54.0	49.0	0,0	625	630	–0.8
Percussion frequency n , Hz	26.3	25.0	28.3	+5.2	8.55	8.6	–0.6
Percussion power N , kW	1.42	1.35	1.39	+5.2	5.34	5.42	–1.4
Flow rate through bit Q_b , m ³ /min	0.69	–	–	–	0	0	–
Total consumption Q , m ³ /min	3.81	4.00	4.50	–4.8	7.85	7.57	+3.7
Specific consumption q , m ³ /J ($\times 10^{-6}$)	44.7	44.4	53.9	+0.7	24.5	23.3	–7.5

Conclusion

1. Energy conservation in the mining industry and the maintenance of required compressed air pressure in underground mining networks can be achieved by reducing the specific air consumption of down-the-hole hammers.

2. Analysis of operating cycles of typical air distribution systems for air hammers, including valve-operated, spoolless, and spool-operated systems, has revealed conditions for ensuring the economic efficiency of an air percussion system. These conditions include eliminating pneumatic resistance to the hammer’s movement and increasing the degree of air expansion in the working chambers.

3. A proposed air distribution system that meets the above requirements includes two elastic valves on the hammer, a cut-off valve for controlling compressed air supply to the forward stroke chamber, and controlled inlet to the backward stroke chamber.

4. An air hammer has been developed based on this air distribution system, designed to be the same size as the batch-produced machine M29T. Numerical simulations have determined its optimal design parameters, emphasizing specific consumption. Calculations show that, despite its similar dimensions and percussion power to M29T, the designed hammer consumes 53% less specific energy and requires 2 times less electric power for compressed air supply.

5. A comparison of the design data, experimental data, and literature sources has demonstrated qualitative and quantitative similarity between experimental and design diagrams of the operating cycle. The deviations of calculated parameters from experimental data are within acceptable limits, with variances of up to 6% for percussion frequency, 1% for percussion energy, 5% for absolute compressed air consumption, and 8% for specific compressed air consumption. This confirms the adequacy of the calculation models and the accuracy of the calculation results.

References

1. Mineeva A.S. Energy efficiency as a factor of sustainable development for a mining company. *Journal of Economy and Entrepreneurship*. 2016;(11–2):565–570. (In Russ.)
2. Lyukhanov V.V., Alferov S.B., Trofimov S.N., Rozhentsov V.F. Pneumatic high-pressure rock drill by Nipigormash OAO and Mashinostroitelny Holding ZAO. *Russian Mining Industry*. 2012;(5): 28–30. (In Russ.)
3. Smolyanitsky B.N., Repin A.A., Danilov B.B. et al. *Improving the efficiency and durability of impulse machines for the construction of long wells in rock masses*. Monograph. Novosibirsk: SB RAS Publ.; 2013. 204 p. (In Russ.)
4. Karpov V.N., Nemova N.A., Reznik A.V. On improving the efficiency of drilling blast wells in the development of solid minerals. In: *Innovations and prospects for the development of mining engineering*



and electromechanics: a Collection of Abstracts of the 8th International Scientific and Practical Conference. St. Petersburg: SPGU; 2021. Pp. 341–345. (In Russ.)

5. Kumykova T.M., Kumykov V.K. Dynamics of mine hydro-pneumatic accumulator. *Journal of Mining Science*. 2013;49(5):763–771. <https://doi.org/10.1134/S1062739149050109> (Orig. ver.: Kumykova T.M., Kumykov V.K. Dynamics of mine hydro-pneumatic accumulator. *Fiziko-Tekhnicheskiye Problemy Razrabotki Poleznykh Iskopayemykh*. 2013;(5):99–109. (In Russ.))

6. Alekseev S.E., Kokoulin D.I. The use of down-the-hole hammers for straight directional drilling. In: *Modern problems in mining and methods of modeling mining and geological conditions in the development of mineral deposits: proceedings of the All-Russian scientific and tech. conf. with international participation. Kemerovo RF, 2015*. Kemerovo: TF Gorbachev Kuzbass State Technical University; 2015 (In Russ.)

7. Gaun V.A. Development and research of down-the-hole hammers with increased impact energy. In: *Improving the efficiency of pneumatic percussion drilling machines: a collection of scientific papers*. Novosibirsk: Institute of Mining SB USSR AS; 1987. Pp. 3–10. (In Russ.)

8. Lipin A.A. Promising pneumatic punchers for borehole drilling. *Journal of Mining Science*. 2005;41(2):157–161. <https://doi.org/10.1007/s10913-005-0078-0> (Orig. ver.: Lipin A.A. Promising pneumatic punchers for borehole drilling. *Fiziko-Tekhnicheskiye Problemy Razrabotki Poleznykh Iskopayemykh*. 2005;(2):74–78. (In Russ.))

9. Emelyanov P.M., Esin N.N., Zinoviev A.A. et al. *Machines for drilling boreholes with down-the-hole hammers in underground conditions*. Novosibirsk: SB USSR AS; 1965. (In Russ.)

10. Ivanov K.I., Latyshev V.A., Andreev V.D. *Drilling technique in the mineral deposit mining*. Moscow: Nedra Publ.; 1987. 272 p. (In Russ.)

11. Sudnishnikov B.V., Esin N.N., Tupitsyn K.K. *Study and designing of pneumatic impact machines*. Novosibirsk: Nauka Publ.; 1985. 134 p. (In Russ.)

12. Wijk G. (Ed.) *Hammer theory and practice*. 2008. URL: https://www.researchgate.net/publication/271527406_Hammer_Theory_and_Practice

13. Gerts E.V. *Pneumatic drives. Theory and calculation*. Moscow: Mashinostroenie Publ.; 1969. 359 p. (In Russ.)

14. Myuntser E.G. Construction of a mathematical model of pneumatic impact mechanisms on a computer. In: *Pneumatic drilling machines: collection of scientific papers*. Novosibirsk: Institute of Mining SB USSR AS; 1984. p.49–55. (In Russ.)

15. Fedulov A.I., Arkhipenko A.P., Mattis A.R. *Selection of gaps in the rubbing pairs of a pneumatic hammer*. Novosibirsk: Siberian dept. of Nauka publ; 1980. 128 p. (In Russ.)

16. Petreev A.M., Primychkin A.Y. Ring-type elastic valve operation in air hammer drive. *Journal of Mining Science*. 2016;52(1):135–145. <https://doi.org/10.1134/S1062739116010224> (Orig. ver.: Petreev A.M., Primychkin A.Y. Ring-type elastic valve operation in air hammer drive. *Fiziko-Tekhnicheskiye Problemy Razrabotki Poleznykh Iskopayemykh*. 2016;(1):132–143. (In Russ.))

17. Tambovtsev P.N. Experimental studies of pneumatic impact device with a reduced specific consumption of compressed air. *Fundamental and Applied Issues of Mining*. 2020;7(2):47–52. (In Russ.) <https://doi.org/10.15372/FPVGN2020070208>

18. Petreev A.M., Primychkin A.Y., Vorontsov D.S. Ring-shape elastic valve in the air percussion machines. *Journal of Mining Science*. 2010;46(4):416–424. <https://doi.org/10.1007/s10913-010-0052-3> (Orig. ver.: Petreev A.M., Primychkin A.Y., Vorontsov D.S. Ring-shape elastic valve in the air percussion machines. *Fiziko-Tekhnicheskiye Problemy Razrabotki Poleznykh Iskopayemykh*. 2010;(4):56–65. (In Russ.))

19. Tymchur A.D. On the issue of improving the pneumatic transport of drill chips when drilling holes in open pits. *Proceedings of USGU*. 2000;(11):277–279. (In Russ.)

20. Esin N.N. *Methods of research and fine-tuning of pneumatic hammers*. Novosibirsk: Institute of Mining SB USSR AS; 1965. 76 p. (In Russ.)

Information about the authors

Pavel N. Tambovtsev – Cand. Sci. (Eng.), Associate Professor, Senior Researcher of the Impulse Systems Modeling Laboratory, N.A. Chinakal Institute of Mining of the Siberian Branch of the RAS, Novosibirsk, Russian Federation; ORCID [0000-0003-1058-2764](https://orcid.org/0000-0003-1058-2764), Scopus ID [7004038110](https://scopus.com/authorid/7004038110); e-mail tambovskiyp@mail.ru

Evgeny P. Rusin – Cand. Sci. (Eng.), Senior Researcher of the Department of Mining and Construction Geotechnics, N.A. Chinakal Institute of Mining of the Siberian Branch of the RAS, Novosibirsk, Russian Federation; ORCID [0000-0001-7220-8589](https://orcid.org/0000-0001-7220-8589), Scopus ID [20434728100](https://scopus.com/authorid/20434728100); e-mail gmmlab@misd.ru

Received 14.12.2022

Revised 31.07.2023

Accepted 25.09.2023